A FRACTURE MECHANICS ANALYSIS OF THE FATIGUE RELIABILITY OF TUBULAR WELDED JOINTS

by

Xiaowen Huang

Submitted to the University of Glasgow

for the degree of

Doctor of Philosophy

November, 1986

ABSTRACT

Fatigue failure is generally the result of crack initiation at a surface followed by stable crack propagation leading finally to unstable fracture. The total fatigue life is often a random variable due to the randomness of fatigue loading, the variability of material properties and the final failure conditions. Fracture mechanics provides a rational description of fatigue, based on which an analytical method has been developed for assessing the reliability of components under random loading. This method can be used for predicting the distribution of crack lengths after a given number of fatigue cycles have been applied to a initial crack; the distribution of the number of cycles needed to grow a crack to a specific length; or the distribution of fatigue lives terminated at a random final crack length.

In order to assess the fatigue reliability of tubular welded joints, the stress intensity factors of surface cracks have been determined by shell analysis with the cracked section modelled by line springs. The surface cracks are generally subjected to mixed mode loadings and the line spring method allows the stress intensity factor for individual modes to be assessed separately. The applicability of the line spring method to stress concentration areas has been verified

in plane strain T joints, which has provided the confidence to apply this method to tubular welded joints. The calculations are compared with available experimental data.

The fatigue life distributions of a tubular welded T joint for three loading modes have been predicted based on an assumed initial crack length. The S-N curve produced from the analytic prediction compares favourably with experimental data in terms of an equivalent hot spot strain range. In the cases studied, the hot spot strain range is seen to be a reasonable but not very accurate parameter for determining fatigue life. In conclusion, fracture mechanics has been demonstrated to be a valid and important method for predicting the residual fatigue life of damaged tubular welded joints.

NOTATION

a	crack length.
a_o	initial crack length.
a_c	critical crack length.
a_f	final crack length.
c	compliance, or "critical" or "correction" if used as a subscript.
d	a locally defined value or a nodal displacement.
e, exp	exponential.
erf	error function.
eff	subscript for "effective".
f	frequency, or any function, particularly the geometric calibration function for the stress intensity factor of cracks.
h	relative frequency of realising an event, or the subscript for "hot spot".
i,j	integers.
k	an integer, for number of repetitions.
l	length, or used as subscript to indicate "the logarithm of" (ln).
m	subscript for "mean".
[m]	element stiffness matrix.

m_n the nth moment of a power spectrum.

max subscript for "maximum".

min subscript for "minimum".

n one of the constants describing the material resistance to fatigue crack propagation.

op subscript for "opening".

p probability density function.

$p_X(y)$ this form of notation is for a probability density function initially in terms of x which is replaced by y

p probability density function represented as a vector.

r radius, or the length of a plastic zone, or the stress ratio: $r=S_{min}/S_{max}$.

s subscript for "stress".

t thickness or time.

u displacement in x direction.

v displacement in y direction.

w displacement in z direction, or work, or weight function.

x a variable or a random signal.

y a variable.

z a variable or a complex variable: $z=x+iy$

A area.

B thickness of a three point bend specimen, or a random event.

C_C locally defined correction factor.

$C, C_1, C_2..$ constants used locally for describing different

theories.

D fatigue damage.

E[ ] "the expectation of".

E Young's modulus.

F force.

G power spectrum, or elastic energy release rate.

G_o a specific power spectrum value.

H Fourier transformation, or the hight of a tubular T joint.

In[ ] the elliptic integration of the second kind.

K stress intensity factor.

K_I, K_{II}, K_{III} the stress intensity factors for the three basic cracking modes.

L a relative crack length index.

M moment.

[M] a matrix, particularly the global stiffness matrix.

M_n the nth moment of stress range distribution.

N number of fatigue cycles, sometimes used as subscript.

N_o minimum fatigue life in terms of fatigue cycles.

P cumulative distribution function.

Pr the probability of a random event.

R autoco-orelation function or resistance to cracking.

$R^{(i)}$ the ith differential of an autoco-orelation function.

R_o plastic zone size.

S stress range, or a particular stress if a subscript is used.

S_o yield stress.

S_a stress amplitude.

U energy or the parameter defined by Eq 10.53.

V, V_1, V_2 variables used locally in the text for describing different theories.

Var variance.

W width.

Z a complex function or defined by Eq 10.47.

α a material constant representing the material resistance to fatigue crack propagation, sometimes used as a subscript.

σ a root mean square value, particularly the root mean square of random stress histories.

σ_n r.m.s of S^n.

μ mean.

μ_n the mean of S^n.

λ the parameter defined by Eq 10.5.

ω angular frequency.

θ, ϕ angles.

γ, τ, β geometric parameters of tubular joints.

ν Poisson's ratio.

δ Dirac's function or "increment"

ϵ power spectrum width parameter.

η normalised stress range: $\eta = S/\sigma$.

ρ distance for a point in a plane crack to the crack front.

π 3.1416

Ψ stress function.

Δ "range of", or "increment of", or critical damage index

Γ Gamma function or an arbitrary curve.

Σ summation.

INTRODUCTION

Many engineering structures, such as the oil rigs in the North Sea are subjected to random loading. In these cases, fatigue is a main cause of damage and final collapse. As more materials are used in severe environments, the ability to understand fatigue mechanisms and predict the fatigue life is essential to improve human safety and equipment reliability while using less material to obtain economic benefits. In the case of offshore platforms, the integrity of the structure as a whole is dependent on the reliability of its joints. It is the object of this thesis to analyse the fatigue behaviour of one common type of joint under realistic random loadings. Although the work is concentrated on a single type of joint, the method of analysis is general and can be easily applied to other joints and geometries.

The fatigue life depends on many factors: loading; temperature; environment; as well as the geometry of the structure and the material properties. Currently, there is no single comprehensive analysis which accounts for all the relevant factors. An appropriate way to tackle the problem is to consider the parameters individually.

Loading is always considered. There are two main types of fatigue loading: constant amplitude loading and random loading. The former usually has a single frequency and constant amplitude cycles. The later can be related to the former in terms of cycles which are defined on the basis of equivalent fatigue damage. The amplitude of the cycle in this case is random and can only be described statistically. The distribution of cycles can be obtained from measurements of the real or simulated random loading, although a more efficient way to achieve this is to use power spectral analysis.

In practical engineering situations, it is arguable that random loading occurs more frequently than constant amplitude loading. However, constant amplitude fatigue tests provide a basis for a fundamental study of fatigue. Such tests can determine the relation between the applied amplitude of the loading and the fatigue life, which is known as the S-N curve. The conventional method of dealing with the problem of random fatigue assesses the damage associated with each cycle in the random loading by reference to the S-N relation. Fatigue damage is accumulated linearly with time and is thus used to predict the fatigue life of the structure. Unfortunately this method sometimes produces inaccurate, non-conservative results, and as there is no physical basis for the method, it does not allow an assessment of the residual life by examining the state of the structure.

The emergence of fracture mechanics provides a more rational way of analysing fatigue. In this method, fatigue damage takes the form of

a growing crack under the fatigue loading, and when the crack reaches a critical length which is a function of the applied load, failure is expected. In many structures pre-existing crack-like defects are almost inevitable and a major part of the fatigue life is spent in crack propagation. The fatigue life is therefore determined by the rate of crack growth per cycle which is frequently expressed as a function of the stress intensity factor range ΔK during the stress cycle

$$\frac{da}{dN} = f(\Delta K)$$

The stress intensity factor K describes the stress field near the crack tip, therefore the influence of loading, geometry and the shape of the crack on the growth rate can be quantified through the stress intensity factor. The determination of the function f is usually a straightforward experimental problem, but the determination of the stress intensity factor K is generally a difficult task, except for some simple planar situations. For a surface crack in a tubular welded joint, the stress intensity factor K varies along the crack front, and a three dimensional analysis is required. If the finite element method is used for such an analysis, a large amount of computer memory and time is needed, which is often not available for economic reasons. An alternative is to increase the efficiency of the calculation so that the amount of computer memory and time can be reduced. This can be achieved by the line spring method which enables part through cracks to be modelled in shell finite element analysis with reasonable accuracy. The efficiency of the method is enormous because the three dimensional analysis can be replaced by a shell analysis.

Deterministic predictions of the fatigue life can be produced by fracture mechanics analysis or by the conventional S-N method. However, fatigue in offshore structures is usually a random event. It is not surprising because even under well controlled laboratory conditions, the variance in crack growth rate has been observed in small fracture mechanics specimens subjected to simple sinusiodal loading. In the case of complicated welded tubular joints under random loading, a wider scatter of the fatigue life is inevitable. Probabilistic and statistical techniques have been used in conjunction with the conventional and fracture mechanics methods to predict life distributions of components under constant amplitude loading and random loading. Although a number of models have been proposed, their application is yet to be universally recognised.

A review of the existing methods for assessing the fatigue reliability of tubular welded joints and their theoretical foundations is given in Chapters 1 to 9. In planing the work, it was believed that the variance in fatigue life should be considered, and a new general method for predicting the random distribution of fatigue life has been developed and presented in Chapter 10. The variance due to the random loading, material properties and the random final crack length have been considered by this analytical method. Predictions by this method are in good agreement both with computer simulations and experimental results. In order to apply the method, the stress intensity factors of semi-elliptical cracks in tubular welded joints have been evaluated using the finite element method incorporating the line spring method. The cracks were

desinged to represent a growing fatigue crack which remains at a position such that the deepest point is always at the original maximum stress site. A comparison of the calculated stress intensity factors with experimentally determined values and other numerical results has been given. In the final chapter, the probabilistic model for predicting fatigue life distribution has been applied to a tubular welded T joint. This produced an estimate of fatigue life distribution of the tubular joint based on an assumed initial crack. This method is particularly useful for assessing the residual fatigue life of an existing structure in which cracks are found. As an illustration, the residual life distribution of the T joint containing a half through crack has been predicted. The method has also been used to produce S-N curves for different level of probability's of survival, which compare favourably with experimental data.

LIST OF CONTENTS

CHAPTER 1 STRUCTURAL RELIABILITY

In some engineering problems, the variance in experimental results or observations is ignored for simplicity. But statistics must be considered whenever the difference between individual results becomes significant in the context of the problem. For example, failure of some critical components before their expected fatigue life must be prevented. In this case, fatigue life can be treated as a random variable and the probability of failure before the designed life represents the reliability of the components.

SECTION 1 Introduction to Reliability

It is generally recognised that structural failures during service can not be completely prevented (Ref 1-3). The possibility of failure of some crucial structures has become a major issue in engineering. Currently, fatigue life can not be predicted exactly and can thus be regarded as a random variable. A random variable can only be described in terms of probability or statistics, the basic mathematical principles of these mathematic topics can be found in a standard text such as that by DeGroot (Ref 4).

The variability in the fatigue life of a structure arises from the randomness of both the material properties which includes the random distribution of any pre-existing cracks and the applied loading. The effect of environment is also a cause of the random distribution of fatigue life. Additional uncertainty can result from the imperfect state of the techniques used currently in design and fatigue life prediction.

SECTION 2 Quantitive Representation of Reliability

The reliability of a structure or component can be quantified in terms of the probability of failure. Let B denote a failure event for which the life of a certain component is less than a given time. The likelihood that this event occurs can be estimated by conducting experiments then determining the ratio of the number of times N_1 in which failure happens during the specific period and the total number of specimens N tested. This ratio is known as the relative frequency h

$$h = \frac{N_1}{N} \tag{1.1}$$

The relative frequency approaches the probability when the number of such experiments is infinite

$$\lim_{N\to\infty} h[B] = \lim_{N\to\infty} \frac{N_1}{N} = Pr[B] \tag{1.2}$$

where Pr[ ] indicates "the probability of".

It is convenient to introduce the concept of a random variable when studying the probability of an event. Depending on the nature of the problem, random variables can be continuous or discrete. Let x be a random variable representing the life of a component and X be a specific value of x. Since the event B includes all the cases in which failure occurs before the specified period of loading is completed, it may be represented as $x \prec X$.

The probability $Pr[x \prec X]$ is known as the cumulative distribution function P(x) which gives the total probability distributed in the region $-\infty$ up to X

$$Pr[B] = P(x) = \int_{-\infty}^{x=X} p(x)\, dx \qquad (1.3)$$

p(x) is the probability density function which is always greater or equal to zero. Its relation with the cumulative distribution function can also be presented in the form

$$dP = p(x)\, dx \qquad (1.4)$$

From Eq 1.3, it can be seen that the probability of failure depends on the fatigue life distribution and the given time. As an example, the Weibull distribution (Ref 5) is considered in which the fatigue life is expressed in terms of a number of cycles.

$$p(N) = \frac{C\,(N - N_o)^{C-1}}{\beta^C}\; e^{-\left(\frac{N - N_o}{\beta}\right)^C} \qquad (1.5)$$

where N_o is the minimum life, C and β are parameters chosen from

curve fitting on the experimental results. In this simple situation, the probability of failure at less than a given life N is the cumulative distribution P(N) as shown in Fig 1.1

$$P(N) = \int_{N_o}^{N} p(N)\, dN = 1 - e^{-\left(\frac{N-N_o}{\beta}\right)^C} \qquad (1.6)$$

Furthermore, the reliability function is defined as the probability of survival P(N|survival) (Ref 6) which is simply 1-P(N)

$$P(N|survival) = e^{-\left(\frac{N - N_o}{\beta}\right)^C} \qquad (1.7)$$

In order to quantify the probability of failure during a particular period, the failure rate, sometimes known as the hazard function can be introduced. For the period between Nth and (N+1)th cycle, the hazard function $H_{(N+1)}$ for the Weibull distribution is

$$H_{(N+1)} = 1 - Pr(\text{survival at } N+1 | \text{survival from } N_o \text{ to } N)$$

$$= 1 - \frac{Pr(\text{survival from } N_o \text{ to } N+1)}{Pr(\text{survival from } N_o \text{ to } N)}$$

$$= 1 - e^{-\frac{(N+1-N_o)^C - (N-N_o)^C}{(\beta - N_o)^C}} \qquad (1.8)$$

SECTION 3 Formulation of Reliability Assessment

In the view of probabilistic fracture mechanics (Ref 3), structures

contain inherent cracks or crack like defects of different sizes. The failure condition can be represented by a crack of a critical length a_c which is a statistical function of the external loading. The chance of realising the condition $a \geq a_c$ is the chance that the structure fails. For fatigue situations, the distribution of crack lengths changes with time due to crack propagation, and thus the reliability of the structure declines as it remains in service.

However, the basic technique for reliability assessment starts by looking at the probability of failure at a given time and incorporates the decrease of the structural strength (Ref 7). It works in terms of the strength Q and load S_r. Let the strength and load have distributions of $p(Q)$ and $p(S_r)$ respectively, for the case that the strength is between Q and Q+dQ, the probability of failure is

$$Pr[\text{failure}|Q] = p(Q)dQ\int_Q^{+\infty} p(S_r)\, dS_r \qquad (1.9)$$

The probability of failure at a time includes all the possible states

$$Pr[\text{failure}] = \int_{-\infty}^{+\infty} \int_Q^{\infty} p(S_L)\, p(Q)\, dS_L\, dQ \qquad (1.10)$$

as shown schematically in Fig 1.2.

It can be seen that the distributions of the structural strength and the loading are essential requirements for any reliability analysis. The probability density function or the cumulative distribution function describes the random variable completely. Unfortunately, it

is often very difficult to obtain such information experimentally, since an infinite number of tests are required; and analytically, it is possible only in very simple cases. In practice, characteristic parameters are often used which describe the important features of the distribution. Perhaps the most important parameter is the mean. If $y=f(x)$ and the possible values of x are x_1, x_2, ... x_k, the mean of y is

$$E[y] = \lim_{N\to\infty} \frac{f(x_1)N_1+f(x_2)N_2+\ldots\ldots f(x_k)N_k}{N}$$

$$= \sum_{i=1}^{k} f(x_i)\ Pr[x_i] \qquad (1.11)$$

where E[ ] indicates "the mean of" and N_1, N_2 ... are respectively the numbers of occurences of the k different values x_1, x_2 ... in the total of N experiments. An integration can be applied when x is continuous

$$E[y] = \int_{-\infty}^{+\infty} f(x)\ p(x)\ dx \qquad (1.12)$$

The mean measures the central location of a distribution (Fig1.3) whereas another important parameter, the variance Var[x] measures the concentration about the mean

$$Var[x] = \int_{-\infty}^{+\infty} (x - E[x])^2\ p(x)\ dx \qquad (1.13)$$

Often, the root mean square is preferred, which is defined as

$$\sigma = \sqrt{Var[x]} \qquad (1.14)$$

A small root mean square or r.m.s indicates that most occurrences of

the event occur close to the mean value. In general, both the mean and variance are special cases of the nth moment Mn about a given value X

$$Mn = E[\ (x-X)^n\ ] = \int_{-\infty}^{+\infty} (x - X)^n\ p(x)\ dx \qquad (1.15)$$

When X=0 and n=1, the moment is the mean; when X=E[x] and n=2, it is the variance.

It is a common practice to assume that the distribution of load or strength has a particular form based on experience. The distribution is then completely determined using characteristic parameters obtained experimentally. A popular form is the normal or Gaussian distribution (Fig 1.3) whose probability density function is

$$p(x) = \frac{1}{\sqrt{(2\pi)}\ \sigma} \exp\left[-\frac{(x - \mu)^2}{2\ \sigma^2} \right] \qquad (1.16)$$

where μ is the mean and σ is the r.m.s of the random variable x. The cumulative distribution function is

$$P(x) = \int_{-\infty}^{X} \frac{1}{\sqrt{(2\pi)}\ \sigma} \exp\left[-\frac{(x - \mu)^2}{2\ \sigma^2} \right] dx$$

$$= \frac{1}{2} \left[1 + \mathrm{erf}\left(\frac{x - \mu}{\sqrt{2}\ \sigma} \right) \right] \qquad (1.17)$$

where erf( ) is defined as

$$\mathrm{erf}(X) = \frac{2}{\sqrt{\pi}} \int_{o}^{x=X} e^{-x^2}\ dx \qquad (1.18)$$

which is called the error function and is tabulated in many handbooks (Ref 8).

LIST OF FIGURES FOR CHAPTER 1

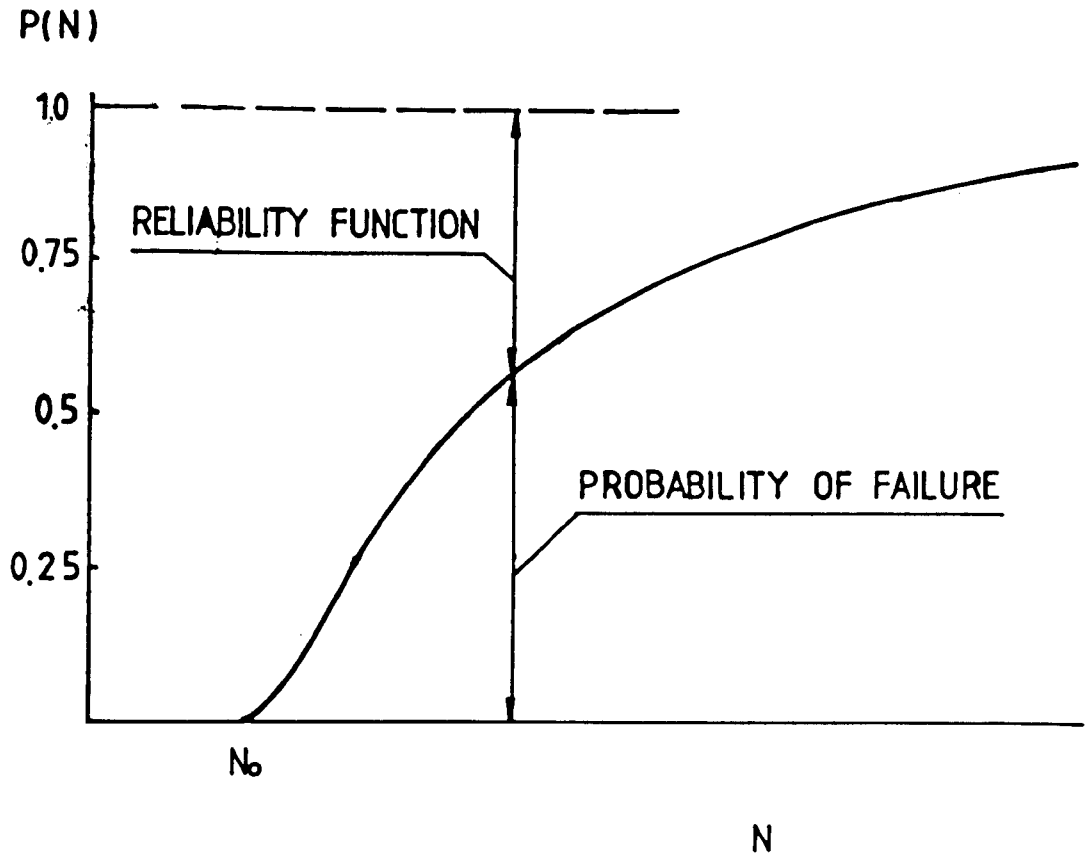
P(N)
1.0
0.75
0.5
0.25
RELIABILITY FUNCTION
PROBABILITY OF FAILURE
N₀
N

Fig 1.1

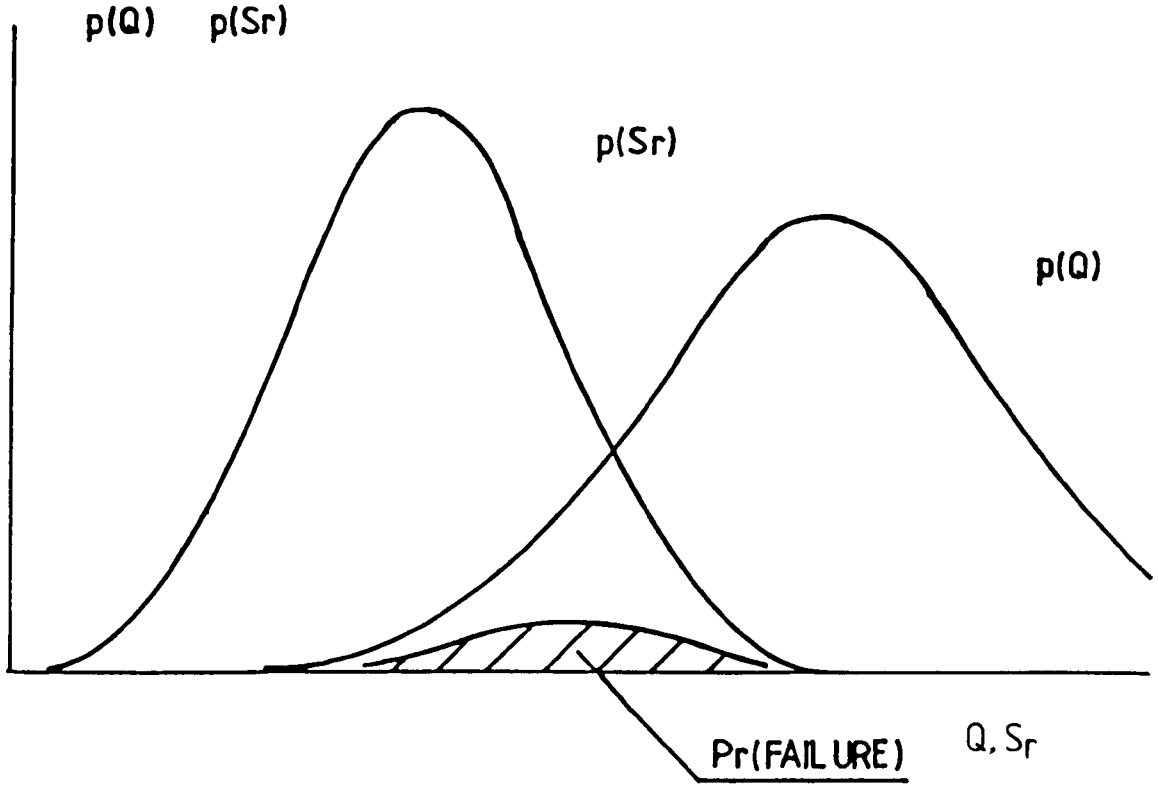

Fig 1.2

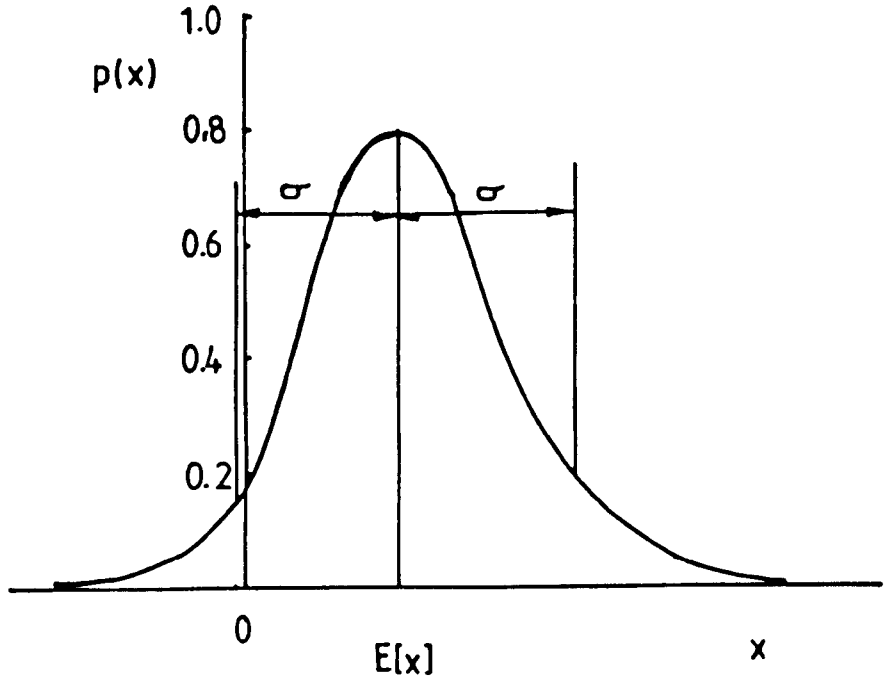

Fig 1.3

CHAPTER 2 RANDOM LOADING

Fatigue occurs in materials subjected to alternating stresses which often comprise a random stress history. A random stress history can be described by its statistic or probabilistic characteristics efficiently. Experiments (Refs 9 and 10) have shown a close relation between the fatigue life and some of the probabilistic characteristics of the fatigue loading, thus it is important to be able to analyse fatigue loadings and obtain the relevant statistical information.

SETCTION 1 Introduction

In the offshore industry, it is usual to record the stress history x(t) at specific points of the structure for maintenance and research purposes. Each time history is regarded as a sample and there is theoretically no limit to the number of samples that can be taken. A random process consists of all such samples which are collectively known as an ensemble (Fig 2.1).

However, when dealing with a random process, it is much more convenient to take one of the samples as being representative of the process as a whole, and this is appropriate only when the process is

ergodic, i.e. when any statistical characteristic measured along any of the samples is the same as that measured across the ensemble. In addition, some processes are called stationary, in which the statistical characteristics across the ensemble are independent of time. An ergodic process must be stationary while a stationary process is not necessarily ergodic. Stationary processes should be infinitely long having neither starting point nor end point, otherwise they will depend on time at those points. In an engineering sense, this condition is interpreted as "reasonably long", depending on the context of the problem. In the following text, random processes are assumed to be ergodic, if not otherwise stated.

Further description of a random history requires the evaluation of the mean, the root mean square and other characteristic parameters. This can be achieved from a knowledge of the probability distribution of the random variable. The probability density function p(x) of a random variable is defined so that at an arbitrarily chosen time, the probability of x(t) falling between X and X+dx is given as (Fig 2.2)

$$P[X<x<X+dx] = p(x)dx = \frac{\Sigma\Delta t}{T} \qquad (2.1)$$

where $\Sigma\Delta t$ is the sum of all the periods x(t) spends between X and X+dx during the total time range T. If the probability density function p(x) is known, the mean, root mean square and other moments can be calculated according to Eqs 1.11 to 1.15.

SECTION 2 The Spectral Density of Random Processes

An essential concept in the analysis of random processes is the representation of a time history by the sum of an infinite number of sine or cosine functions with random phases.

$$x(t) = \lim_{i \to \infty} \sum_{i=1}^{i} C_i(\cos\omega_i t - \Phi_i) \qquad (2.2)$$

where Φ_1, Φ_2 ..... Φ_i are independent random phase angles, C_1, C_2 ..... C_i amplitudes and ω_1, ω_2 ..... ω_i angular frequencies.

$$\omega_i = 2\pi i \Delta f \qquad (2.3)$$

Δf is the frequency difference between the harmonic components which can be arbitrarily small. Based on this, S.O. Rice (Ref 11) and later Cartwight and Longuet-Higgins (Ref 12) have established many significant results. It was assumed that Φ_i is uniformly distributed between 0 and 2π. The amplitudes of the harmonic components C_i can be determined through the power spectrum of the process G(f)

$$C_i^2 = 2\, G(f)\, \Delta f \qquad (2.4)$$

when Δf is very small. A physical interpretation of the result is that, if the random signal is a current flowing through a unit resistance, the dissipated power arising from the components having frequencies between f_i and $f_i+\Delta f$ is given by $G(f)\Delta f$. The difference between the samples of an ergodic random process is entirely due to the random phase angles, while the power spectrum for them is the same.

The relation between a random process and its power spectrum can be illustrated in another way. This utilizes the autocorrelation function which was first introduced by Taylor (Ref 13). The autocorrelation $R(\tau)$ of a random history is the average of the product $x(t)x(t+\tau)$, i.e:

$$R(\tau) = E[\, x(t)\, x(t+\tau)\,] \tag{2.5}$$

where τ is the time gap between the sampling points. It is obvious that

$$R(0) = E[\, x^2(t)\,] \tag{2.6}$$

and

$$R(\tau) = R(-\tau) \tag{2.7}$$

S.O. Rice (Ref 11) has described the relation between the autocorrelation and the power spectrum, as well as showing that the Fourier transformation of the autocorrelation is identical to the power spectrum. The Fourier transformation H(f) of a function x(t) can be defined in complex form as

$$H(f) = 2 \int_{-\infty}^{\infty} x(t)\, e^{-i2\pi ft}\, dt \tag{2.8}$$

H(f) exists when

$$\int_{-\infty}^{\infty} \left| x(t) \right| dt < \infty \tag{2.9}$$

The coordinates for the magnitude of the signal can be adjusted so

that the mean of the signal is zero and the autocorrelation function satisfy the above condition. The power spectrum can be given by

$$G(f) = 2 \int_{-\infty}^{\infty} R(\tau)\, e^{-i2\pi f\tau}\, d\tau \qquad (2.10)$$

or

$$G(\omega) = 2 \int_{-\infty}^{\infty} R(\tau)\, e^{-i\omega\tau}\, d\tau \qquad (2.11)$$

Since $R(\tau)$ is a even function of τ, the imaginary part of the right hand side of the equation vanishes. The autocorrelation function can be regained by an inverse Fourier transformation

$$R(\tau) = \frac{1}{\pi} \int_{-\infty}^{\infty} G(\omega)\, e^{i\omega\tau}\, d\omega \qquad (2.12)$$

SECTION 3 Narrow Band and Broad Band Random Processes

A random process whose power spectrum occupies a narrow band of frequencies Δf is naturally called a narrow band process. If the frequency range occupied is considered to be large, the process is known as broad band random. Furthermore, in the extreme case, if the power spectrum covers the whole range from 0 to $+\infty$ uniformly, the process is called "white noise". In practice, narrow band processes occur when a lightly damped structure is excited by a large band of frequencies, and broad band processes are intermediate situations between narrow band processes and white noise. Two typical examples of narrow and broad band random histories are illustrated with their

corresponding power spectra in Fig 2.3. It can be seen that in a narrow band random history, there are clearly defined cycles and a dominant frequency, which does not exist in broad band random signals. The property of these random processes is very well demonstrated in the following artificial situation (Ref 14). Suppose a narrow band spectrum has a uniform height G_0 (Fig 2.3b)

$$G = \begin{cases} G_0 & \omega_1 \leq \omega \leq \omega_2 \\ 0 & \omega < \omega_1 \text{ or } \omega > \omega_2 \end{cases} \tag{2.13}$$

The corresponding autocorrelation function is

$$R(\tau) = \frac{1}{2\pi} \int_0^\infty G(\omega) \cos\omega\tau \, d\omega$$

$$= \frac{2G_0}{\pi\tau} \cos\left(\frac{\omega_1+\omega_2}{2}\right)\tau \sin\left(\frac{\omega_2-\omega_1}{2}\right)\tau \tag{2.14}$$

For white noise, that is $\omega_1=0$, $\omega_2 \to \infty$

$$R(\tau) = \lim_{\omega_2\to\infty} G_0 \frac{\sin\omega_2\tau}{\pi\tau} \tag{2.15}$$

Following the argument in Ref 14, the autocorrelation function for white noise is finally expressed as

$$R(\tau) = \frac{1}{2} G_0 \delta(\tau) \tag{2.16}$$

where $\delta(\tau)$ is the Dirac's delta function (Ref 15), which is zero everywhere except at $\tau=0$ where it is infinite in a way such that

$$\int_{-\infty}^{+\infty} \delta(\tau) \, d\tau = 1 \tag{2.17}$$

It can be concluded that for a narrow band random process, there is a strong correlation when τ is close to times of half mean period $2\pi/(\omega_1+\omega_2)$, while generally the correlation decays as the time τ becomes large. But for white noise, there is no correlation (R=0) except at one point τ=0. The correlation functions for both situations are shown in Fig 2.4.

SECTION 4 The Distribution of Peaks and Cycle Counting

2.4.1 The Peak Distribution in Narrow Band Random Loading

The distributions of peaks, maxima, and level crossings are frequently of interest in engineering. It has been shown (Ref 12) that for a narrow band random process, if the p.d.f of the signal x(t) is Gaussian, the distribution of peaks S* is

$$p(S*) = \frac{S*}{\sigma^2} \exp\left(- \frac{S*^2}{2\,\sigma^2} \right) \qquad (2.18)$$

which is the well known Rayleigh distribution. Here σ is the r.m.s of x(t). The range S of a cycle can be assumed to be twice the magnitude of the peak. In a normalised form

$$\eta = \frac{S}{\sigma} \qquad (2.19)$$

the distribution of η is

$$p(n) = \frac{n}{4} \exp\left(- \frac{n^2}{8} \right) \qquad (2.20)$$

2.4.2 Cycle Counting

In broad band processes, however, cycles are not clearly defined. A number of cycle counting methods have been proposed to allow broad band loading to be related to narrow band or simple sinusoidal loadings in terms of fatigue damage (Ref 16-19). Among them, the rainflow method is popular (Ref 19).

The details of the rain flow method can be found in Ref 16. The broad band random signal is plotted such that the time axis is vertically downwards, and the lines connecting the stress peaks are imagined to be a series of pagoda roofs (Fig 2.5). Each rain flow begins successively at the inside of each stress peak and is allowed to drip down vertically to another roof. This procedure is continued until the flow stops when it comes opposite to a minimum more negative than that from which the flow starts. Similarly, if the flow initiates at a maximum, it stops when it comes opposite to a maximum more positive than the one at which it starts. For example, in Fig 2.5, a half cycle begins at peak 4 and stops opposite peak 8. A half cycle is thus counted between the starting point and the end point that the flow has covered. The over all rule is that every part of the stress time history is counted once and only once, thus a flow must stop when it meets the rain from a roof above. The final step is to produce a rather artificial random cyclic history from the half cycles counted.

2.4.3 Fatigue Cycles in Broad Band Loading

From the output of any cycle counting method applied to broad band random loading, the distribution of cycles can be constructed. If the cycles are defined in a simple manner such as by peak or range counting, analytical expressions for the distributions are available.

The peak counting method identifies cycles by taking every positive maxima (or maxima above the mean load) as the peak of a load cycle. Based on the distribution of maxima by S.O. Rice (Ref 11), the distribution of cycles has been shown to be (Ref 19 and 21)

$$p(n)= \frac{1}{\sqrt{(2\pi)}\ (1-C)} \left[\epsilon\ e^{\frac{-n^2}{8\epsilon^2}} + \sqrt{(1-\epsilon^2)}\ \frac{n}{2}\ e^{\frac{-n^2}{8}} \int_{-\infty}^{\frac{n\sqrt{(1-\epsilon^2)}}{2\epsilon}} e^{\frac{-x^2}{2}}\ dx\right] \qquad (2.21)$$

where C is the percentage of negative maxima and ϵ the power spectral width parameter. Both are defined in terms of moments of the power spectrum

$$r = \frac{1}{2}\ [\ 1 - \frac{m_2}{\sqrt{(m_0 m_4)}}\ ] \qquad (2.22)$$

$$\epsilon = [1 - (\frac{m_2^2}{m_0\ m_4})\ ]^{\frac{1}{2}} \qquad (0<\epsilon\leq 1) \qquad (2.23)$$

Generally, the nth moment is given as

$$m_n = \int_{-\infty}^{\infty} f^n G(f)\, df \qquad (2.24)$$

For the range counting method in which the range of a cycle is defined to be the rise from a minimum to the succesive maximum or the fall from a maximum to the following minimum, J.R. Rice (Ref 22) has shown that the average range is the mean of the absolute value of the differential dx(t)/dt, divided by the mean number of maxima j per unit time.

$$E[S] = \frac{E\left[\left|\frac{dx}{dt}\right|\right]}{j} \qquad (2.25)$$

which is

$$E[S] = -R_{(0)}^{(2)} \left[\frac{2\pi}{R_{(0)}^{(4)}}\right] \qquad (2.26)$$

Here $R^{(i)}$ is the ith differential of the autocorrelation function of the original random signal. An analytical procedure to calculate the distribution of ranges has also been given in J.R. Rice's work (Ref 22).

Apart from these analytic expressions, the distribution of ranges in broad band random loading can be measured experimentally from the output of cycle counting methods. Different cycle counting methods generally lead to different answers for a single random signal. Hancock and Gall (Ref 21) have conducted an investigation into the effect of cycle counting methods including peak, range and rainflow methods. They suggested that for the rainflow method, the distribution of ranges can be approximated by a Weibull function in which the range S is normalised by the r.m.s. of the stress signal

o.

$$P(n) = 1 - \exp\left[- \left(\frac{n}{\sqrt{2}\,\gamma}\right)^{\gamma} \right] \qquad (2.27)$$

For a given stress signal, γ is a parameter defined as

$$\gamma = 2 - \epsilon^2 \qquad (2.28)$$

Eq 2.28 reduces correctly to the Rayleigh distribution for narrow band random loading when the spectral band width parameter ϵ is zero. However, the authors found that this expression severely underestimates the number of small cycles when ϵ is large. A better equation for the distribution of cycles was proposed as

$$P(n) = C_1 + (1-C_1)\left[1 - \exp\left[-\left(\frac{n}{8}\right)^2\right]\right] \qquad (2.29)$$

where

$$C_1 = 1 - \left(1 - \epsilon^2 \right)^{\frac{1}{2}} \qquad (2.30)$$

LIST OF FIGURES FOR CHAPTER 2

Fig 2.5

The rainflow cycle counting method.

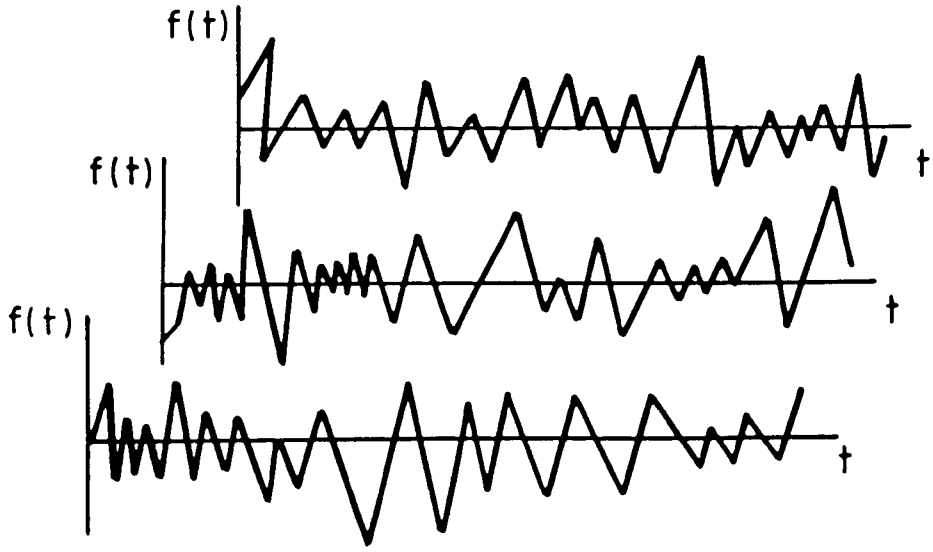

Fig 2.1

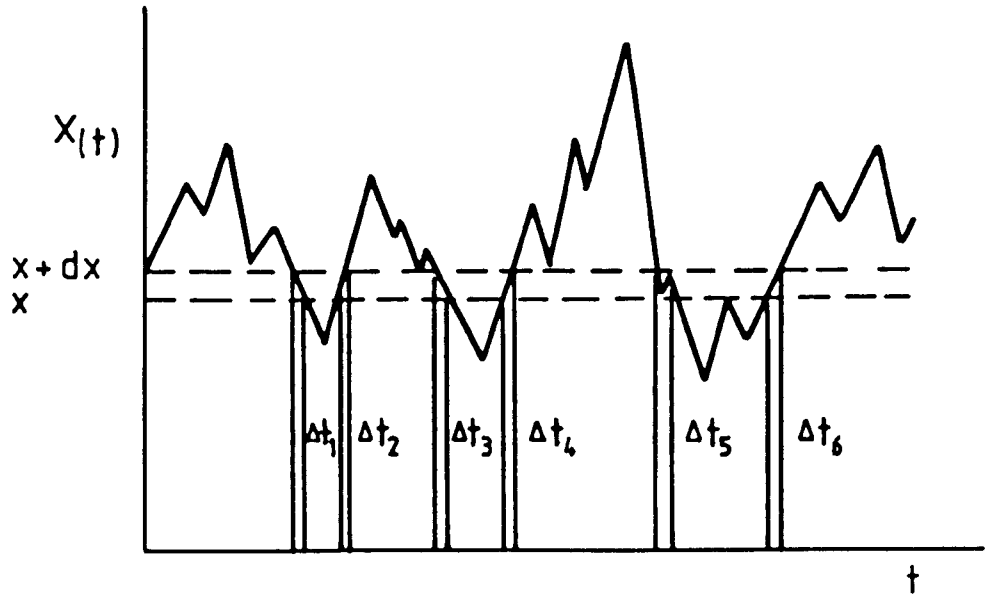

Fig 2.2

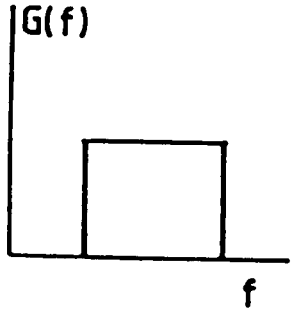

(a)

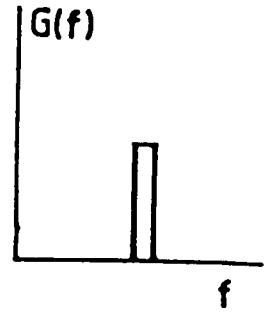

(b)

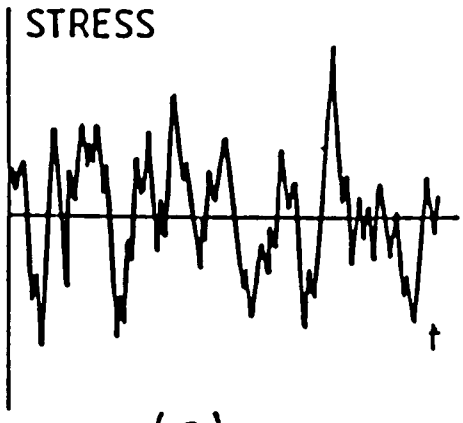

(c)

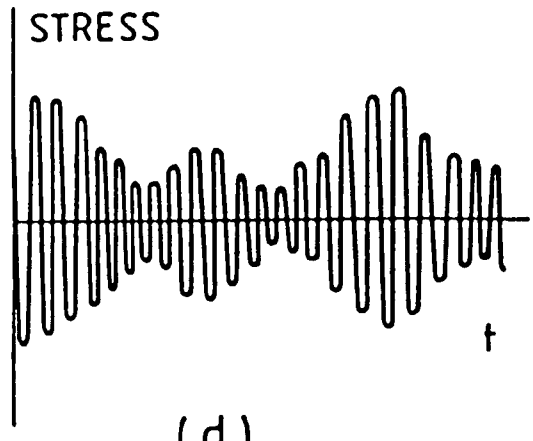

(d)

Fig 2.3

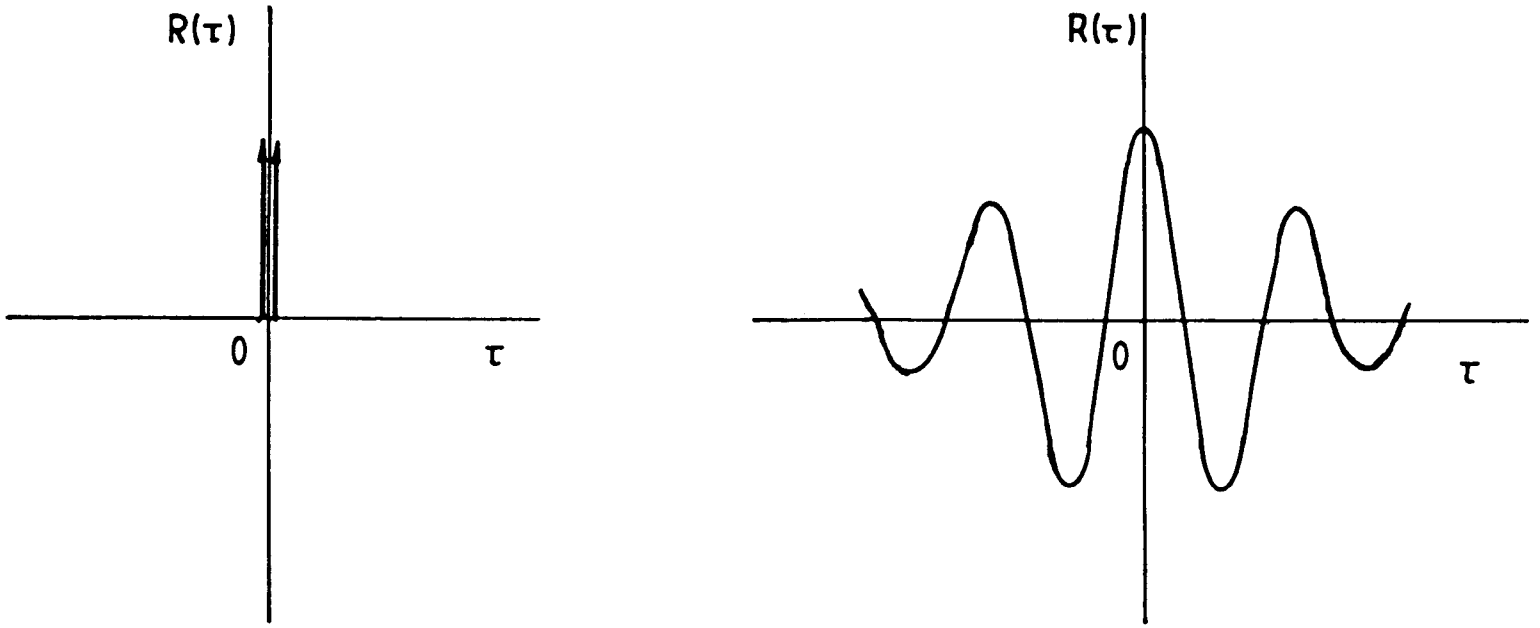

Fig 2.4

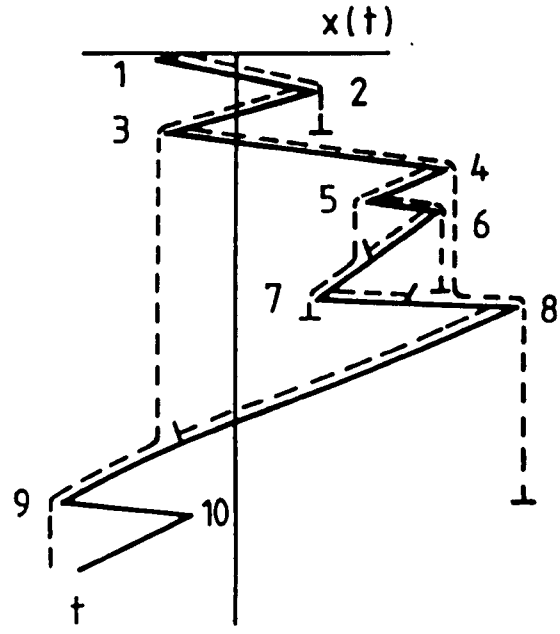

Fig 2.5

CHAPTER 3 THE CONVENTIONAL ASSESSMENT OF RANDOM FATIGUE

For over a hundred years, a major problem in the design and maintenance of engineering structures has been random fatigue which is difficult to analyse because of the complicated nature of the loading. Engineers have developed a conventional way of assessing the fatigue life under random loading using Miner's law in conjunction with S-N curves obtained from tests on small specimens under constant amplitude loading. The conventional method is still the basis of engineering design against fatigue today.

SECTION 1 Miner's Law

Despite the fact that random loading frequently occurs in practice, it is often more convenient to perform tests using constant amplitude loading. Fig 3.1 shows a typical example of constant amplitude loading, which has a zero mean and a superimposed sinusoidal stress. The Figure also indicates the notation which is to be used henceforth.

Under sinusoidal loading, small smooth specimens may be tested to determine the relation between the applied stress range S and the number of cycles to failure N, which often has the form shown

schematically in the S-N curve in Fig 3.2. For some materials, the life seems to approach infinity when S is less than a critical value known as the fatigue limit. In practice when N is greater than an arbitrarily chosen large number, the corresponding S is assumed to reach a limit under which fatigue failure will not occur.

Fatigue under sinusoidal loading is a simple situation to analyse, because the description of a loading involves only two parameters, namely the mean load and the amplitude. Under variable amplitude loading, the fatigue life is predicted by referring to that under constant amplitude loading. Palmgren (Ref 23) and later Miner (Ref 24) have suggested a relation which is now called the Palmgren-Miner law or simply the Miner's law.

The Palmgren-Miner law indicates that a component experiences an increment of damage D_i when a cycle of range S_i is applied

$$D_i = \frac{1}{N_i} \tag{3.1}$$

where N_i is the life of the component under a constant amplitude loading in which the stress range is S_i. As more cycles are applied, the damage accumulates linearly, for N cycles of different ranges

$$D = \sum_{i=1}^{N} D_i = \sum_{i=1}^{N} \frac{1}{N_i} \tag{3.2}$$

When the damage D reaches unity, failure is expected.

SECTION 2 The Application of Miner's Law

In current design codes, such as that of the A.W.S (Ref 25), and the D.n.V Rules for Offshore Construction (Ref 26), the S-N approach is used. Its main advantages are simplicity and the fact that no other proposed rules have been shown to be consistently better than it.

However, in comparison with the fracture mechanics approach, the shortcomings must be recognized. First of all, Miner's law has no physical basis, therefore, it is not possible to assess the residual strength by examining the state of the component. For the same reason, the original design life of a structure given by Miner's law can not be adjusted if the environment or the operation method have been changed during service. Secondly, there is no reason to believe that a cycle applied at different stages causes the same amount of damage. Thirdly, in Miner's law, no consideration has been given to overloads and sequential effects which can play a significant role in the fatigue process (Ref 27).

The Miner's law approach has been checked against results from experiments using random fatigue loading. Smith and Malme (Ref 28) and Hillberry (Ref 29) found that Miner's law over-estimated the fatigue life, while Barsom (Ref 30), Kowalewski (Ref 31) found it agreed with the experiment results for random loading. Swanson (Ref 32) has collected a large amount of experimental data and shown that some of the data agrees with Miner's law while the rest does not.

Probably, the characteristics of the random loading used in the experiments need to be considered more closely. It has been shown (Ref 33) that in the case of constant amplitude loading which includes occasional overloads, the fatigue life is affected strongly by the frequency of the overloads. The fatigue life is longer than the Miner's law prediction when the interval for occasional overload is more than 10^4 cycles, but shorter when the overload occurs every 100 cycles or more often. The usual explanation is based on the residual stress field. If the overload is tensile, the residual stress produced by it in the maximum stress areas, where the most serious fatigue damage takes place, is in inverse sense to the stress of the following load peaks. A relatively detailed explanation is considered in Section 5.3 from the fracture mechanics point of view.

Apart from the objections already mentioned, there are other difficulties with the application of the Miner's law approach, for instance, the definition of life N. This is somewhat arbitrary and may be taken as either fracture or loss of stiffness. The correlation of the S-N curve obtained from small smooth specimen with the real structure is also a major practical problem (Ref 34).

SECTION 3 Developments

3.3.1 Considering the Effect of the Mean Load and Overloads

Awareness of the shortcomings of the S-N curve approach has led to

attempts to produce a better correlation between cyclic loading and the fatigue life. S-N data can be amended in many ways to accommodate parameters, such as the mean stress which is often represented by the stress ratio r

$$r = \frac{S_{min}}{S_{max}} \tag{3.3}$$

where S_{min} and S_{max} are the minimum and maximum respectively in a stress cycle. One of the proposed formulae for assessing the mean stress effect is the "modified Goodman equation" (Ref 35) in which the range S for a given fatigue life is adjusted by

$$\frac{S}{S_1} + \frac{S_m}{S_o} = 1 \tag{3.4}$$

Here S_1 is the fatigue strength for the given fatigue life when the cycles are fully reversed (S_m=0, r=-1) and S_o is the yield stress of the material. This equation is necessarily true at these two points. When the range is zero, it reduces to

$$S_m = S_o \tag{3.5}$$

which is the monotonic failure condition; when S_m=0,

$$S = S_1 \tag{3.6}$$

which is the definition of S_1

As an example of a modifications to the Miner's law approach to include the influence of overloads, the Corten-Dolan theory (Ref 36) may be considered. If S_a denotes the stress amplitude, this theory

takes the form

$$N = \frac{N_1}{\sum_{i=1}^{k} c_i \left(\frac{S_{ai}}{S_{a1}}\right)^d} \qquad (3.7)$$

Here, N is the total number of cycles to failure, c_i the percentage of cycles at S_{ai} which is one of the k stress amplitude levels, correspondingly, N_1 is the fatigue life at stress S_{a1} which is the biggest amplitude which ever appears in the whole life, d is a material constant. The formula reduces to Miner's law if the S-N curve can be expressed as

$$N S^d = 1 \qquad (3.8)$$

3.3.2 Using Statistical Representation of Random Loading

Based on the assumption that the S-N curve has the form

$$N S^d = C \qquad (3.9)$$

where C is a material constant, Wirshing and Light (Ref 37) have described a model which aims at predicting fatigue life under either narrow or broad band loading. No cyclic interaction was considered and the damage by N cycles was given by

$$D = N \frac{E[S^d]}{C} \qquad (3.10)$$

$E[S^d]$ is the average of S to the power of d. For a narrow band loading, the distribution of stress peaks is a Rayleigh distribution and the normalised stress range S/σ is given by Eq 2.20, the mean of

S^d can be evaluated as

$$E[S^d] = \int_0^\infty S^d \, p(S) \, dS$$

$$= (2\sqrt{2}\,\sigma)^d \, \Gamma\left(\frac{d}{2} + 1\right) \qquad (3.11)$$

$\Gamma(\ )$ is the Gamma function tabulated in many texts, for instance, in Ref 8. Let the dominant frequency be f_o, the damage during a period T is D_{nb}

$$D_{nb} = \frac{f_o T}{C} (2\sqrt{2}\,\sigma)^d \, \Gamma\left(\frac{d}{2}+1\right) \qquad (3.12)$$

A correction number C_C was introduced while estimating damage by broad band loading D_{bb}

$$D_{bb} = C_C \, D_{nb} \qquad (3.13)$$

where D_{nb} is determined by Eq 3.10 in which the stress ranges are identified by performing cycle counting on the broad band loading. The rain flow counting method was used. C_C was found to be a function of d and the spectral width parameter ϵ. For the best curve fitting to the experimental results, an empirical relation was given

$$C_C = C_1 + (1-C_1)\,(1-\epsilon)^{C_2} \qquad (3.14)$$

where

$$\left.\begin{aligned} C_1 &= 0.926 - 0.033d \\ C_2 &= 1.587\,d - 2.323 \end{aligned}\right\} \qquad (3.15)$$

3.3.3 Accounting for the Variance in Fatigue Life

The theories described so far have tended to regard fatigue life as a deterministic value. In fact, fatigue life exihibits variability. In light of this, Shin and Lukens (Ref 38) and Shin (Ref 39) have treated the cumulative damage D, called fatigue damage index in their paper, as a random variable. A critical damage value Δ was introduced as a random variable incurred from property differences of specimens and environmental factors. For convenience in presenting their results, another value Z was introduced which is defined as

$$\ln Z = \ln\Delta - \ln D \tag{3.16}$$

lnD and lnΔ are assumed to follow normal distributions thus lnZ also has a normal distribution. Failure was defined to occur when the damage index exceeded the critical damage value Δ, thus the probability of failure is

$$P_f = Pr[D \geq \Delta] = Pr[\ln Z < 0]$$

$$= \int_{-\infty}^{0} \frac{1}{\sqrt{(2\pi)}\ \sigma_{\ln Z}} e^{-\frac{(\ln Z - E[\ln Z])^2}{2\ \sigma_{\ln Z}^2}} d(\ln Z) \tag{3.17}$$

E[lnZ] and $\sigma_{\ln Z}$ are respectively the mean and r.m.s of the distribution of lnZ, which have been expressed in terms of the distribution parameters of D and Δ. The final form for the failure probability was

$$P_f = \Phi\left[- \frac{\ln\left[\frac{E[\Delta]}{E[D]}\right] + \ln\sqrt{\left[1+\frac{\sigma_D}{E^2[D]}\right]} - \ln\sqrt{\left[1+\frac{\sigma_\Delta}{E^2[\Delta]}\right]}}{\ln^{1/2}\left[\left[1+\frac{\sigma_D^2}{E^2[D]}\right]\left[1+\frac{\sigma_\Delta^2}{E^2[D]}\right]\right]} \right] \qquad (3.18)$$

where σ_D and σ_Δ are the root mean square of D and Δ respectively. The function $\Phi(\ )$ is the cumulative function of a standard normal distribution which is a normal distribution with zero mean and unit root mean square.

LIST OF FIGURES FOR CHAPTER 3

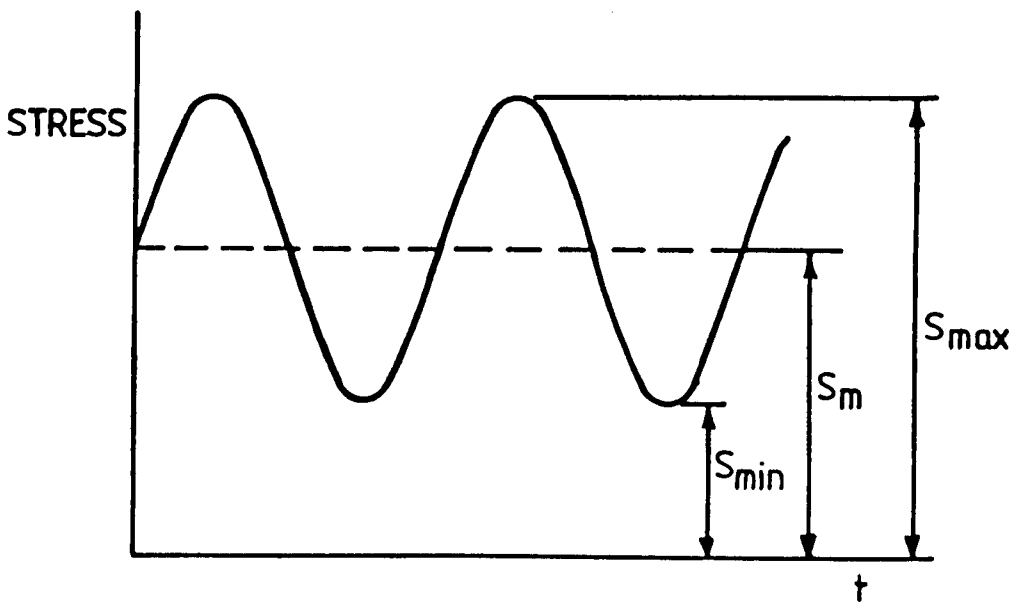

$$r = \frac{S_{min.}}{S_{max.}}$$

$$S_m = \frac{S_{min} + S_{max.}}{2}$$

Fig 3.1

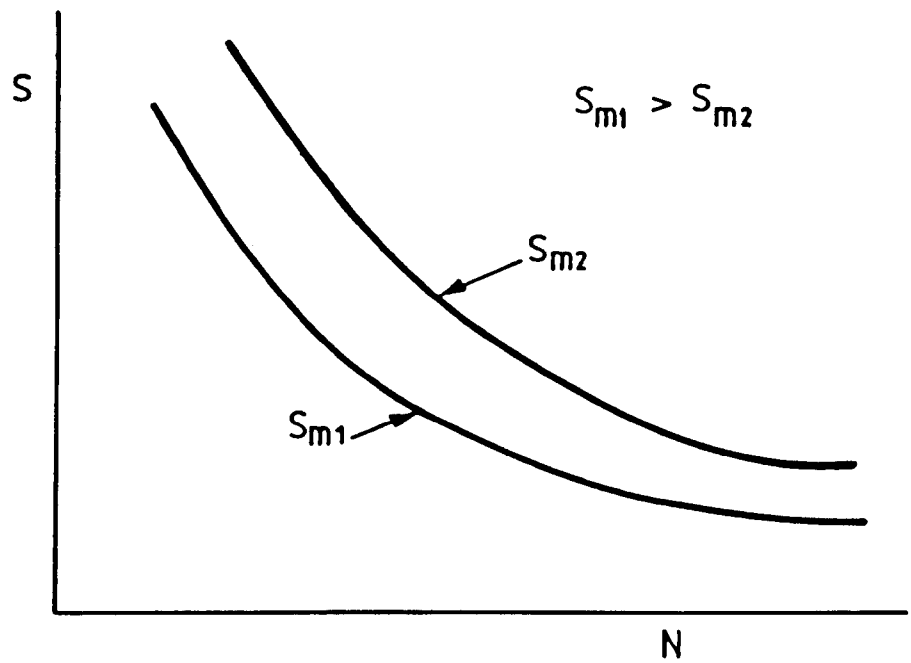

Fig 3.2

CHAPTER 4 FRACTURE MECHANICS

Structural failure can be due to massive plastic deformation or plastic collapse which is controlled by the yield stress of the material. However, failure can also occur at loads much lower than the limit load owing to the cracks in the structure. In many engineering situations, cracks can appear as a result of fatigue. Even the manufacturing process can introduce cracks or crack-like defects. It is thus important to be able to predict the behavour of cracks and defects to maintain the integrity of the structure, and this is the principle purpose of fracture mechanics.

SECTION 1 Cracks in Linear Elastic Materials

A crack can be subjected to three basic forms of loading, namely the opening mode or mode *I*, sliding mode or mode *II*, and the anti-plane mode or mode *III* (Fig 4.1). Among the three, the opening mode is most common, and is often the dominant mode in combined modes of loading.

Westergaard (Ref 40) has studied the stress field of an infinite plate of a linear elastic material containing a central crack under

remote tensile loading (Fig 4.2). The method of solution is to construct a stress function which satisfies the appropriate boundary conditions. Following the notation shown in Fig 4.2, the stress field around the crack tip was found to be

$$S_x = \frac{S_\infty \sqrt{a}}{\sqrt{(2r)}} \cos\frac{\theta}{2}\left[1 - \sin\frac{\theta}{2}\sin\frac{3\theta}{2}\right]$$

$$S_y = \frac{S_\infty \sqrt{a}}{\sqrt{(2r)}} \cos\frac{\theta}{2}\left[1 + \sin\frac{\theta}{2}\sin\frac{3\theta}{2}\right] \qquad (r \ll a) \qquad (4.1)$$

$$\tau_{xy} = \frac{S_\infty \sqrt{a}}{\sqrt{(2r)}} \cos\frac{\theta}{2}\sin\frac{\theta}{2}\cos\frac{3\theta}{2}$$

S_∞ is the remote stress. The restriction for plane stress or plane strain applies, i.e.

$$S_z = \tau_{xy} = \tau_{yz} = 0 \qquad (4.2)$$

for plane stress and

$$S_z = \nu\,(S_x + S_y) \qquad (4.3)$$

$$\tau_{xy} = \tau_{yz} = 0 \qquad (4.4)$$

for plane strain. A stress singularity exists at r=0. In fact, whatever the geometry and loading, the stress at a crack tip has a singularity of the order $1/\sqrt{r}$ as r approaches zero. Therefore, the limit

$$K_I = \lim_{r \to 0^+} \sqrt{(2\pi r)}\; S_y(r,0) \qquad (4.5)$$

has a finite value which is called the stress intensity factor. K_I

so defined describes the stress field near crack tip for different geometries and loadings. For the infinite plate in Fig 4.2

$$K_I = S_\infty \sqrt{(\pi a)} \tag{4.6}$$

It has been pointed out (Ref 41) that there is a mistake in the Westergaard calculation, but this mistake does not affect the solution of the stress intensity factor or the strength of the stress singularity. Generally, for any case in which the loading is represented by a stress S_n, the stress intensity factor can be expressed as

$$K_I = f(\frac{a}{W})\ S_n \sqrt{(\pi a)} \tag{4.7}$$

where $f(a/W)$ is a general form of a dimensionless function of the geometry. Expressions of $f(a/W)$ for many cases have been collected in Refs 42 and 43. For the popular three point bend specimen (Fig 4.3) often used in fatigue tests, K_I can be presented as (Ref 44)

$$K_I = \frac{F\ L}{B\ W^{\frac{3}{2}}} \left[2.9(\frac{a}{W})^{\frac{1}{2}} - 4.6(\frac{a}{W})^{\frac{3}{2}} \right.$$

$$\left. + 21.8(\frac{a}{W})^{\frac{5}{2}} - 37.6(\frac{a}{W})^{\frac{7}{2}} + 38.7(\frac{a}{W})^{\frac{9}{2}} \right] \tag{4.8}$$

where F is the applied load, B, L and W are dimensions of the specimen given in Fig 4.3. In a similar manner, the stress intensity factors for cracks under sliding mode loading or anti-plane mode loading have been defined using the $r^{-1/2}$ singularity of the stress

field at the crack tip. The stress intensity factors for the three modes are known as K_I, K_{II} and K_{III}. They have an energy significance which arises from an original concept due to Griffiths (Ref 45). The basic argument is that as the crack extends in a brittle material such as glass, elastic energy in the material is released to create the new crack area which absorbs energy. For metals, it has been noted (Ref 46) that a large part of the energy released is consumed to form a new plastic zone ahead of the crack as it propagates. Nevertheless, crack extension takes place only when the energy release rate is greater or equal to the energy consumption rate. If the elastic energy be U_e and its release rate G

$$G = \frac{\partial U_e}{\partial a} \tag{4.9}$$

the energy release rate G is related to the stress intensity factors for plane strain by the equation

$$G = \frac{(1-\nu^2)K_I^2}{E} + \frac{(1-\nu^2)K_{II}^2}{E} + \frac{(1+\nu)K_{III}^2}{E} \tag{4.10}$$

SECTION 2 K_{Ic} and the Validity of Linear Elastic Fracture Mechanics

The stress intensity factor provides a quantitative measurement of the effect of the crack through its ability to characterise the crack tip stress field. However, the whole argument is based on the assumption of a linear elastic material, which is not possible in

practice since the stresses S_x and S_y close to the crack tip can not go to infinity as Eq 4.1 indicates. There must be a area ahead of the crack tip where plastic deformation occurs as depicted in Fig 4.4. If the material yield stress is denoted S_o, the radius of the plastic zone R_o along x axis can be estimated in a concise procedure (Ref 47). The stress S_y evaluated from Eq 4.1 is approximated as

$$S_y(r,0) = \frac{K_I}{\sqrt{(2\pi r)}} \qquad (r \ll a,\ \theta=0) \qquad (4.11)$$

A first estimation of the plastic zone in plane stress can be taken as the area in which the stress given by Eq 4.11 is more than or equal to the yield stress S_o. Since Eq 4.11 represents a situation in which the equilibrium between the external loading and the the internal stresses is maintained and the part of $S_y(r,0)$ which is more than S_o does not appear in the material, the corresponding part of the loading has to be carried by other areas. The effect of this is to spread the plastic area. If the stress distribution profile in the range $S_y(r,0) \angle S_o$ is simply shifted away from the crack tip to give space for the plastic zone, the radius of the plastic zone R_o along the crack line is easily determined to be

$$R_o = \frac{1}{\pi} \left(\frac{K_I}{S_o}\right)^2 \qquad (4.12)$$

for plane stress. For plane strain, the plastic zone is smaller because of the constraint in the third direction. Usually it is taken as one third of that in plane stress (Ref 48)

$$R_o = \frac{1}{3\pi} \left(\frac{K_I}{S_y}\right)^2 \qquad (4.13)$$

Since the size of the plastic zone indicates the amount of energy consumed by plastic deformation, it is not surprising that the critical stress intensity factor K_C at fracture is lower in plane strain than in plane stress. The limiting value of the stress intensity factor for thick plates for which perfect plane strain condition applies, is a material constant known as the material toughness (Ref 49) and usually denoted as K_{IC}. For a valid K_{IC} test, there are quantative requirements (Ref 50) concerning the specimen dimensions to ensure that small scale yielding and plane strain prevails. These requirements are usually defined as (Ref 50)

$$B,\ a,\ (W-a) \geq 2.5\left(\frac{K_I}{S_o}\right)^2 \qquad (4.14)$$

where B, W, are the specimen dimensions. For a bend specimen, the notation for B, W and a are shown in Fig 4.3. As long as the plastic zone at the crack tip is small in respect to the dimensions of the body, the deformation is dominated by the surrounding elastic field. For such small scale yielding situation, linear elastic fracture mechanics is applicable. However, K_{IC} may be affected by mode *II* or mode *III* cracking when there is a deviant angle of the crack in the specimen as indicated by Pook (Ref 51)

SECTION 3 Methods for Determining Stress Intensity Factors

There are so many ways for assessing the stress intensity factors that they can not be exhaustively mentioned here. However, some of the methods are briefly described and the emphasis is placed on those methods which are suitable to be applied to surface cracks in tubular joints. Additional relevant information can be found in a

paper by Cartwright and Rooke (Ref 52).

4.3.1 Experimental Methods

An obvious experimental approach to stress intensity factors is to measure the stress or strain close to the tip of a crack. The photoelastic technique is a popular method among those using this approach (Ref 53).

An alternative is to measure the stress intensity factor indirectly by making use of the relation between the compliance c and the stress intensity factor (Ref 54)

$$K_I^2 = EG = \frac{E F^2}{2 B} \left(\frac{\partial c}{\partial a}\right) \qquad (4.15)$$

where B is the thickness of the plate containing a crack of length a. The compliance for several crack lengths needs to be measured so that $\partial c/\partial a$ can be evaluated.

James and Anderson (Ref 55) have proposed a method for determining the stress intensity factor by using the relation between the stress intensity factor and the measurable crack growth. This method is theoretically simple and can be applied to any three dimensional crack problems when crack growth measurements are possible. However, it is generally regarded as unreliable (Ref 52) due to the complicated physical process occuring in fatigue.

4.3.2 Analytic Methods

Analytic methods are most successful in two dimensional problems for which the Airy function Ψ can be used. The stresses can be given by

$$\sigma_{xx} = \frac{\partial^2 \Psi}{\partial y^2} \qquad \sigma_{yy} = \frac{\partial^2 \Psi}{\partial x^2} \qquad \tau_{xy} = \frac{\partial^2 \Psi}{\partial x \partial y} \tag{4.16}$$

which satisfy the compatability and equilibrium requirements automatically since the Airy function is a double harmonic function

$$\nabla^2 \nabla^2 \Psi = 0 \tag{4.17}$$

The exact form of the Airy function for a particular problem is determined by applying the boundary conditions. A general form of Airy function for opening mode crack configurations has been proposed by Westergaard (Ref 40) in terms of a complex function

$$\Psi = \mathrm{Re}Z^{**} + y\ \mathrm{Im}Z^{*} \tag{4.18}$$

Here Z is a complex analytic function of the complex variable $z=x+iy$, and

$$\frac{dZ^{**}}{dz} = Z^{*} \tag{4.19}$$

$$\frac{dZ^{*}}{dz} = Z(z) \tag{4.20}$$

Several two dimensional crack problems have been studied using this form of Airy function. The simplest case is that of a crack in an infinite plate subjected to uniform biaxial tension S_∞ (Fig 4.2) for which the function was given as

$$Z = \frac{S_\infty z}{\sqrt{(z^2 - a^2)}} \qquad (4.21)$$

The stress intensity factor can be evaluated from the calculated stress field according to the definition (Eq 4.5). This approach has been applied to other problems (Ref 56 and 57)

4.3.3 Direct Finite Element Methods

The finite element method is a powerful technique in determining stresses (see Section 3, Chapter 7). A simple and direct approach for assessing stress intensity factors is to evaluate the stress distribution near the tip of a crack using the finite element method. For the opening mode of a plane crack, the stress intensity factor is related to the stress by the asymptotic solution

$$S_{ij} = \frac{K_I}{\sqrt{(2\pi r)}} f_{ij}(\theta) \qquad (4.22)$$

where f_{ij} is a function of θ. The evaluation of the stress intensity factor can be carried out by substituting the stress and r, θ and f_{ij} for any point near the crack tip. It has been shown that this procedure is not accurate when the elements around the crack tip are not very small (Ref 58).

4.3.4 Elastic Line Spring Method

If a direct finite element method is used for evaluating the stress intensity factor of surface cracks, a three-dimensional analysis is necessary because of the variation of the crack depth and the

different stress distributions along the crack length. In theory, the finite element method makes it possible to calculate stresses and fracture mechanics parameters for any combination of conceivable geometries, cracks and loadings, but there are practical limitations due to such factors as the computing power and the financial sources available and efficiency is an important factor to be considered.

An very efficient method is the line spring concept initiated by Rice and Levy (Ref 59) in 1972. Fig 4.5 is presented to illustrate the line spring concept for mode *I* stress intensity factor calculations. Let the thickness of the plate be T and the depth of the surface crack vary with the x coordinate, a=a(x). The cracked section of the shell is modeled by a series of line springs (Fig 4.5c). The response of the line springs to the local loads F(x) and M(x) can be represented by

$$\begin{bmatrix} \delta(x) \\ \theta(x) \end{bmatrix} = \begin{bmatrix} C_{11}(x) & C_{12}(x) \\ C_{21}(x) & C_{22}(x) \end{bmatrix} \begin{bmatrix} F(x) \\ M(x) \end{bmatrix} \tag{4.23}$$

where [C] is the compliance matrix whose elements can be determined by reference to a simple plane strain strip having a crack of identical depth of the surface crack at the point concerned. $\delta(x)$ and $\theta(x)$ are taken as the additional displacements of one end of the strip to the other due to the presence of the crack. For convenience, the above equation can be written as

$$\begin{bmatrix} \delta \\ \theta \end{bmatrix} = \begin{bmatrix} C_{11} & C_{12} \\ C_{21} & C_{22} \end{bmatrix} \begin{bmatrix} F \\ M \end{bmatrix} \tag{4.24}$$

The local loads and moments are now determined by shell analysis. Rice and Levy also assumed that the stress intensity factor at a

point in the cracked section is the same as in the reference strip containing a crack of equal depth. In this case

$$K_I = [\ C_1\ F(x) + C_2\ M(x)\ ] \tag{4.25}$$

where C_1 and C_2 can be determined from the known value of stress intensity factor, such as that given by Gross and Srawley's results (Ref 60).

In order to determine the matrix [C], consideration has been given to the energy balance, from Eq 4.9

$$G = \frac{1}{2}\ [\ F\ \frac{\partial \delta}{\partial a} + M\ \frac{\partial \theta}{\partial a}\ ] \tag{4.26}$$

so,

$$G = \frac{1}{2}\ [\ F^2\ \frac{dC_{11}}{da} + 2M\ F\ \frac{dC_{12}}{da} + M^2\ \frac{dC_{22}}{da}\ ] \tag{4.27}$$

Also from Eq 4.10 and 4.25

$$G = \frac{1 - \nu^2}{E}\ K_I^2$$

$$= T\ [C_1^2\ F\ + 2C_1C_2\ F\ M + C_2^2\ M\ ] \tag{4.28}$$

Comparison of Eqs 4.27 and 4.28 gives the following result

$$\left.\begin{aligned} C_{11} &= 2T \int_0^a C_1^{\,2}\ da \\ C_{12} &= C_{12} = T \int_0^a C_1\ C_2\ da \\ C_{22} &= 2T \int_0^a C_2^{\,2}\ da \end{aligned}\right\} \tag{4.29}$$

The line spring method has been utilized (Ref 61) to assess the opening mode stress intensity factors for semi-elliptic cracks in a plate. In comparison with a three dimensional finite element solution (Ref 62), it was found that the method is accurate (difference less than 3%) in the central part of the semi-elliptical cracks, while not surprisingly, inaccurate in the two end regions where the crack front is almost normal to the plate and the line spring concept has a poor physical basis.

This line spring mode has been expanded to account for mode *II* and mode *III* cracking by Desvaux (Ref 63). Using similar assumptions, after introducing shear loads and one more moment (Fig 4.6) which may occur in shells, the constitutive relation for the reference strip is as follows

$$\begin{bmatrix} \delta_z \\ \theta_x \\ \delta_y \\ \delta_x \\ \theta_z \end{bmatrix} = \begin{bmatrix} C_{11} & C_{12} & C_{13} & C_{14} & C_{15} \\ C_{21} & C_{22} & C_{23} & C_{24} & C_{25} \\ C_{31} & C_{32} & C_{33} & C_{34} & C_{35} \\ C_{41} & C_{42} & C_{43} & C_{44} & C_{45} \\ C_{51} & C_{52} & C_{53} & C_{54} & C_{55} \end{bmatrix} \begin{bmatrix} F_z \\ M_x \\ F_y \\ F_x \\ M_z \end{bmatrix} \qquad (4.30)$$

The notation for this is shown in Fig 4.5, δ_y and θ_x are seen the equivalents of δ and θ in Rice and Levy's model. Since the loads contribute to individual modes of cracking, a number of the coefficients in the compliance matrix are zero. By considering the K_I, K_{II} and K_{III} modes separately, the remaining coefficients were evaluated and the subsequent calculation of K_{II} and K_{III} was performed in the same manner of Rice and Levy.

4.3.5 Virtual Crack Extension Method

The virtual crack extension method is a finite element technique developed by Parks (Ref 64 and 65). The stress intensity factor is determined from the J-integral (see Section 5) which is equal to G, the potential energy release rate of the solid containing the crack in linear elastic cases. For plane strain

$$\frac{(1-\nu^2)\ K^2}{E} = J = G = -\frac{\partial U_p}{\partial a} \qquad (4.31)$$

The potential energy can be expressed in terms of the global stiffness matrix [M], the nodal forces {F} and movements {V} (Ref 66)

$$U_p = \frac{1}{2} \{V\}^T [M] \{V\} - \{V\}^T \{F\} \qquad (4.32)$$

where the superscript T indicates "transpose". The global stiffness matrix [M] and the nodal forces {f} are related to the coordinates (see Section 3, Chapter 7). Let the nodes surrounding the crack tip be arranged in two contours Γ_1 and Γ_2 and the x coordinate be in the direction of the crack as shown in Fig 4.7a. The virtual crack extension can be modelled by moving the nodes at the crack tip and at the first contour Γ_1 in x direction a small distance δa such that the elements between the two contours maintain a proper shape (Fig 4.7b). This causes a change in potential energy δU_p which divided by the crack extension δa gives the energy release rate

$$G = -\frac{\partial U_p}{\partial a}$$

$$= \frac{-\delta\{V\}^T}{\delta a}\left[[M]\{V\}-\{F\}\right] - \frac{1}{2}\{V\}^T\frac{\delta[M]}{\delta a}\{V\}+\{V\}^T\frac{\delta[F]}{\delta a} \qquad (4.33)$$

The equation can be reduced since the terms in the first pair of brackets is zero (see Eq 7.4)

$$G = -\frac{1}{2}\{V\}^T\frac{\delta[M]}{\delta a}\{V\} + \{V\}^T\frac{\delta[F]}{\delta a} \qquad (4.34)$$

If there is no load applied to the crack surface, the second term in Eq 4.34 is zero

$$\frac{\delta\{F\}}{\delta a} = 0 \qquad (4.35)$$

The first term can be evaluated by

$$\frac{\delta[M]}{\delta a} = \frac{1}{\delta a}\left\{[M]_{a+\delta a} - [M]_a\right\} \qquad (4.36)$$

where the subscripts a and a+δa represents the state before and after crack extension. The global stiffness matrix is dependent on the individual element geometries, displacement functions and material properties, which are unchanged after the crack extension, except in the group of elements between the two contours. Let the element group be numbered from 1 to k, the potential energy release rate, and therefore the stress intensity factor can be determined by

$$\frac{(1-\nu^2)\,K^2}{E} = G = -\frac{1}{2\,\delta a}\{V\}^{T*}\sum_{i=1}^{k}\left\{[mi]_{a+\delta a} - [mi]_a\right\} \qquad (4.37)$$

where $[m_i]$ represents the element stiffness matrix. $\{V\}^{T*}$ contains the corresponding nodal displacements. The biggest advantage of this

technique is that it avoids solving the global stiffness matrix twice for the potential energy before and after crack extension. Application of the virtual crack extension method to three dimensional problems has been suggested (Ref 64). The change in potential energy due to a virtual crack extension at a single crack front node can be used to evaluate the potential energy release rate for a virtual crack extension of the whole crack. The method is also applicable to elastic-plastic problems (Ref 65).

4.3.6 Weight Function Method

The weight function method is a popular technique in determining the stress intensity factor (Ref 67). As illustrated in Fig 4.8, the stress intensity factor at the crack tip x=a due to a pair of point forces F_Q opening the crack is given as

$$K_I = F_Q \, w \tag{4.38}$$

where w is known as the weight function which depends on the geometry and the relative position of the force and crack tip. This can be used to evaluate the opening mode stress intensity factor of a crack. If in the absence of the crack, the stress along the crack line is $-\sigma_z(x,0)$, the stress intensity factor under this external loading is identical to the situation when only $\sigma_z(x, 0)$ is applied to the crack faces. The distribution of $\sigma_z(x,0)$ can be regarded as an infinite series of point loadings $\sigma_z(x,0)dx$ and the stress intensity factor is given by an integrating these loads over the crack surface. For a crack of length 2a

$$K_I = \int_{-a}^{a} w(x)\ \sigma_z(x, 0)dx \qquad (4.39)$$

The weight function method has been applied to irregularly shaped cracks embedded in an infinite solid (Ref 68) subjected to an arbitrary normal stress field. For this case, it is necessary to specify the point Q' (Fig 4.9) on the crack front where the stress intensity factor is calculated.

$$K_{Q'} = \iint_A w(x, y)\ \sigma_z(x, y)dA \qquad (4.40)$$

where both the weight function w and the internal stress σ_z are two dimensional variables. The problem is to find the generalised weight function. After considering the weight functions for three particular cases, i.e. for a circular crack and a semi-infinite straight crack front in an infinite solid (Ref 43), and for a circular ligament in an infinite cracked solid (Ref 69), Oore and Burns (Ref 68) have suggested a general form of weight function

$$w_{QQ'} = \frac{\sqrt{2}}{\pi} \frac{1}{l_{QQ'} \left[\int_\Gamma \frac{ds}{\rho^2} \right]^{1/2}} \qquad (4.41)$$

for the contribution to the stress intensity factor at Q' from a point load applied at Q. $l_{QQ'}$ is the distance between Q and Q', ρ is measured from Q to a point on the crack front Γ where an element of Γ is taken as ds. There is no rigorous proof of this weight function, but calculations for several cases using this weight function gave results which show agreement with existing solutions.

For surface cracks, the stress distribution near the crack front is

different from the situation of an embedded crack discussed above. It was assumed that the stress intensity factor for a surface crack can be obtained from that of an embedded crack using a simple correction factor C_C. The solid containing the reference embedded crack has mirror symmetry with respect to the crack shape and loading such that a half of the solid is identical to the surface cracked solid. Furthermore, the correction factor C_C was supposed to be

$$C_C = \frac{\text{Stress intensity factor at a point on the front of the surface crack}}{\text{Stress intensity factor at a corresponding point of the embedded crack}}$$

$$= \text{function depending on geometry but not on loading} \qquad (4.42)$$

The assumption enables the stress intensity factor for surface cracks to be evaluated (Ref 70). The discrepancy due to this can be as high as 14%.

4.3.7 Other Methods

Parellel to the compliance experimental method (Section 4.3.1), there is a finite element method which determines the stress intensity factor from the compliance of the cracked plate (Ref 71). Based on the relation expressed by Eq 4.15, accurate solutions can be produced from rather coarse mesh, while in the direct finite element method, a very fine mesh is required in the crack tip area.

It is possible to improve the efficiency of the finite element method by making use of special crack tip elements (Refs 72 and 73). One of the techniques is to arrange second order isoparametric elements to diverge from the crack tip and along the divergent boundaries of the elements, the side nodes are located at positions such that the distance from the side node to the corner node nearer to the crack tip is one third of that to the other side node further from the crack tip. This arrangement allows the displacement in the crack tip elements to have the correct asymptotic form. The use of such elements reduces the number of elements required for a given level of accuracy.

There are other methods available such as the boundary collocation method. In this method the stress function is represented by a series which satisfies the boundary condition for the crack surfaces. There are unknown parameters in the series which are determined by matching the stress function to any remaining boundary conditions (Refs 74 and 75). It is also proposed that stress intensity factors can be determined from stress concentration factors of notches by considering a crack as a notch whose curvature at the tip approaches zero (Ref 76).

SECTION 4 The Stress Intensity Factors of Elliptic Cracks in Plates

The surface crack is the most common type of crack found in

engineering structures, the shape of such cracks is usually idealised as semi-ellipses. This kind of crack has been studied extensively due to the importance of the problem, as has the problems of embedded elliptical cracks.

4.4.1 An elliptical crack in an infinite plate

Irwin (Ref 77) considered a flat elliptic crack embedded in a solid of infinite dimensions under a remote uniformly distributed stress S_∞ (Fig 4.10a). He derived an expression for the stress intensity factor around the perimeter of the ellipse from the stress and displacement field reported previously (Ref 78)

$$K_I = \frac{S_\infty \sqrt{(\pi a)}}{In[k]} \left(\sin^2\theta + \frac{a^2}{c^2}\cos^2\theta\right)^{\frac{1}{4}} \qquad (4.43)$$

θ, a, c are as specified in Fig 4.10a. In[k] is the elliptic integral of the second kind.

$$In[k] = \int_0^{\pi/2} \left(1 - \frac{c^2-a^2}{c^2}\sin^2\theta\right)^{\frac{1}{2}} d\theta \qquad (4.44)$$

4.4.2 A Semi-elliptic Crack in a Semi-infinite Plate

If a cut is made along the major axis of the ellipse in Fig 4.10a the crack intersects the surface as shown in Fig 4.10b. Suppose the remote loading remains as the uniform tensile stress S_∞, corrections must be made to the K_I evaluation of Eq 4.43 corresponding to the geometrical change. This can be achieved for the deepest point ($\theta=\pi/2$) and the surface intersection point ($\theta=0$) by introducing a

the front face correction factor C_f

$$K_I(\theta=\frac{\pi}{2}) = \frac{S_\infty}{In[k]} \sqrt{(\pi a)}\ C_f(\theta=\frac{\pi}{2}) \qquad (4.45)$$

$$K_I(\theta=\frac{\pi}{2}) = \frac{S_\infty}{In[k]} \sqrt{(\pi a)}\ C_f(\theta=0) \qquad (4.46)$$

Adopting the result of Hartranft and Sih (Ref 79) which is the preferred solution recommended by Scott and Thrope (Ref 80), C_f is given by

$$C_f[\theta=\frac{\pi}{2}] = 1 + 0.12(1 - \frac{a}{2c})^2 \qquad (4.47)$$

$$C_f[\theta=0] = [1.21 -0.1(\frac{a}{c})+0.1(\frac{a}{c})^4\ ]\frac{\sqrt{a}}{\sqrt{c}} \qquad (4.48)$$

4.4.3 A Semi-elliptic Crack in a Plate of Finite Thickness

A. Under tensile loading

The correction for the crack in semi-infinite plate is sometimes referred as the front face correction. As the plate thickness is reduced to finite thickness t, the influence of the back face should be also accounted for. Newman (Ref 81) has proposed that for the tension case

$$K_I = [C_f+(In[k]\frac{\sqrt{c}}{\sqrt{a}} - C_f)(\frac{a}{t})^{C_b}]\ \frac{S_\infty}{In[k]} \sqrt{(\pi a)} \qquad (4.49)$$

where C_b is the back face correction factor. One advantage of the equation is that when $a/t=1$, no matter what C_b is, it reduces to

$$K_I = S_\infty \sqrt{(\pi\ c)} \qquad (4.50)$$

which is the exact K_I expression for a through thickness crack of length 2c. The value of C_b monitors how K_I varies with the fractional crack depth a/t. Raju and Newman (Ref 62) have performed a three dimensional finite element analysis in which a large number of elements have been used, to represent their findings C_b is given as (Ref 80)

$$C_b(\theta=\frac{\pi}{2}) = 1.6+3(\frac{a}{c})^3+ 8(\frac{a}{c})(\frac{a}{t})^5+0.008(\frac{c}{a}) \qquad (4.51)$$

$$C_b(\theta=0) = 0.3 +1.15(\frac{c}{a})^{[1.3\times\frac{a}{t}(\frac{a}{c})^{0.2}]} +0.8(\frac{a}{c})^3 \qquad (4.52)$$

The results of Raju and Newman (Ref 62) have been successfully used to predict surface crack growth patterns and to correlate surface crack fracture data for a brittle epoxy material (Ref 82).

B. Bending

In bending, K_I at the deepest point should drop to zero somewhere as the fractional crack depth increases, because the back face is in compression. Let $S_{\infty m}$ denote the remote stress on tension side surface due to the bending moment, the three dimensional solution of Koterrazawa and Minamisaka (Ref 83) can be represented by

$$K_I(\theta=\frac{\pi}{2}) = C_f(\theta=\frac{\pi}{2})[1-1.36(\frac{a}{t})(\frac{a}{c})^{0.1}]\frac{S_{\infty m}}{In(k)}\sqrt{(\pi a)} \qquad (4.53)$$

$$K_I(\theta=0)=[C_f(\theta=0)(1-0.3\ \frac{a}{t})(1-\frac{a}{t})^{12}\ ]$$

$$+[0.394\ \ln(k)(\frac{a}{t})^{12}\ \frac{\sqrt{c}}{\sqrt{a}}]\ \frac{S_{\infty m}}{\ln(k)}\sqrt{(\pi a)} \qquad (4.54)$$

4.4.4 A Semi-Elliptical Crack in a Finite Plate

It is often found in engineering that plates can not be treated as "infinite". The finite area correction should be considered when the crack dimensions are appreciable in comparison with the plate dimensions (Fig 4.10c). This has been studied by Holdbrook and Dover (Ref 84). The stress intensity factors can be expressed by introducing correction factors C_t and C_b to the results of Irwin (Ref 85) for tensile loading cases and of Shah and Kobayashi (Ref 86) for bending. The correction factor C_t for tensile loading cases is

$$C_t = 1+ \frac{f_1(\frac{a}{c})f_2(\frac{c}{w})f_3(\frac{a}{t})}{0.0599^2} \qquad (4.55)$$

The empirical expressions for f_1, f_2 and f_3 are as follows

$$f_1(\frac{a}{c}) = 0.059+0.108(\frac{a}{c}) -0.734(\frac{a}{c})^2$$

$$+1.85(\frac{a}{c})^3 -2.01(\frac{a}{c})^4 +0.89(\frac{a}{c})^5$$

$$f_2(\frac{c}{w}) = -0.00252 + 0.274(\frac{c}{w})$$

$$-0.354(\frac{c}{w})^2 +1.008(\frac{c}{w})^3$$

$$f_3(\frac{a}{t}) = 0.0126 -0.132(\frac{a}{t}) +0.857(\frac{a}{t})^2$$

$$-1.182\left(\frac{a}{t}\right)^3 + 0.746\left(\frac{a}{t}\right)^4 \qquad (4.56)$$

For bending, the equation for the correction factor C_b takes a similar form

$$C_b = 1 + \frac{f_1\left(\frac{a}{c}\right) f_2\left(\frac{c}{w}\right) f_3\left(\frac{a}{t}\right)}{0.2745^2} \qquad (4.57)$$

f_4, f_5 and f_6 can be evaluated by using the empirical equations

$$f_4\left(\frac{a}{c}\right) = 0.381 - 0.141\left(\frac{a}{c}\right) - 0.366\left(\frac{a}{c}\right)^2 + 0.569\left(\frac{a}{c}\right)^3 - 0.248\left(\frac{a}{c}\right)^4$$

$$f_5\left(\frac{c}{w}\right) = -0.0239 + 1.434\left(\frac{c}{w}\right) - 2.984\left(\frac{c}{w}\right)^2 + 7.822\left(\frac{c}{w}\right)^3$$

$$f_6\left(\frac{a}{t}\right) = -0.0113 + 0.323\left(\frac{a}{t}\right) + 0.749\left(\frac{a}{t}\right)^2 - 0.535\left(\frac{a}{t}\right)^3 \qquad (4.58)$$

It has been indicated that (Ref 84) surface cracked plate subjected to tension loading, undergoes bending when a considerable part of the cross sectional area of the plate is taken by the crack. This is because of the eccentric loading on the crack plane. A procedure for assessing this effect has been given in Ref 84.

SECTION 5 Overview of Elastic/Plastic Fracture Mechanics

When the plastic zone is large compared to the dimensions of the cracked body or the crack length, linear elastic fracture mechanics

is no longer applicable and elastic/plastic fracture mechanics must be applied. There are two current ductile fracture mechanics parameters for assessing cracks associated with large scale plastic deformation: the J integral and the crack tip opening displacement (CTOD).

4.5.1 The J Integral

The J integral was proposed by Rice (Ref 87) for a non-linear elastic material and is defined as

$$J = \int_{\Gamma} [\ w dy - \mathbf{F} \frac{\partial u}{\partial x} ds\ ] \qquad (4.59)$$

Γ is an arbitrarily closed curve traversed in an anticlockwise direction surrounding the crack tip in the stressed solid (Fig 4.11), w is the strain energy density defined as

$$w = \int_0^{\epsilon} \sigma_{ij}\, d\epsilon_{ij} \qquad (4.60)$$

The other parameters, F, u and ds are respectively the traction vector along an outward unit vector normal to the curve Γ , the displacement vector and the element of the curve Γ. The J integral can be shown to be path independent (Ref 88) in non-linear elastic materials.

Rice (Ref 87) has shown that for a non-linear elastic material, J is equal to change in potential energy for a virtual crack extension ∂a.

$$J = -\frac{\partial U_p}{\partial a} \tag{4.61}$$

Of course this conclusion holds for a linear elastic material. In this case,

$$J = G \tag{4.62}$$

Assuming the stress-strain behaviour of a non-linear material can be presented as

$$\frac{\epsilon}{\epsilon_f} = C_1 \left(\frac{\sigma}{\sigma_f}\right)^{C_2} \tag{4.63}$$

where σ_f and ϵ_f are the flow stress and strain respectively, C_1 and C_2 are constants for a specific material, the stress and strain singularity close to the crack tip are found in polar coordinates to be

$$\sigma(r) = \frac{C_3}{r^{\frac{1}{C_2 + 1}}} \tag{4.64}$$

and

$$\epsilon(r) = \frac{C_4}{r^{\frac{C_2}{C_2 + 1}}} \tag{4.65}$$

by Hutchinson (Ref 89), Rice and Rosengren (Ref 90). Here C_3 and C_4 are parameters determined by individual configuration and loading. The singularities represented by these two equations are often referred to as the HRR fields. In addition, Hutchinson (Ref 89) has also shown that for this case the crack tip stress field can be

expressed in terms of J

$$\sigma_{ij} = \sigma_f \left(\frac{J}{C_2\ \sigma_f\ \epsilon_f\ V\ r}\right)^{\frac{1}{C_2+1}} f_{ij}(\theta) \qquad (4.66)$$

$$\epsilon_{ij} = C_1\ \sigma_f \left(\frac{J}{C_2\ \sigma_f\ \epsilon_f\ V\ r}\right)^{\frac{C_2}{C_2+1}} g_{ij}(\theta) \qquad (4.67)$$

f_{ij} and g_{ij} are functions of θ only and V is a parameter depends only on the stress-strain relation. This indicates that the J integral characterises the crack tip stress and strain fields and is not only a energy parameter, but also a stress field parameter. However, this argument is restricted to a non-linear elastic material. If the J integral is to be applied to elastic-plastic materials, unloading is not permissible, because during the unloading, the material follows a stress-strain route other than the non-linear route which is followed in loading. When a crack advances, unloading takes place in the wake of the crack and the application of J concept becomes questionable. In practice however, this does not appear to be a serious shortcoming for crack advance of less than 10% of its initial length (Ref 91).

4.5.2 The Crack Tip Opening Displacement

An alternative to the J integral approach is the crack tip opening displacement (CTOD) concept proposed by Wells (Ref 92). CTOD can be shown related to the stress intensity factor for the case of a linear elastic material. If the CTOD is defined as the displacement at x=a for an original crack of 2a under remote tensile loading (Fig

4.2), using the Dugdale approach for assessing the displacement (Ref 93), it can be expressed as

$$CTOD = \frac{K_I^2}{E\,\sigma_o} = \frac{G}{\sigma_o} \qquad (4.68)$$

for plane stress. The crack tip opening displacement however depends upon the position where it is determined, and in general

$$CTOD = \frac{G}{C\,\sigma_o} \qquad (4.69)$$

Different values for C can be found in the literature (Refs 87, 94 and 95).

For elasto-plastic cases, CTOD can be determined from the measurable crack opening displacement (Ref 96). It is assumed that COD or CTOD is still a parameter controlling the crack tip stress and strain field when extensive plastic deformation appears, thus its value at failure represents the severity of crack tip deformation for a given material, environment and loading, but does not depend on the geometry of the structure. So far, experiments (Ref 97) have been shown to be broadly in agreement with this elastic-plastic fracture mechanics model. The application of a critical value of COD as a failure criterion has been demonstrated and a design curve has been established (Ref 98).

LIST OF FIGURES FOR CHAPTER 4

Fig 4.6

The notation of the stresses concerned in the line spring element capable of assessing stress intensity factors separately.

Fig 4.7

The arrangement of the nodes in the crack tip area for virtual crack extension method.

Fig 4.8

The principle of the weight function method.

Fig 4.9

The extended weight function method (Ref 79).

Fig 4.10

Elliptical cracks in plates.

a. An elliptical crack in a infinite solid;

b. A semi-elliptical surface crack in a semi-infinite solid;

c. A semi-elliptical surface crack in a finite plate.

Fig 4.11

The J-integral.

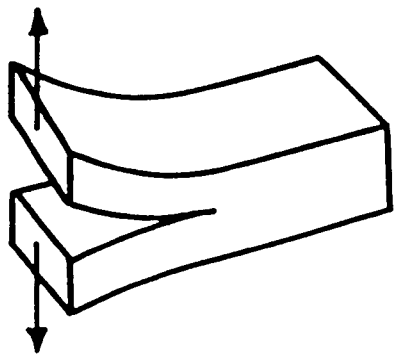

Mode 1

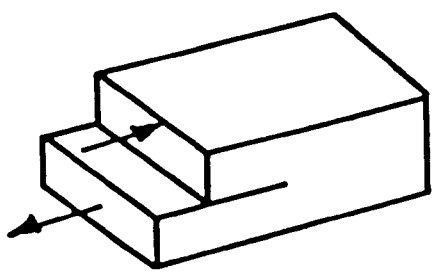

Mode II

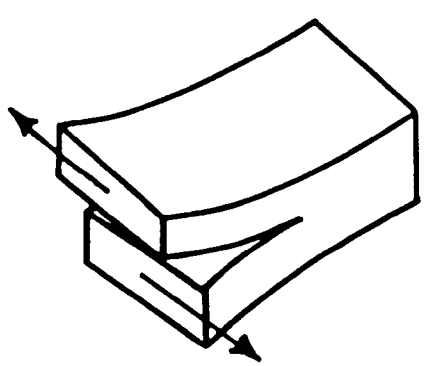

Mode III

Fig4.1

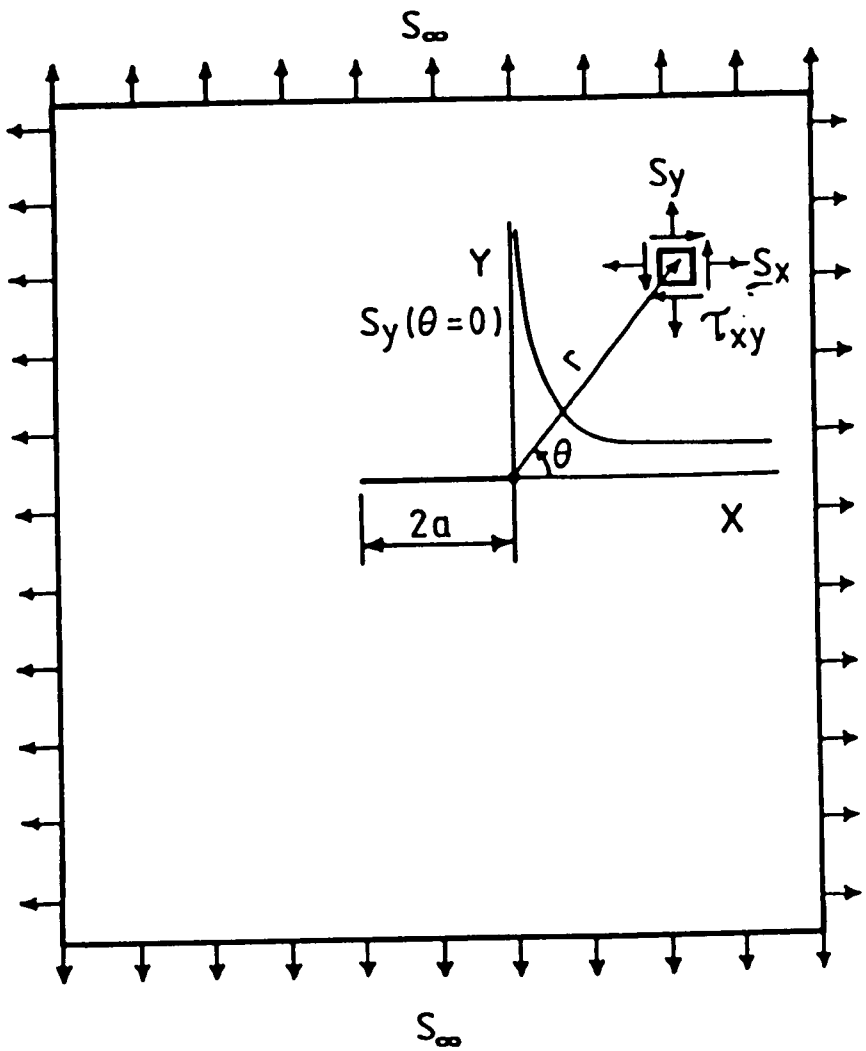

Fig4.2

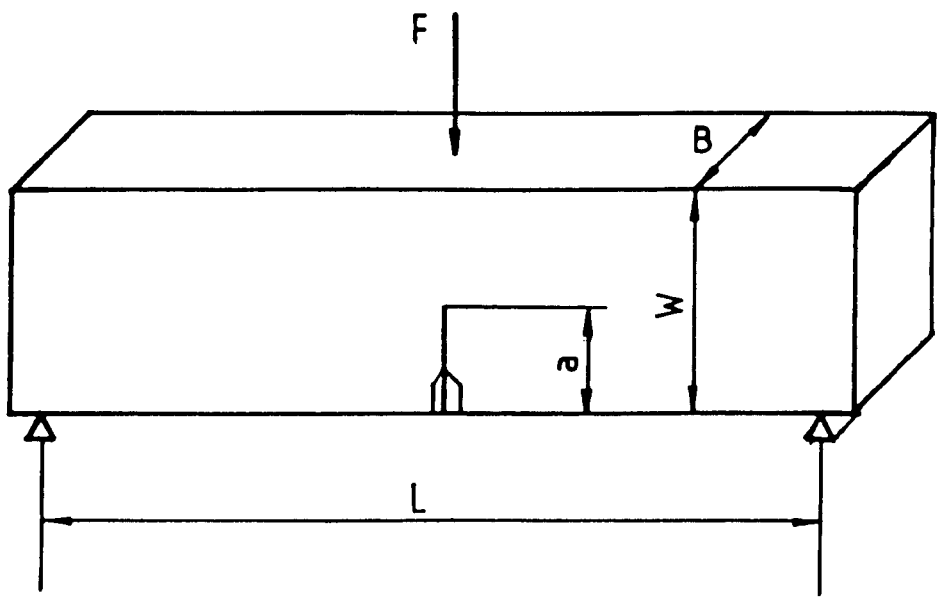

L = 200mm

B = 25 mm

W = 50 mm

Fig 4.3

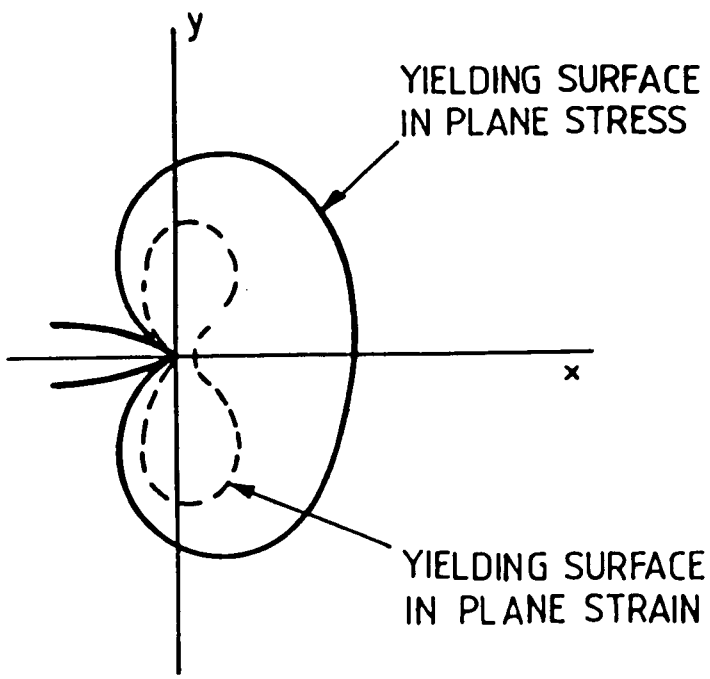
y
YIELDING SURFACE
IN PLANE STRESS
x
YIELDING SURFACE
IN PLANE STRAIN

Fig 4.4

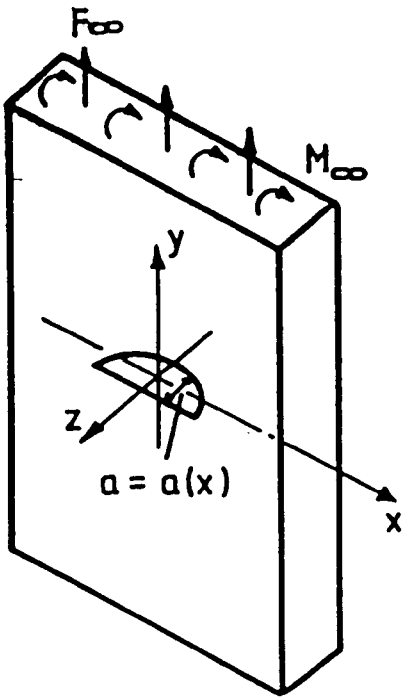

(a)

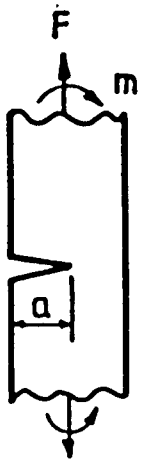

(b)

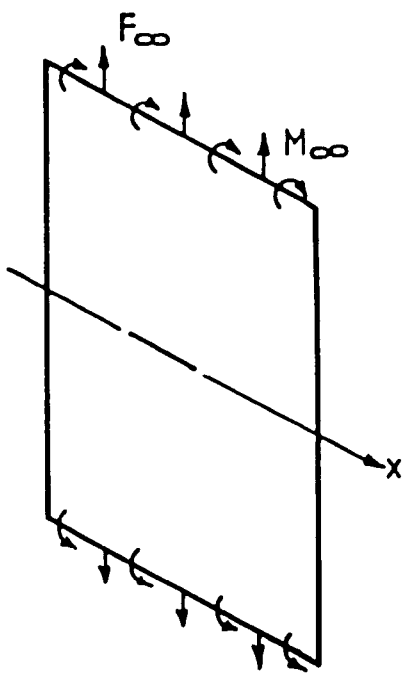

(c)

Fig 4.5

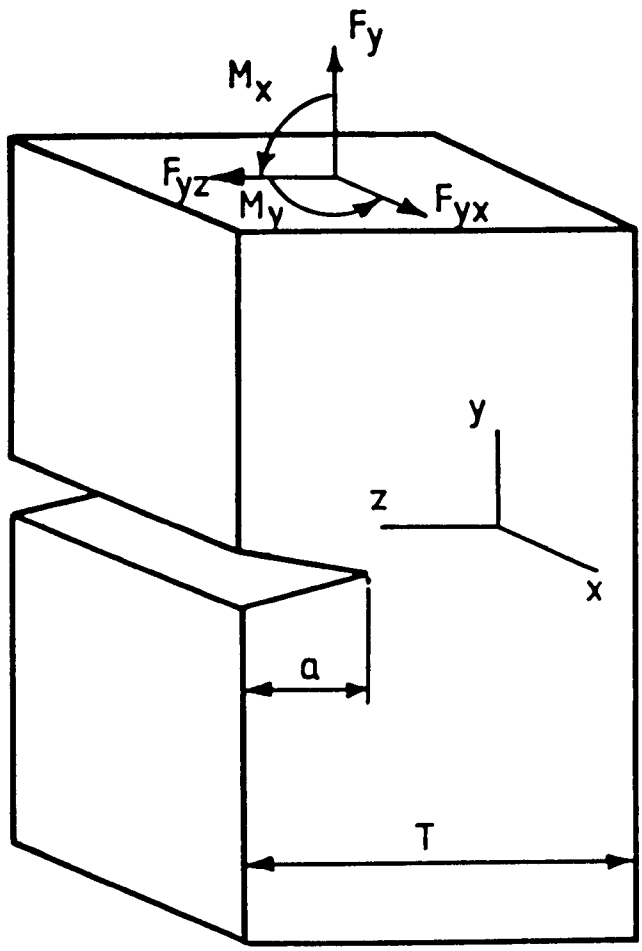

Fig 4.6

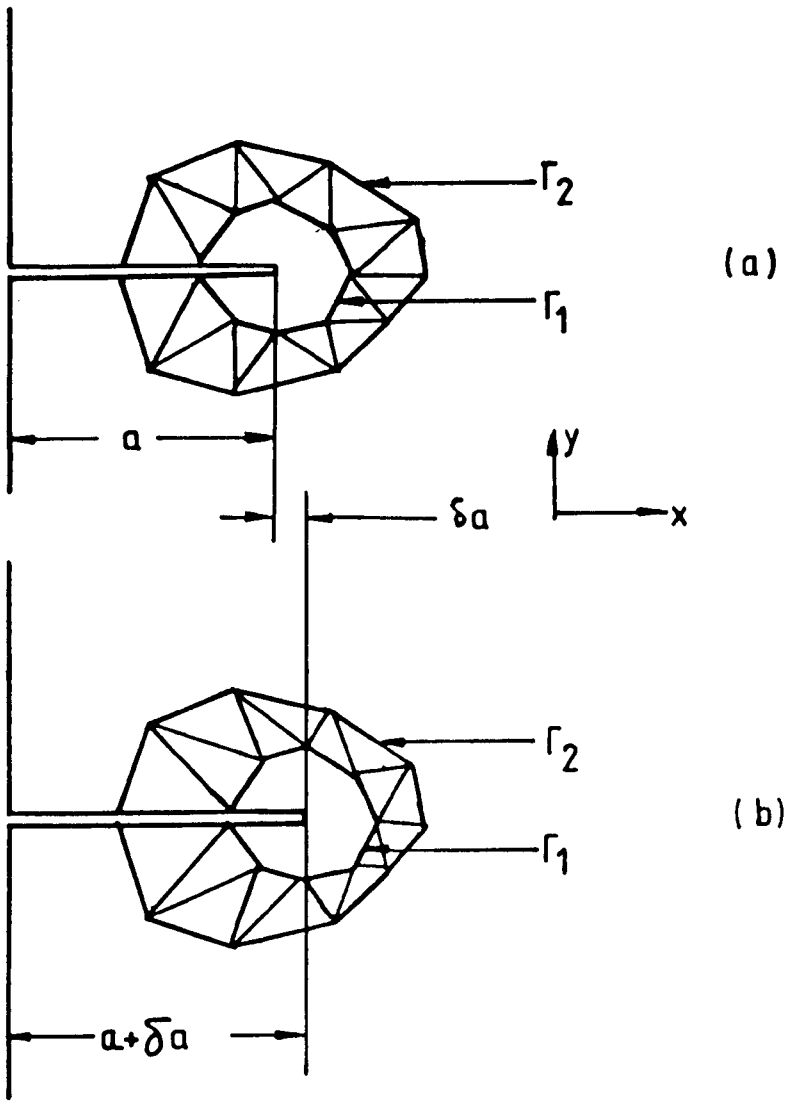

Fig 4.7

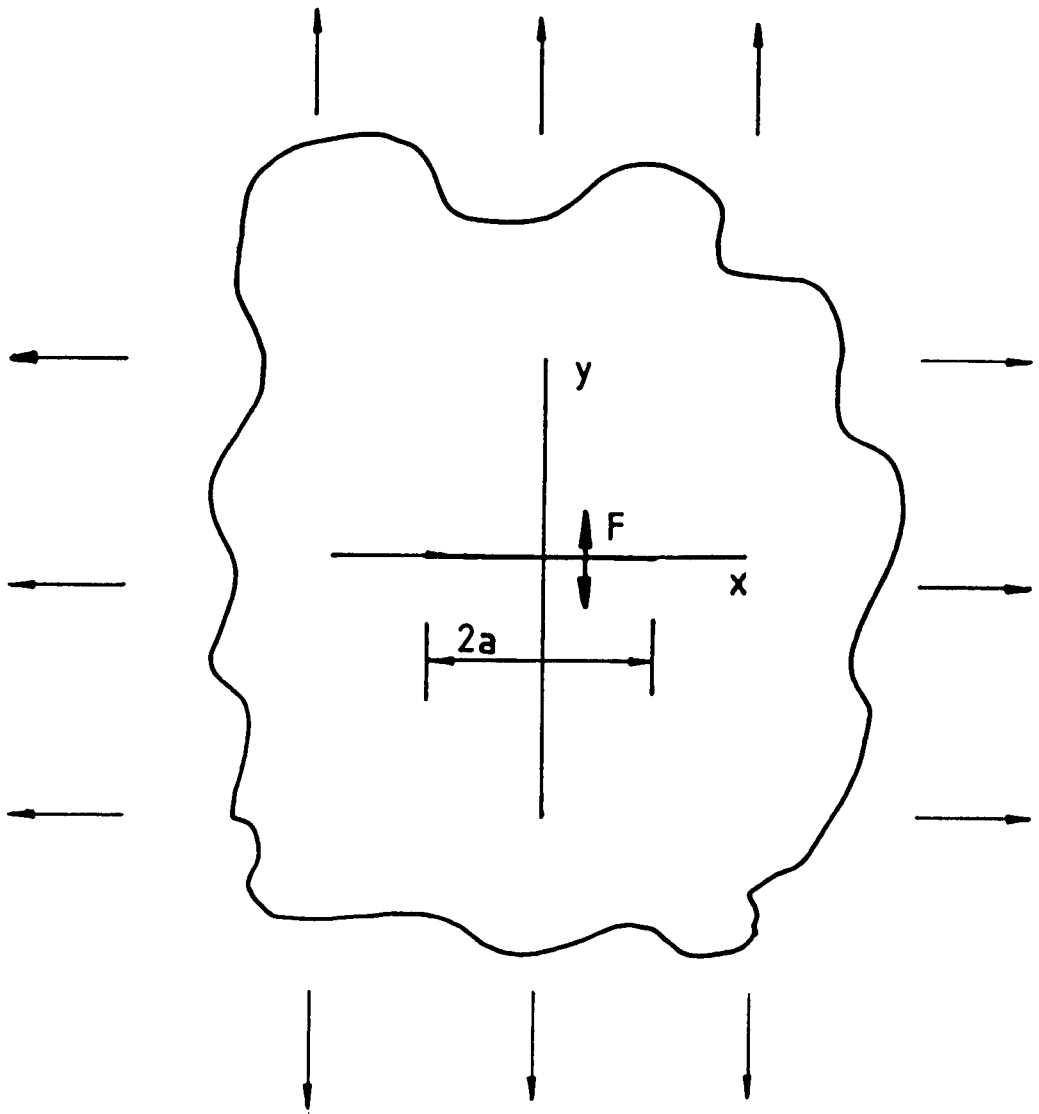

Fig 4.8

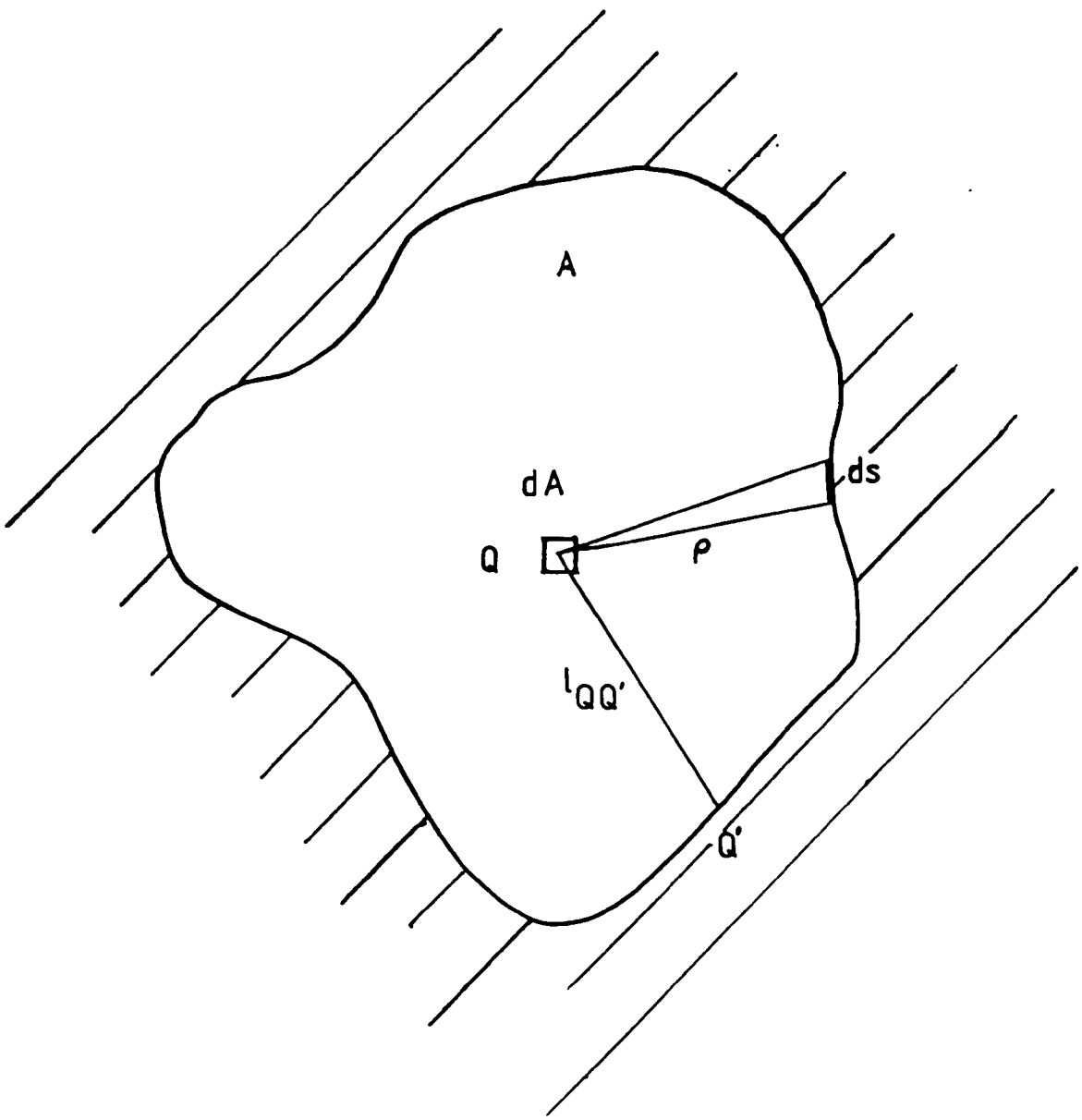

Fig 49

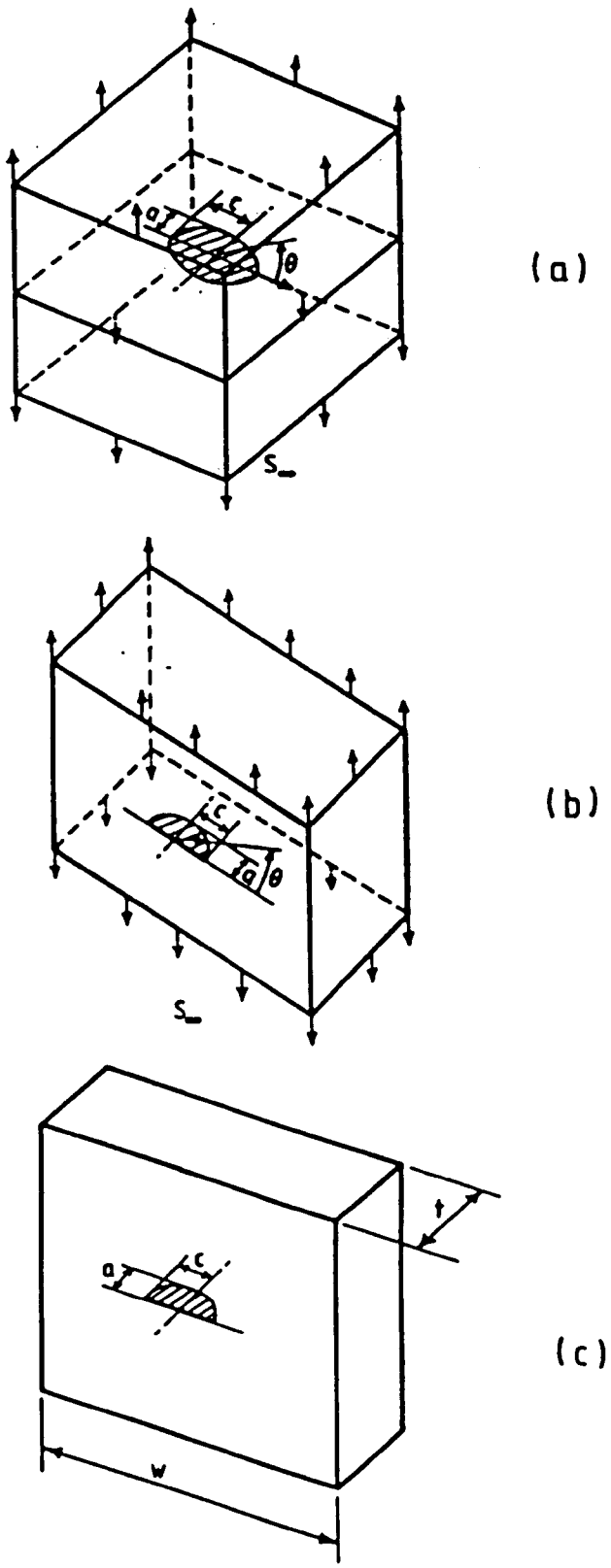

Fig 4.10

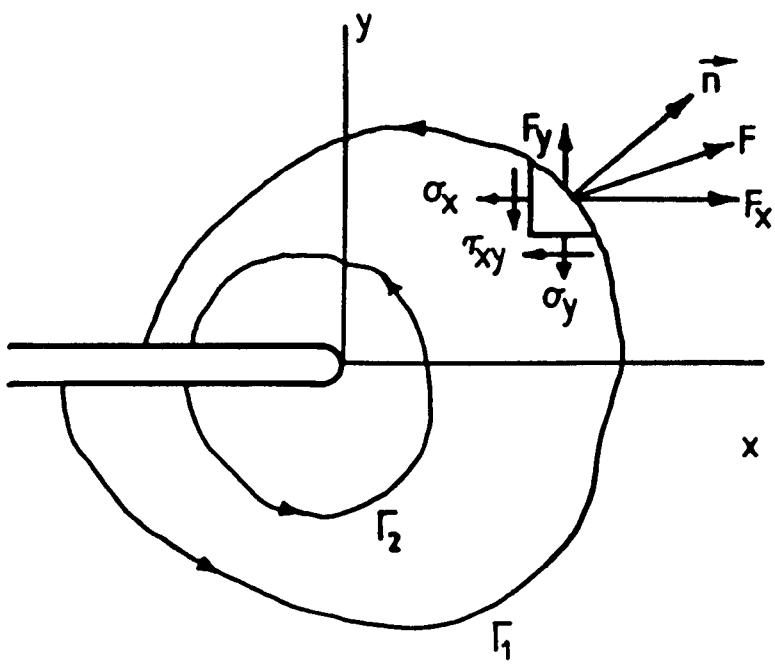

Fig 4.11

CHAPTER 5 FATIGUE ASSESSMENT BY FRACTURE MECHANICS

Fatigue failure is generally recognized to be the result of crack initiation followed by crack propagation and final fracture. The physical processes of fatigue at a crack tip are complicated and difficult to analyse. However, fracture mechanics can provide a phenomenological description of the crack growth rate which is particularly important in developing inspection and repair regulations for structures. It is also possible to predict the fatigue life using fracture mechanics in cases in which crack propagation occupies the dominant period of the life. A detailed descritption of the various aspects of matel fatigue can be found in a book by Pook (Ref 99)

SECTION 1 The Fatigue Process

5.1.1 Cracked Surface

Generally, fatigue has three stages which can be observed on typical cracked surfaces (Ref 100). Crack initiation often accounts for a very small portion of the whole cracked surface, which is difficult to identify. The area which represents the propagation stage is

often macroscopically smooth, but microscopically striations which are the result of individual loading cycles can be detected. Any change in the statistical characteristics of the loading alters the average crack growth rate and thus leads to the formation of a "beach mark" which can be utilized to indicate the crack front. (Ref 101). The final part of the surface is frequently rough, and fibrous in appearance, which is produced by ductile tearing and ultimate fracture.

5.1.2 The Fatigue Process in Metals

Most commercial metals and alloys are polycrystalline. Such materials consist of many crystals with each crystal having its own orientation and mechanical properties. Whenever a metal component is subjected to a cyclic loading, some of the crystals may have their slip plane oriented in the direction of maximum shear stress and the first slip occurs in those crystals. Both slip band intrusions and extrusions are formed where the slip planes intersect the surface (Ref 102). As the cyclic loading continues, some intrusion areas may become more distinct and cracks grow from these persistent slip bands.

The initial cracks grow under fatigue loading. The discontinuity due to the crack tip causes a high stress concentration, and the main factor driving the crack forward changes to the normal stress as opposed to the shear stress. Therefore, the crack propagation direction gradually turns from the direction of maximum shear stress to a direction perpendicular to the biggest principal stress. Mode *I*

cracking is usually the dominant mode although the other two modes may also present. A crack can grow by a wide range of fatigue mechanisms. Among the most common are striation formation, microvoid coelescence and microcleavage which can be identified from the cracked surface using a scanning electron microscope (Ref 103). As the crack becomes longer, the growth rate usually increases. When the stress intensity factor associated with the maximum in the fatigue load cycle approaches K_C, the growth rate accelerates and failure follows in a few cycles.

It has been argued that (Refs 104 and 105) there is no crack initiation period and cracks are contained in the slip bands. Crack propagation starts immediately as fatigue loading is applied and if the loading is very small, the cracks stop at the grain boundaries. This explains the fatigue limit behaviour of materials and furthermore indicates the damage accumulation under a loading lower than the fatigue limit. Fatigue life predictions have been produced for tests using fatigue loadings which contain many stress cycles lower than the fatigue limit (Ref 104). Such predictions were found to be significantly closer to the experimental data than predictions by either Miner's law (Ref 24) or Corten and Dolan's model (Ref 36) which ignore the damage due to stress cycles lower than the fatigue limit. However, this finding has yet to be widely confirmed.

SECTION 2 Crack Growth Rate Models

For engineering structures under fatigue loading, subcritical crack

propagation often occupies a major part of the fatigue life. In general, cracks tend to grow under mode *I* conditions and the current study is restricted to this kind of crack propagation. However, mixed mode fatigue crack propagation is also a major form of fatigue (Ref 106).

For fatigue crack propagation involving a large number of cycles to failure, the applied stress range is low, and the plastic zone at the crack tip is small compared to all other dimensions. The stress intensity factor in this case can be used to give a good description of the crack tip stress field. Therefore, it is not surprising that the crack growth rate can be correlated with stress intensity factor range as originally proposed by Paris and Erdogan (Ref 107).

In the constant amplitude loading depicted in Fig 3.1, when the minimum stress $S_{min} \geq 0$, the stress intensity range ΔK associated with each cycle is defined as

$$\Delta K = K_{max} - K_{min} \qquad (5.1)$$

where K_{max} and K_{min} are stress intensity factors corresponding to the maximum and minimum stresses in a cycle, S_{max} and S_{min}. Let da/dN be the crack growth per cycle, if $\ln(da/dN)$ is plotted against $\ln\Delta K$, the curve will generally exhibit three regions as shown in Fig 5.1. When K_{max} approaches K_C, a sharp increment in the crack growth rate is observed because of the presence of ductile tearing. At the other end of the curve, region *I*, when ΔK decreases to near a threshold value ΔK_{th}, the growth rate decreases abruptly. It is thought that when the stress intensity range ΔK is less than the

threshold value ΔK_{th}, the crack does not grow. While the central part of the curve, region *II*, can be approximated by a straight line,

$$\ln\left(\frac{da}{dN}\right) = n \ln\Delta K + \alpha \qquad (5.2)$$

Therefore,

$$\frac{da}{dN} = \alpha \Delta K^{n} \qquad (5.3)$$

where α and n are material constants. This is the very popular equation due to Paris and Erdogan (Ref 107). Originally, there were some models which did not recognize the connection of the crack growth rate to the applied stress intensity factor range. For example, Liu (Ref 108) suggested

$$\frac{da}{dN} = C \; S^{2} \; a \qquad (5.4)$$

where C was thought to be a material constant. This kind of model (Refs 108-110) has lost its popularity, because they only describe the individual sets of experimental results studied by the authors. Experimental data analysed using such models have been re-analysed using the Paris law and the results were satisfactory (Ref 111).

However, the Paris law approximates only to the central part of the crack growth behaviour. To represent the whole range of crack growth rate, an inverse hyperbolic tangent model (Ref 112) can be used.

$$\log\left(\frac{da}{dN}\right) = C_1 + C_2 \; \mathrm{Tanh}^{-1}[f(K_{eff})] \qquad (5.5)$$

where C_1, C_2 are material constants, and $f(K_{eff})$ is a function of the effective stress intensity range which can be determined by considering the crack closure stress (see 5.3.3). This equation represents a sigmoidal curve in the $\ln(^{da}/_{dN})$ and $\ln\Delta K$ coordinates, therefore, by choosing appropriate parameters and the function $f(K_{eff})$, it can be used to express the fatigue crack growth behaviour for the whole range of the applied ΔK.

Alternatively, Forman et al (Ref 113) have proposed an expression in which the material behaviour in region *III* is accounted for.

$$\frac{da}{dN} = \frac{\propto \Delta K^n K_{max}}{K_{IC} - K_{max}} \qquad (5.6)$$

Here the material parameters $\propto$ and n are not necessarily the same as in the Paris law.

The relation proposed by Walker (Ref 114) can be taken as a further example of a similar model.

$$\frac{da}{dN} = \propto K_{max}^{m} \Delta K^n \qquad (5.7)$$

where m is a material constant. There have been attempts to relate the crack growth rate to the crack opening displacement (Refs 115 and 116). Generally in the form of

$$\frac{da}{dN} = C \left(\frac{\Delta K}{E}\right)^2 \qquad (5.8)$$

where E is Young's modulus.

SECTION 3 Factors Affecting the Fatigue Crack Growth Rate

Many factors affect the crack growth rate, the temperature, material, mean load, environment and sequence effects (including overloads). Here however, discussion is limited to the effect of mean stress, environment and random loading which are the dominant factors for fatigue crack growth in offshore structures.

5.3.1 The Mean Stress

It has been found (Refs 117-119) that the influence of mean stress on the crack growth rate is usually small in region *II* of the $\ln(da/dN)$ vs. $\ln\Delta K$ sigmoidal curve (Fig 5.2). While in region *I*, the mean stress may have a substantial effect on the threshold stress intensity range. In region *III*, the crack growth rate increases as the K_{max} of the stress cycle approaches K_C or K_{IC}. Since K_{max} is directly connected to the mean stress through the relation

$$K_{max} = f(\frac{a}{w})\, S_{max} \sqrt{(\pi a)} = f(\frac{a}{w})(S_m + S_a)\sqrt{(\pi a)} \qquad (5.9)$$

it is not surprising that the upper transition region (region *III*) shifts to a lower ΔK value for large mean stresses. A modified form of Forman model (Ref 113) can be used to estimate the influence of the mean stress

$$\frac{da}{dN} = \frac{\propto \Delta K^n}{(1-r)\, K_C - \Delta K} \qquad (5.10)$$

where r is the stress ratio.

5.3.2 Environment

Fatigue takes place in diverse situations in which the influence of environment may be substantial. For offshore structures, the main detrimental effect is the corrosive action of sea water. It has been shown that on a metal surface submerged in sea water, pits are formed which cause stress concentrations and reduce the crack initiation time. Fresh material surfaces in the crack tip region are continually exposed to the corrosive sea water as the protective oxide layer is broken by the cyclic loading. Due to the interaction between the external loading and the corrosive action, the crack growth is generally enhanced. For one particular case in NaCl solution, the enhancement of crack growth has been found to be about 2.5 to 3 times greater than that in air (Ref 120).

The frequency of the loading in corrosion fatigue is an important parameter. Crooker et al (Ref 121) have shown that the difference between crack growth rates in sea water and air is smaller when the frequency is high than when it is low. This can be explained by the fact that there is less time available for the interaction between corrosion and the repeated stress cycles in high frequency fatigue.

5.3.3 Interaction Between Cycles

It is generally agreed that occasional overloads have a marked effect on the fatigue life (Refs 122 and 123). This effect is often

referred to as a sequence effect or the interaction between cycles. For narrow band random loading, Priddle (Ref 124) indicates that calculations which do not consider the interaction between cycles are in agreement with experiments. Barsom (Ref 30) found no interaction effect in experiments using random amplitude loading. Gall and Hancock (Ref 125) found increasing interaction effects with increasing spectral band width. Their experiment shows that as the band width of the power spectrum of a random loading increases, the slope of the line representing the crack growth rate against stress intensity range relation in logarithmic coordinates decreases.

Sequence effects in cyclic loading have been studied extensively and a number of models have been proposed. There are two well known models and their modified versions which represent the basic features of such models (126-129).

In the model proposed by Wheeler (Ref 126), it is believed that the plastic deformation at the crack tip during an application of a tensile overload produces a residual compression stress which slows down the subsequent crack growth. The assessment of retardation is achieved by introducing an empirical parameter C in the crack increment calculation

$$\frac{da}{dN} = C \quad f(\Delta k) \qquad (5.11)$$

$f(\Delta K)$ is determined by crack growth laws, such as the Paris law. C is determined according to the plastic zone sizes (Fig 5.3). For the ith cycle, $C_i=1$ if the instantaneous crack length plus the associated plastic zone passes beyond the plastic zone left by a

previous over-load. If not, C_i is evaluated from the equation

$$C_i = \left[\frac{r_i}{(a_d + r_d) - a_i} \right]^m \qquad (5.12)$$

where a_d+r_d is the furthest point in the plastic zone left by an overload, a_i and r_i are the crack length at ith cycle and the corresponding plastic zone size while m is an experimental shaping parameter.

The model proposed by Elber (Ref 128) handles crack growth retardation by introducing an effective stress concept to reduce the applied stress and hence the stress intensity factor of the crack. The effective stress range is defined as

$$S_{eff} = S_{max} - S_{op} \qquad (5.13)$$

where S_{op} is the crack opening stress. This is based on the finding that a crack tip closes before the applied load reduces to zero, in other words, part of the applied stress is used to open the crack tip. S_{op} has been found to be dependent on the material, thickness, environment and the magnitude of previous stress peaks (Ref 128). The effective stress range is employed in determining the range of effective stress intensity factor which is used to replace the stress intensity factor range in crack growth laws. For example, the Paris law can be adjusted to

$$\frac{da}{dN} = \alpha (\Delta K_{eff})^n = \alpha[f(\frac{a}{w})(S_{max}-S_{op})\surd(\pi a)]^n \qquad (5.14)$$

The crack length a after the application of a number of cycles N can

be estimated by

$$a = a_o + \sum_{i=1}^{N} \Delta a_i \qquad (5.15)$$

Δa_i may be given by various crack growth models. This procedure is simple if Δa_i only depends on the current size of the crack a and the stress cycles history. The models which consider interaction effects, such as Wheeler's model (Ref 126) and Elber's model (Ref 128), almost inevitably use this procedure. The cycle by cycle calculation method is thus time consuming and computer programs are often used. Predictions of fatigue life with and without considering the interaction effects have been compared by Chang et al (Ref 131) and there was no significant improvement in the predictions by introducing interaction effects.

SECTION 4 Single Parameter Crack Growth Models

5.4.1 ΔK_{rms}

It would be convenient to predict fatigue life if a single statistical parameter of a random loading could fully describe the fatigue process for a given specimen under random loading. One such parameter is ΔK_{rms} (Refs 9, 10 and 125). Barsom (Ref 9) used variable-amplitude random-sequence stress loading, and defined ΔK_{rms} as the root mean square of the stress intensity factor ranges. Hudson took ΔK_{rms} as

$$\Delta K_{rms} = f(\frac{a}{w}) \ (S_{max\text{-}rms} - S_{min\text{-}rms})\sqrt{(\pi a)} \qquad (5.16)$$

Here $S_{max\text{-}rms}$ and $S_{min\text{-}rms}$ are the root mean square's of the maxima and minima for fatigue loadings with zero mean load, and are given as

$$S_{max\text{-}rms} = \left\{E[S_{max}^2]\right\}^{\frac{1}{2}} \qquad (5.17)$$

and

$$S_{min\text{-}rms} = \left\{E[S_{max}^2]\right\}^{\frac{1}{2}} \qquad (5.18)$$

In some fatigue crack growth models, the stress ratio is required. This can be replaced by a rather artificial "root mean square stress ratio" r_{rms}

$$r_{rms} = \frac{S_{min\text{-}rms}}{S_{max\text{-}rms}} \qquad (5.19)$$

In addition, ΔK_{rms} can be defined as (Ref 125)

$$\Delta K_{rms} = 2 \ f(\frac{a}{w}) \ \sigma \ \sqrt{(\pi a)} \qquad (5.20)$$

where σ is the root mean square of the random stress. It has been shown that in some steels, fatigue crack growth rates under constant amplitude loading and variable amplitude loading are related in terms of ΔK_{rms} (Ref 9). This gave a basis for the application of the ΔK_{rms} method to predict fatigue life.

5.4.2 ΔK_h

An alternative to ΔK_{rms} is ΔK_h which is defined as

$$\Delta K_h = f(\frac{a}{w}) \quad Mn[S]^{\frac{1}{n}} \quad \sqrt{(\pi a)} \tag{5.21}$$

where Mn[S] is the nth moment of the distribution of stress ranges about zero, specified by Eq 1.11. The stress range can be given by various definitions or cycle counting methods (Ref 125). The reason for using ΔK_h can be seen from the following argument. Suppose the sequence effects negligible, the average crack growth rate can be estimated for a given crack length a by the Paris law

$$\frac{da}{dN} = \alpha E\left\{ [\ f(\frac{a}{w}) \quad S\ \sqrt{(\pi a)}\ ]^n \right\}$$

$$= \alpha\ [\ f(\frac{a}{w})\ \sqrt{(\pi a)}\ ]^n\ M_n[S] \tag{5.22}$$

By comparing with the previous equation

$$\frac{da}{dN} = \alpha\ \Delta K_h{}^n \tag{5.23}$$

ΔK_h has been used to represent the results of fatigue experiments on tubular welded joints by Dover and co-workers (Ref 132-133). The fatigue life of these joints was estimated based on this characteristic range of stress intensity factor. More details of the experiments are given in Chapter 8.

LIST OF FIGURES FOR CHAPTER 5

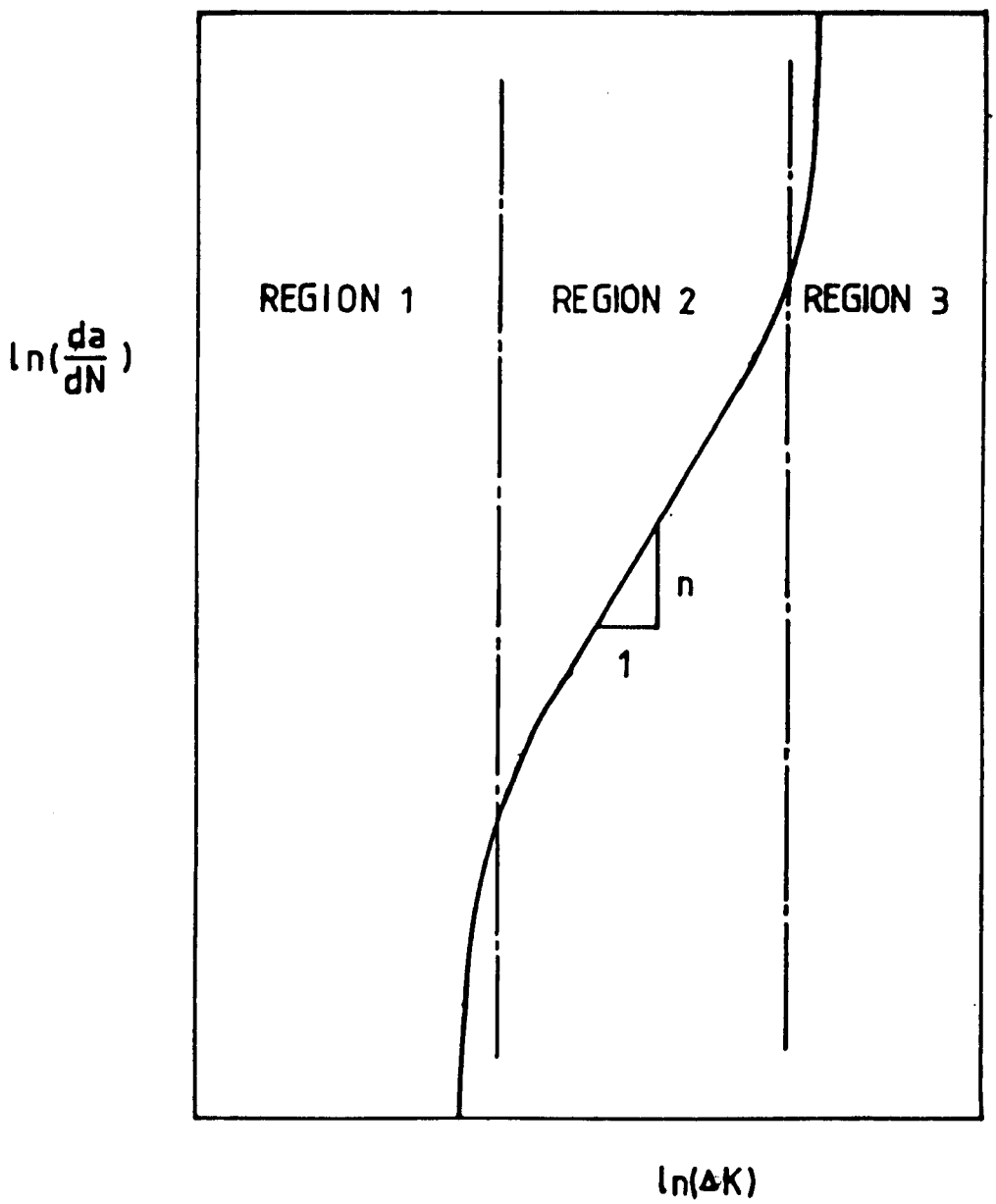

Fig 5.1

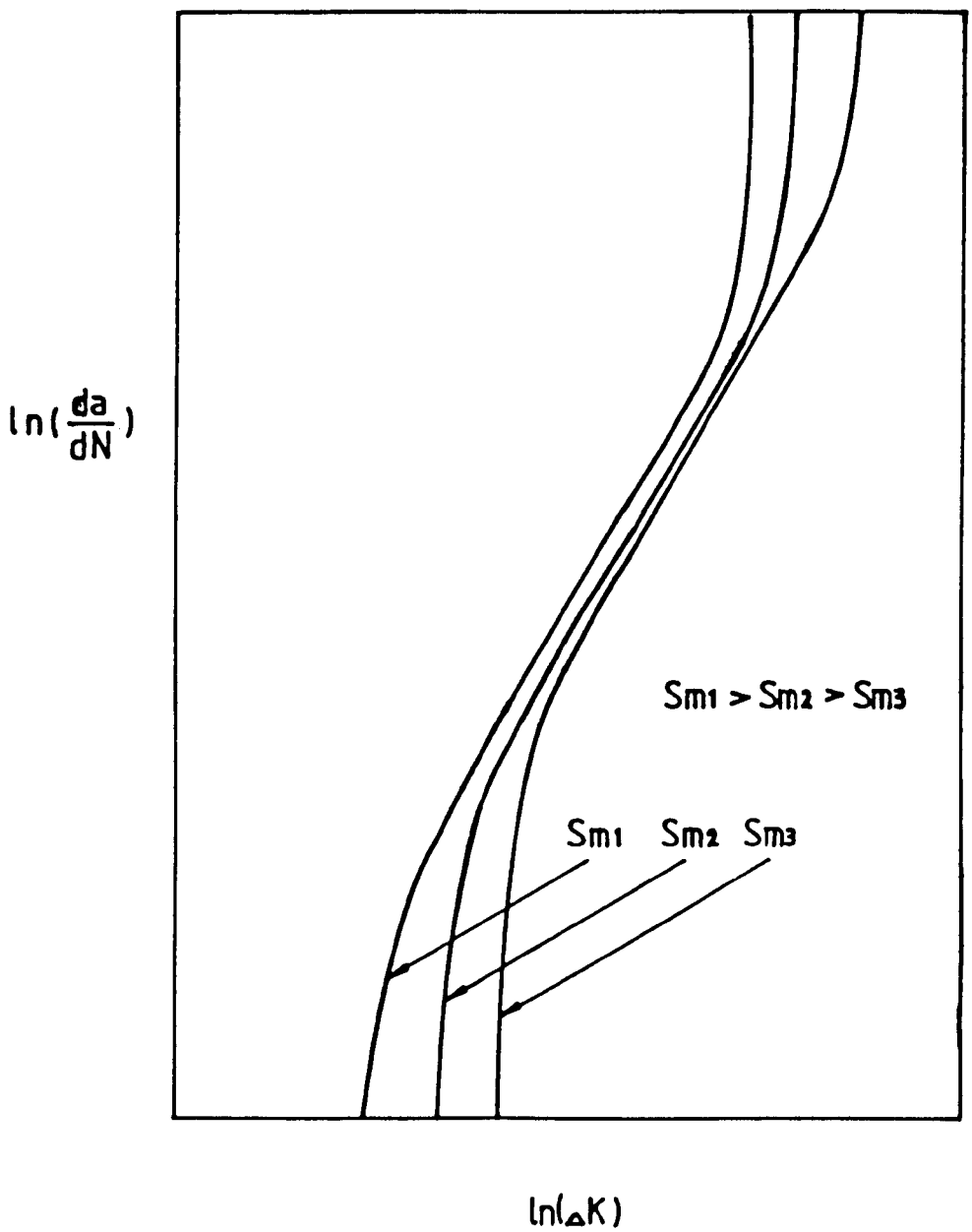

Fig 5.2

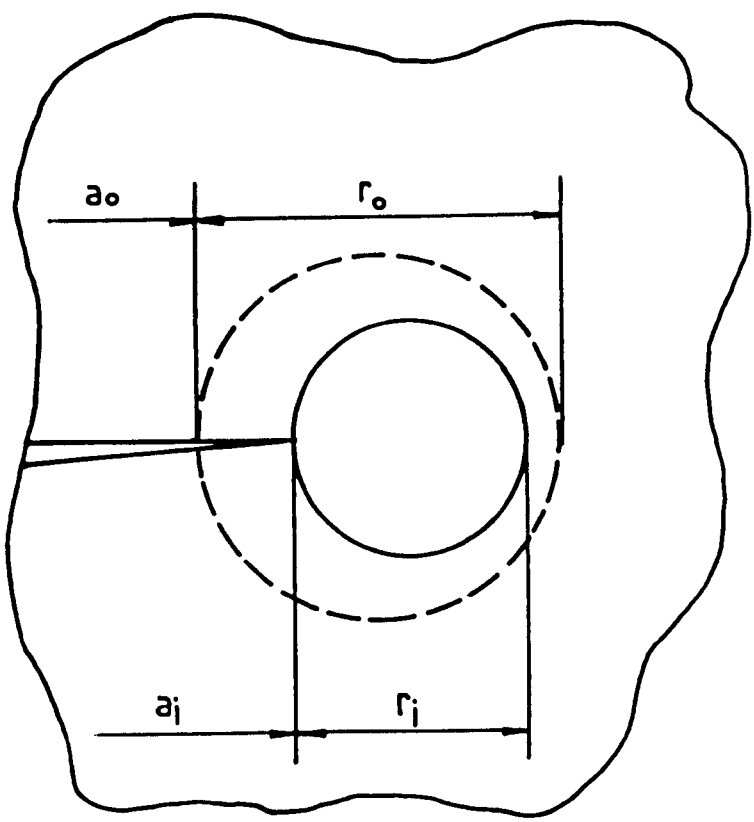

Fig 5.3

CHAPTER 6 PROBABILISTIC APPROACH TO FATIGUE CRACK GROWTH AND LIFE PREDICTION

A difficulty with fatigue analysis is the experimentally observed variance in crack growth rates and fatigue lives. This may be attributed to the variability in material properties, environment, and loading. These factors often occur simultaneously and the interaction between them produces a complicated picture. A knowledge of the mean crack growth rate or mean fatigue life is adequate for some engineering problems. But in other cases, the chance of premature failure is very important and the crack growth rate or the fatigue life must be treated as a random variable.

SECTION 1 Monte-Carlo Simulation

In an engineering design, the life of a structure in terms of number of cycles N can be defined by the loading, environment and material parameters which are random variables. Let these parameters be V_1, V_2 and V_3 respectively, then

$$N = f(V_1, V_2, V_3) \tag{6.1}$$

The random variables V_1, V_2 and V_3 may have normal, Weibull, or any

other kind of distribution, although in general, analytic expressions for the distribution of N are too difficult to be derived. However, a numerical approach can be used to determine the distribution of N. The general scheme is to use a digital computer to generate random numbers having the specified distribution, these numbers are used as the input of Eq 6.1 to give a random sample of N, so that the probabilistic distribution of N can be approximated by the "empirical" distribution produced from the sample. The general method is known as a Monte-Carlo simulation (Ref 134).

It can be seen that a wide range of probabilistic problems concerning fatigue can be solved by Monte-Carlo simulation, provided that the generated numbers follow the required distribution. It is easy to find a computer capable of producing random numbers uniformly distributed between 0 and 1. Let such a variable be x, it can be transferred into other kind of distribution through the mathematic technique called transformation (Ref 4).

The transformation involves two random variables x and y connected by y=f(x). The distribution of y can be deduced through the following relation if the distribution of x is known.

$$p_y(y) = \begin{cases} p_x(x) \left|\frac{dx}{dy}\right| & \text{when y is in a region corresponding to the x domain} \\ 0 & \text{other regions} \end{cases} \qquad (6.2)$$

To employ this equation, the reciprocal function $x=f^*(y)$, should be single valued. If not, the function can be treated separately in several intervals such that in any of the intervals it meets this

condition. The function y=f(x) can be manipulated to produce an appropriate distribution of y for Monte-Carlo simulation.

SECTION 2 Constant Amplitude Loading Cases

6.2.1 The Scatter in Crack Growth Rate

It is generally recognized that crack growth under constant amplitude loading exhibits sample variation (Refs 135 and 136). It is useful to provide a description of this situation in a probabilistic way rather than the usual mean crack growth rate against ΔK curve.

Virkler et al (Ref 135) have conducted 68 fatigue crack growth tests on a 2024-T3 aluminum alloy using constant amplitude loading. The general trend of the crack length a vs. N curves is shown schematically in Fig 6.1. The crack growth rate distributions were determined for a number of ΔK levels. Five probability models were used to fit the experimental data and the number of times that each model was selected as the best at a ΔK level was recorded. It was found that each model gave a fair but not outstanding performance in providing a fit to the experimental results, this was thought to be due to the large amount of variability existing in the experimental data. A Monte-Carlo simulation scheme was used to provide an prediction of the crack length a against the number of cycles N curve, in which the crack growth rate was simulated by computer generated random numbers satisfying the given distribution. It was

found that this scheme gave an accurate prediction of the mean crack length but did not describe the variance well.

6.2.2. The Possible Influence of Measurement and Data Processing Procedure

The differences in crack growth rate are probably mainly due to the variability of the material properties. The significance of the contributions from the measurement precision and data processing procedure has been studied by Wei et al (Ref 136) and others (Ref 137). In Ref 136, the Paris law was integrated using an experimentally determined α and n to yield an "error free" curve of a versus N, from which the practical measurements of the crack length a were simulated by introducing errors which were assumed to have normal distributions with the appropriate variances. The simulated data was then processed again to produce a Paris law expression. The difference between this expression and the original expression was therefore solely due to the measurement precision and the data processing procedure used. By comparing the two sets of data, the authors concluded that the measurement precision and the associated data processing procedure may contribute considerably to the variance in crack growth rate.

SECTION 3 Simplified Fatigue Life Distribution

It is a simple but useful idea to regard the fatigue life as a random variable having a specific distribution, and the problem of random fatigue life prediction is reduced to predict the controlling

parameters of the assumed distribution. There are two popular models: the log-normal and Weibull distributions.

6.3.1 Log-normal

This model assumes the logarithm of fatigue life has a normal distribution

$$p_{\ln N}(\ln N) = \frac{1}{\sqrt{(2\pi)}\ \sigma_{\ln N}} e^{-\frac{(\ln N - \mu_{\ln N})^2}{2\ \sigma_{\ln N}^2}} \qquad (6.3)$$

where $\mu_{\ln N}$ and $\sigma_{\ln N}$ are respectively the mean and the r.m.s of lnN. The advantage of this model in comparison to normal distribution is it does not allow negative values of fatigue life. In addition, it has been found experimentally that the distribution of life N has a long tail in the positive direction (Ref 122), thus the logarithm of the life has a more symmetric distribution which is closer to a normal distribution.

6.3.2 Weibull

The Weibull distribution has also been proposed to fit experimental data (Ref 5). It is sometimes used in preference to the log-normal distribution because of its flexibility, and is often expressed in a three parameter form as

$$P_N(N) = 1 - e^{-\left(\frac{N - N_0}{\beta}\right)^C} \qquad (6.4)$$

N is the random variable, N_o represents the minimum life, β and C are constants determined by curve fitting. When the minimum life is zero, it has a simpler form known as a two parameter Weibull distribution

$$P_N(N) = 1 - e^{-\left(\frac{N}{\beta}\right)^C} \qquad (6.5)$$

The Weibull distribution has been used in analysing fatigue data and predicting fatigue life (Refs 139 and 140) and transformation between Weibull and log-normal distributions has been discussed by Nash (Ref 141).

SECTION 4 Probabilistic Evaluation of Life Distribution

In order to develop probabilistic models of fatigue, it is invariably necessary to make some simplfying assumptions, which usually limit the general applicability of the models. Examples are now discussed.

6.4.1 Bogdanoff's Model

Bogdanoff (Refs 7 and 142) has proposed an interesting model for predicting the fatigue life distribution. Fatigue damage is assumed to be associated with various levels which increase from 1 to b with state b corresponding to failure or retirement. The probability of the component being in the jth level of damage after N cycles is represented as the jth element of a row vector p_N

$$p_N = [V_1, V_2, \ldots V_b] \tag{6.6}$$

At the start of the test, the probability of being in the failure state is assumed to be zero

$$p_0 = [V_1, V_2, \ldots V_{b-1}, 0\ ] \tag{6.7}$$

The fatigue loading is specified in terms of duty cycles. Each duty cycle represents a repetitive period of fatigue loading. The severity of the cycle is defined by a (b×b) matrix

$$C_f = \begin{bmatrix} C_{1,1} & C_{1,2} & 0 & 0 & \ldots\ldots & 0 & 0 \\ 0 & C_{2,1} & C_{2,2} & 0 & \ldots\ldots & 0 & 0 \\ & & & & \vdots & & \\ 0 & 0 & 0 & 0 & \ldots\ldots & C_{b-1,2} & C_{b-1,2} \\ 0 & 0 & 0 & 0 & \ldots\ldots & 0 & 1 \end{bmatrix} \tag{6.8}$$

in which $C_{i,j}$ are parameters determined from the loading. The elements satisfy the conditions: $C_{i,1} \geq 0$, $C_{i,2} \geq 0$ and to maintain the total probability to be unit, $C_{i,1} = 1 - C_{i,2}$. The fatigue process is assumed to be a Markoff process (Ref 143) in which the probabilistic characteristics of the future are independent of those in the past if the probabilistic characteristics for present are known. In other words, the probability distribution of damage states at the end of a duty cycle can be determined from that at the beginning of the duty cycle and the duty cycle itself. Thus the effect of applying a duty cycle on the distribution of damage states is modelled such that the probability of high damage levels is increased by multiplying the damage vector by the severity matrix.

$$p_j = p_{j-1}\ C_f \tag{6.9}$$

If the severity of the duty cycles is constant

$$p_N = p_o \, C_f^N \tag{6.10}$$

From this the cumulative distribution of failure as a function of cycles is given by the last element of the damage vectors, which can be represented as

$$P_{failure}(N) = V_b(N) \tag{6.11}$$

The model has been adjusted to consider the possibility that failure may take place in a number of damage states (Ref 142).

For cases in which the duty cycles are not the same, the probability distribution of damage can be determined by treating the duty cycles on a individual and average basis (Ref 144).

6.4.2. Lin and Yang's Model

Lin and Yang (Refs 145 and 146) have studied a model, in which the crack growth rate was presented as

$$\frac{da}{dt} = f(K, \Delta k, S, a, r) \, x(t) \tag{6.12}$$

where f was a function of the loading and the geometry which was taken to be the Paris law in the model. t is the time and x(t) a random variable introduced in the analysis. It was assumed that

$$x(t) = \sum_{k=1}^{N(t)} C_k \, w(t, \tau_k) \tag{6.13}$$

where N(t) is a homogeneous Poisson counting process, denoting the total number of pulses which arrive in the period $(-\infty,t)$. C_k is the random amplitude of the kth pulse which arrives at time τ_k (Ref 143). It can be seen that if x(t) is independent of the time, the model can be represented in statistical terms as a group of curves with different α values in the Paris law (Fig 6.2). When x(t) is a function of the time t, the model represents a situation in which α value changes with time, thus the sample curves of a vs. N mix up in a random manner similar to that observed in experiments, as shown in Fig 6.1.

The fatigue process is also assumed to be a Markoff process (Ref 143). Expressions have been given for the mean crack length and the distribution of crack length at a given time t (Ref 146).

6.4.3 Payne and Graham's Model

An analysis by Payne (Ref 147) and Payne and Graham (Ref 148) established a model for two distinct situations: the first is called ultimate load failure; the other is failure in service. In the first situation, the material resistance to cracking Q and the loading S_r are both considered to be random variables. The failure probability in the remaining population at the Nth cycle is specified as

$$\begin{aligned} \Pr[\text{ultimate failure}] &= \Pr[\, Q \prec S_r] \\ &= P_f(N)dN \\ &= p_f(N) \end{aligned} \qquad (6.14)$$

where the interval dN is taken as one cycle and $p_f(N)$ is the risk at

life N. If Q and S_r are both positive, $Q=S_r$ becomes the boundary between safety and failure in the first quarter of the coordinate system of Q and S_r, any points in the area between $Q=S_r$ and $Q=0$ represent failure, therefore

$$P_r(\text{failure}) = \int\int_{\substack{Q<S_r \\ Q\geq 0}} p_Q(Q,N)\, p_{Sr}(S_r)\, dQ\, dS_r$$

$$= \int_0^\infty p_Q(Q,N) \int_Q^\infty p_{Sr}(S_r)\, dQ\, dS_r \qquad (6.15)$$

It was assumed that p(Q,N) can be approximated by $p_Q(Q)$, which is appropriate only when crack growth is negligible. So that $p_f(N)$ is independent of N

$$p_f = \int_0^\infty p_Q(Q) \int_Q^\infty p_{S_r}(S_r)\, dQ\, dS_r$$

$$= \int_0^\infty p_Q(Q)\, [\, 1-P_{S_r}(Q)\,]\, dQ \qquad (6.16)$$

To obtain a non-dimensional expression let $z=Q/\mu_Q$ where μ_Q is the mean of Q, i.e the average level of resistance to cracking. μ_Q is supposed to be known from the design analysis. Eq 6.16 can be solved by assuming that z has a Gaussian distribution with mean μ_z and root mean square σ_z, and S_r is distributed as

$$P(S_r) = e^{-\frac{C_1}{S_u}(S_r - S_m)} \qquad (6.17)$$

where S_u is the ultimate load at failure, S_m the mean load and C_1 is a parameter introduced to adjust the equation to suit the real behaviour. The calculation leads to the final form

$$p_f=\left\{1-\Phi\left[\frac{C_m z^*-C_m(\mu_Z-C_1 C_m^2\ \sigma_Z^2\ )}{C_m\ \sigma_Z}\right]\right\}\ \exp\left[\frac{(C_1 C_m \sigma_Z)^2}{2}\ -\ C_1 C_m(\mu_Z-z^*)\right] \tag{6.18}$$

where

$$C_m\ =\ \frac{\mu_Z}{S_u} \tag{6.19}$$

and

$$z^*\ =\ \frac{S_m}{\mu_Z} \tag{6.20}$$

This is shown schematically in Fig 1.2.

The second situation is failure during service in which the influence of fatigue crack growth is pronounced. Again, failure during service was considered to have two forms: "static" failure caused by an overload which is beyond the capacity of the structure and failure due to "wear out". The second form represents a situation in which the residual strength is lost continuously under fatigue until the mean load can initiate the fracture. The total risk is the sum of the two

$$p_f(N)\ =\ p_t(N)\ +\ p_w(N) \tag{6.21}$$

where $p_t(N)$ and $p_w(N)$ are the failure rates of the first and the second type respectively. Let L denote the degree of "wear-out" and be defined as

$$L = \frac{a}{a_f} \tag{6.22}$$

where a_f is the critical crack size at which the second mode failure takes place. Since the relative wear-out after a number of cycles N is a random variable, the risk of static failure is

$$p_t(N) = \int_0^{L_f} p_S(N|L)\, P_L(L)\, dL \tag{6.23}$$

$p_t(N|L)$ is the probability density function when the relative wear-out is L. L_f corresponds to the value of L at fracture.

In comparison with ultimate load failure, it is clear that static failure is simply ultimate failure at different wear-out levels. Therefore, let $z(L)=Q(L)/\mu_Q(L)$

$$p_W(N) = \int_{z_o}^{\infty} p_W(N|z)\, P(z)\, dz \tag{6.24}$$

where z_o is the lower limit of z and $p_W(N|z)$ is the probability density function of failure at the relative residual strength z when the wear out is L. Eq 6.24 is true only under the assumption that P(z) is the same for all L, although such an assumption is unlikely to be appropriate for most practical fatigue situations.

Combining Eqs 6.23 and 6.24 gives the risk of failure. When applying these equations, a large amount of input data is required as illustrated in Ref 149.

An additional model by Shin and Lukens (Ref 39) is described in Section 3 of Chapter 3. All the statistical models require a large

number of input data and can be very sensitive to the input, thus it is hard to verify them. This is one of the reasons why none of these probabilistic models has been generally accepted.

LIST OF FIGURES FOR CHAPTER 6

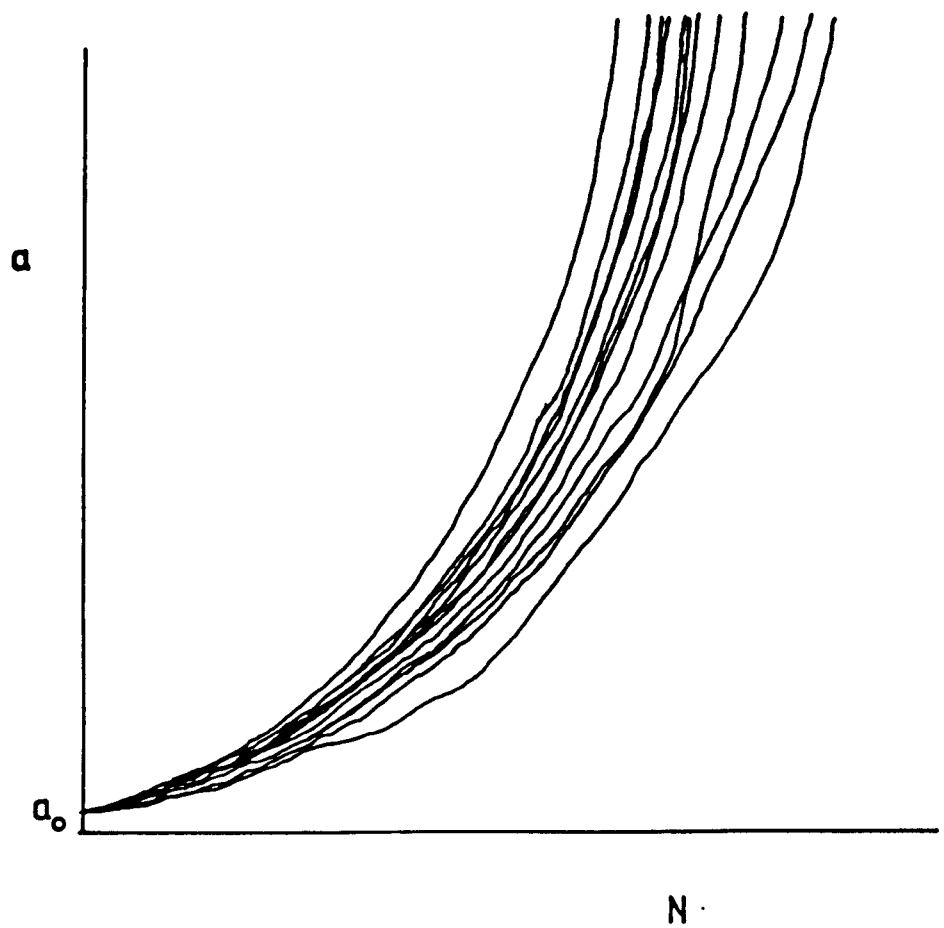

Fig 6.1

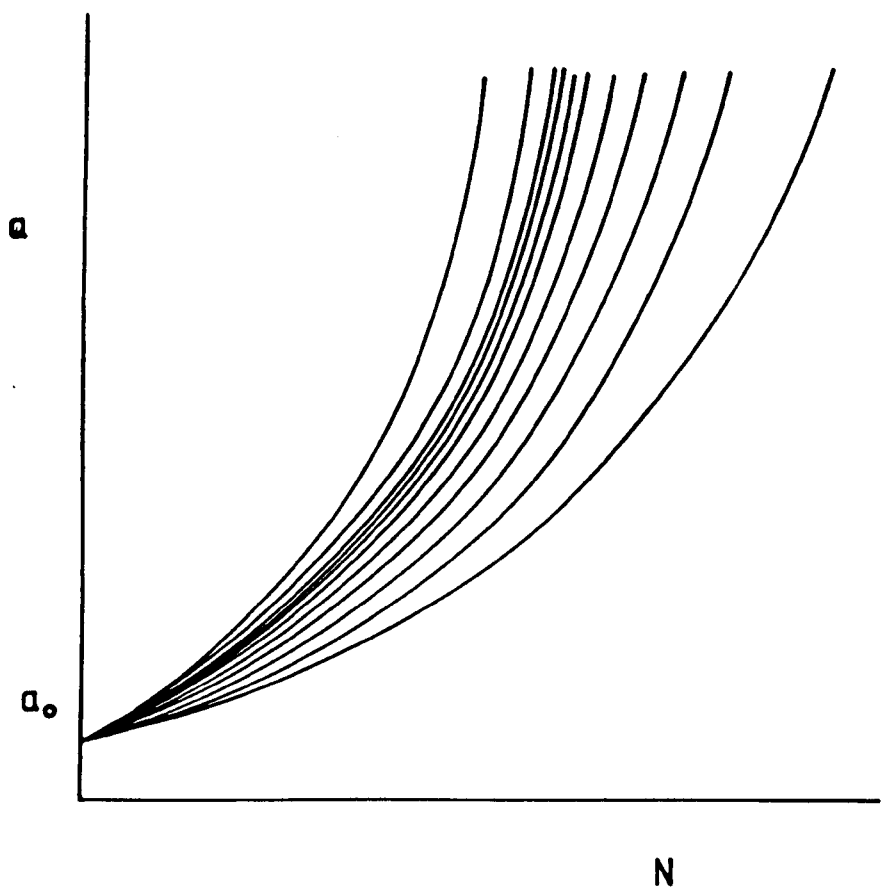

Fig 6.2

CHAPTER 7 THE STRESS ANALYSIS OF TUBULAR WELDED JOINTS

In offshore structures, the connections between the tubes are critical areas where a stress concentration is inevitable. A static or fatigue assessment of the reliability of such tubular joints requires a description of the stress state which is often characterized by the stress concentration factor. Such information can be obtained using analytical, numerical and experimental methods. The procedures used and the results achieved are now discussed.

SECTION 1 The Representative Stress and Strain

Welded tubular joints used in offshore structures can be generally classified as T, K, X, TK and V types. Fig 7.1 shows a T joint with the definitions of its geometrical parameters α, β, τ and γ. The horizontal member in Fig 7.1 is denoted the chord, and the vertical member is the brace. A loading applied to the end of the brace can be generally represented by the combinations of the three basic cases, namely axial loading, in plane bending and out of plane bending (Fig 7.2).

The stress concentrations for all loading modes occur in the brace-chord intersection. The maximum stress arises from three main sources (Ref 150): the basic response of the joint to the load (nominal stresses), the stress due to maintenance of compatability between tubes (geometric stresses) and the stress caused by the local geometry, such as the weld profile (notch stresses). It seems reasonable to use the maximum stress to characterize tubular joints. However, the maximum stress appears in a region where the stress gradient is very steep, and is thus experimentally difficult to measure and reproduce. Furthermore, the notch stress is probably only pronounced near the surface. During the fatigue life of the joint, cracks are inevitably developed in the intersection area and as the cracks grow into the wall the notch stress decays rapidly. Therefore, the maximum stress is expected to determine the site where fatigue cracks are initiated, but its subsequent effect on the growth rate of part-through cracks is debateable.

An alternative to the maximum stress is the "hot spot stress" or "hot spot strain". Based on the observation that the stress distribution is fairly linear in a area near the chord-brace intersection, the "hot spot stress" is defined to be the principal stress extrapolated from this region to the weld toe. It is hoped that the hot spot stress excludes the effect of the notch stress and represents only the nominal and the geometric stresses. In tests of steel models, the linear extrapolation of the stress can be achieved from two strain gauges mounted at positions (indicated in Fig 7.3) recommended by the E.C.S.C. Technical Working Party (Ref 150). These points can be described in terms of the dimensions of the joint

(given in Fig 7.1) as follows:

A. At the saddle on the chord side: a point the greater of 0.2√rt or 4mm from the weld toe and a point which is a 5° arc of the chord away from the weld toe.

B. At the crown on the chord side: a point the greater of 0.2√rt or 4mm from the weld toe and a point 0.5√Rt from the weld toe.

C. At the saddle and crown on the brace: a point the greater of 0.2√rt or 4mm from the weld toe and a point 0.65√(rt) from the weld toe.

Due to the high stress concentration at the wall surface near the chord-brace intersection, yielding may take place, therefore the extrapolated hot spot strain is sometimes used in preference to the hot spot stress (Ref 151).

SECTION 2 Theoretical Consideration of the Stress Distribution

The tubular joints used in offshore structures can be regarded as a particular kind of shell. The ratio of thickness to the radius of the tube is usually less than 1/20, and thin shell theories are applicable. Thin shell theory involves two assumptions, which are that the deflections are small compared to the thickness, and the plane sections through a shell, taken normal to the midsurface, remain normal to the deformed midsurface. The stresses in a thin shell can be viewed as the combination of the membrane stresses and

the bending stresses (Refs 152 and 153). A membrane is identified as a body of the same shape as the shell, but incapable of withstanding moments or shear forces. A complete analysis comprises a membrane solution, adjusted by accounting for the effect of bending in those areas where there are abrupt changes in geometry or loading. The superposition of the membrane and bending stresses results in a linear distribution of stress across the shell wall from which the forces and moments are easily identified as shown in Fig 7.4.

For a single tube, when the applied load is axisymetric with respect to its central line, the solution is simple. Under general loading the effect of bending must be recognised. For a tubular welded T joint, there have been attempts to determine the stresses in an analytic way, for example, by Scordelis and Bouwkamp (Ref 154). It is possible by conventional shell theory to assess the stress in a half circular shell segment subjected to a point force loading or displacement loading. This situation becomes a tube under a point loading by adding another half shell to the original half and defining the boundary condition between the two halfs by an appropriate Fourier series. A tubular T joint has been modelled as a tube subjected to a group of point loadings which represent the effect of the brace. It was considered that the effect of the brace was best represented by a forces which produce a uniform displacement along the intersection. The stress field under a group of point displacements was determined by superimposing the streses in the tube under individual point displacements. It can be seen that analytical methods do not give a good simulation of the connections between tubular members and the stress distribution

calculated in the intersection area is not expected to be accurate.

SECTION 3 Numerical Methods for Shell Analysis

The finite element method is the most successful numerical approach to problems involving complicated geometries and loadings. The basic principles of this technique remain unchanged from the early description given by Zienkiewicz (Refs 66 and 155). To begin with, the method may be viewed as an implementation of the principle of minimum potential energy. If the potential energy U_p for a system is defined as the strain energy U_e stored in the material minus the work done by the external forces W

$$U_p = U_e - W \tag{7.1}$$

The principle of minimum potential energy indicates that the change in potential energy due to an arbitrary infinitesimal increment of displacement is zero

$$\delta U_p = \delta(U_e - W) = 0 \tag{7.2}$$

This concept can be applied to any elastic situation provided that the potential energy is expressed in terms of displacement. In finite element analysis, the solid continuum is firstly discretized by a number of elements connected at their hypothetical inter-element boundaries. Within each of these elements the displacement pattern related to the movements at the nodes is given which automatically satisfies the compatibility condition between

and inside the elements. The stresses may not satisfy the equilibrium condition but when the size of the elements become small, this condition is approached. This is why, as the number of the elements increases and the size of the elements decreases, the results generally converge to the true values. The potential energy corresponding to an individual element can be expressed by its nodal displacements, after suming all these, the potential energy for the whole continuum can be obtained in the form

$$U_p = U_p(d_{11}, d_{12}, d_{13}, d_{14}, d_{15}, d_{16}, d_{21}, \ldots) \qquad (7.3)$$

where d_{ij} is the displacement of the ith node in the jth degree of freedom. Because of the arbitrary nature of the virtual increment of the displacements, the application of Eq 7.2 to each individual degree of freedom at the nodes produces a equation. The total number of the equations is thus the same as the number of the degrees of freedom in the problem and the equation set can be written as

$$[M]\ \{V\} - \{F\} = 0 \qquad (7.4)$$

Here {V} is the vector representing the nodal displacements and {F} is the vector representing the external loading applied at the nodes. [M] is known as the global stiffness matrix. In stead of carrying out the differentiation given by Eq 7.2, the global stiffness matrix is often constructed from element stiffness matrix which is produced by considering the relation between the nodal force and displacement in the element. The equation set can be solved for nodal displacement which are then used to calculate the

stresses and strains in the elements.

The elements described above are known as the displacement elements which are based on assumed displacement patterns. There are elements known as equilibrium elements which are based on assumed stress functions while hybrid elements are based on both assumed stress and displacement patterns (Ref 156). However, the displacement element is the most successful and popular kind for elastic analysis. For the analysis of stresses in tubular welded T joints, the finite elements can be constructed using the procedure described above combined with shell analysis to simplify the process.

SECTION 4 Experimental Methods

To determine the stresses in tubular joints, the most commonly used experimental methods involve strain gauging steel or acrylic models and photoelastic techniques. These methods have different advantages and can be used to conduct a check on any numerical solution.

7.4.1 Strain Gauge Tests on Steel Models

Strain gauges can be bonded to points of interest in steel tubular joints. By measuring the change of the gauge resistance, the strain at the points can be determined. Steel models may be fabricated by the standard procedures to produce very realistic results. However, such experiments are expensive and the steel models tested to determine the static stresses are usually used for fatigue

experiments at a later date (Ref 34).

7.4.2 Strain Gauge Tests on Acrylic Models

The use of acrylic models in static tests has a number of advantages notably that the material is cheap and the model can be manufactured rapidly. Other advantages are that only small loads and simple facilities are required for the test due to the low Young's modulus of the material, and that welds can be modelled by gluing acrylic strips according to the weld shape. Seeing these advantages, Wordsworth and Smedley (Ref 157) and Wordsworth (Ref 158) have made an extensive use of acrylic models.

7.4.3 The Photoelastic Method

The value measured by a strain gauge is an average strain in the area covered by the gauge. Thus it can not produce accurate results in a region where sharp stress gradients occur. Photoelastic methods can be used to overcome this difficulty, which is why photoelastic techniques are frequently utilized to analyse the effect of welding profile and thickness of the tube wall on the stress field in the weld (Ref 159).

SECTION 5 Stress Concentration in Tubular Joints

In linear elastic structures, the hot spot stress is proportional to the applied external loading. To be generalise, a stress concentration factor C_s is introduced to characterize the response

of a tubular welded joint under external loading

$$C_S = \frac{S_{hot}}{S_n} \tag{7.5}$$

where S_{hot} is the hot spot stress at the chord-brace intersection and S_n the maximum nominal stress in the brace remote from the joint. Since the hot spot stress excludes the notch stress due to the weld, the stress concentration factors are functions of only the geometrical parameters.

$$C_S = C_S(\alpha, \beta, \gamma, \tau) \tag{7.6}$$

For a T joint under axial loading or out of plane bending, the hot spot is at the saddle point, while in the case of in-plane bending, the hot spot is at the intersection somewhere between the saddle and the crown. In most cases, the hot spot is at the chord side of the intersection (Ref 157).

An early investigation into the stress concentration factors of tubular joints carried out by Kuang et al (Ref 160), which covers not only T joints, but also K and KT joints. The hot spot stress was evaluated by extrapolating to the brace-chord middle surface intersection. The calculated stress concentration factors have been utilized to deduce parametric equations in terms of the geometric parameters. For stress concentration factors calculated from the principal stress extrapolated from the chord side in T tubular welded joints, the equations are

$$C_S = 1.177(2\gamma)^{0.808}\, e^{-1.2\beta^3}\, \tau^{1.333}(\alpha/2)^{0.057}$$

(Axial load) (7.7)

$$C_S = 0.41(2\gamma)^{0.6}\ \beta^{-0.04}\ \tau^{0.86}$$

(IPB) (7.8)

$$C_S = 0.465\ (2\gamma)^{1.014}\ \beta^{0.787}\ \tau^{0.889}$$

(OPB, $0.3<\beta<0.55$) (7.9)

$$C_S = 0.199(2\gamma)^{1.014}\ \beta^{-0.619}\ \tau^{0.889}$$

(OPB, $0.5<\beta<0.75$) (7.10)

Gibstein (Ref 161) has carried out extensive finite element analyses of tubular welded T joints under the three basic loading conditions. Consideration has been given to the stress concentration factor at the brace side and chord side separately, thus two sets of parametrical formulae are produced. The set for chord side is

$$C_S = [1.5 - 3.88(\beta-0.47)^2]\gamma^{0.87}\ \tau^{1.37}\ (\frac{\alpha}{2})^{0.06}$$

(Axial load) (7.11)

$$C_S = 1.65-1.1\ (\beta-0.42)^2\ \gamma^{0.382}\ \tau^{1.05}$$

(IPB) (7.12)

$$C_S = [1.01-3.36\ (\beta-0.64)^2]\ \gamma^{0.952}\ \tau^{1.18}$$

(OPB) (7.13)

The stress concentration factors have also been determined from acrylic modelling (Ref 157) by Wordsworth and Smedley. Parametric formulae for the hot spot stress concentration factors in T tubular joints were produced from these experimental results.

$$C_S = \gamma \tau \beta (6.78-6.42 \beta^{1/2})$$

(Axial, saddle position, chord side) (7.14)

$$C_S = 0.75 \gamma^{0.6} \tau^{0.8} (1.6\beta^{1/4} - 0.7\beta^2)$$

(IPB, crown position, chord side) (7.15)

$$C_S = \gamma \tau \beta (1.6-1.15 \beta^5)$$

(OPB, saddle position, chord side) (7.16)

LIST OF FIGURES FOR CHAPTER 7

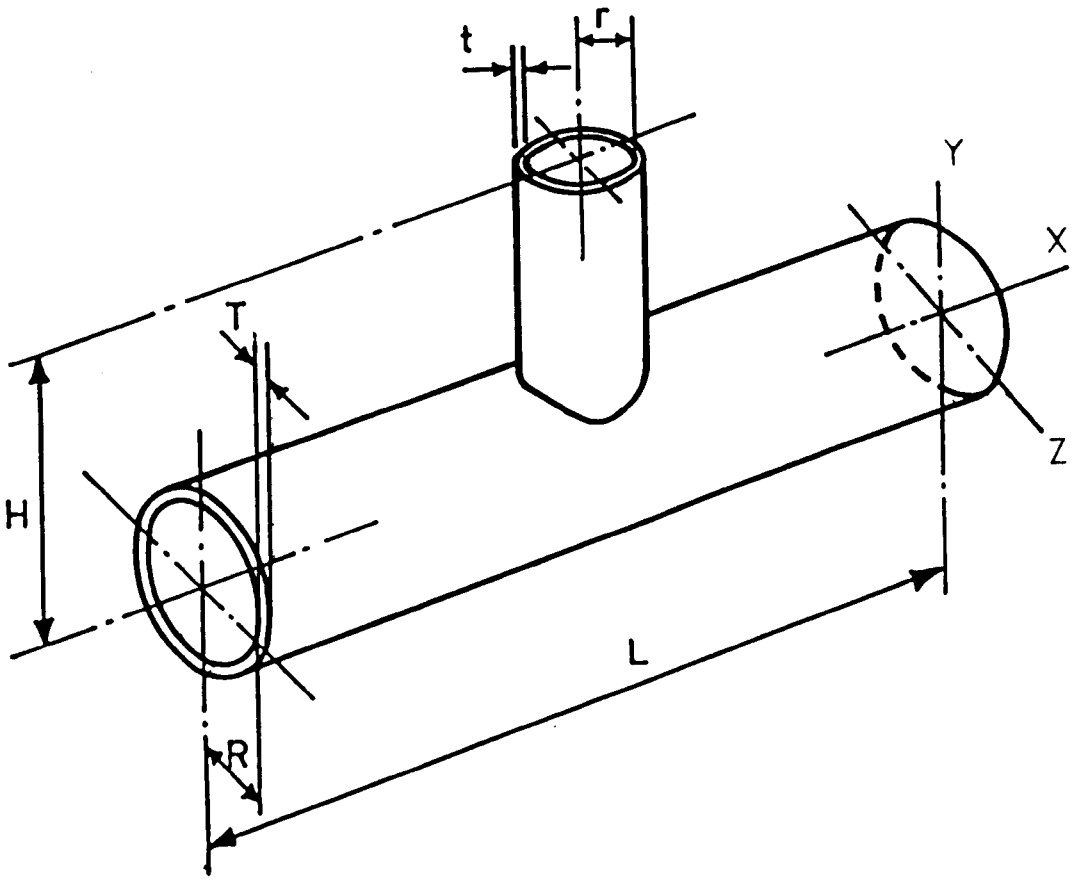

$$\tau = \frac{t}{T} = 0{\cdot}79$$

$$\beta = \frac{r}{R} = 0{\cdot}71$$

$$\gamma = \frac{R}{T} = 14{\cdot}4$$

$$\alpha = \frac{L}{R} = 10$$

Fig 7.1

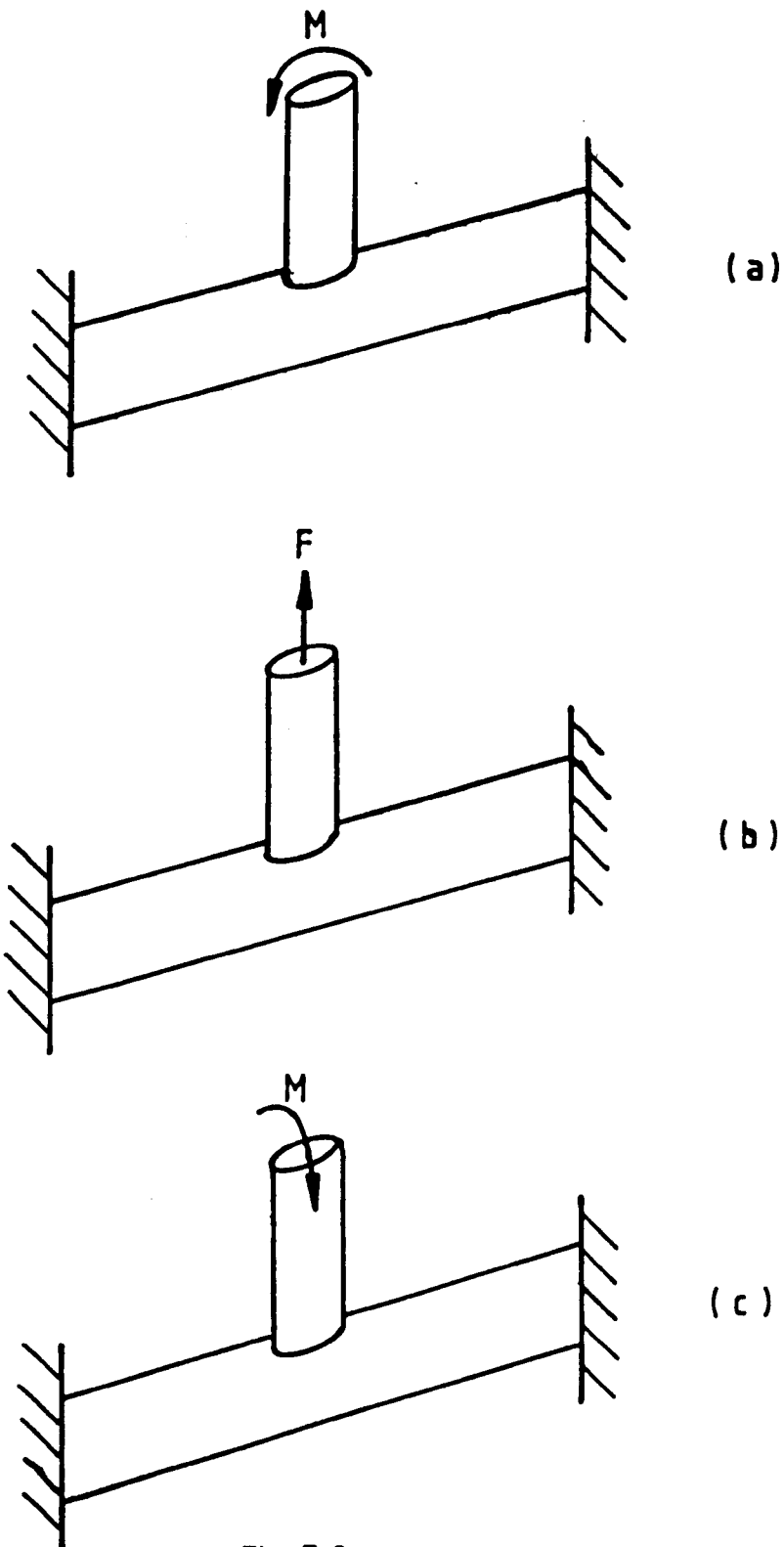

Fig 7.2

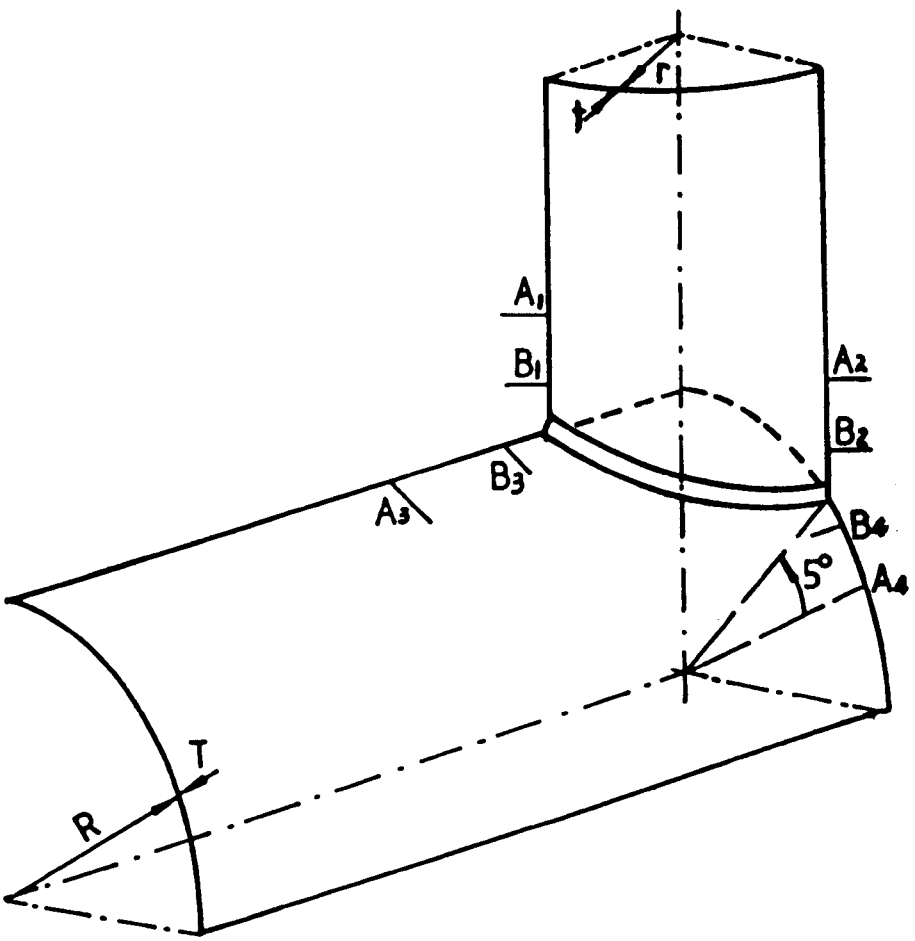

Fig 7.3

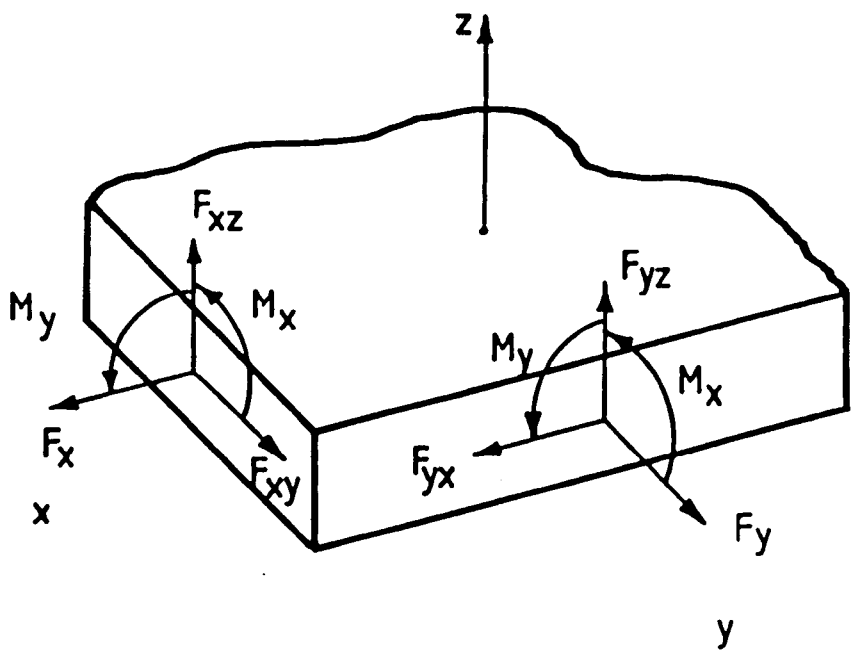

Fig 7.4

CHAPTER 8 THE ANALYSIS OF SURFACE CRACKS IN TUBULAR T JOINTS

In tubular welded joints, fatigue cracks are frequently initiated at the weld toe of the chord-brace intersection where a stress concentration occurs. The subsequent surface crack propagation takes up a large part of the fatigue life, which can be predicted using fracture mechanics if the stress intensity factor can be determined. The stress intensity factors K_I, K_{II} and K_{III} for many relatively simple cases have been evaluated and are well documented in handbooks such as Ref 43. However, the evaluation of the stress intensity factors for surface cracks in tubular T joints is a significant challenge, due to the complex geometry of the chord-brace intersection, the crack shapes and the load shedding caused by the cracks.

SECTION 1 The Influence of Weldment

The influence of the weldment on fatigue cracks in tubular welded joints should be considered at least for the crack initiation and early propagation stages. Extensive experimental fatigue studies have been carried out on various welded specimens (Ref 162) and a simple specimen particularly relevant to the geometry of tubular

joints is the cruciform weldment (Fig 8.1).

The crack initiation site and propagation route depend on not only the weldment, but also the loading. Fatigue cracks can initiate at the weld toe due to the stress concentration or at internal slag inclusions (Ref 163). Hayes and Maddox (Ref 164) have studied a through crack at the weld toe in a plate of a cruciform joint and the cracked plate was subjected to a tensile load (Fig 8.1). It was proposed that the stress intensity factor of the crack could be determined by introducing the front face correction C_f, back face correction C_b and stress concentration correction C_s

$$K_I = C_f\ C_b\ C_s\ S_n\ \sqrt{(\pi a)} \qquad (8.1)$$

Here S_n is the norminal stress in the load carrying plate. A finite element method was used to calculate the stress intensity factor of the through crack at the weld toe of the cruciform weldment which was compared with the stress intensity factor of a through crack in a plate of the same thickness T of the load carrying plate in the weldment. The difference between the two cases is the stress concentration. The results are shown in Fig 8.2, from which, it can be seen that the influence of stress concentration decreases rapidly as the crack becomes deeper. In addition, the angle of the fillet makes a small difference for the range of angles which commonly occur in engineering structures. Other finite element calculations confirmed this finding (Ref 165).

Fatigue cracks which initiate from the weld root (inside the fillet weldment) of a cruciform joint have been studied by Frank and Fisher

(Ref 166). This models the situation in which a fatigue crack results from lack of penetration during welding. The finite element method was used to evaluate the stress intensity factor, and the fatigue life of the weldment was predicted based on fracture mechanics.

SECTION 2 Fatigue Crack Development in Tubular Welded Joints

In tubular welded joints, the fatigue cracks often initiate at the weld toe near the maximum stress site of the chord-brace intersection. This can be explained (Refs 163 and 167) by the presence of small defects at the weld toe in the form of slag inclusions combined with the hot spot stress. The small defects are randomly distributed, thus the initial cracks may be formed anywhere in the hot spot region. These cracks have a high aspect ratio a/c and gradually coalesce to form a single crack of much lower a/c ratio as they propagate. Sometimes the early cracks are not in one plane and there are unbroken ligaments even at the end of the fatigue life.

At the surface the single crack propagates around the chord-brace intersection. In the thickness direction, the surface crack frequently does not grow perpendicular to the wall of the tube, but rather in an angle to it. This was observed in Delft University (Ref 101) and in University College of London (Refs 168). After penetration of the wall, the surface crack grows into a through crack along the whole length of the crack before any significant

growth occur in the length direction (Ref 167). Some propagation away from the intersection may also take place to form branches of the main crack.

The shape of the surface crack is important in the analysis of fatigue life. Unfortunately, this is subjected to some variability (Fig 8.3) due to the random growth behaviour of the crack. In an out-of-plane bending fatigue test (Ref 168), the crack depth a versus the number of cycles N was measured at five different points around the hot spot region of the welded chord-brace intersection (Fig 8.4). It was noted that when the crack was active at one point, it might be stationary at other points and the active area continually changed. Similar phenominon has been reported by Martin (Ref 169). Additionally, asymmetry in the distribution of cracks as well as stress distribution contribute to this variability. Evidence of the asymmetry can be obtained from fatigue tests (Ref 101) on a tubular welded T joint using constant amplitude axial loading, in which only one dominant surface crack was found on one side of the joint, while ideally, there should be a dominant crack on both sides of the joint since the configuration is symmetric.

The difficulty of describing the shape of surface cracks can be illustrated by the experimental data (Fig 8.5) published in a U.K.O.S.R.P project report (Ref 170). The aspect ratio a/c of cracks for the crack depth range $0.1 \leq a/T \leq 1$ covers virtually the whole range between 0.05 and 0.3

8.3.1 The Experiments

The experimentally observed development of semi-elliptical cracks in plates can indicate the stress intensity factor distribution along the crack profile. This has been utilized to check the accuracy of various numerical calculations (Ref 80). In principle, it is always possible to evaluate the stress intensity factors for surface cracks through their relation to the crack growth rate which can be measured in complicated geometries and loading cases, although the contributions from different crack modes can not be distinguished for a mixed mode problem.

Dover et al (Ref 171) have applied this method to surface cracks in tubular welded T joints. The relation between the crack growth rate and the stress intensity factor range was obtained from tests on standard fracture mechanics specimens made of the same material as the tubular joints (BS4360 50C steel).

$$\frac{da}{dN} = 1.09 \times 10^{-12} \quad \Delta K^{3.85} \qquad (8.2)$$

The fatigue loading was 5Hz sine wave with a stress ratio r=0. In comparison, the crack growth rate under a broad band random loading in a T pipe joint of the same material was determined experimentally

$$\frac{da}{dN} = 8.76 \times 10^{-12} \quad \Delta K_h^{3.29} \qquad (8.3)$$

where ΔK_h was calculated from the nth root of the nth moment of individual rises S in the local stress on the crack site

$$\Delta K_h = f(\frac{a}{T})\sqrt{(\pi a)}\ \left\{E[S^n]\right\}^{\frac{1}{n}} \qquad (8.4)$$

The local stress was estimated from a rosette about 8mm away from the weld toe and because the crack was very long, it was initially assumed to behave like an edge crack in the calculation of the stress intensity factor. The crack growth rates given by Eq 8.2 and 8.3 were regarded as similar. However, it was pointed out that (Ref 172), the load shedding effect in the joint must be accounted for when determining the stress intensity factor. This was achieved by adopting a different geometric calibration function f(a/T) which was taken as that of an edge crack in a plate under uniformly distributed constant displacement loading. In this case, f(a/T) decreases as the crack depth increases, while in the previous calculation f(a/T) was taken as a constant 1.12 (Ref 171). As a result, the stress intensity range became smaller and a better correlation between the data from the in situ measurement and from the test on precracked small specimens resulted (Fig 8.6).

8.3.2 The Results

The stress intensity factor for surface cracks in a tubular joint can always be expressed in the general form (Eq 4.7)

$$K_I = f(\frac{a}{T})\ S_h\ \sqrt{(\pi a)} \qquad (8.5)$$

where S_h is the hot spot stress and f(a/T) is a non-dimensional

geometrical calibration function which has been determined experimentally for tubular T, Y and K joints (Refs 173 and 174). f(a/T) can also be given in a slightly different form

$$K_I = Y_{st}\, Y_{sh}\, S_h \sqrt{(\pi a)} \qquad (8.6)$$

where Y_{st} and Y_{sh} were defined respectively as the correction factor for the load transfer and crack shape, which vary during the life of the tubular joint. The shape factor Y_{sh} was considered to be important only at the beginning of the life and was taken to be unity, therefore

$$f(\frac{a}{T}) = Y_{st} = \frac{K_I}{S_h \sqrt{(\pi a)}} \qquad (8.7)$$

Y_{st} for some tubular joints determined by fatigue tests have been presented as a function of the geometric parameters and stress concentration factors (Fig 8.7), and this allows a prediction of the stress intensity factor.

An analysis of the data of these experiments has shown that (Ref 173) the crack growth rate for a T joint under axial loading is higher than that under out of plane bending for a similar hot spot stress. The crack growth rate under axial loading was taken from the result of a constant amplitude fatigue test by Gibstein (Ref 175). It was concluded that hot spot stress alone is not adequate to describe crack growth in tubular joints. By further studies on the stress distribution in the intersection area, it was revealed that the average of stress concentration factor C_{av} over the chord-brace intersection is a significant factor. It has been found that the

experimentally inferred Y_{st} can be expressed as

$$Y_{st} = C_1 \left(\frac{a}{T}\right)^{C_2} \tag{8.8}$$

where C_1 and C_2 are constants for a given geometry and loading. The effect of C_{av} and C_s is accommodated in the determination of C_1 and C_2 through the relations

$$C_1 = 0.73 - 0.18 \frac{C_s}{C_{av}} \tag{8.9}$$

$$C_2 = 0.24 + 0.06 \frac{C_s}{C_{av}} \tag{8.10}$$

SECTION 4 Numerical Evaluation of the Stress Intensity Factor

The stress intensity factor calibration function f(a/T) can be determined both experimentally and numerically. Scott and Thorpe (Ref 176) have suggested that the load shedding and local compliance change due to a surface crack in a tubular joint are similar to that due to a crack in an infinite plate. Therefore, given that it is possible to model the surface crack by such a cracked plate, then the problem is to determine the relevant loading. In areas near the chord-brace intersection in a tubular joint, the stress distribution is not linear in the thickness direction, due to the local geometry. A further simplification is to assume that the plate model is subjected to a linear stress field. Strain gauging or two dimensional finite element analysis can be used to obtain information about the stress distribution in the joint from which the relevant load, which consists of a bending stress and a membrane

stress, can be determined.

In an analysis of a tubular Y joint (Ref 174), the ratio of the bending stress to the membrane stress was assumed to be constant at 4.73. Using the hot spot stress S_h, the stress intensity factor has been estimated. However which was consistently high in comparison with the experimental results (Fig 8.8).

It was argued that the hot spot stress represents the stress state at one point in the chord-brace intersection, but the influence of stresses in the rest of the chord-brace intersection areas need to be accounted for. The average stress concentration C_{av} over the intersection of the tubes (Eqs 8.9 and 8.10) was considered. Using the corresponding stress $S_n C_{av}$ as the loading applied to the infinite plate has improved the accuracy of the calculations. However, the average stress concentration treats equally the stress distribution away from and near to the hot spot and it was argued that the stresses nearer the hot spot, where the crack initiates, should have more influence. Therefore, a weighted average C_{wa} was proposed as

$$C_{wa} = \frac{E[e^{l}]}{l_1 - l_2} \int_{l_1}^{l_2} C_s(l)\, e^{-|l|}\, dl \qquad (8.11)$$

where l_1-l_2 is the region along the chord-brace intersection for which averaging is carried out, l is measured along the intersection from the hot spot. It has been shown that using C_{wa} gives the best result in the three calculations.

The weight function method of Oore and Burns (Ref 68) has also been employed for the evaluation of stress intensity factors of surface cracks in the same Y joint (Ref 174). The crack was assumed to be subjected to a stress field determined by using an assumed bending to membrane stress ratio and the surface stress distribution along the intersection between the tubes. The position of the crack in the stress field was chosen to correspond its actual position in the intersection, this implies that the deepest point of the crack was not necessarily situated at the point of maximum stress. The cracked area was divided into elements over which the integration (Eq 4.40) was performed numerically. The stress intensity factor determined by this method is better than all the three previous solutions using the infinite plate model.

LIST OF FIGURES FOR CHAPTER 8

Fig 8.1

A through crack at the weld toe of a cruciform weldment under axial loading.

Fig 8.2

The stress intensity factors of through cracks in a cruciform joint and a plat.

Solid line: edge cracked plate;

Broken line: cruciform joint of 45° fillet;

Dotted line: cruciform joint of 30° fillet.

Fig 8.3

A fatigue crack at different number of cycles in a tubular welded joint (Ref 174).

Fig 8.4

The crack depth a against the number of cycles N curve for five points in the hot spot area of a tubular welded T joint (Ref 168).

Fig 8.5

Crack development in tubular welded joints (Ref 170).

Fig 8.6

The load shedding correction of crack growth rate data.

The closed points are the data before correction;

The open points are the data after correction.

Fig 8.7

Experimentally determined f(a/T) as function of a/T for some T, Y and K joints (Ref 173)

a. K joint axial loading;

b. Y joint axial loading;

c. T joint axial loading;

d. Y joint in-plane-bending;

e. T joint out-of-plane bending.

Fig 8.8

Comparison between experimental data and the calculational results by Dover and Connolly (Ref 174).

A1: Using hot spot stress;

A2: Using average stress along the chord-brace intersection;

A3: Using weighted average stress along the chord-brace intersection;

A4: Using weight function method.

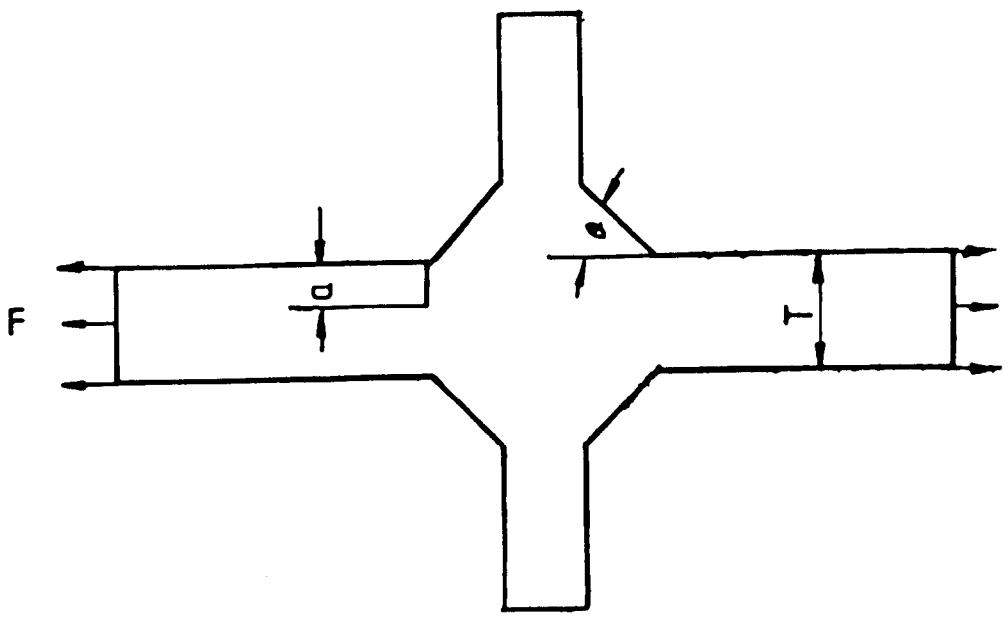

Fig 8.1

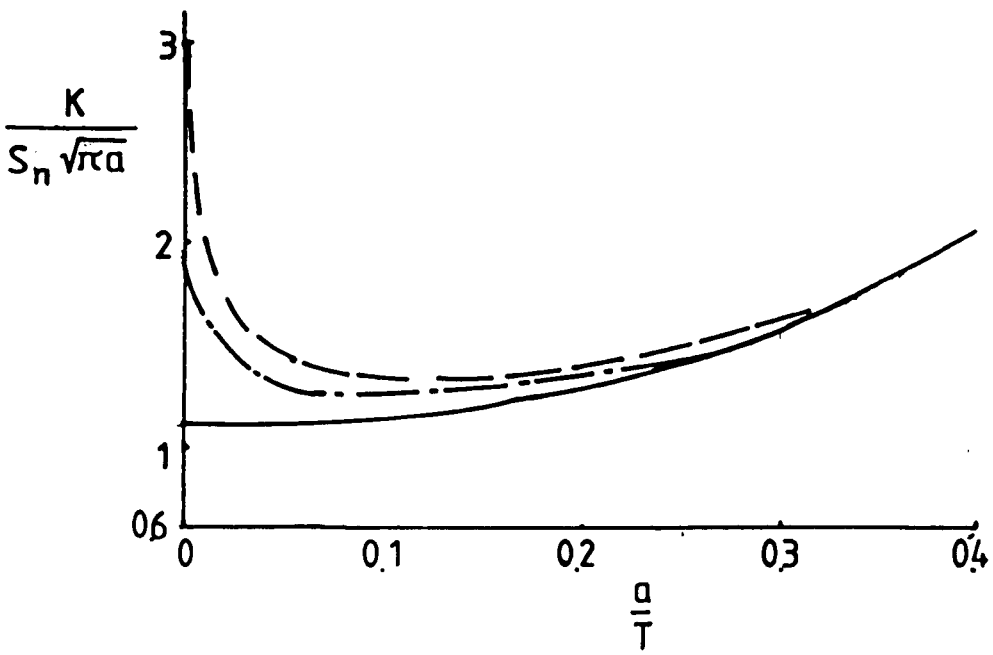

Fig 8.2

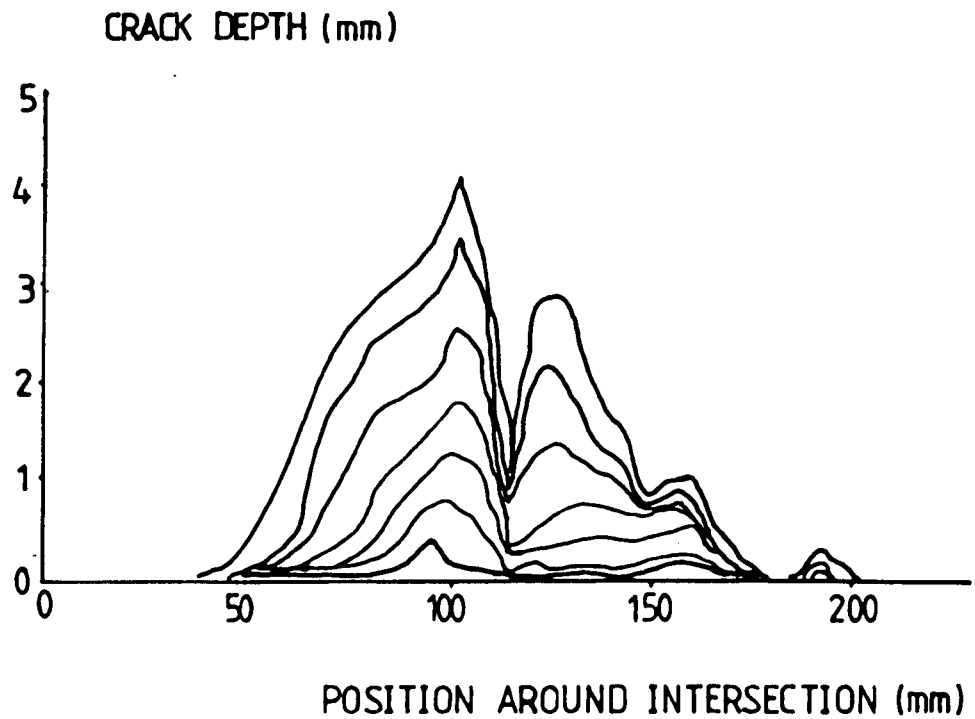
CRACK DEPTH (mm)
5
4
3
2
1
0
0
50
100
150
200
POSITION AROUND INTERSECTION (mm)

Fig 8.3

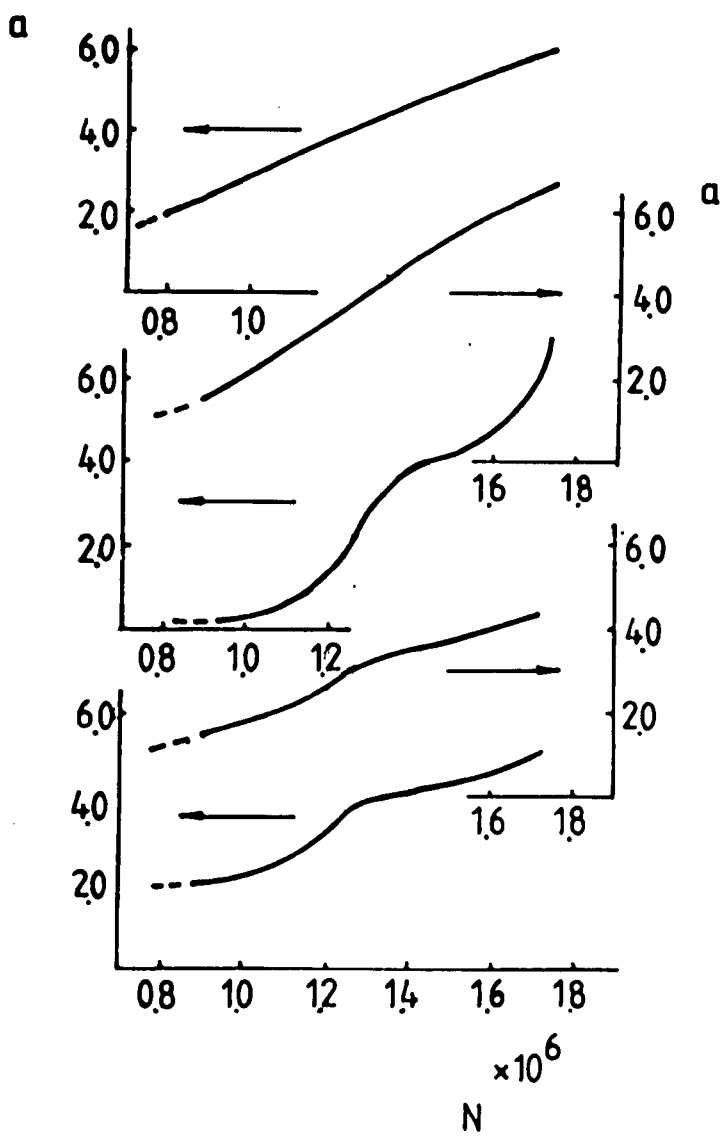
a
6.0
4.0
2.0
0.8
1.0
a
6.0
4.0
2.0
1.6
1.8
6.0
4.0
2.0
0.8
1.0
1.2
6.0
4.0
2.0
1.6
1.8
6.0
4.0
2.0
0.8
1.0
1.2
1.4
1.6
1.8
×10^6
N

Fig 8.4

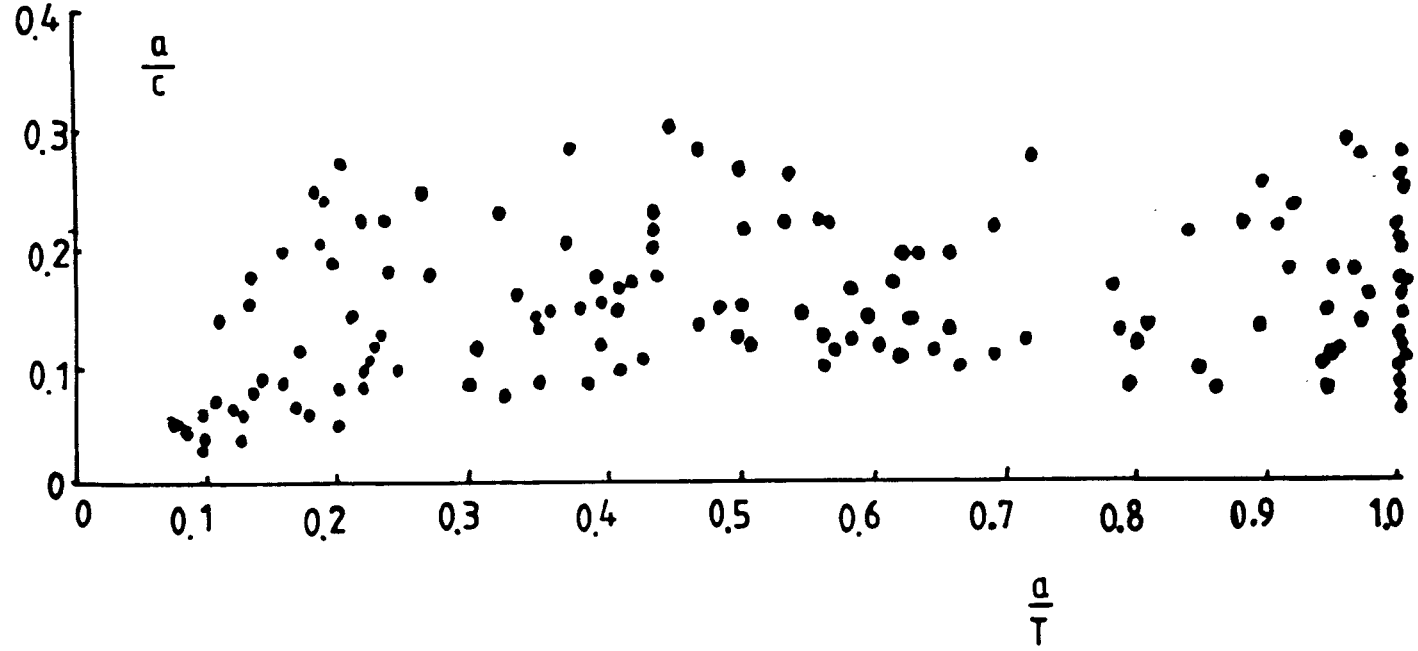

Fig 8.5

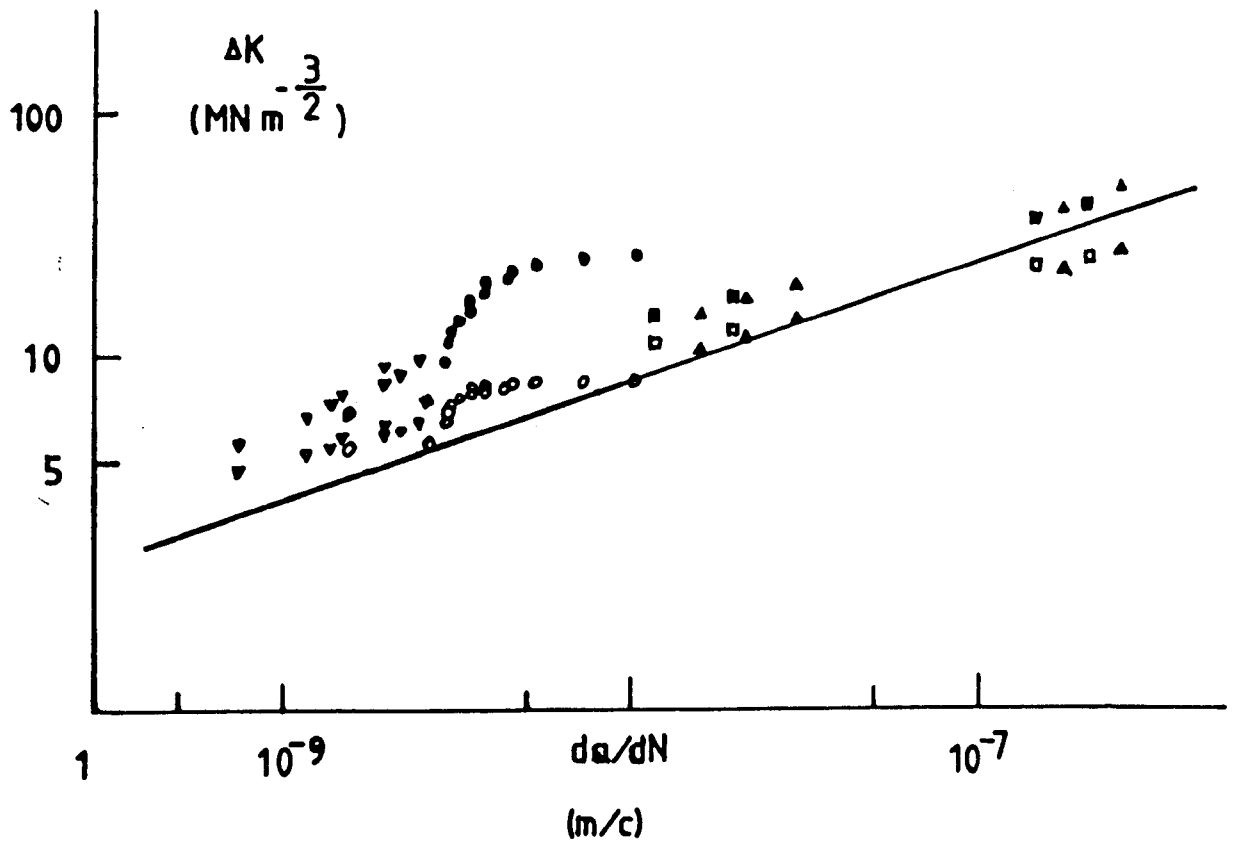

Fig 8.6

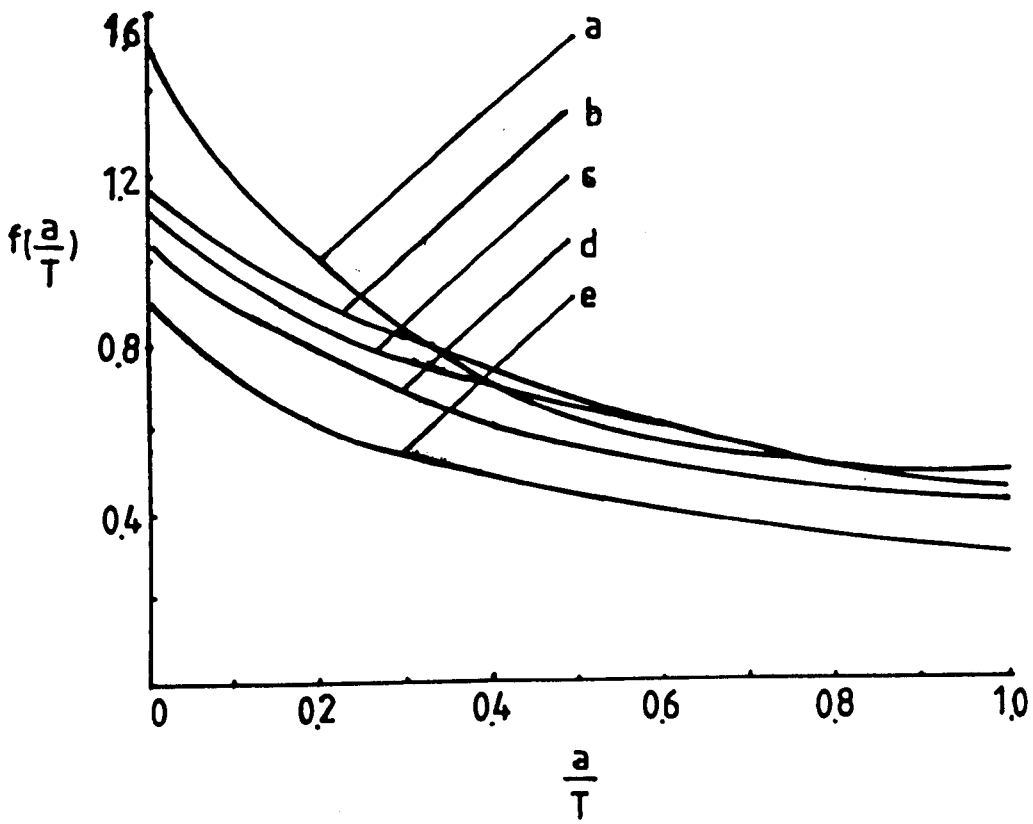

Fig 8.7

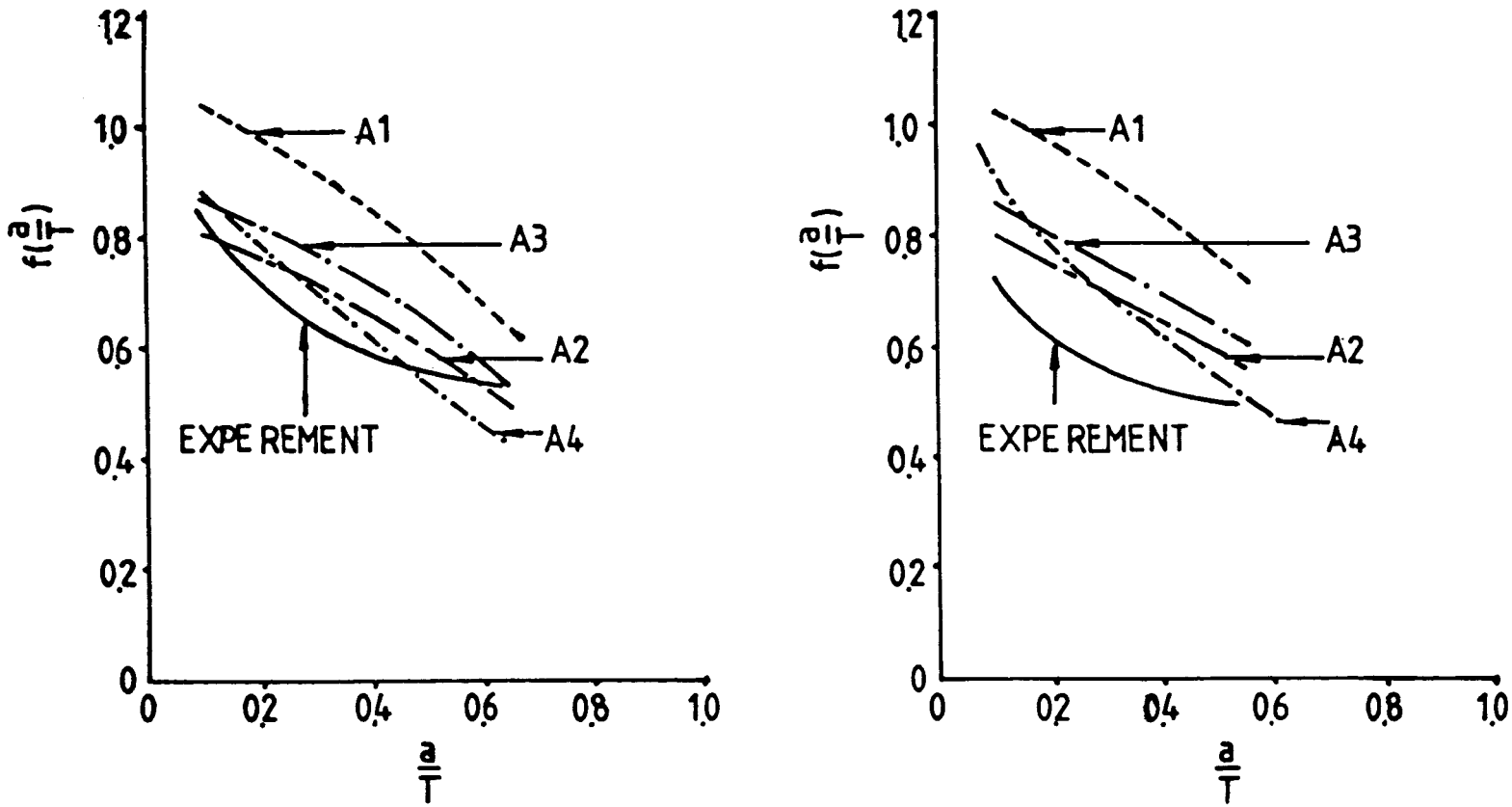

Fig 8.8

CHAPTER 9 LIFE PREDICTION OF TUBULAR WELDED T JOINTS

The ability to predict the fatigue life of tubular joints is very important in maintaining the safety of offshore structures. An enormous amount of work has been carried out for this purpose, as described in previous Chapters. However, procedures for predicting fatigue life are still under development and there are factors such as the influence of the marine environment which have yet to be precisely accounted for.

SECTION 1 Assessment of Fatigue Life Based on Miner's Law

Much of the philosophy of the design of tubular joints against fatigue is based on the conventional S-N curve approach in conjunction with Miner's law. Here S is taken as the hot spot stress range which is regarded as relevant to the stress state at which the most serious cracks in the joint initiate and propagate. This method needs a precise prediction of the load in the structure, the stress concentration factors in the joints and an appropriate S-N curve for welded tubular steel joints of realistic dimensions.

The experimental life of a large scale tubular welded joint consists of three parts: N_1 is the number of cycles to the appearance of a

visible crack; N_2 is the number of cycles to the penetration of the wall of the tube; N_3 is the number of cycles at the termination of the test which is often determined by the maximum displacement the testing machine can produce (Ref 167).

Experimental programs, such as the U.K. Offshore Steel Research Project, have accumulated data about the fatigue strength of steel joints. It was found (Ref 151) that fatigue strength of tubular joints decreases as the chord dimensions increases. This indicates that the hot spot stress range is not a very good parameter with which to correlate fatigue lives of tubular joints if there is a big difference in the scale of the joints. Some experimental data points from tests on models of realistic dimensions were found to be on the unsafe side of the American Welding Society S-N curve (Fig 9.1). McDonald and Wylde (Ref 151) have also demonstrated that the hot spot strain range can be used to characterize the fatigue strength of tubular joints. This is essentially the same as using the hot spot stress range when the material behaviour remains elastic. The argument is that when there is a plastic deformation, the hot spot strain range is a better parameter because it can indicate plasticity.

Fatigue experiments have increased the understanding of fatigue behaviour of tubular joints. As a result improvements on previous S-N curves such as the curve by the American Welding Society (Ref 25) have been made and new S-N curves and design guides are constantly being published (Ref 177).

SECTION 2 Assessment of Fatigue Life Based on Fracture Mechanics

In 1981, Clayton (Ref 178) outlined a fracture mechanics model of crack growth in tubular joints. The main requirements were recognized to be the stress distributions, including residual stresses, the initial flaw size and shape, the material behaviour and the effect of environment, while the crack shape variation during propagation and the stress redistribution due to the presence of the crack were regarded as part of the problem to be solved.

The work by Dover and co-workers was aimed at a scheme based on fracture mechanics for predicting the fatigue life of tubular welded joints (Refs 132 and 133). The large amount of information required for a complete fracture mechanics assessment model has inevitably at this stage led to simplifying assumptions, one of which usually concerns the initial crack size. Nevertheless, it has been found (Ref 179) that the initial size of the crack is not as sensitive to the fatigue life as was thought, due to the load transfer that prevents the crack growth from accelerating rapidly with crack length, and the high local stress concentration (include notch stresses) at the intersection which reduces the number of cycles for crack initiation.

A simple fracture mechanics model of Dover and Hildbrook (Ref 168) assumed the initial crack depth a_i to be 1mm. The end of the fatigue life was defined as the penetration of the chord wall, thus the fatigue life is determined by the crack growth rate which was

expressed as

$$\frac{da}{dN} = \alpha \ \Delta K^n \qquad (9.1)$$

where the constants α and n were determined by experiment on precracked simple specimens. For the BS 4060 50C steel, they are (Ref 168)

$$\left.\begin{aligned} \alpha &= 4.5 \times 10^{-12} \\ n &= 3.3 \end{aligned}\right\} \qquad (9.2)$$

ΔK was determined simply using the stress intensity calibration for an edge crack in a semi-infinite plate

$$\Delta K = 1.1 \ \Delta S_h \ \sqrt{(\pi a_i)} \qquad (9.3)$$

where a_i is the initial crack depth and ΔS_h the hot spot stress range. ΔK determined in this way is constant in the course of crack propagation for a constant loading test, and the crack growth rate given by Eq 9.1 is a constant, therefore

$$N = \frac{T - a_i}{\frac{da}{dN}} \qquad (9.4)$$

This has been called the linear model. It is claimed that the model can be modified if more information concerning the crack growth rate is available. Without giving verification, Dover et al (Ref 179) have suggested the following expression for predicting the fatigue life of 16mm chord thickness joints

$$N = \frac{T - a}{1.39\times10^{-13}\,(T-0.001)(T/0.016)^{0.75}(\Delta S_h)^3} \qquad (9.5)$$

A rather more complicated method was proposed by Dharmavasan and Dover (Ref 180). The fatigue life of a tubular joint was divided into 3 stages. In the first stage, the crack initiation defined as the period from the start of the test until a crack of 0.25mm deep is formed. This can be estimated by using strain-life data as proposed by Iida et al (Ref 181). The second stage involves crack growth from 0.25mm to 1.3mm deep. In this stage small thumbnail cracks coalesce to form a long semi-elliptical crack and the corresponding part of fatigue life can be substantial. The crack was treated as a edge crack in an infinite plate. Constant crack growth rate was assumed, which was determined by

$$\Delta K_h = 1.1\ \Delta S_h \surd(\pi a) \quad \text{but } a=0.25\text{mm} \qquad (9.6)$$

and the corresponding Paris crack growth law. The final stage involves the growth of a long semi-elliptical crack to wall penetration, ie. from a=1.3mm to T, the thickness of the wall. The estimation of this part of life was given by

$$\Delta K_h = Y_{st}\ \Delta S_h \surd(\pi\ T/2) \qquad (9.7)$$

and the fatigue crack growth rate of the material. Here Y_{st} is a function of a/T which can be estimated by Eq 8.10. The stress intensity factor range is again constant. This bi-linear model provides a better description of the relation between crack depth and the number of cycles than the linear model (Fig 9.2).

LIST OF FIGURES FOR CHAPTER 9

Fig 9.1

The experimental data (Refs 151 and 176) for tubular T joint of chord diameter of 914mm and thickness 32mm, in comparison with a AWS S-N curve.

Fig 9.2

Experimentally observed crack depth a against the number of cycles curve, with "linear" and "bi-linaer" models (Ref 180)

The brocken line represents the linear model;

The doted line represents the bi-linear model;

The solid line is experimental data.

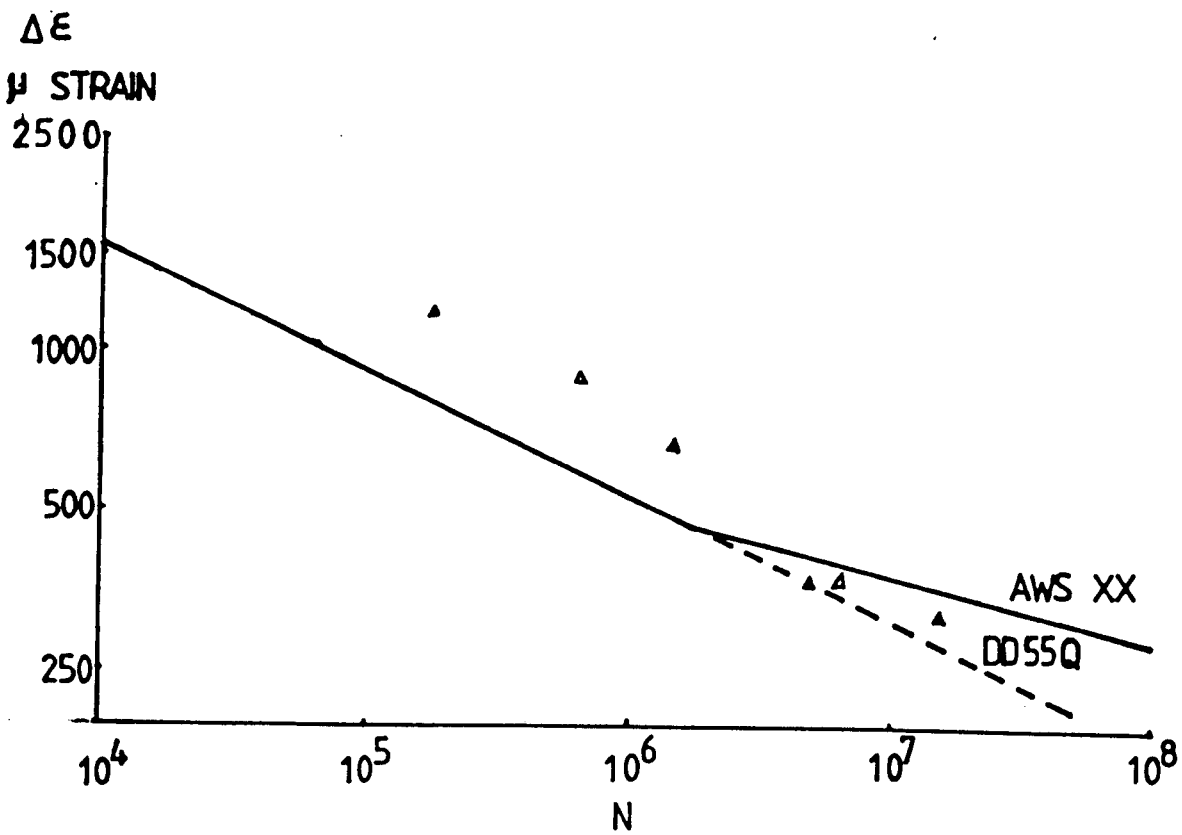
Δε
μ STRAIN
2500
1500
1000
500
250
AWS XX
DD55Q
10^4
10^5
10^6
10^7
10^8
N

Fig 9.1

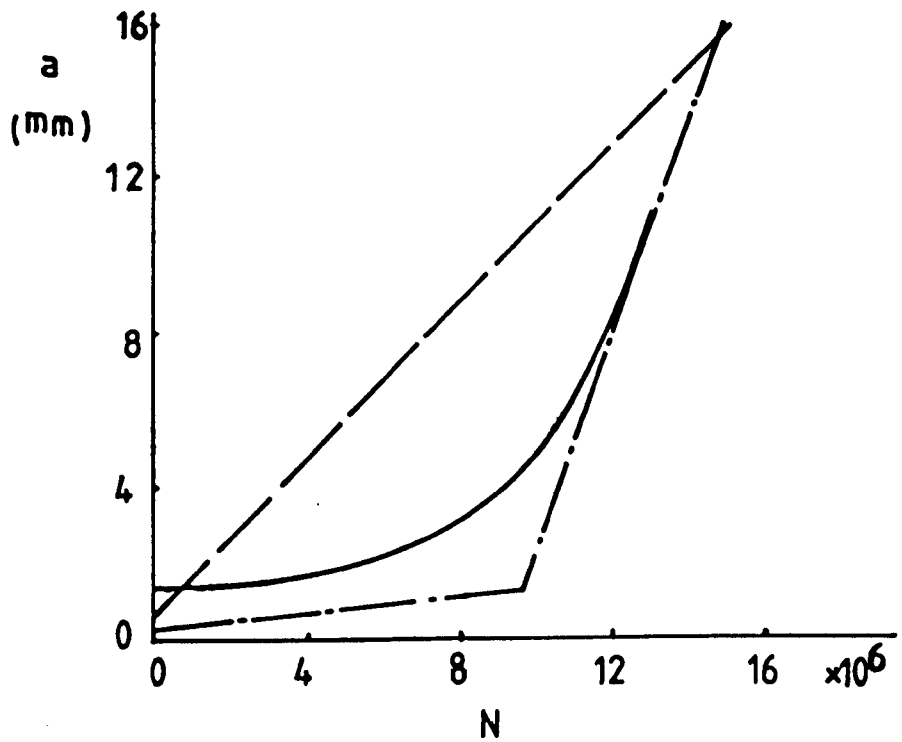

Fig 9.2

CHAPTER 10 PROBABILISTIC ANALYSIS OF FATIGUE RELIABILITY

It has been shown in previous chapters that the analytic methods for assessing fatigue reliability have explicit and implicit assumptions. Since each set of asssumptions may only suit a particular situation, or a particular group of tests, care must be taken when applying these methods. It is believed that for offshore structures, random loading and the variance of material properties are two major factors which contribute to the scatter of the fatigue life. A method which incorporates these factors in fatigue life calculations was not available and has been developed in this work. The new method has been designed to be analytic and adaptable to a wide class of problems; to require simple input data and to account for as many parameters as possible. The development of this model is described in the current chapter.

SECTION 1 Crack Growth Rate due to Random Loading

In structures such as oil platforms, a basic mode of damage is crack propagation. The present analysis therefore neglects crack initiation and considers only fatigue crack growth. Generally, it is recognised that the crack growth rate is related to the stress intensity factor representing the stress field at the crack tip. A

widely known and simple form for the relation has been given by Paris and Erdogan (Ref 107)

$$\frac{da}{dN} = \alpha\ (\Delta K)^n \qquad (10.1)$$

which has been adopted for the present study. ΔK is the stess intensity factor range which can always be expressed in the form

$$\Delta K = f(\frac{a}{w})\ S\ \sqrt{(\pi a)} \qquad (10.2)$$

where $f(a/w)$ is a function of the geometry of the component and the crack length while S is the stress range for narrow band or constant amplitude loading. For broad band loading, the stress range S can be obtained from a cycle counting method.

In the following text, f will be used instead of $f(a/w)$ for reasons of brevity. The crack growth rate then becomes

$$\frac{da}{dN} = \alpha \left[\ fS\sqrt{(\pi a)}\ \right]^n \qquad (10.3)$$

For generality, the equation is written in a non-dimensional form in which the crack length is normalized in respect of its initial size a_o, the stress range S with respect to the root mean square of the signal σ

$$\frac{d(a/a_o)}{dN} = \lambda\ f^n\ \pi^{\frac{n}{2}}\ (\frac{S}{\sigma})^n\ \ (\frac{a}{a_o})^{\frac{n}{2}} \qquad (10.4)$$

Here λ is a non-dimensional value defined as

$$\lambda = \alpha\ \sigma^n\ \ a_o^{\frac{n-2}{2}} \qquad (10.5)$$

Since the applied stress range at any instant is a random variable,

the crack growth rate at a specific crack length is also a random variable whose average value is denoted as $E[^{da}/_{dN}]$, from Eq 10.4

$$E[\frac{d(\frac{a}{a_o})}{dN}] = \lambda f^n \left[\pi \frac{a}{a_o}\right]^{\frac{n}{2}} \int_0^\infty (\frac{S}{\sigma})^n p(\frac{S}{\sigma}) d(\frac{S}{\sigma}) \qquad (10.6)$$

The integration involves a non-dimensional nth moment of the stress range which can be evaluated if the distribution of the ranges is known. For the distribution given by Hancock and Gall (Ref 21)

$$p(\frac{S}{\sigma}) = \frac{\gamma}{(\sqrt{2}\ \gamma)^\gamma} (\frac{S}{\sigma})^{\gamma-1} \exp[\ -(\frac{S}{\sqrt{2}\gamma\sigma})^\gamma] \qquad (10.7)$$

where γ is a function of the power spectral width parameter ϵ (Eq 2.23), the nth moment can be expressed as

$$\mu_n = E[(\frac{S}{\sigma})^n] = (\sqrt{2}\gamma)^n\ \Gamma(\frac{n}{\gamma} + 1) \qquad (10.8)$$

where $\Gamma(\ )$ is a Gamma function (Ref 8). The equation represents a narrow band case when $\gamma=2\sqrt{2}$. Generally

$$E[\frac{d(a/a_o)}{dN}] = \lambda f^n \left[\pi \frac{a}{a_o}\right]^{\frac{n}{2}} \mu_n \qquad (10.9)$$

Eq 10.9 thus gives the mean crack growth rate but it is important to realise that under random loading both the crack growth rate and the crack length are also random variables. As an example Fig 10.1 shows relations between the crack length and the number of cycles which could result from a central crack in an infinite plate under perfect narrow band random loading, growing at the average rate and the average plus and minus one and two standard deviations. The equation

for the central line is

$$\frac{a}{a_o} = \left[\frac{2-n}{2} \lambda (8\pi)^{\frac{n}{2}} \Gamma(\frac{n}{2}+1) N + 1 \right]^{\frac{2}{2-n}} \qquad (10.10)$$

In practice, the fatigue load does not approach infinity as the ideal Rayleigh distibution of narrow band random loading requires. Generally if the theoretical expression for the distribution of the random stress range is represented as $p_{th}(n)$ where $n=S/_o$, the true distribution $p(n)$ truncated at a position ξ, can be estimated as

$$p(n) = \begin{cases} \dfrac{p_{th}(n)}{1 - \int_{\xi}^{\infty} p_{th}(n)\, dn} & 0 < n < \xi \\ 0 & \text{otherwise} \end{cases} \qquad (10.11)$$

which maintains unity for the total probability. In this case, a numerical integration can be performed to determine μ_n and the mean crack growth rate.

SECTION 2 The Distribution of Crack Lengths under Random Loading

The final crack length a_f produced by random loading is given by summing the increments of crack growth in each cycle. Eq 10.4 can be rearranged to give

$$\int_{1}^{\frac{a_f}{a_o}} \frac{d(\frac{a}{a_o})}{f^n \pi^{n/2} (\frac{a}{a_o})^{n/2}} = \lambda \sum_{i=1}^{N} (\frac{S_i}{\sigma})^n \qquad (10.12)$$

where N is the number of cycles in the fatigue loading, a_o and a_f

are the initial and the final crack lenths. The summation on the right hand side of this equation produces a random variable, therefore, the left hand side of Eq 10.12 is a random variable which may be denoted as X

$$X = \int_{1}^{\frac{a_f}{a_o}} \frac{d(\frac{a}{a_o})}{f^n \ \pi^{n/2} \ (\frac{a}{a_o})^{n/2}} \tag{10.13}$$

X is a function of a_f/a_o. For a central crack in an infinite plate subjected to remote tensile loading, X has a simple form

$$X = \frac{2}{(2-n) \ \pi^{n/2}} \left[(\frac{a_f}{a_o})^{\frac{2-n}{2}} - 1 \right] \qquad (n \neq 2) \tag{10.14}$$

According to the central limit theorem, a summation of random variables, here represented as the nth power of the stress range, has a normal distribution whose mean and variance equal to N times the mean and the variance of the population from which each individual variable is drawn. Therefore, the distribution of X is

$$p(X) = \frac{e^{-(\frac{X}{\lambda} - N\mu_n)^2 / [2N \ \sigma_n^2]}}{\lambda \ \sigma_n \ \sqrt{(2\pi N)}} \tag{10.15}$$

where μ_n and σ_n are respectively the mean and the root mean square of n^n. σ_n is given as

$$\sigma_n = (\sqrt{2\gamma})^n \left[\Gamma(\frac{2n}{\gamma} + 1) - \Gamma^2(\frac{n}{\gamma} + 1) \right]^{\frac{1}{2}} \tag{10.16}$$

Since X is related to a_f, the distribution of the final crack length

a_f normalised in respect to the initial length a_o, can be determined by transforming the variable from X to (a_f/a_o)

$$p(\frac{a_f}{a_o}) = \frac{e^{-(\frac{X}{\lambda} - N\mu_n)^2/[2N\,\sigma_n^2]}}{\lambda\,\sigma_n\,\sqrt{(2\pi N)}} \left|\frac{dX}{d(\frac{a_f}{a_o})}\right| \qquad (10.17)$$

Physically, the crack can never become shorter under fatigue loading. Eq 10.17 can be regarded as valid only when $a_f/a_o \geq 1$ and the probability distributed in the region $a_f/a_o < 1$ is negligible as long as the number of cycles N is large. For the simplest situation, f=1, the equation has this form

$$\frac{dX}{d(\frac{a_f}{a_o})} = \frac{1}{\pi^{n/2}\,(\frac{a_f}{a_o})^{n/2}} \qquad (10.18)$$

The probability density function can be evaluated by substituting Eqs 10.14, 10.8, 10.16 and 10.18 in to Eq 10.7. For this case, direct integration can be performed on Eq 10.7 to produce a cumulative distribution function, but it is easier to use numerical integration techniques.

Monte-Carlo simulations (see Appendix A) have been carried out to check the prediction of Eq 10.17. Constants λ=1.5E-6 and n=3 were chosen to give convenient numbers for a central crack in a infinite plate after 5000 cycles. In the simulation, stress ranges for a narrow band loading (having Reyleigh distribution) and for a broad band loading (having a distribution determined by Eq 10.7 with the spectral width parameter ϵ=2/3) were generated by a digital computer. The corresponding increments of crack length were

calculated for each cycle according to the Paris law and summed to give the crack length after 1000, 3000, 5000 cycles. This simulation was performed 100 times and the results are presented together with the analytic values in Figs 10.2 and 10.3 in which the agreement is seen to be excellent. It can also be seen that as the crack length increases the variance of crack length increases.

SECTION 3 Distribution of Number of Cycles to Reach a Given Crack Length

If failure is defined to occur when the crack reaches a critical length, the distribution of number of cycles to reach that length provides a reliability assessment. Let a single sample of the fatigue process, say the jth sample, be considered, the product of the number of cycles N_j and the average of $(S/\sigma)^n$ in this particular sample is the summation in Eg 10.12, therefore,

$$\frac{X}{\lambda} = N_j \mu_j \qquad (10.19)$$

where μ_j is the average of $(S/\sigma)^n$ for the ith sample which has N_j cycles. For different samples, μ_j and N_j are different but the product of the two is the same. Now let μ be the random variable representing the average of $(S/\sigma)^n$ for every sample, the above equation can be generalised as

$$\frac{X}{\lambda} = N \mu \qquad (10.20)$$

In this case, the initial and the final crack lengths are given, X is a deterministic value while μ and N are random variables. A variation of the central limit theorem, sometimes described as the Lindeberg-Levy theorem (Ref 8) indicates that μ has a normal distribution with a mean value μ_n and a root mean square $\sigma_n/\sqrt{N}$.

$$p(\mu) = \frac{\sqrt{N}}{\sqrt{2\pi}\,\sigma_n} \exp\left[\frac{-N\,(\mu - \mu_n)^2}{2\,\sigma_n^{\,2}}\right] \qquad (10.21)$$

N and μ are the two random variable correlated by Eq 10.20, therefore the distribution of cycles N to a given crack length can be deduced

$$p(N) = \frac{X}{\sqrt{2\pi}\,\sigma_n\,\lambda\,N^{3/2}} \exp\left[\frac{\mu_n^{\,2}}{2\,\sigma_n^2}\,\frac{\left(\frac{X}{\lambda\,\mu_n} - N\right)^2}{N}\right] \qquad (10.22)$$

Monte-Carlo simulation (see Appendix A) has also been carried out to check the validity of Eq 10.22 and the results are given in Figs 10.4 and 10.5. The probability for $N<1$ is neglected, which does not produce any significant error in practice.

$$\mu_N = \frac{X}{\lambda\,\mu_n} \qquad (10.23)$$

On the condition that

$$\frac{\mu_N - N}{\mu_N} = \frac{\Delta N}{\mu_N} \ll 1 \qquad (10.24)$$

the exponent in Eq 10.22 can be simplified as follows

$$\frac{(\mu_N - N)^2}{N} = \frac{(\mu_N - N)^2}{\mu_N - \Delta N}$$

$$= \frac{(\mu_N - N)^2}{\mu_N} \left[1 - \frac{\Delta N}{\mu_N} + \left(\frac{\Delta N}{\mu_N}\right)^2 - \ldots.\right]$$

$$\approx \frac{(\mu_N - N)^2}{\mu_N} \qquad (10.25)$$

Eq 10.22 can be simplified further by replacing N by μ_N in the denominator. This procedure results in an expression

$$p(N) = \frac{X \ \sigma^n}{\sqrt{2\pi}\ \lambda\ \sigma_n\ \mu_N^{3/2}} \exp\left[\frac{\mu_n^2}{2\ \sigma_n^2} \ \frac{(\mu_N - N)^2}{\mu_N}\right]$$

$$= \frac{1}{\sqrt{2\pi}\ \sigma_N} \exp\left[\frac{(\mu_N - N)}{2\ \sigma_N^2}\right]^2 \qquad (10.26)$$

which is a normal distribution. Its root mean square is

$$\sigma_N = \frac{\sqrt{\mu_N}}{\mu_n} \qquad (10.27)$$

In cases in which the difference between N and the mean life μ_N is big (in comparison with the mean life itself), this approximation may lead to substantial errors in terms of the probability density. Nevertheless, the mean life μ_N and the root mean square σ_N so defined can be used to evaluate the fatigue life distribution because the approximation describes the part of the probability density function arround the mean life where the probability concentrates. The effect of n and λ on the mean μ_N of the number of cycles are shown in Figs 10.6 and 10.7 respectively with a Monte-Carlo simulation which confirms the analytic calculation. It

can be seen that factors which increase the crack growth rate decrease both the mean number of cycles and the standard deviation, but increase the coefficient of variation (Figs 10.2-6). This can be seen from the limiting cases

$$\lim_{\mu_N \to \infty} \sigma_N = \infty \tag{10.28}$$

while

$$\lim_{\mu_N \to \infty} \frac{\sigma_N}{\mu_N} = \lim_{\mu_N \to \infty} \frac{1}{\mu_n \sqrt{\mu_N}} = 0 \tag{10.29}$$

SECTION 4 Material Variance

10.4.1 The Distribution of Fatigue Life

Experiments such as those by Virkler et al (Ref 135) indicate the existence of variance in the fatigue crack growth rate under constant amplitude loading, which is attributable to the the variance in material properties. It is important to account for this influence in predicting the fatigue life and this is achieved by treating one of the material parameters, α as a random variable. α is simply assumed to have a normal distribution

$$p(\alpha) = \begin{cases} \frac{1}{\sqrt{(2\pi)}\ \sigma_\alpha} e^{-\frac{(\alpha - \mu_\alpha)^2}{2\sigma_\alpha^2}} & \alpha \geq 0 \\ 0 & \alpha \leq 0 \end{cases} \tag{10.30}$$

where μ_α and σ_α are the mean and the root mean square respectively. When α is reasonably concentrated about a mean value, the part of probability in the area $\alpha \leq 0$ can be neglected to avoid any negative

crack growth rates. In order to separate the new random variable, Eq 10.20 is written as

$$\ln X = \ln \lambda + \ln \mu + \ln N \tag{10.31}$$

By introducing a new notation, the above equation can be written as

$$X_1 = \lambda_1 + \mu_1 + N_1 \tag{10.32}$$

It is convenient to introduce a convention at this stage that if a probability density function is written as $p_X(y)$, where the suffix x indicates the expression is a function of x but the variable x is replaced by y. When the distribution of number of cycles needed to grow a crack to a specific length is considered, X_1 is constant, λ_1, μ_1 and N_1 are random variables. The distribution of λ_1 and μ_1 determines the distribution of N_1 in such a way that (Ref 7)

$$p(N_1) = \int_{-\infty}^{\infty} p_{\mu_1}(\mu_1) \; p_{\lambda_1}(X_1 - N_1 - \mu_1) \; d\mu_1 \tag{10.33}$$

The distribution of λ_1 can be obtained from that of α

$$p(\lambda_1) = \frac{e^{\lambda_1}}{\sqrt{(2\pi)}\, N\, \sigma_\alpha\, \sigma^n\, a_o^{\frac{n-2}{2}}} \exp\left\{ - \frac{\left[\frac{e^{\lambda_1}}{\sigma^n\, a_o^{\frac{n-2}{2}}} - \mu_\alpha \right]^2}{2\, \sigma_\alpha^2} \right\} \tag{10.34}$$

The distribution of μ_1 can be deduced from the distribution of μ in a similar manner

$$p(\mu_1) = \frac{e^{\mu_1}\sqrt{N}}{\sqrt{(2\pi)}\, \sigma_n} \exp\left\{ - \frac{N\,(e^{\mu_1} - \mu_n)^2}{2\, \sigma_n^2} \right\} \tag{10.35}$$

An expression for the distribution of N_1 can be obtained by substituting Eq 10.34 and Eq 10.35 into equation 10.33. This can be converted to produce the distribution of the fatigue life

$$p(N)= \frac{X}{2\pi\, \sigma_\alpha\, \sigma_n\, \sigma^{\frac{n-2}{n}}\, a_o^2\, N^{\frac{3}{2}}} \int_{-\infty}^{\infty} \exp\left\{ - \frac{N\,(e^{\mu_1} - \mu_n)^2}{2\,\sigma_n^2} - \frac{\left[\frac{X\, e^{-\mu_1}}{\sigma^{\frac{n-2}{n}}\, a_o^2\, N} - \mu_\alpha \right]^2}{2\quad \sigma_\alpha^2} \right\} d\mu_1 \qquad (10.36)$$

10.4.2 The Distribution of Crack Lengths after a Given Number of Cycles

When considering the probability distribution of crack lengths a_f after a initial crack a_o has been subject to a given number of cycles, Eq 10.32 can be rearranged into the form

$$X_1 = \lambda_1 + Y_1 \qquad (10.37)$$

Each of the three terms is a random variable with

$$Y_1 = \mu_1 + N_1 \qquad (10.38)$$

Similar to the case of crack length distribution, a general form of the distribution of X_1 can be given as

$$p_{X_1}(X_1) = \int_{-\infty}^{\infty} p_{Y_1}(Y_1)\; p_{\lambda_1}(X_1 - Y_1)\; dY_1 \qquad (10.39)$$

The distribution of λ_1 is represented by Eq 10.34, the distribution of Y_1 is given by the central limit theorem through the relation

$$\log Y_1 = \log(\mu N) = \log \sum_{i=1}^{N} \left(\frac{S_i}{\sigma}\right)^n \qquad (10.40)$$

Therefore

$$p(Y_1) = \frac{1}{\sqrt{(2\pi N)}\ \sigma_n} \exp\left\{ - \frac{(e^{Y_1} - N\ \mu_n)^2}{2\ N\ \sigma_n^{\ 2}} \right\} \qquad (10.41)$$

The expression for the distribution of the final crack length a_f can be obtained from Eq 10.39, 10.41 and 10.34

$$p\left(\frac{a_f}{a_o}\right) = \frac{a_o}{(2\pi)^{\frac{n+2}{2}}\ f^n\ \sigma_\alpha\ \sigma_n\ \sigma^n\ a_f^{\frac{n}{2}}\ N^{\frac{1}{2}}} \int_{-\infty}^{\infty} \exp\left\{ - \frac{(e^{Y_1} - \mu_n N)^2}{2\ N\ \sigma_n^{\ 2}} \right.$$

$$\left. - \frac{\left[\dfrac{X\ e^{-Y_1}}{\sigma^n\ a_o^{\frac{n-2}{2}}} - \mu_\alpha \right]^2}{2\ \ \sigma_\alpha^{\ 2}} \right\} dY_1 \qquad (10.42)$$

SECTION 5 The Variability of the Critical Crack Length

The distribution of the number of cycles to grow a crack from an initial length to a given length has been studied for cases with and without material property variability. These expressions can be regarded as estimates of the fatigue life distribution given that failure occurs when the crack reaches a constant critical length. But failure may take place at various combinations of crack length and the external random loading during a fatigue process. For a refined method the variability of the critical length should be

considered.

It is convenient to consider the probability that failure takes place at an arbitrary ith cycle while the crack length is between a specific crack length a' and a'+da'. This event consists of two statistically independent evénts. That is to say that the crack length is in a certain range given as $a' \prec a \prec a'+da'$ and the failure in the ith cycle, which is conditional on surviving the previous i-1 cycles. The failure condition can be represented as that the crack length reach a critical length a_c or simply $a_c \prec a$. The probability for realising the two events simultaneously is

$$\Pr[\text{failure} | a' \prec a \prec a'+da] = p(a)da \Pr[a_c \prec a]$$

$$= p(a)da \Big|_i \int_o^a p(a_c)\, da_c \qquad (10.43)$$

where i indicates the crack length distribution at the ith cycle. a_c is the critical crack length representing the crack length at fracture and is a random variable independent of the number of cycles i. Generally, failure can be regarded as possible at any crack length between zero and infinity. To cover the whole range of crack length an integration must be carried out

$$\Pr[\text{failure}] = \int_0^\infty p(a) \int_0^a p(a_c)\ da_c\, da \qquad (10.44)$$

The probability of failure at the ith cycle can be presented in a non-dimensional form with Pr[i] as an alternative notation

$$\Pr[\text{failure}] = P(i)$$

$$= \int_1^{\infty} p\left(\frac{a}{a_o}\right) \int_1^{\frac{a}{a_o}} p\left(\frac{a_c}{a_o}\right)\, d\left(\frac{a_c}{a_o}\right)\, d\left(\frac{a}{a_o}\right) \qquad (10.45)$$

An initial crack is assumed to exist at the beginning of the random fatigue loading, thus the two lower integration limits are 1. This gives the probability of failure, i.e the failure rate at the ith fatigue cycle which can be utilized to determine the probability of failure in the first N cycles of a random loading. Let B_i be the event of surviving the ith cycle

$$\Pr[\text{surviving N cycles}] = \Pr[B_1]\Pr[B_2|B_1]\Pr[B_3|B_1 \cap B_2]\ldots$$

$$= \prod_{i=1}^{N} [1-P(i)] \qquad (10.46)$$

This indicates that fatigue is a Marcoff process (Ref 143). As a fatigue life often comprises hundreds of thousands of cycles, it is not practical to evaluate Eq 10.46 cycle by cycle and it is necessary to perform a numerical integration

$$Z(N) = \int_1^N \log[1-P(i)]\, di$$

$$\approx \log[1-P(1)] + \log[1-P(2)] + \ldots. \qquad (10.47)$$

where the integers N and i have to be regarded as continuous in the integration. Comparison of Eq 10.47 with 10.46 gives the probability of surviving the first N cycles is

$$\Pr[\text{survive}] = e^{Z(N)} \qquad (10.48)$$

The probability of failure in the first N cycles is therefore

$$\Pr[\text{failure}] = 1 - e^{Z(N)} \tag{10.49}$$

The essential part in this calculation is the determination of P(i) given by Eq 10.45. It is necessary to be able to evaluate the distribution of crack length which is a function of the number of cycles i

$$p\left(\frac{a}{a_o}\right) = p\left(\frac{a}{a_o}, i\right) \tag{10.50}$$

The methods described in previous sections are adequate for this purpose. As regards the question of the distribution of critical crack lengths a_c, it may initially be considered that the critical crack length is a function of the external fatigue loading using a linear elastic fracture mechanics criterion

$$a_c = \frac{K_c}{f\sqrt{\pi}\sqrt{\left(\frac{S}{2} + S_m\right)}} \tag{10.51}$$

where K_c is the material toughness and S_m the mean stress. The distribution of the critical crack length a_c for this case can be determined from a variable transformation and can be adapted if other criteria are used

SECTION 6 The Implementation of the Probabilistic Calculation

Analytic evaluation of the proposed calculation is not possible due to the complex form of the expressions for $p(^{a}/a_o)$ and $p(^{a}c/a_o)$, therefore a numerical method has to be used A computer program called PANA has been compiled in which particular attention has been paid to accuracy and efficiency.

10.6.1. The Main Structure of the Computer Program

The program was designed to evaluate the probabilistic distributions described in the previous sections, so that sharing subroutines and functions between different purposes is possible. A logic flow chart of the program is presented in Fig 10.8. The program was compiled and run on a ICL 2988 machine at Glasgow University. A typical calculation, allowing both α and a_c to be random variables, needs 4 cpu seconds.

10.6.2. Evaluation of X and $P(a_c)$

The preliminary evaluation of X and the cumulative distribution function $P(^{a}c/a_o)$ are straight forward procedures using the trapezoidal rule (Ref 182). However, two points require particular care. The first concerns the geometric calibration function which was defined such that f is extremely big when the crack length is larger than a limiting value a_t at which the applied mean load causes failure. The second point is that the limits of integration of $p(^{a}c/a_o)$ are restricted by the ability of computers to handle very small numbers without underflow error. The integration area was expanded by scaling the distribution of a_c by an artificially large number and the effect of this was corrected later in the calculation.

10.6.3. Evaluation of P(i)

The difficult part of the calculation is to evaluate P(i) according to Eq 10.45. This requires two dimensional numerical integration, so that accuracy is very critical. The logic of this part of the calculation is shown in Fig 10.9.

The evaluation of P(i) needs the integration on $p(a_c)$. It also needs distribution of crack length $p(a/a_o, i)$ which can be given by Eq 10.42 using a and i instead of a_f and N. The calculation of the distribution of crack lengths (Eq 10.42) involves another integration and it was found to be important to perform integration in the correct area, failure to do so leads to waste of computer time and very poor precision. The exponential in the expression (Eq 10.42) for the probability density function $p(^af/a_o)$ denoted as U here

$$U = \exp\left\{-\frac{(e^{Y_1} - \mu_n N)^2}{2 N \sigma_n^2} - \frac{\left[\frac{X e^{-Y_1}}{\sigma^n a_o^{\frac{n-2}{2}}} - \mu_\alpha\right]^2}{2 \sigma_\alpha^2}\right\} \qquad (10.53)$$

was regarded as the parameter which determines the integration interval out of which any input of Y_1 causes underflow. The two terms in the exponent were considered separately to give two regions which exclude the under flow areas, and the integration domain was taken to be the overlapped area of the two regions. The exponent has been increased by an artificial factor which was compensated at the end of the calculation.

The integration domain for crack length in the caculation of P(i) (Eq 10.45) is the area in which the domain for the calculation for $p(a/a_o, i)$ exists. The main integration technique was the Romberger method (Ref 182) and a subroutine for this integration procedure is presented in Appendix 2. In this method the integral is estimated from a number of integration points with equal intervals. After more integration points are added to each interval, a new version of the estimation can be obtained which is compared with the previous estimate. More iteration may be necessary depending on whether the difference between the estimations is smaller than the required precision. In this way, by changing the criterion for accuracy, confidence concerning the precision of the program can be obtained.

The Romberger method (Appendix B) has also been used in the evalaution of distribution of crack length given by Eq 10.42 and the distribution of number of cycles given by Eq 10.36.

SECTION 7 Comparison with Experimental Results

So far, this method for fatigue life prediction has been compared with Monte-Carlo simulation to verify the procedure. The comparison can be extended to experiments by Talreja (Ref 183). In these experiments, a narrow band random loading of stress r.m.s σ=182.4 MPa with a mean stress S_m=167 MPa was applied to Cr-Mo-V steel bars of cross section 10×15mm dimensions. On one of the 15mm faces of the specimen, an initial crack was introduced by electro-discharge machining. The crack was 0.05mm deep and 0.15mm long on the surface.

The failure of the specimen was defined as the fracture of the specimen and the experimental data are presented in Table 1. The fatigue life was measured in terms of the periods (each period consists of 200×12.5 cycles). Since Groups 2, 3 and 4 are not comparable, they are omitted.

TABLE 1 - Experimental data from Talreja's paper (Ref 183)
Group 5 and 6 were tested for 150 and 200 periods
"*" indicates "the rest of the group did not fail"

Group No.	Specimen	Periods of Loading to Failure											
		1	2	3	4	5	6	7	8	9	10	11	12
1 (10 specimens)		95	101	144	145	160	163	171	220	235	296		
5 (30 specimens)		137	149	*									
6 (18 specimens)		132	136	151	152	159	159	176	180	184	188	199	*

To establish a basis for comparison between the probabilistic calculation and the experiments, it is assumed that the exponent n in the Paris law is 3 and the crack was always a semi-ellipse which follows a preferred route given by Scott and Thorpe (Ref 80). The stress intensity factors were determined dased on Raju and Newman's results (Ref 62). The finite area correction due to Holdbrook and

Dover (Ref 84) has also been introduced into the calculation of stress intensity factors. The crack length at fracture in the specimen is not available and in the probabilistic calculation, the definition of failure is a crack penetration of three quarters of the material thickness. Information on the randomness of the material resistance to cracking is not known either, but the input of $\mu_\alpha=3.2\times10^{-12}$ and $\sigma_\alpha=0.95\times10^{-12}$ into Eq 10.36 produces good curve fitting to the data of Group 1 as shown in Fig 10.10. These values of the parameters were used in the evaluation of the survival probabilities based on Eq 10.41 after 150 and 200 periods of loading, which were found to be 70.4% and 29.5% respectively. The analytical results are in good agreement with the experiment data of 93.3% and 38.9%.

A comparison with a fatigue test by Gall (Ref 184) on a standard three point bending specimen (Fig 4.3) has been conducted. The material was BS 4360 50D steel whose fatigue behaviour has been reported by Gall and Hancock (Ref 125) as

$$\frac{da}{dN} = 8.02 \times 10^{-12} \Delta K^{2.92} \qquad (10.54)$$

for the mean growth rate and

$$\frac{da}{dN} = 1.12 \times 10^{-11} \Delta K^{2.92} \qquad (10.55)$$

for 95% upper band of the growth rate. A narrow band random loading of r.m.s of 2.86 kN superimposed onto a mean loading of 30 kN has been applied to the specimen containing an initial crack of length a_o=7.1996mm. Failure initiated at a crack length of a_c=30mm after

3.159×10^6 cycles. The 95% upper band of the crack growth rate was utilized to produce a root mean square growth rate assuming α has a normal distribution

$$\sigma_\alpha = 1.59 \times 10^{-12} \tag{10.56}$$

This provides adequate information for a calculation according to Eq 10.36 which produces an estimation that the probability is 37% for the crack to reach 30mm in less than 3.159×10^6 cycles (Fig 10.11). To consider the variance of critical crack length a_c, it is appropriate to use the failure criterion of plastic collapse given (Ref 185) for a bar of unit thickness

$$F = 0.728 \frac{S_o (W-a)^2}{L} \tag{10.57}$$

where S_o is the yield stress, which is 329 MN/m^2 in this case, F is the applied force, and W and L are dimensions given in Fig 4.3. This criterion has been used instead of the linear elastic fracture mechanics criterion (Eq 10.51) and the distribution of critical crack lengths was produced from that of the force F. Based on this random final crack length, the probability of failure within 3.159×10^6 cycles was estimated according to Eq 10.49 to be 64% as shown in Fig 10.11. The result has once more added confidence to the present probabilistic analysis method.

LIST OF FIGURES FOR CHAPTER 10

a_o to a final length a_f under broad band random loading.

The solid line is the prediction of Eq 10.22;

The open circles represent Monte-Carlo simulation data.

Fig 10.6

The mean of the number of cycles as a function of n.

The solid line is the prediction of Eq 10.23;

The open circles represent Monte-Carlo simulation data.

Fig 10.7

The maen of the number of cycles as a function of λ.

The solid line is the prediction of Eq 10.23.

The open circles represent Monte-Carlo simulation data.

Fig 10.8

Main structure of the computer program PANA

Fig 10.9

Detailed logic flow chart for the computation of P(i)

Fig 10.10

Experimental result of Talreja (Ref 183) and the curve fitting to it

Experimental result are indicated by a broken line;

Curve fitting given by Eq 10.36 is given by a solid line.

Fig 10.11

Predictions of the fatigue life of the three point bending

specimen

The prediction of Eq 10.36 is represented by a broken line;

The prediction of Eq 10.49 is represented by a solid line.

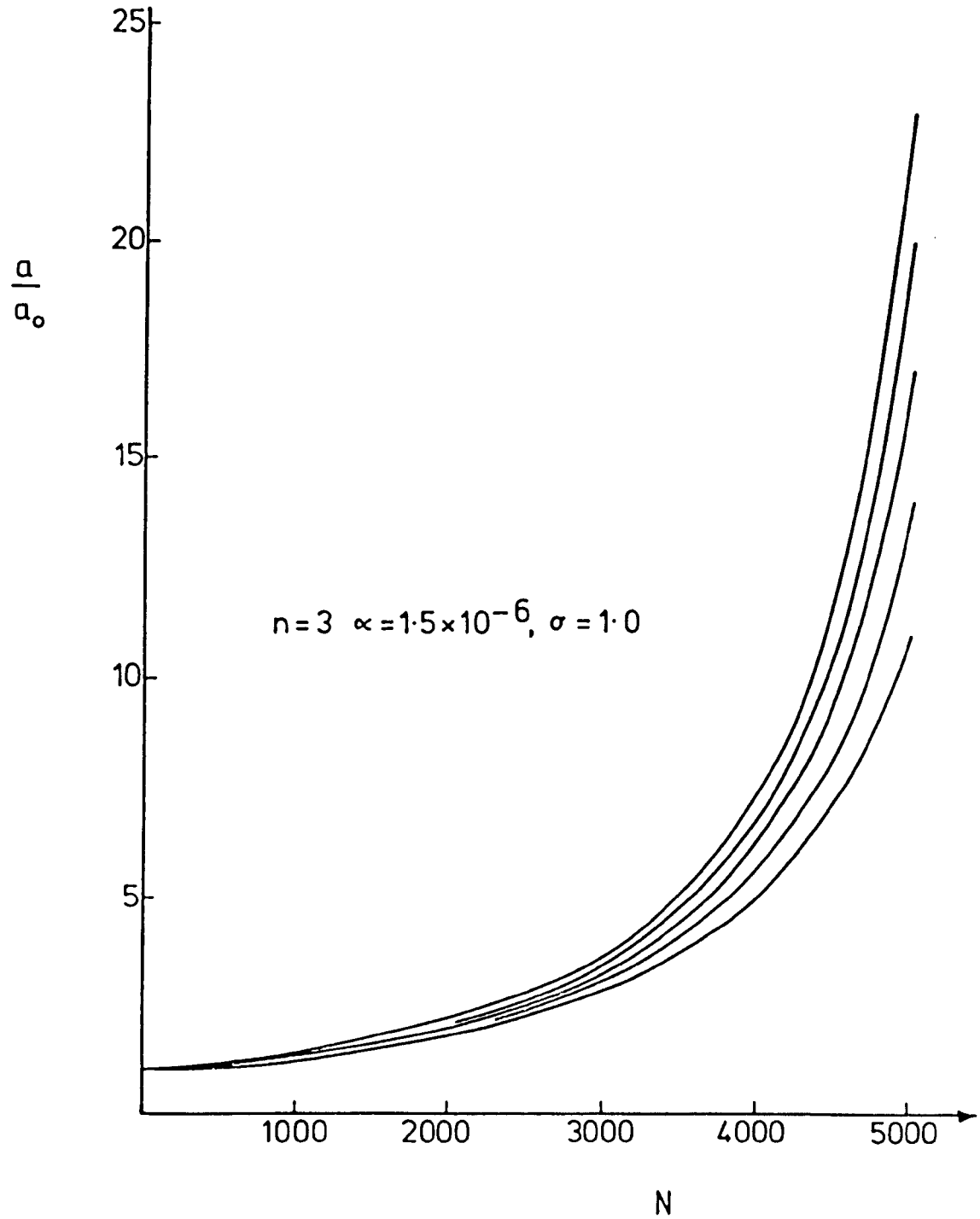

Fig 10.1

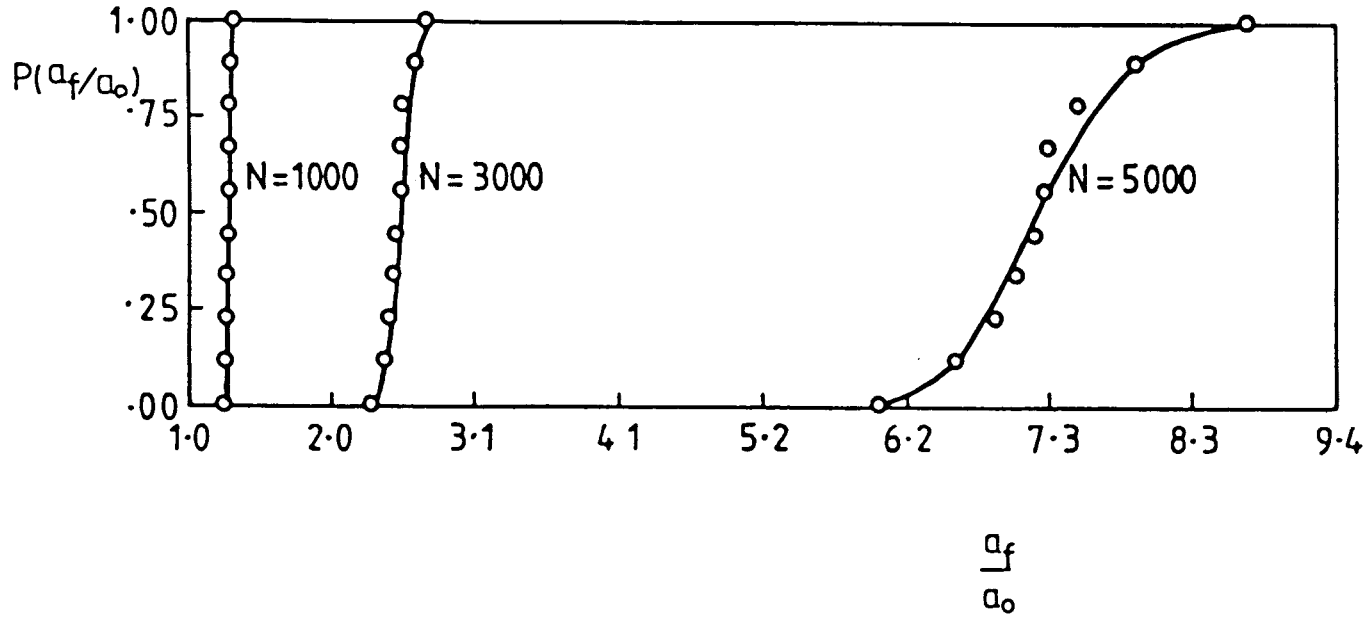
1·00
P(af/ao)
·75
·50
·25
·00
N=1000
N=3000
N=5000
1·0
2·0
3·1
4 1
5·2
6·2
7·3
8·3
9·4
af
ao

Fig 10.2

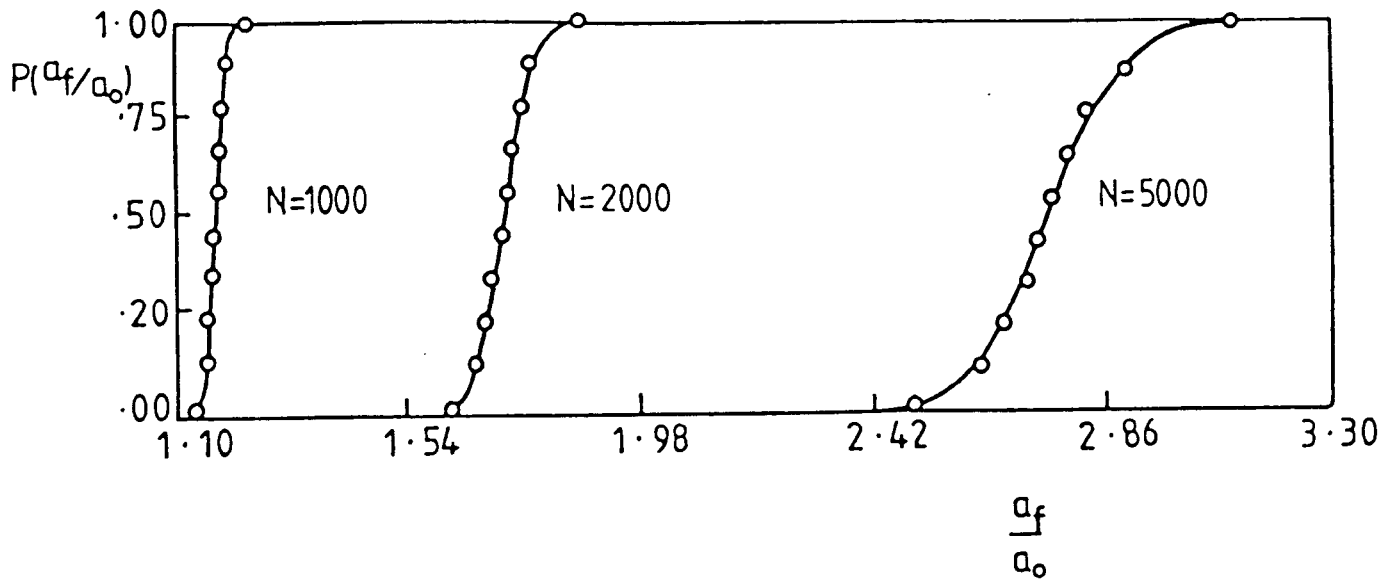
1·00
P(af/ao)
·75
·50
·20
·00
N=1000
N=2000
N=5000
1·10
1·54
1·98
2·42
2·86
3·30
af
ao

Fig 10.3

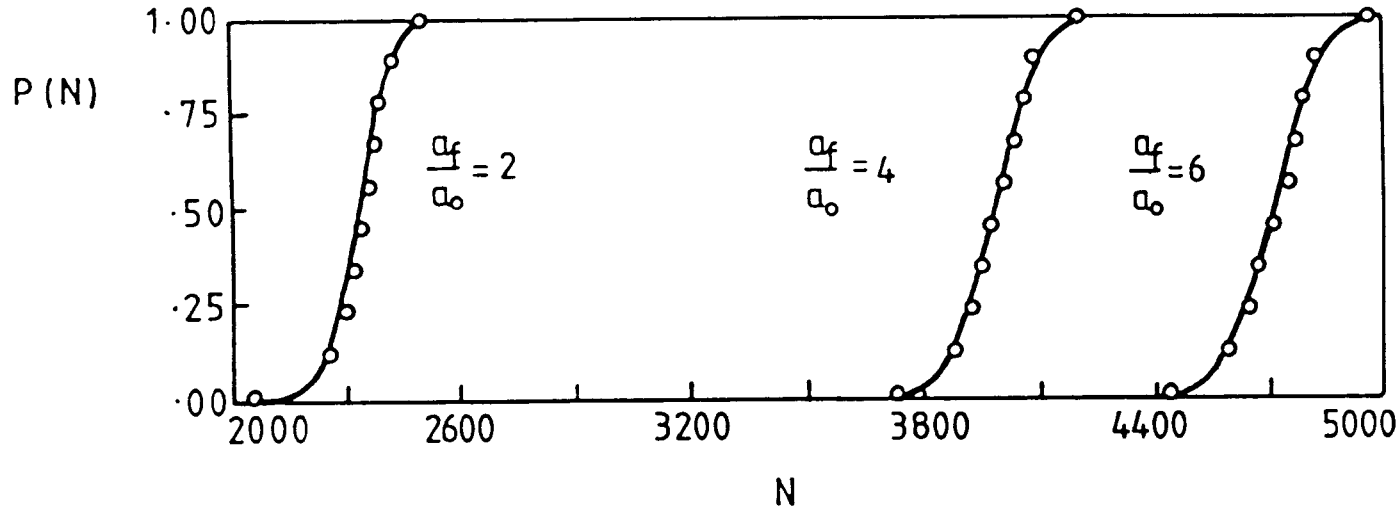
P (N)
1·00
·75
·50
·25
·00
2000
2600
3200
3800
4400
5000
N
$\frac{a_f}{a_o} = 2$
$\frac{a_f}{a_o} = 4$
$\frac{a_f}{a_o} = 6$

Fig 10.4

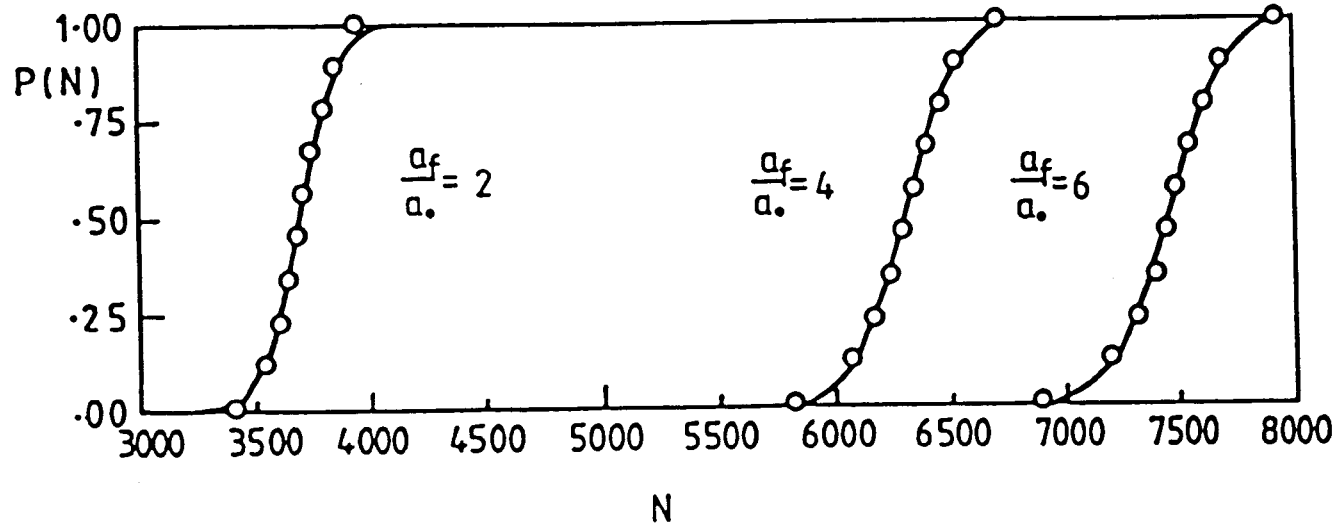
1·00
P(N)
·75
·50
·25
·00
3000
3500
4000
4500
5000
5500
6000
6500
7000
7500
8000
N
$\frac{a_f}{a_\circ} = 2$
$\frac{a_f}{a_\circ} = 4$
$\frac{a_f}{a_\circ} = 6$

Fig 10.5

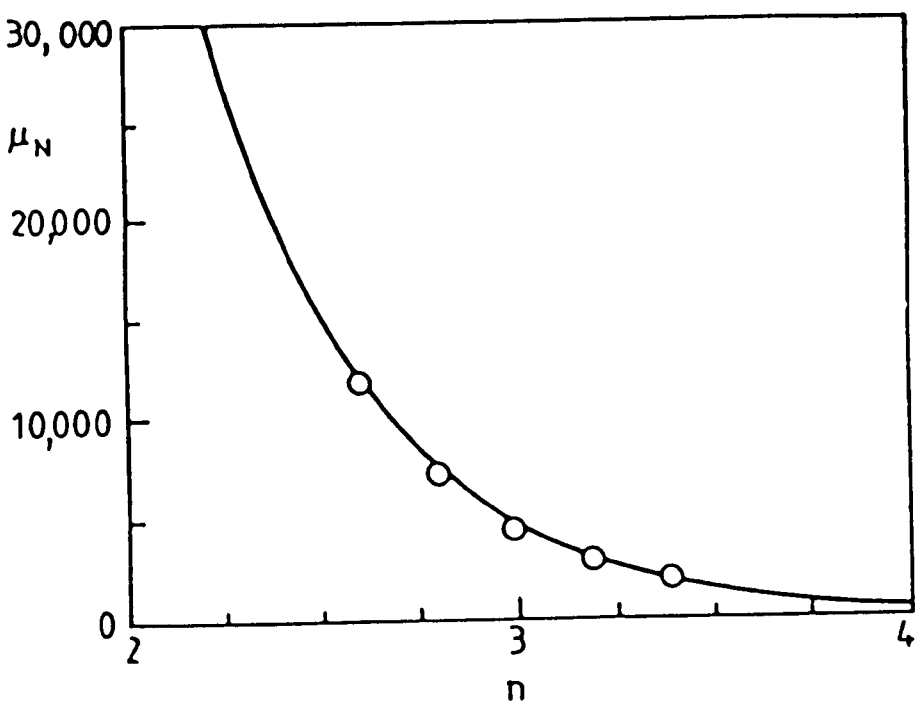

Fig 10.6

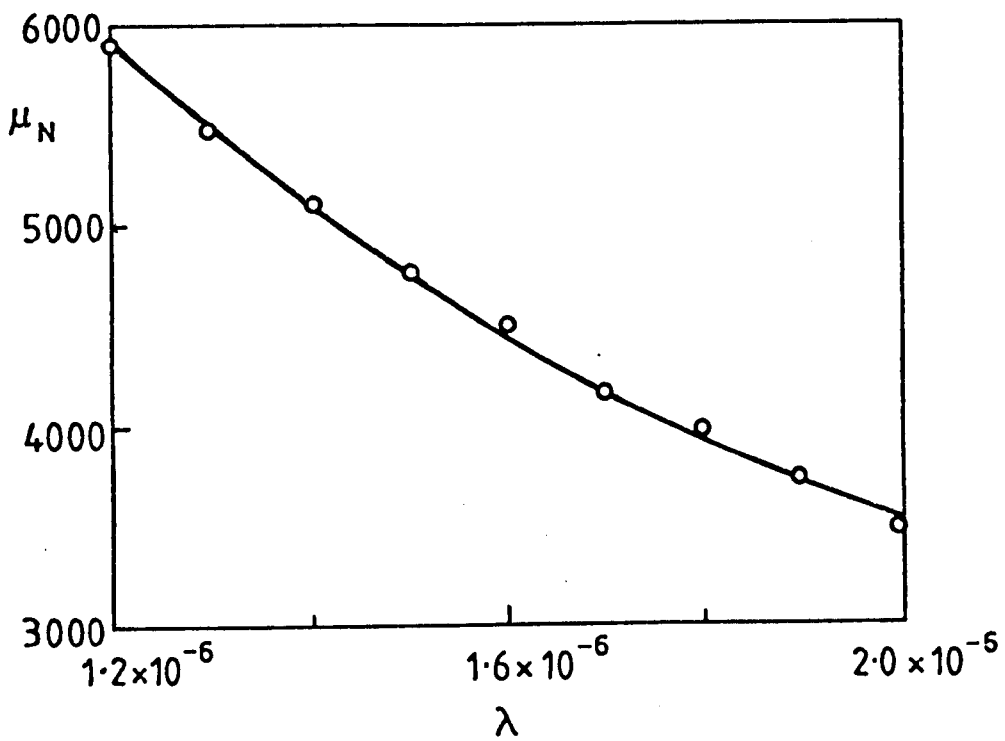
6000
μ_N
5000
4000
3000
$1{\cdot}2\times10^{-6}$
$1{\cdot}6\times10^{-6}$
$2{\cdot}0\times10^{-6}$
λ

Fig 10.7

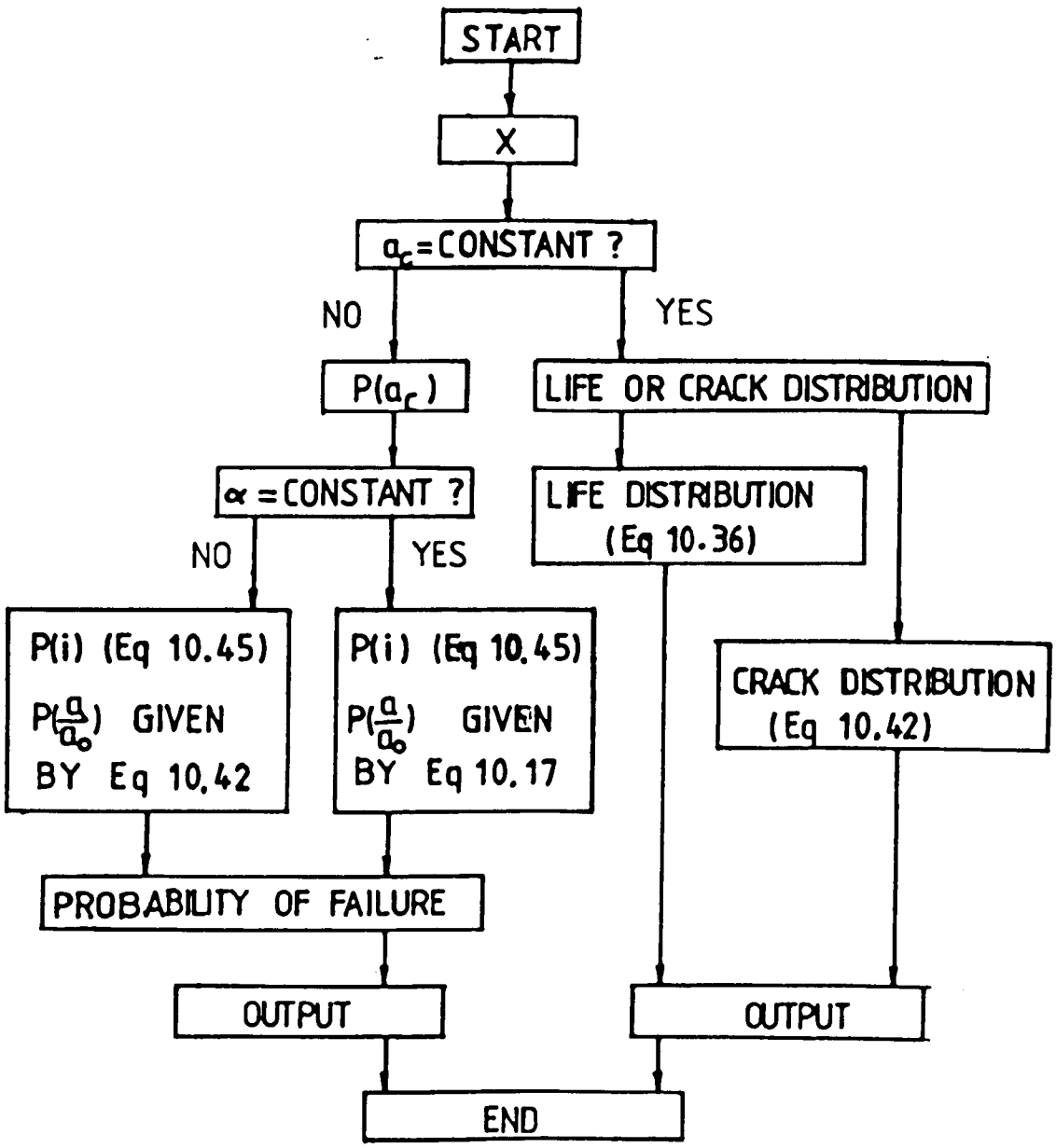
START
X
a_c = CONSTANT ?
NO
YES
$P(a_c)$
LIFE OR CRACK DISTRIBUTION
α = CONSTANT ?
LIFE DISTRIBUTION (Eq 10.36)
NO
YES
P(i) (Eq 10.45) $P(\frac{a}{a_0})$ GIVEN BY Eq 10.42
P(i) (Eq 10.45) $P(\frac{a}{a_0})$ GIVEN BY Eq 10.17
CRACK DISTRIBUTION (Eq 10.42)
PROBABILITY OF FAILURE
OUTPUT
OUTPUT
END

Fig 10.8

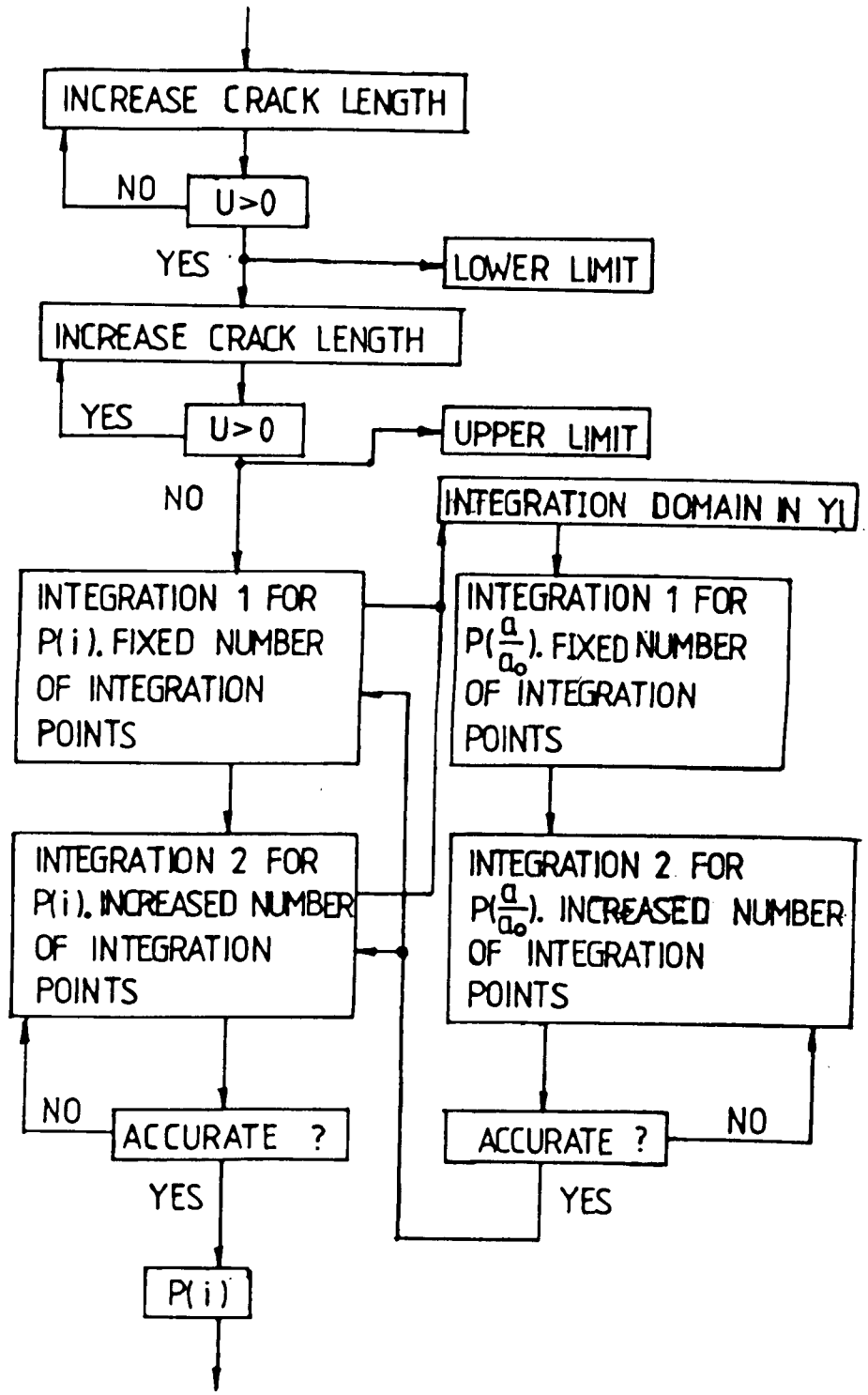
INCREASE CRACK LENGTH
NO
U>0
YES
LOWER LIMIT
INCREASE CRACK LENGTH
YES
U>0
UPPER LIMIT
NO
INTEGRATION DOMAIN IN Yi
INTEGRATION 1 FOR P(i). FIXED NUMBER OF INTEGRATION POINTS
INTEGRATION 1 FOR P(a/a0). FIXED NUMBER OF INTEGRATION POINTS
INTEGRATION 2 FOR P(i). INCREASED NUMBER OF INTEGRATION POINTS
INTEGRATION 2 FOR P(a/a0). INCREASED NUMBER OF INTEGRATION POINTS
NO
ACCURATE ?
YES
ACCURATE ?
NO
YES
P(i)

Fig 10.9

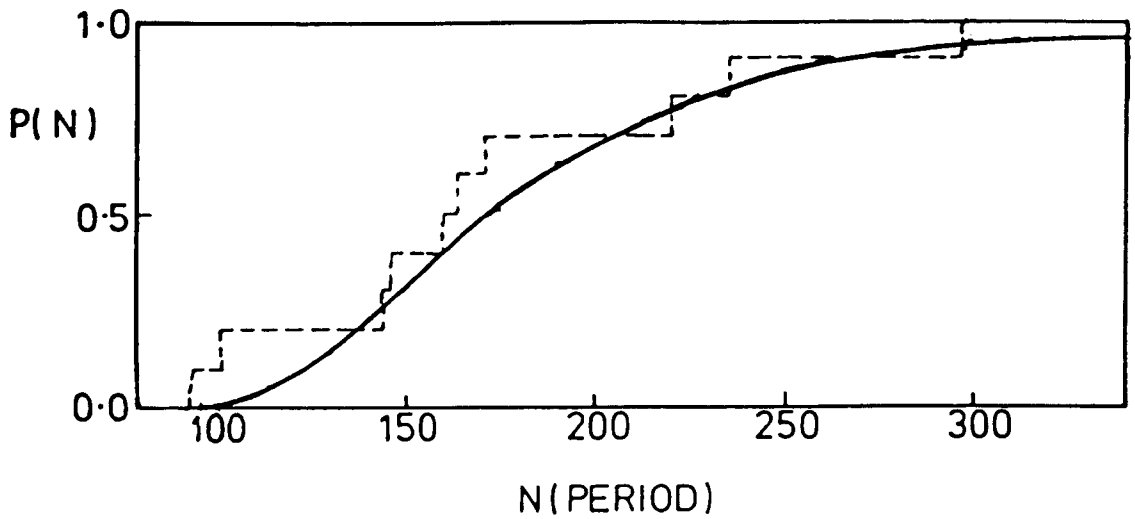

Fig 10.10

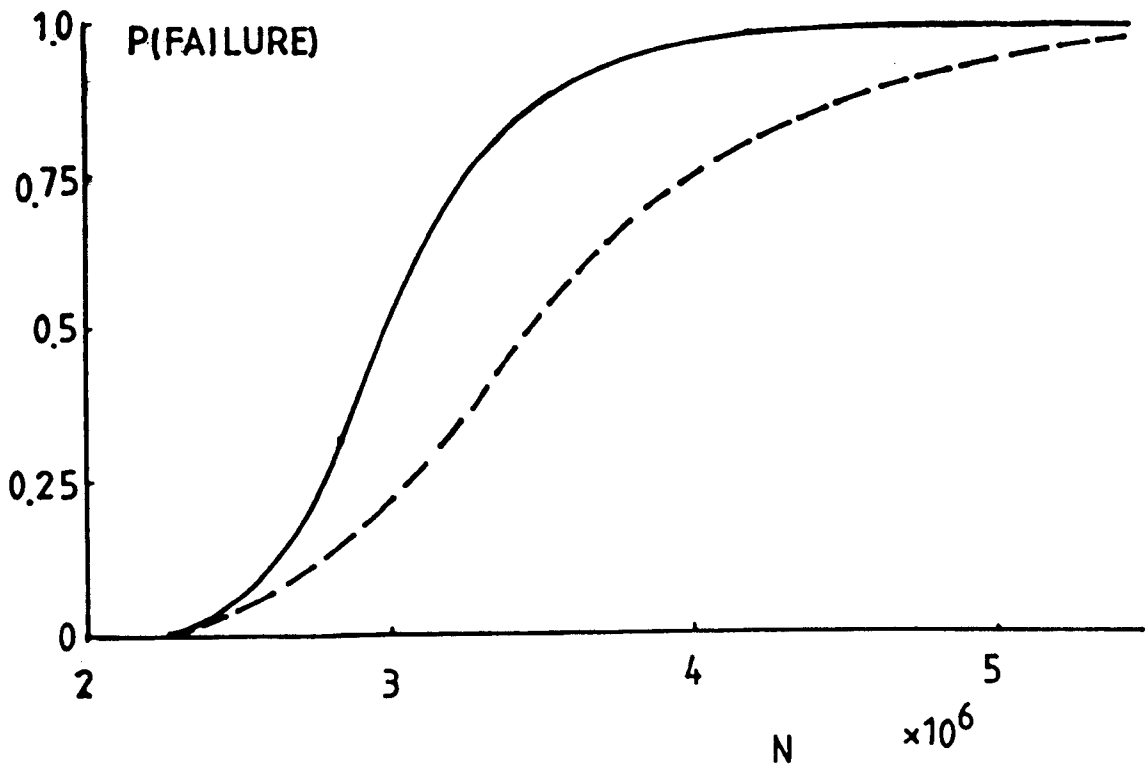

Fig 10.11

CHAPTER 11 FRACTURE MECHANICS ANALYSIS OF A TUBULAR WELDED T JOINT

In order to use fracture mechanics to assess the fatigue life of a tubular welded T joint, an analysis of cracks in the joint has been carried out and is described in this chapter. The analysis considers a number of crack depths representing different levels of crack propagation. The technique used in the analysis is based on the shell finite element method in conjunction with the line spring concept of Rice and Levy (Ref 59). An investigation of the applicability of this concept to the modelling of surface cracks in sites of stress concentration has been conducted prior to application of the technique to tubular welded joints.

SECTION 1 A T Plate Joint

Numerical analysis of structures such as the tubular joint shown in Fig 7.1 using shell elements is computationally efficient in comparison with three dimensional analysis. The line spring concept allows the simulation of surface cracks near the chord-brace intersection by a shell analysis, which otherwise requires three dimensional analysis. However, a shell analysis does not provide a model of any weld details such as the size or the curvature of the

weldment which may affect the fracture mechanics parameters of a crack at such sites.

To verify the applicability of line spring elements, part through cracks in a plate T joint (Fig 11.1) have been studied using two essentially different techniques. The analysis was carried out by means of a finite element code known as ABAQUS (Ref 186) mounted on a VAX 11/750 in the C.A.E. Centre of Glasgow University. A crack was located in a horizontal plate at a position one vertical plate thickness away from the central line of the vertical plate which is approximately the position of the weld toe where cracks are frequently found. The joint was designed to be a simple model of part of the chord-brace intersection in a tubular T joint, and plane strain was imposed. The ratio between the thickness of the vertical plate t and the thickness of the horizontal plate T was 0.79 which is identical to the thickness ratio of the tubular T joint analysed subsequently.

In the first technique, eight noded isoparametric quadrilateral plane strain elements were used with which the local geometry of the weldment was modelled. Three situations were considered: a sharp corner joint, a 45° weld profile and a smooth circular profile as shown in the meshes (Fig 11.2). 124 elements with 445 nodes were used to model the sharp corner joint, and 150 elements with 529 nodes were used for the 45° weld profile and the smooth profile.

In the first loading case a pure couple was applied to each end of the horizontal plate while allowing the end of the vertical plate to

be unrestrained. The J-integral was evaluated using the virtual crack extension method of Parks (Ref 64) for crack depths of a/T=0.2, 0.3, 0.5 and 0.8 as shown in Fig 11.3. Since the crack was subjected to a purely mode I loading under perfectly elastic conditions, the J-integral can be converted into the stress intensity factor K_I by

$$K_I = \left[\frac{J\,E}{1 - \nu^2} \right]^{\frac{1}{2}} \qquad (11.1)$$

The results are presented in Fig 11.4 in which K_I is normalised in respect to $S_n\sqrt{a}$ where S_n is the maximum fibre stress in the horizontal plate remote from the intersection and a is the crack depth

$$\frac{K_I}{S_n \sqrt{a}} = \left[\frac{J\,E}{(1-\nu)^2\, a\, S_n^2} \right] \qquad (11.2)$$

In the second loading case, the two ends of the horizontal plate were built in and the end of the vertical plate was subjected to a vertical force loading. The crack was subjected to mixed mode loading, thus the J integral contains contributions from mode *I* and mode *II* stress intensity factors K_I and K_{II} which can be combined

$$\frac{J\,E}{1 - \nu^2} = (K_I^2 + K_{II}^2) \qquad (11.3)$$

Fig 11.5 shows the non-dimensional results but in this case S_n is the stress in the vertical plate remote from the intersection.

A shell analysis of the same plate T joint has been conducted in which 15 eight noded shell elements with 73 nodes were used (Fig

11.6) and the crack was represented by a line spring element (Ref 59). The plate was restrained in plane strain state and the same loadings and crack depths as in the first analysis were considered. The results are presented in Figs 11.4 and 11.5 together with those from the first analysis. Although the second analysis using line spring elements does not allow the modelling of weld details, the results compare very favourably with that of the first. Generally, the scatter is smaller for pure bending than that for vertical force loading. For both loading cases, $^{a}/_{T}$=0.2 is the worst situation. For vertical force loading, the difference at this crack depth between the round corner T plate calculation and the line spring calculation is less than 12%. If the line spring results are compared with that of sharp corner plate T joint, the difference is less than 7%. The difference between the 45° weld profile result and the line spring calculation is the biggest, as much as 14%. This can be attributed to the stress concentration at the point where the crack was introduced. It is clear that the line spring model may not produce accurate results when the surface crack concerned is very shallow. But when the crack becomes deeper, the influence of the local geometry decreases and as the stress field surounding the crack becomes dominated by the membrane forces and the bending moments which can be determined by a shell analysis of the overall goemetry, the line spring element produces an accurate estimation.

In addition, it can be seen from the calculations that when there is not a load shedding effect, the stress intensity factor naturally increases as the crack becomes deeper (Fig 11.4). In the case of load shedding, the stress intensity is determined by both the effect

of decreased load passing through the cracked section and the increased crack depth. In the load shedding case studied, the stress intensity increases to a maximum then decreases (Fig 10.5).

SECTION 2 The Tubular Welded T Joint and Its Finite Element Model

Having established the validity of the method applied to plane strain weldments, it is now natural to extend the analysis to three dimensional problems such as the tubular welded T joint shown in Fig 7.1. The dimensions of the joint are given in the figure and are identical to the joint Dover and Holdbrook (Ref 173) have tested using random fatigue loading. The joint has been analysed under three basic loading cases, namely axial loading, in-plane bending and out-of-plane bending. For all the cases the two ends of the chord were built in and force boundary conditions were applied to the end of the brace.

Under in plane bending, half of the geometry is adequate for the analysis. The half geometry concerned was idealized by 444 8 noded linear elastic shell elements provided by ABAQUS as shown in Fig 11.7. The calculation of the stress distribution in the uncracked geometry is a problem with 2664 degrees of freedom. For axial loading, because of the symmetry of the loading, the problem can be reduced further to a quarter of the geometry (Fig 11.8). The number of elements along the chord-brace intersection has been increased while the multi-point constrain technique (Ref 186) has been utilized to reduce the number of elements elsewhere. The mesh

presented in Fig 11.8 consists of 208 eight noded linear elastic shell elements. This results in a problem with 4128 degrees of freedom. Under out of plane bending, it is necessary to analyse half of the geometry and the mesh in this case was generally produced by adding another quarter of the geometry to that for axial loading situation. 416 eight noded linear elastic shell elements were used (Fig 11.9) and the number of degrees of freedom for the problem was 7932.

Surface cracks were introduced into the model at the site of maximum stress concentration. Despite the somewhat irregular shape of cracks in experiments, they were idealized as semi-ellipses with a surface length of 2c and a depth a as shown in Fig 11.10. Although a variety of crack shapes may occur in fatigue tests on tubular welded joints (Ref 168 and 172), the evolving shapes of the crack were taken as a simple function of crack depth from an inspection of experimental data (Ref 172)

$$\frac{a}{c} = 0.05 + \frac{a}{6\ T} \qquad (11.4)$$

as illustrated in Fig 11.11. Crack shapes observed in a test on a similar T joint ($\tau=\beta=0.5$) using constant amplitude loading (Ref 101) are also shown in this Figure, and have been used to conduct a check on the accuracy of the line spring method at a later date.

Surface cracks in tubular joints have been observed to propagate in a direction at an angle to the surface of the chord wall (Ref 101), while in the line spring element model, the crack is always assumed to be normal to the shell at every point. The numerical analysis

represents the cracks by discrete line springs in the chord distributed along a perimeter which is on the chord side and one brace wall thickness away from the chord-brace mid-surface intersection. This perimeter is at approximately the position of the weld toe where fatigue cracks are frequently found. The surface length of the cracks was measured along the perimeter and the centres of the cracks were assumed to remain at the original maximum stress concentration sites under the individual loading cases.

SECTION 3 Results of the Numerical Analysis

11.3.1 In-Plane Bending

Analysis of the uncracked tubular welded T joint under in plane bending gives the hot spot stress concentration factor, which is defined as the hot spot stress divided by the maximum fibre stress in the brace remote from the chord-brace intersection. The hot spot stress is determined by extrapolating the principal stress at the surface from the linear distribution region to a point half wall thickness away from the central line of the brace wall. It is designed to achieve the same result as the recommended experimental procedure (Ref 150). The calculated hot spot stress concentration factor was 3.28 which compares favourably with 3.4 and 2.8 from the parametric formulae of Wordsworth and Smedley (Ref 157) and Kuang et al (Ref 160). In order to introduce surface cracks in the following analysis, the position of the hot spot was determined to be 36° from the crown on the chord side of the chord-brace intersection.

Semi-elliptic cracks were introduced following the procedure described in the previous section. To define positions along the crack front, an angular coordinate system was defined such that the origin was the centre of the brace, the $\Theta=0^{o}$ line passes through the initial hot spot, and Θ increases in the anti-clockwise direction (Fig 11.12), such that $\Theta=-36^{o}$ defines the crown position and $\Theta=54^{o}$ defines the saddle point.

Stress intensity factors K_I, K_{II} and K_{III} along the perimeter of the crack were normalised by $S_n\sqrt{a}$ and presented for different crack depths in Figs 11.13-15. In all cases the results from the two end points of the semi-elliptical crack have been neglected because of the abrupt change in crack depth which can not be accurately modelled by the spring elements.

The cracks were subjected to a mixed mode loading and the three stress intensity factors can be combined through the J-integral which is equivalent to G for linear elastic fracture mechanics

$$G = J = \frac{1 - \nu^2}{E} (K_I^2 + K_{II}^2) + \frac{1 + \nu}{E} K_{III}^2 \qquad (11.5)$$

The J-integral is presented along the crack length in Fig 11.16 in a non-dimensional form.

The stiffness of the joint is given in an appropriate non-dimensional form in Fig 11.17 in which u is the horizontal displacement of the nodes on the end of the brace in x direction and M the applied pure couple. The notation for dimensional parameters

such as H and r and the Cartesian coordinate system are defined in Fig 7.1. Although diplacements in the y and z directions exist, they are negligible in comparison with the x direction displacement. The stiffness of the joint has been shown to be maintained even after the penetration at the original hot spot, but a marked loss of stiffness occurs when penetration takes place at the crown position.

11.3.2 Axial Loading

The hot spot in the axial load case is the saddle position. Following the procedure described above, the hot spot stress consentration factor was determined to be 9.35, while the values given by the parametric formulae of Kuang et al (Ref 160) and Wordsworth and Smedley (Ref 157) are 8.5 and 9.35 respectively.

The stress intensity factors K_I, K_{II} and K_{III} along the crack length are presented in Figs 11.18-11.20.

The angular position is given by ϕ which is more convenient for this case. As shown in Fig 11.12, the coordinate system represented by ϕ can be obtained from that represented by θ, by moving the 0° line to the crown point, thus the difference between the two angles is 36°. The half crack concerned is in the region $0^\circ \angle \phi \leq 90^\circ$. From Fig 11.20, it can be seen that in general mode *III* cracking exists, but at the saddle position, where both the symmetric planes of loading and geometry pass, the corresponding stress intensity factor K_{III} decreases to zero.

The magnitude of the J-integral along the crack front is presented in Fig 11.21. Data concerning the stiffness of the joint is given in Fig 11.22 in which v is the vertical displacement of the nodes on the end of the brace. The crack shape after penetration at the saddle is rather arbitrary. As in the case of in plane bending, the stiffness of the joint is maintained before the penetration at the original maximum stress concentration position and decays steadily afterwards.

11.3.3 Out-of-Plane Bending

For the out of plane bending case, the maximum stress concentration is located at the saddle on the chord side of the intersection. The same procedure has been carried out to extrapolate the principal stress to a point a half brace wall thickness from the mid-surface intersection at the saddle. This produces a hot spot stress concentration factor of 9.42, which is in good agreement with the results given as 9.57 by Gibstein's (Ref 161) and 11.26 from Wordsworth and Smedley's (Ref 157) parametric formulae.

It is not surprising that the stress intensity factors K_I, K_{II} and K_{III} along the crack length shown in Figs 11.23-25 vary in a similar way to that in the axial loading case. The variation of the J-integral along the crack length is presented in Fig 11.26 and the stiffness of the joint in Fig 11.27.

11.3.4 Summary of the Results

Under the three basic load cases, the analysis of the uncracked T tubular joint gives hot spot stress concentration factors which are in good agreement with parametric formulae derived from the measurements on acrylic models (Ref 157) and from finite element analysis (Refs 160 and 161). The difference between the results of the present analysis for in-plane bending and that from the formulae of Kuang et al (Ref 160) can be attributed to among other factors, the fact that Kuang et al used the stress concentration at the crown position to construct their parametric formula for this loading case.

The opening mode stress intensity factor is generally the dominant component of the mixed mode cracking. Fig 11.28 shows the opening mode stress intensity factor at the deepest point of the cracks under the three loading cases. The stress intensity factor does not increase rapidly as the crack becomes deeper. This can be explained by the load shedding effect in the tubular welded joint which reduces the load carried by the damaged section.

The evaluated mode two and mode three stress intensity factors are not stable in some cases, and this may be probably attributed to the mathematical techniques used in the extended model of the line spring element (Ref 63). However, mode two and mode three stress intensity factors are small in comparison with the mode one stress intensity factor. In addition, the mode three stress intensity factor is zero at the saddle point under both axial loading and

out-of-plane bending as shown in Figs 11.20 and 11.25, which is physically correct.

SECTION 4 Discussion

The opening mode stress intensity factor at the deepest point of the crack is compared with experimentally inferred data by Dover et al (Refs 172 and 173) in Fig 11.29 for the three loading cases studied. Despite the fact that the crack in a joint is subjected to a mixed mode loading, the experimental method basically determines a stress intensity factor by comparing the crack growth rate in the tubular welded T joint and the crack growth rate in pure mode *I* loading in simple fracture mechanics specimens. Therefore the comparison is not on an exactly equivalent basis.

For very small cracks, for example, when $a/T \leq 0.1$, the cracks are in the process of coalescing to form a single long crack, the experimental data are not comparable. For very deep cracks, plastic tearing can be substantial as the crack propagates through the remaining ligament, thus the experimental data is questionable in this area. In the central range of crack depth, satisfactory agreement has been achieved in axial loading case. For out-of-plane bending case, the results from the two methods are closer (as also shown in Fig 11.30) when a/T is about 0.3 or 0.8. While around $a/T=0.5$, where the line spring element is expected to perform well, the experimental data is low in comparison with the finite element analysis. The experimental results for the in-plane bending case

increase as a/T approaches about 0.5 and experimental data for a/T≥0.5 is not available. There is an obvious difference which may be attributed to the stress concentration factor. The stress concentration factor used in deriving the experimental function f(a/T) was 6.67 and the dimensions for the tubular T joint have not been given (Ref 172). While in the current study, the hot spot stress concentration factor was 3.32. If the stress intensity factor is presented as $K/(S_n\sqrt{\pi}\sqrt{a})$, there is a general agreement between the experimental data and the current study (Ref 187).

The corelation between the finite element results and the experimentally inferred results is better in the axial loading case than in the other two cases. This is because the experimental data for in-plane and out-of-plane bending is much lower than that in the axial loading case. In the range a/T≥0.1, the difference between the axial loading case and the out-of-plane bending case is consistently more than 36%. This implies that if the exponent in the Paris law n is 3, the part of fatigue life corresponding to crack propagation from a visible crack to a through crack under out-of-plane bending test is 2.5 times longer than that in axial loading case for a similar hot spot stress range. This can be partly attributed to the nature of the experimental method. The evidence is that (Ref 174) the function f(a/T) determined from two nominally similar cracks in a fatigue test of a K joint using constant amplitude loading were significantly different (Fig 11.31). The K joint has two braces with same angle to the chord and diameter, the braces were loaded in the plane on the brace and chord such that the material between the braces was subjected to a fatigue loading of r=-1.

Three main factors which contribute to the difference between the current study and the experimental data can be identified. Firstly, differences in the crack shape. Exact information on the crack shapes in the experiments with which the current study is compared are available. The crack shapes used were rather arbitrarily chosen and a variety of crack shapes is expected to occur in the experiments. In order to illustrate the influence of the crack shape, a calculation has been carried out for out-of-plane bending using a different crack shape. The a/c ratio was increased from 0.15 given by Eq 11.4 for a/T=0.6 to a/c=0.2, and the corresponding value of f(a/T) for the deepest point droped by 13%. In the test reported by Delft University (Ref 101), the ratio a/c for the same crack depth ratio a/T was observed to be 0.3, and if this value was used, an even larger decrease in the function f(a/T) is expected.

The second factor is the assymetry in crack shapes and stress distribution. In the numerical analysis symetrical situations were always assumed, and this is not always true in reality. For instance, in the experiment conducted in Delft University (Ref 101), on one side of the tubular T joint under axial fatigue loading there was a major crack while on the other side, there was not. The assymetry of crack shape and position enhances the assymetry of stress distribution, and this results in a more biased distribution of cracks. A third factor which can be considered is the variance in material resistance to cracking. Assuming the variance in growth rate in tests using constant amplitude loading is attributed to variance of the applied stress intensity factor range in the

experiment, the likely scatter band of the inferred stress intensity factor can be determined. The 95% scatter band in crack growth rate under constant amplitude loading has been determined by Gall and Hancock (Ref 125) for BS 4360 50D steel, which indicates that such a scatter corresponds to a scatter band of about ±10% in stress intensity factor. When using random loading as the experimental case by Dover and co-workers (Refs 171 and 172), an even larger scatter can not be avoided as shown in the last chapter.

Ideally it would be desireable to track surface cracks on an individual basis, although to achieve this, detailed information is required which involves both financial resources and time. For the experiment performed in Delft University (Ref 101), the information about the configuration of the joint and the crack position and shapes are available. A line spring calculation has been carried out and the results are compared with experimental data given by Ritchie (Ref 188). The experimental results have a scatter band (Fig 11.32): if the line spring calculation is compared with the mean experimental data, the difference is less than 12.5% for the range of cracks considered. Ritchie (Ref 188) has also indicated that a finite element analysis using solid element for modelling the intersection area and shell elements for modelling the rest of the tubular joint yield a value of $K/S_n/\sqrt{a}=6.29$ for crack depth $a/T=0.563$, and the corresponding line spring result is 6.91. Obviously the line spring calculation has achieved a satiafactory agreement baring in mind that it does not allow modelling of the weld detail.

In comparison with the experimental method and three dimensional analysis, the main advantage of line spring element method is its efficiency, without which it would be impossible to carry out such an analysis at low cost and in a short time. Although the line spring element model of surface cracks is a simple simulation of the real structure, it can be used to evaluate the stress intensity factors K_I, K_{II} and K_{III} with a reasonable accuracy when the crack in hot spot region is more than 20% of ~~the~~ the thickness of the plate.

LIST OF FIGURES FOR CHAPTER 11

Fig 11.1

Basic dimensions of the plate T joint.

Fig 11.2

Finite element meshes of the plate T joint using eight noded isoparametric quadrilateral elements.

Fig 11.3

Mesh details for the smooth circular weldment for a/T=0.2, 0.3, 0.5 and 0.8 cases.

Fig 11.4

The stress intensity factor of the cracks in T plate joint subjected to pure bending determined from J-integral and from line spring calculations.

Sharp corner weldment: triangles;

45° weld profile: crosses;

Smooth circular weldment: circles;

Line spring calculation: squares.

Fig 11.5

The stress intensity factor of the cracks in T plate joint subjected to pure bending determined from J-integral and line spring calculations.

Sharp corner weldment: triangles;

45° weld profile: crosses;

Smooth circular weldment: circles;

Line spring calculation: squares.

Fig 11.6

The mesh for the analysis of plate T joint using shell elements.

Fig 11.7

The mesh for the analysis of tubular T joint under in-plane bending. The crack is one element away from the intersection.

Fig 11.8

The mesh for the analysis of tubular T joint under axial loading. The crack is one element away from the intersection.

Fig 11.9

The mesh for the analysis of tubular T joint under out-of-plane-bending. The crack is one element away from the intersection.

Fig 11.10

Notation of a semi-elliptic crack.

Fig 11.11

Original experimental data of shape ratio from an fatigue test on a tubular T joint (Ref 172), the crack shapes used in current study and crack ratios observed in Delft University (Ref 101)

Experimental data (Ref 172): closed circles;

Experimental data (Ref 101): crosses;

Crack shapes used in the current study: straight line.

Fig 11.12

Definitions of θ and ϕ.

Fig 11.13

Opening mode stress intensity factor of semi-elliptic cracks in tubular T joint subjected to in-plane bending.

Fig 11.14

Sliding mode stress intensity factor of semi-elliptic cracks in tubular T joint subjected to in-plane bending.

Fig 11.15

Anti-plane mode stress intensity factor of semi-elliptic cracks in tubular T joint subjected to in-plane bending.

Fig 11.16

In-plane bending: J-integral as a function of the angular position for cracks in the tubular T joint.

Fig 11.17

Stiffness of the tubular welded T joint under in-plane bending.

Fig 11.18

Opening mode stress intensity factor of semi-elliptic cracks in tubular T joint subjected to axial loading.

Fig 11.19

Sliding mode stress intensity factor of semi-elliptic cracks in tubular T joint subjected to axial loading.

Fig 11.20

Anti-plane mode stress intensity factor of semi-elliptic cracks in tubular T joint subjected to axial loading.

Fig 11.21

Axial loading: J-integral as a function of the angular position for cracks in the tubular T joint.

Fig 11.22

Stiffness of the tubular welded T joint under axial loading.

Fig 11.23

Opening mode stress intensity factor of semi-elliptic cracks in tubular T joint subjected to out-of-plane bending.

Fig 11.24

Sliding mode stress intensity factor of semi-elliptic cracks in tubular T joint subjected to out-of-plane bending.

Fig 11.25

Anti-plane mode stress intensity factor of semi-elliptic cracks in tubular T joint subjected to out-of-plane bending.

Fig 11.26

Out-of-plane bending: J-integral as a function of the angular position for cracks in the tubular T joint.

Fig 11.27

Stiffness of the tubular welded T joint under out-of-plane bending.

Fig 11.28

Opening mode stress intensity factor at the deepest point of the semi-elliptic cracks for the three loading cases.

The solid line represents in-plane bending;

The broken line represents axial loading;

The dotted line represents out-of-plane bending.

Fig 11.29

Comparison of the results of the line spring analysis of surface cracks and experimentally inferred results.

Fig 11.30

Comparison of the results of the line spring analysis of surface cracks for out-of-plane case and experimentally inferred results showing random characteristics.

Current study: crosses

Experimental results (Ref 172): closed circles

Fig 11.31

Experimentally inferred function f(a/T) for two cracks in a test on a tubular K joint.

Fig 11.32

Comparison between experimental data (Ref 188) and line spring results.

The solid lines represent the experimental data;

The crosses represent line spring results.

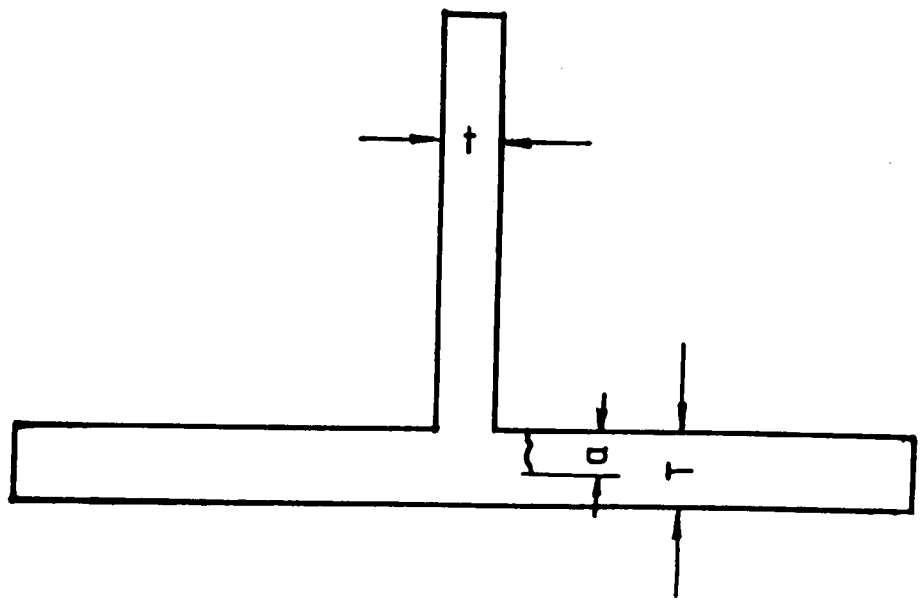

$\frac{t}{T} = 0.79$

Fig 11.1

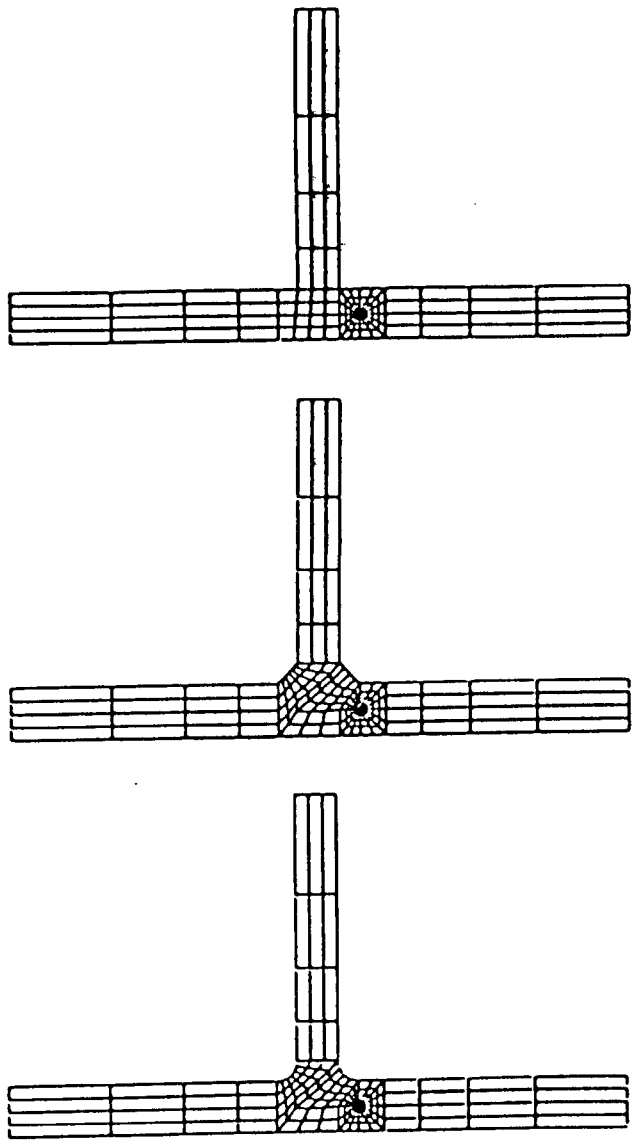

Fig 11.2

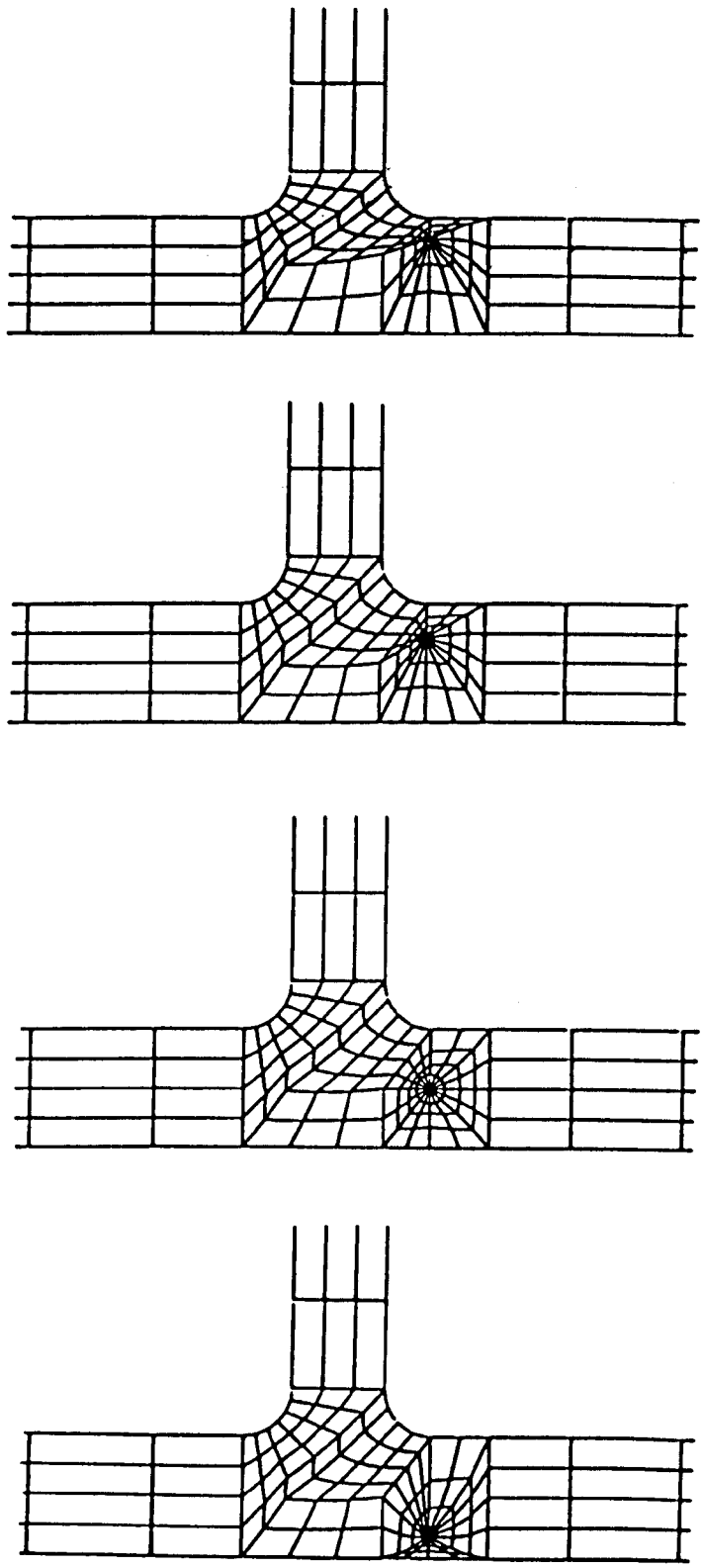

Fig 11.3

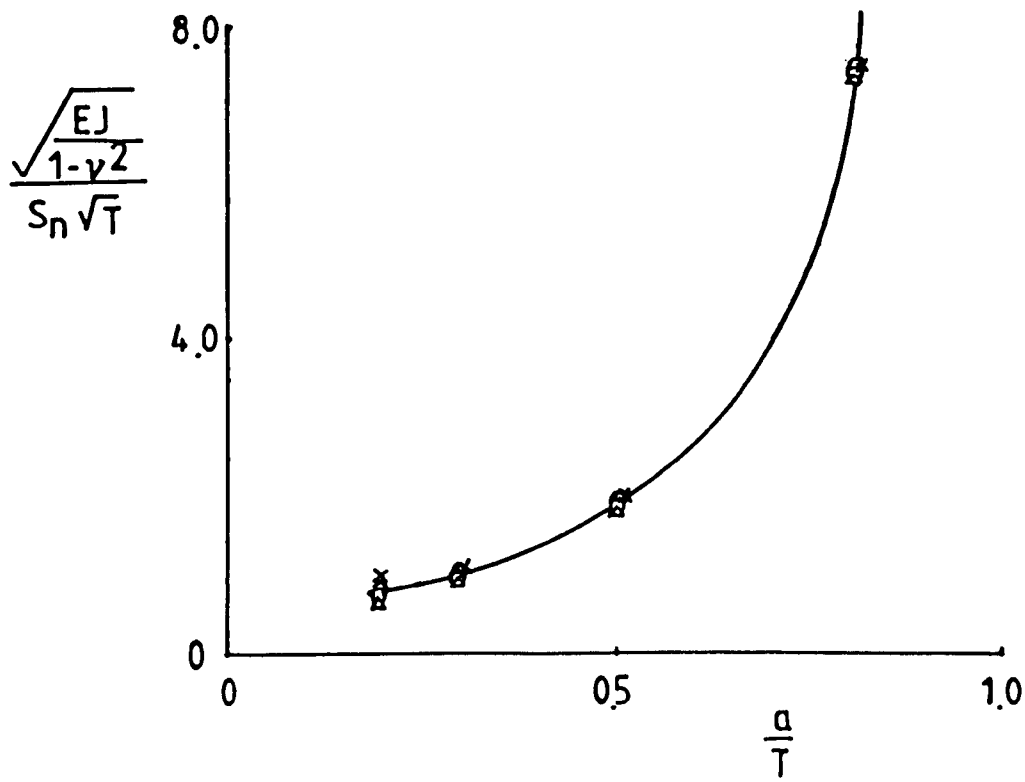

Fig 11.4

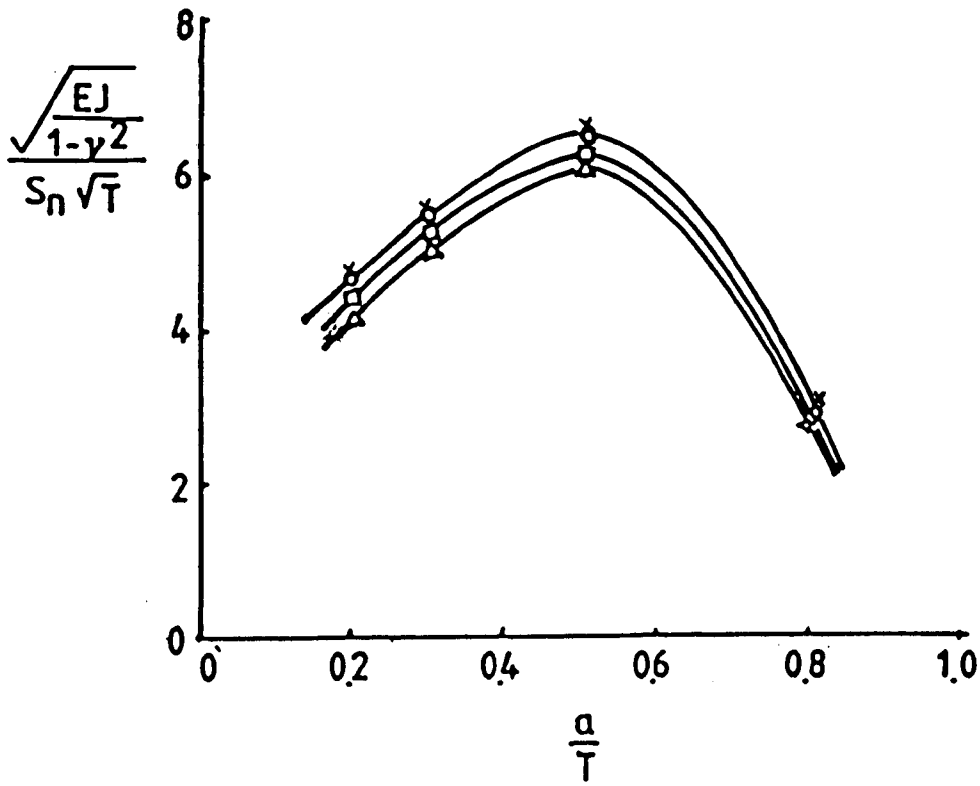

Fig 11.5

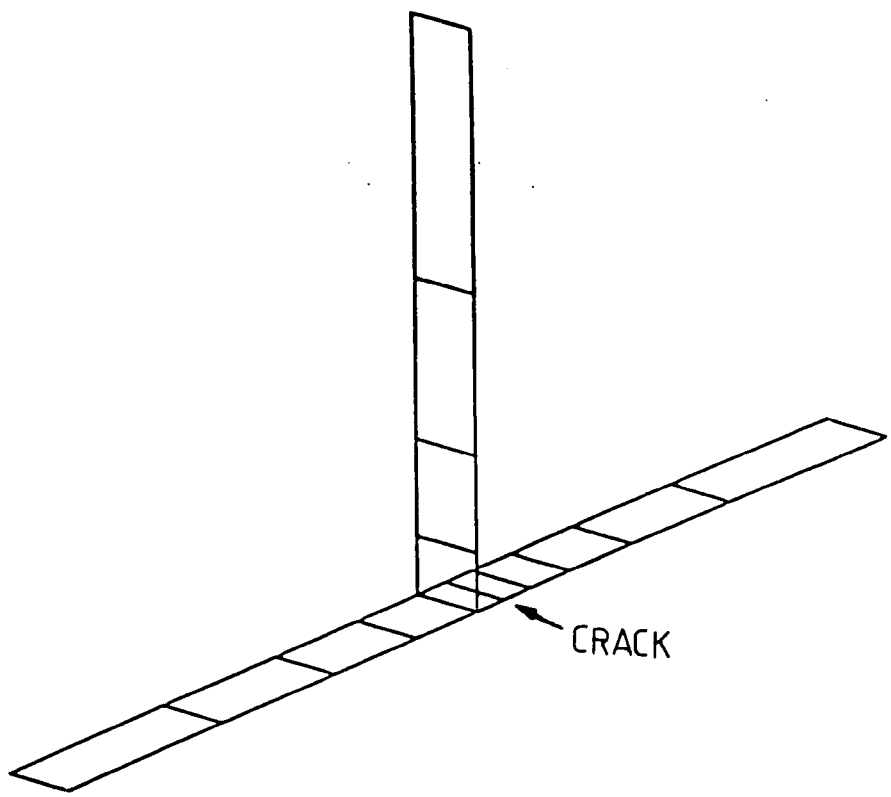

Fig 11.6

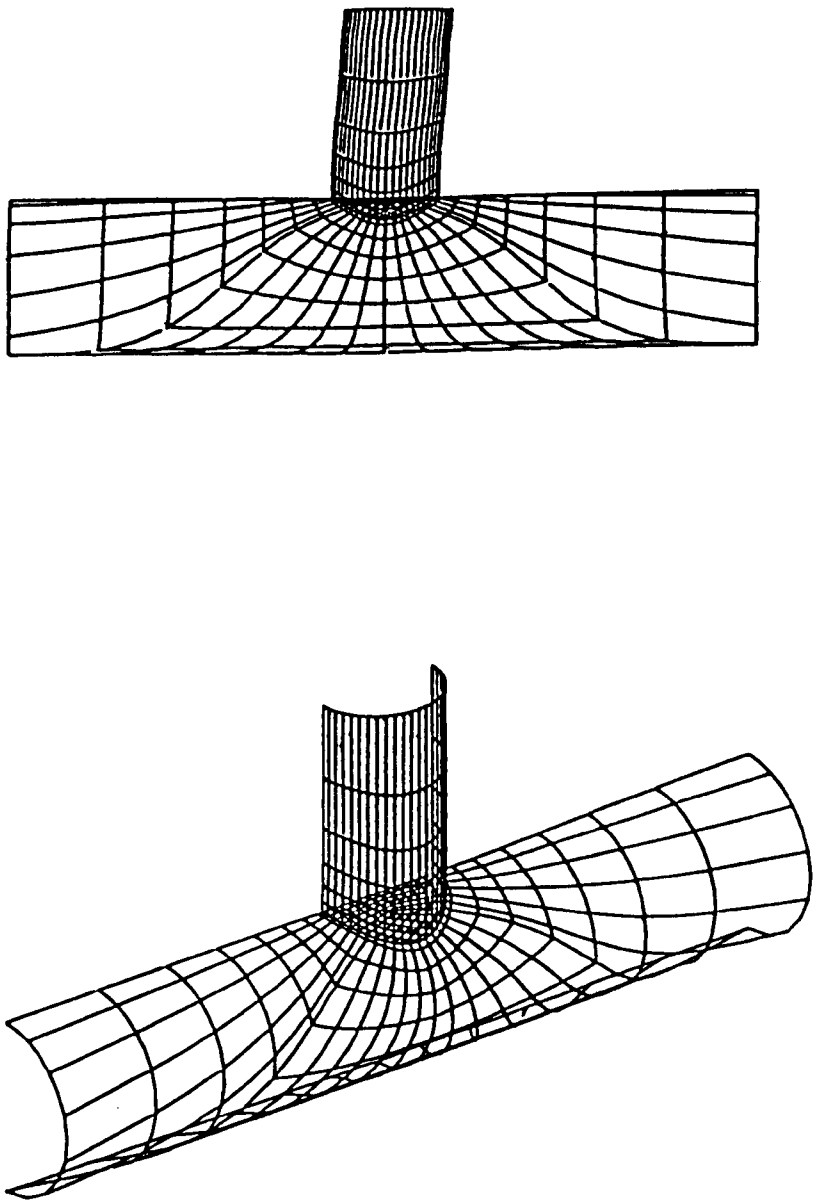

Fig 11.7

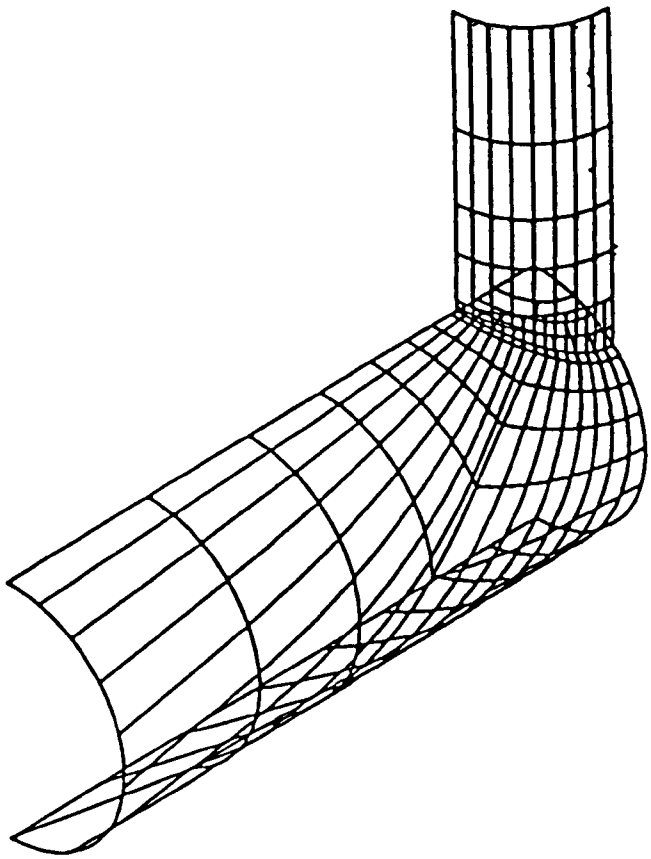

Fig 11.8

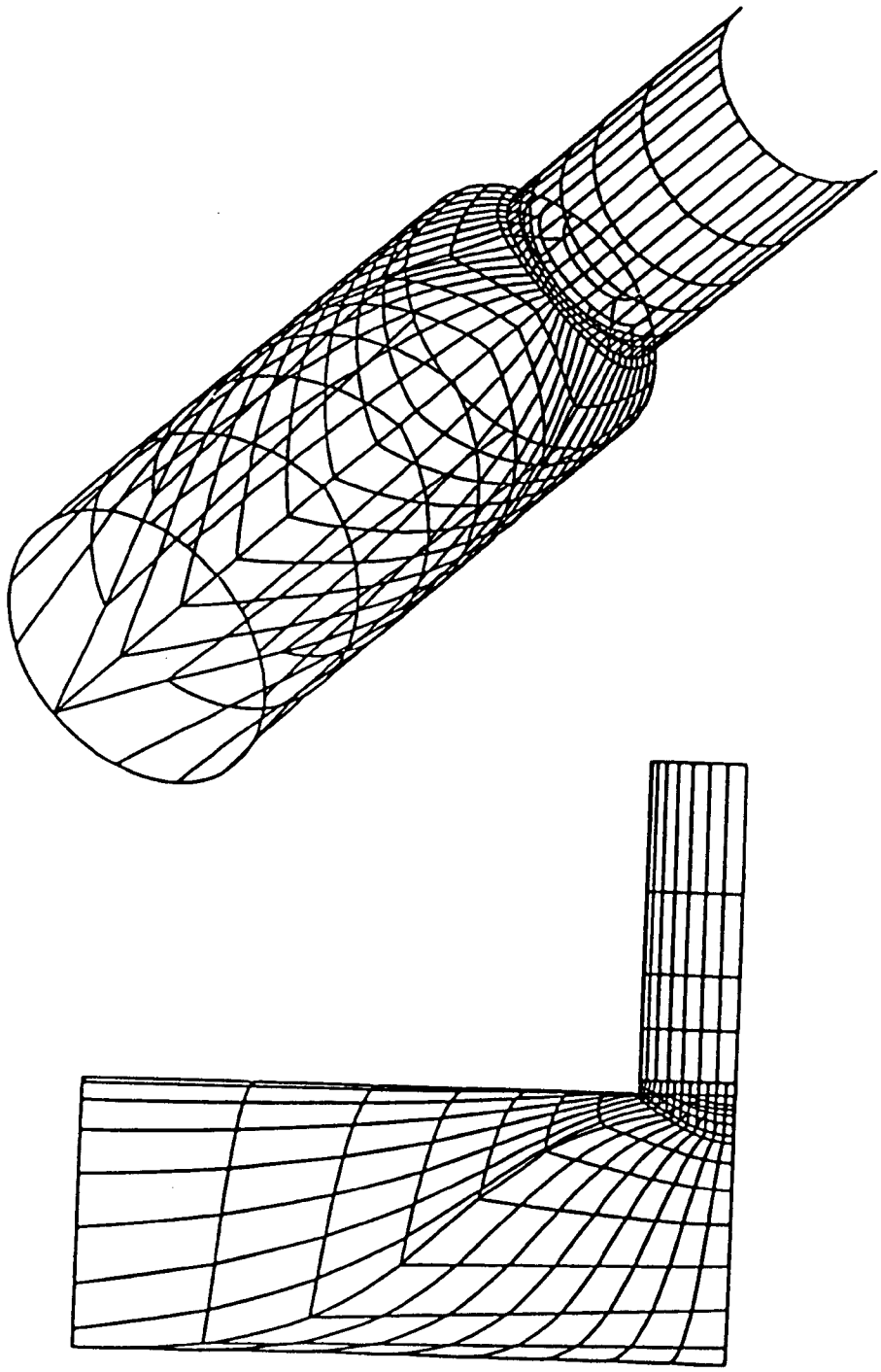

Fig 11.9

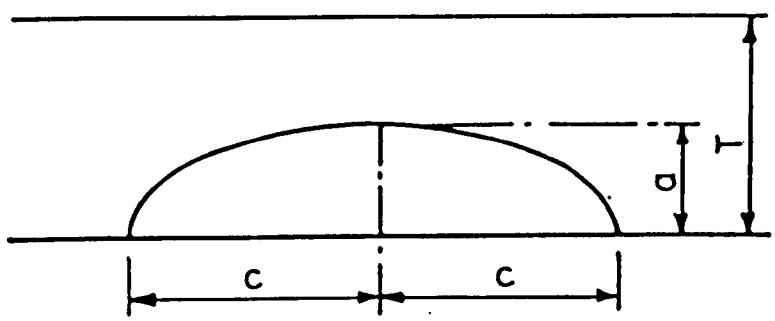

Fig 11.10

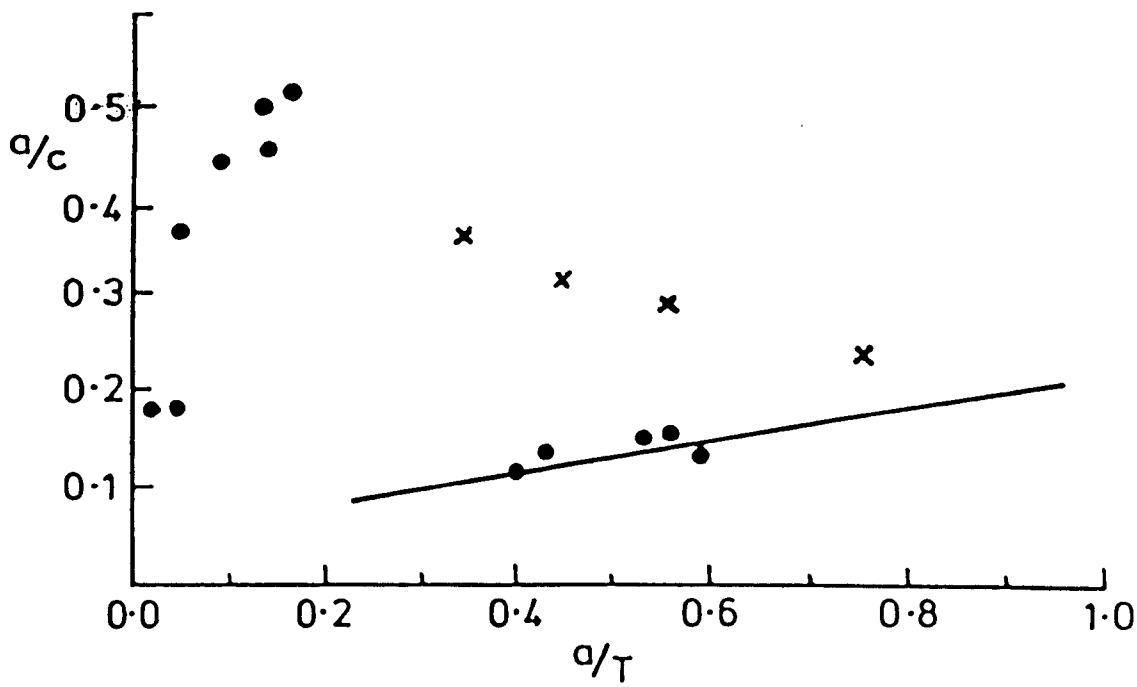

Fig 11.11

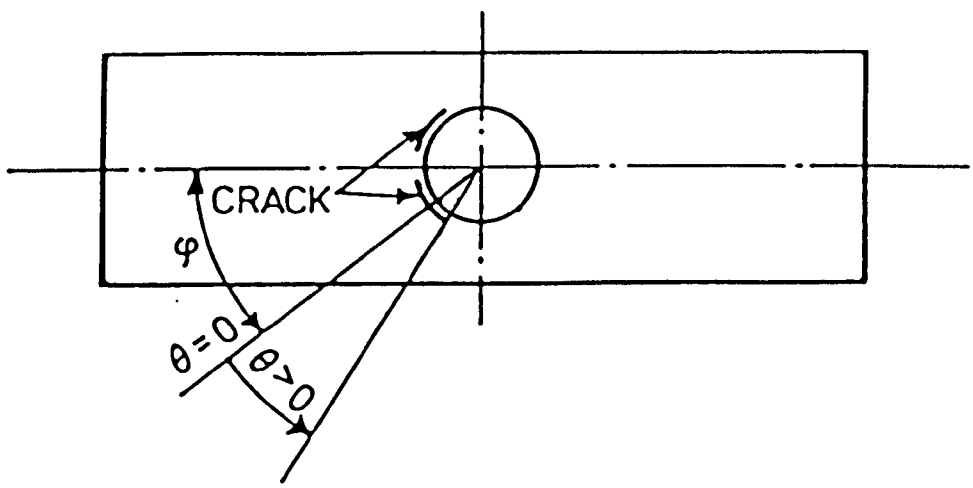

Fig 11.12

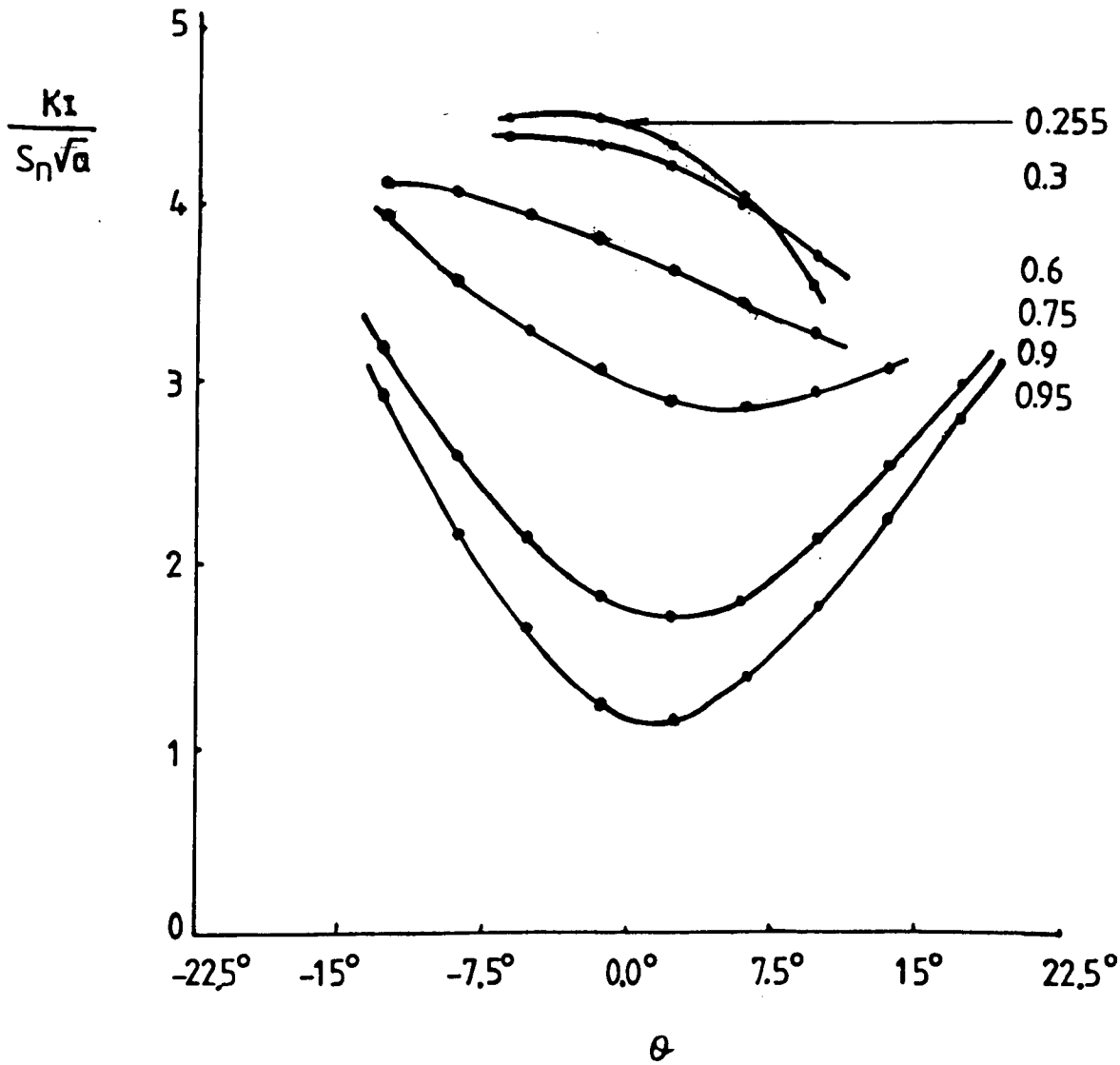
$\frac{K_I}{S_n\sqrt{a}}$
5
4
3
2
1
0
0.255
0.3
0.6
0.75
0.9
0.95
-22.5°
-15°
-7.5°
0.0°
7.5°
15°
22.5°
θ

Fig 11.13

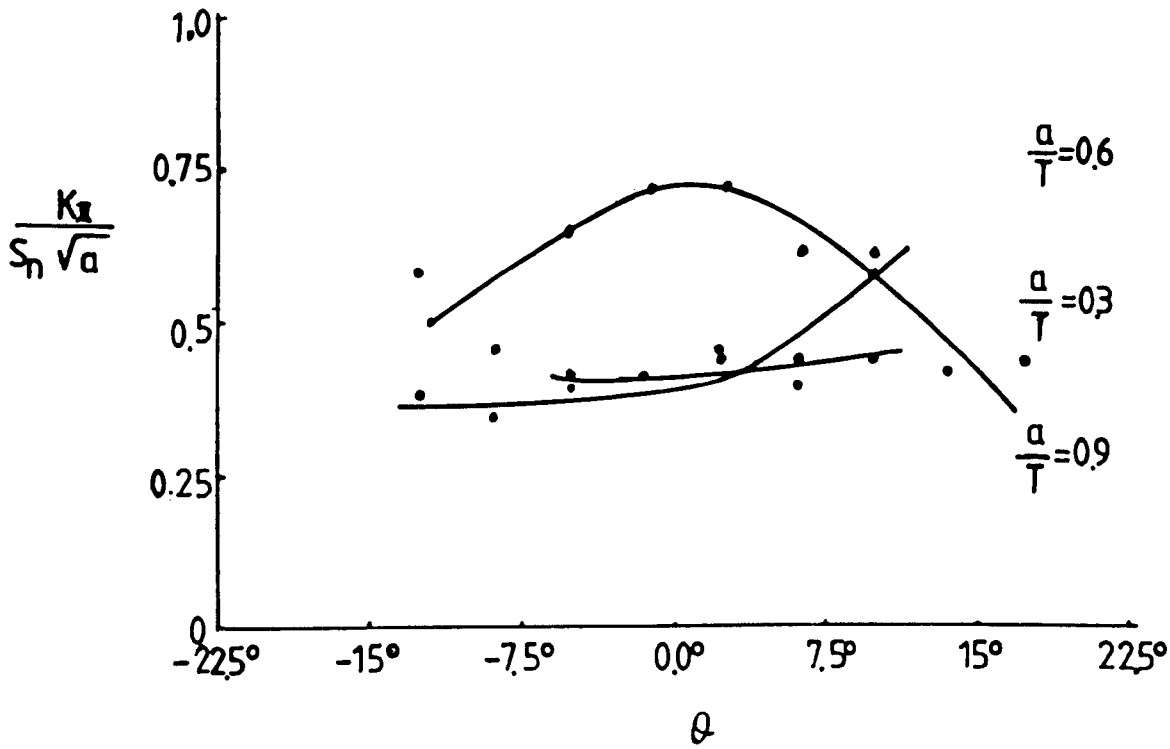
1.0
0.75
0.5
0.25
0
$\frac{K_I}{S_n\sqrt{a}}$
$\frac{a}{T}=0.6$
$\frac{a}{T}=0.3$
$\frac{a}{T}=0.9$
-22.5°
-15°
-7.5°
0.0°
7.5°
15°
22.5°
θ

Fig 11.14

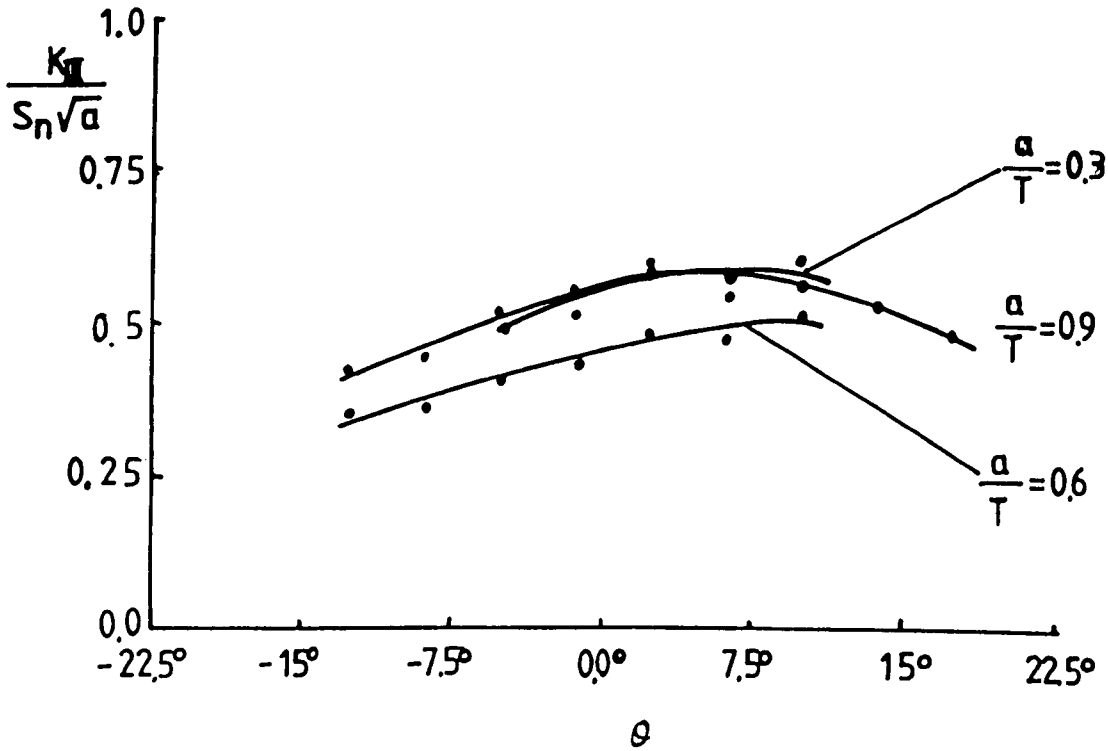
1.0
$\frac{K_{II}}{S_n\sqrt{a}}$
0.75
0.5
0.25
0.0
-22.5°
-15°
-7.5°
0.0°
7.5°
15°
22.5°
θ
$\frac{a}{T}$=0.3
$\frac{a}{T}$=0.9
$\frac{a}{T}$=0.6

Fig 11.15

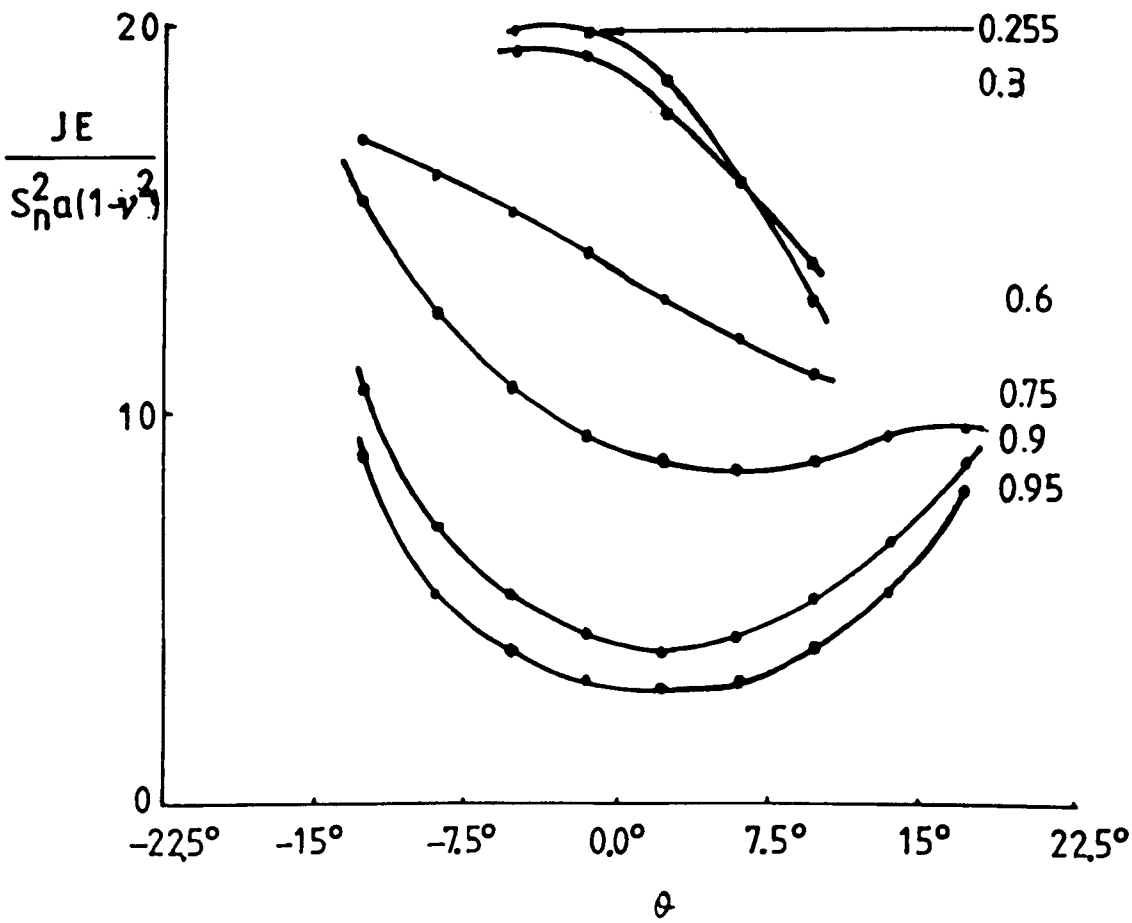

Fig 11.16

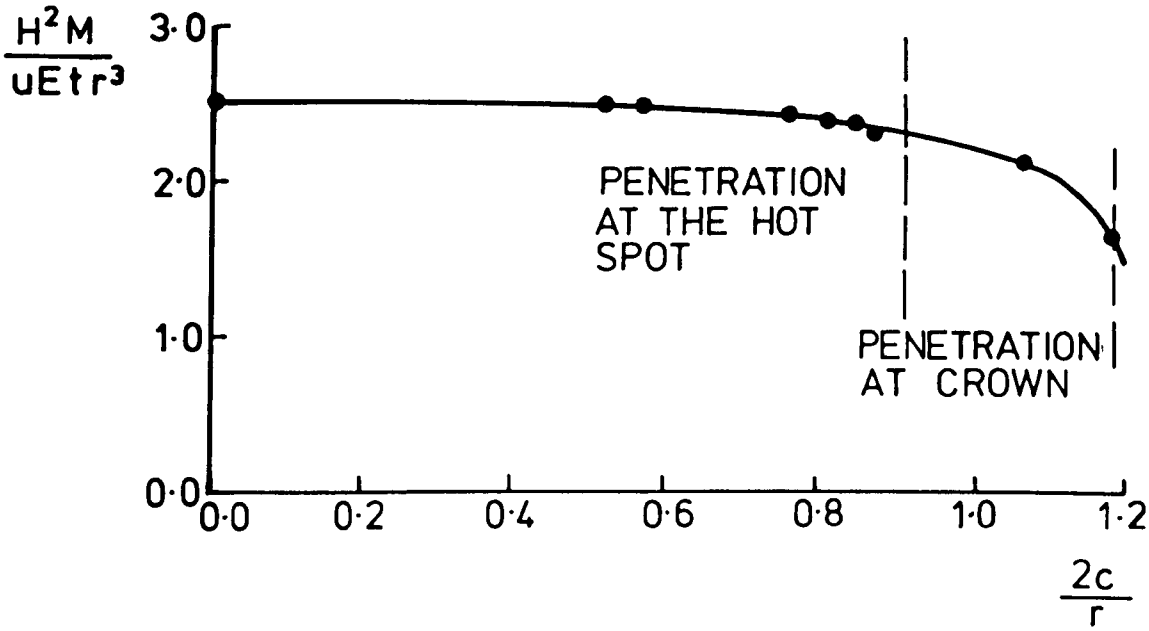
$\frac{H^2M}{uEtr^3}$
3·0
2·0
1·0
0·0
0·0
0·2
0·4
0·6
0·8
1·0
1·2
PENETRATION AT THE HOT SPOT
PENETRATION AT CROWN
$\frac{2c}{r}$

Fig 11.17

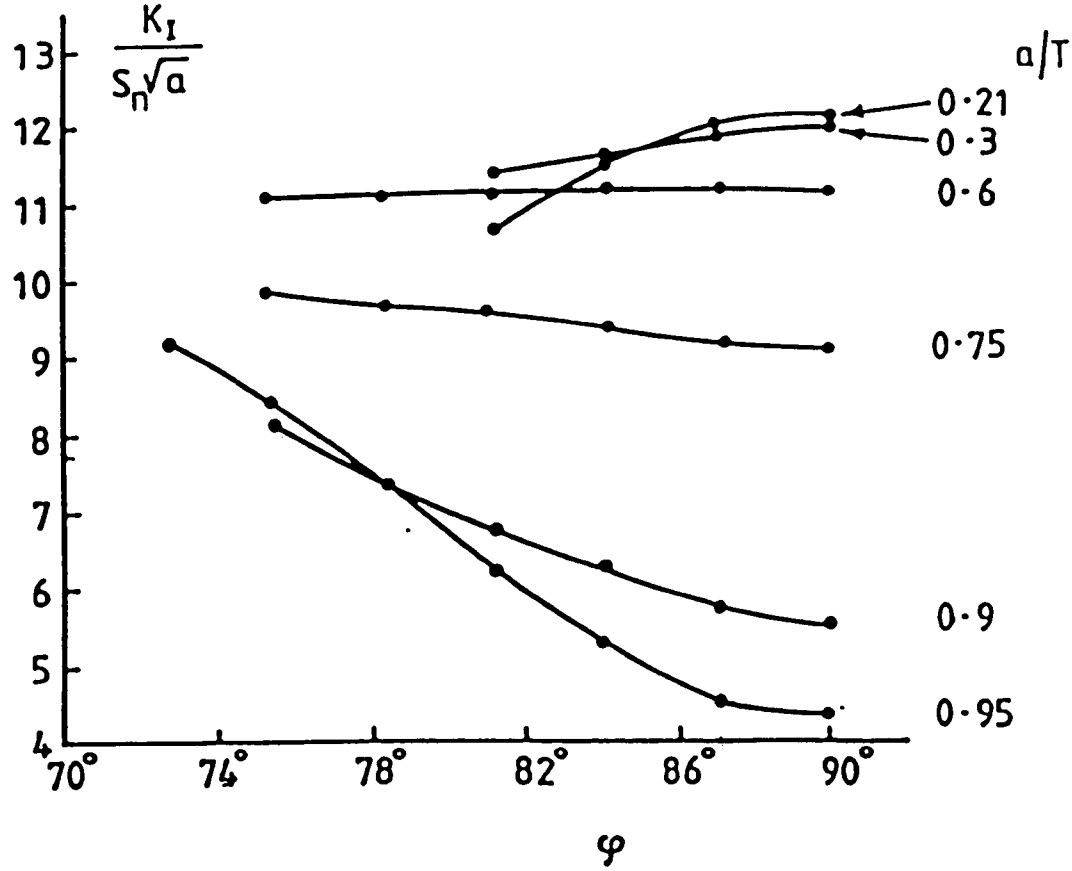
$\frac{K_I}{S_n\sqrt{a}}$
a/T
13
12
11
10
9
8
7
6
5
4
70°
74°
78°
82°
86°
90°
φ
0·21
0·3
0·6
0·75
0·9
0·95

Fig 11.18

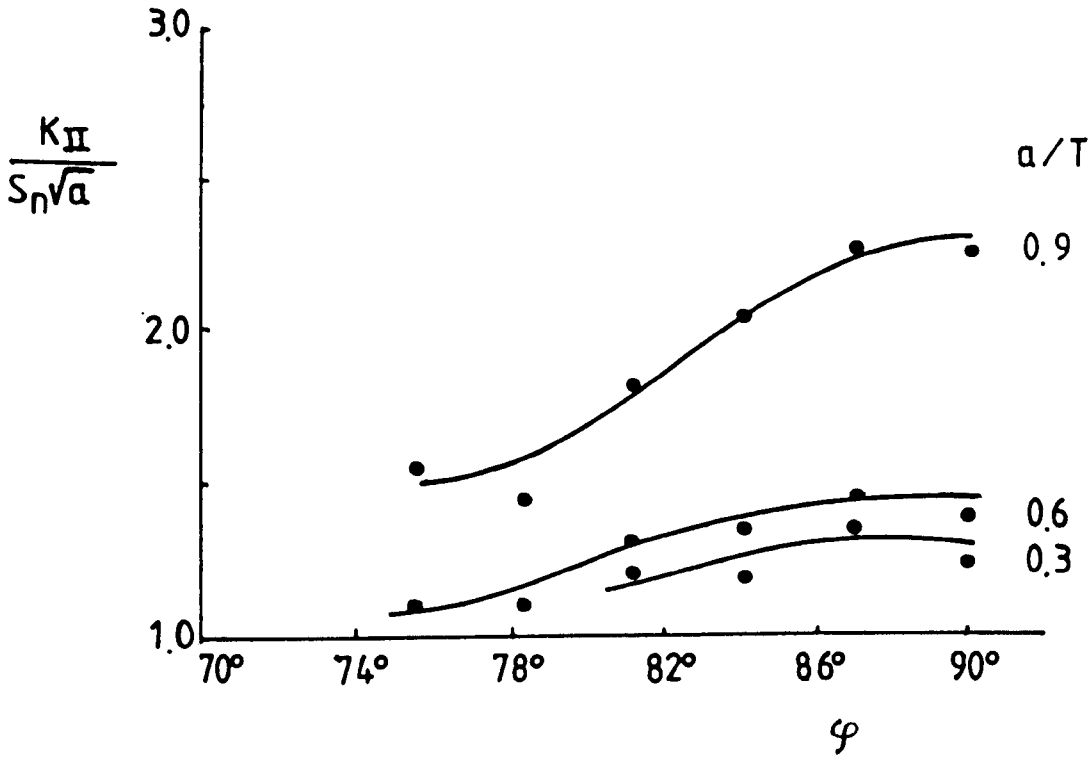

Fig 11.19

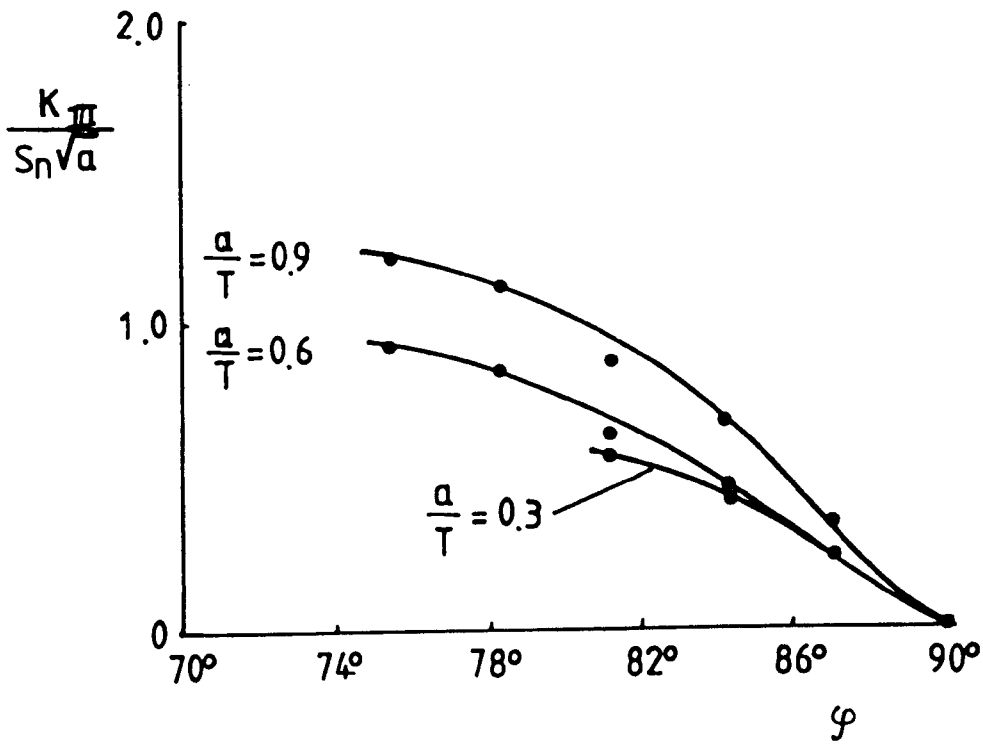
2.0
$\frac{K\sqrt{\pi}}{S_n\sqrt{a}}$
1.0
0
$\frac{a}{T}=0.9$
$\frac{a}{T}=0.6$
$\frac{a}{T}=0.3$
70°
74°
78°
82°
86°
90°
φ

Fig 11.20

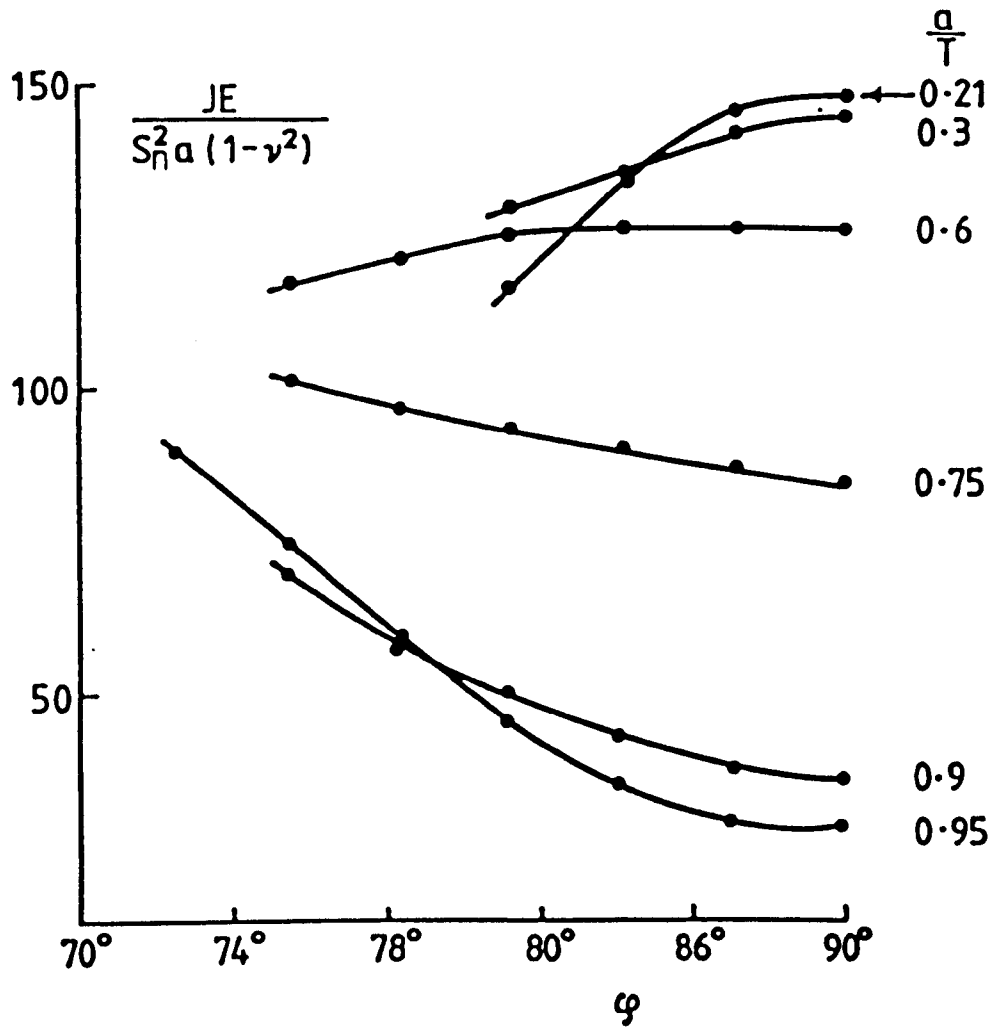

Fig 11.21

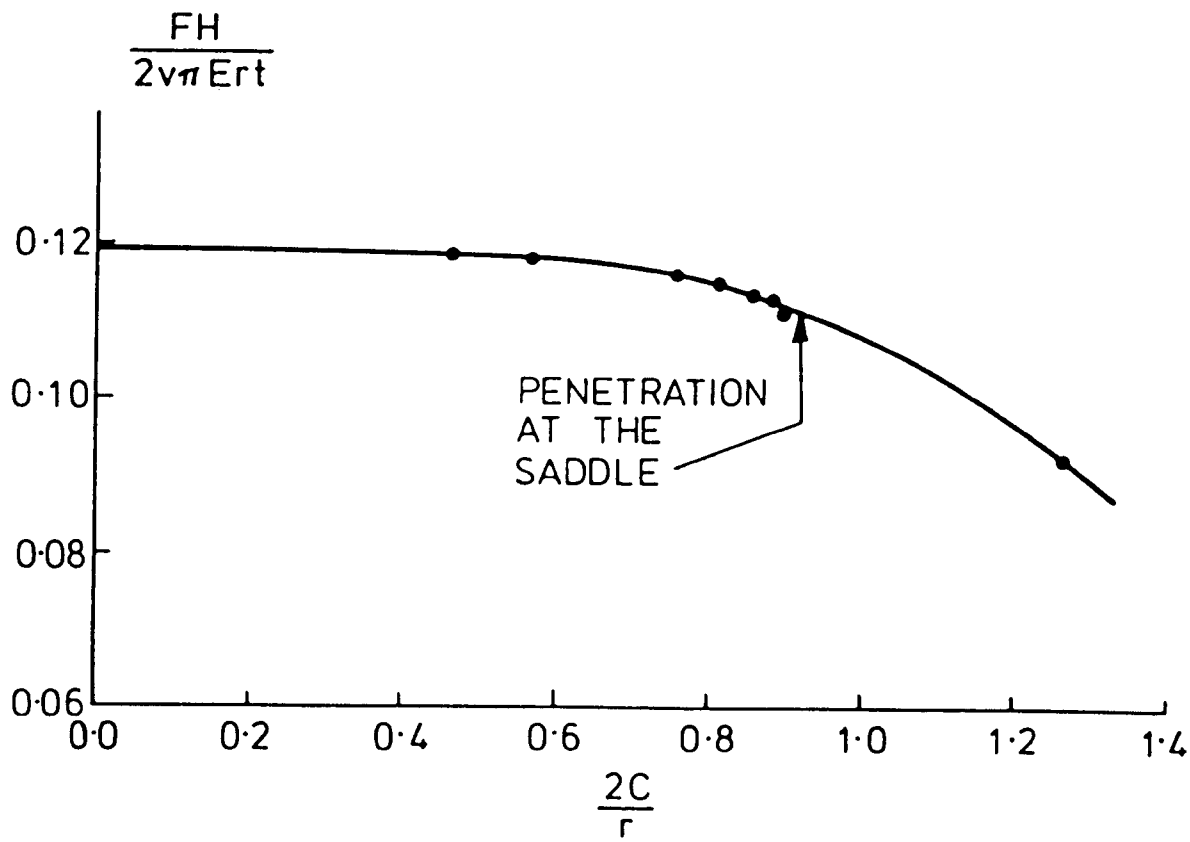
FH
2vπ Ert
0·12
0·10
0·08
0·06
0·0
0·2
0·4
0·6
0·8
1·0
1·2
1·4
2C
r
PENETRATION
AT THE
SADDLE

Fig 11.22

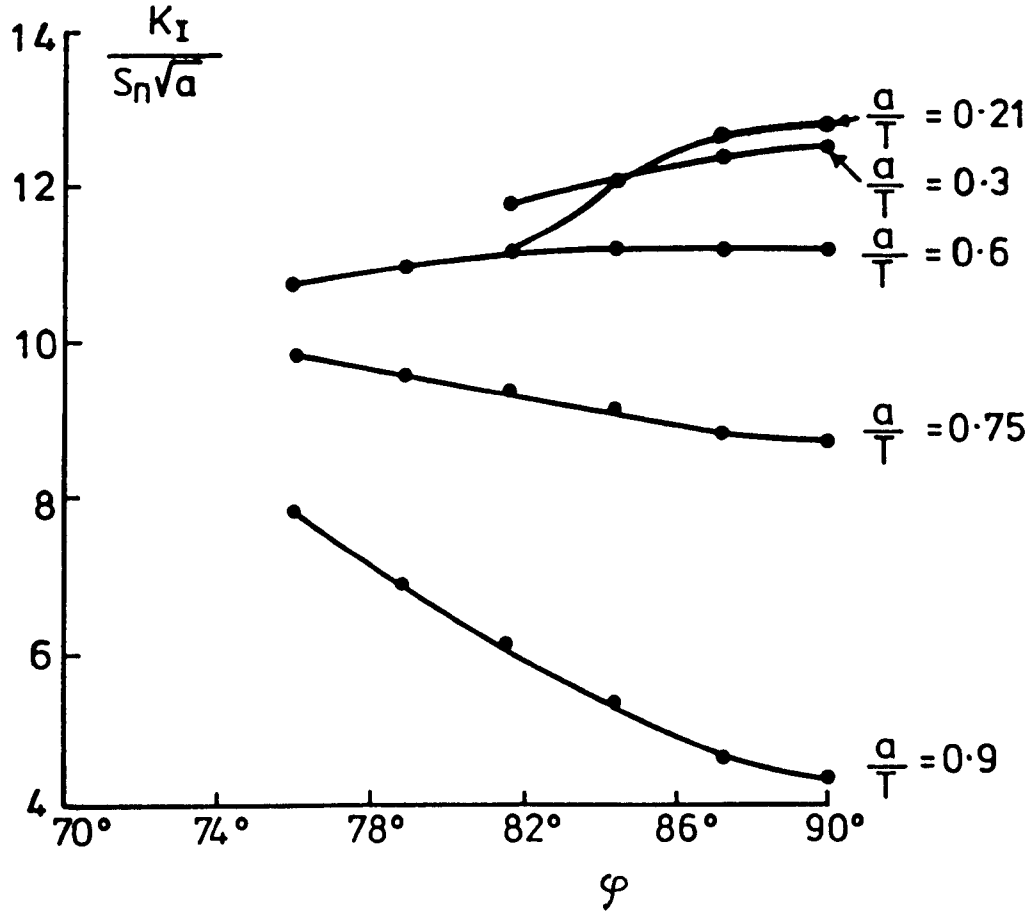
$\frac{K_I}{S_n\sqrt{a}}$
14
12
10
8
6
4
70°
74°
78°
82°
86°
90°
φ
$\frac{a}{T}$ = 0·21
$\frac{a}{T}$ = 0·3
$\frac{a}{T}$ = 0·6
$\frac{a}{T}$ = 0·75
$\frac{a}{T}$ = 0·9

Fig 11.23

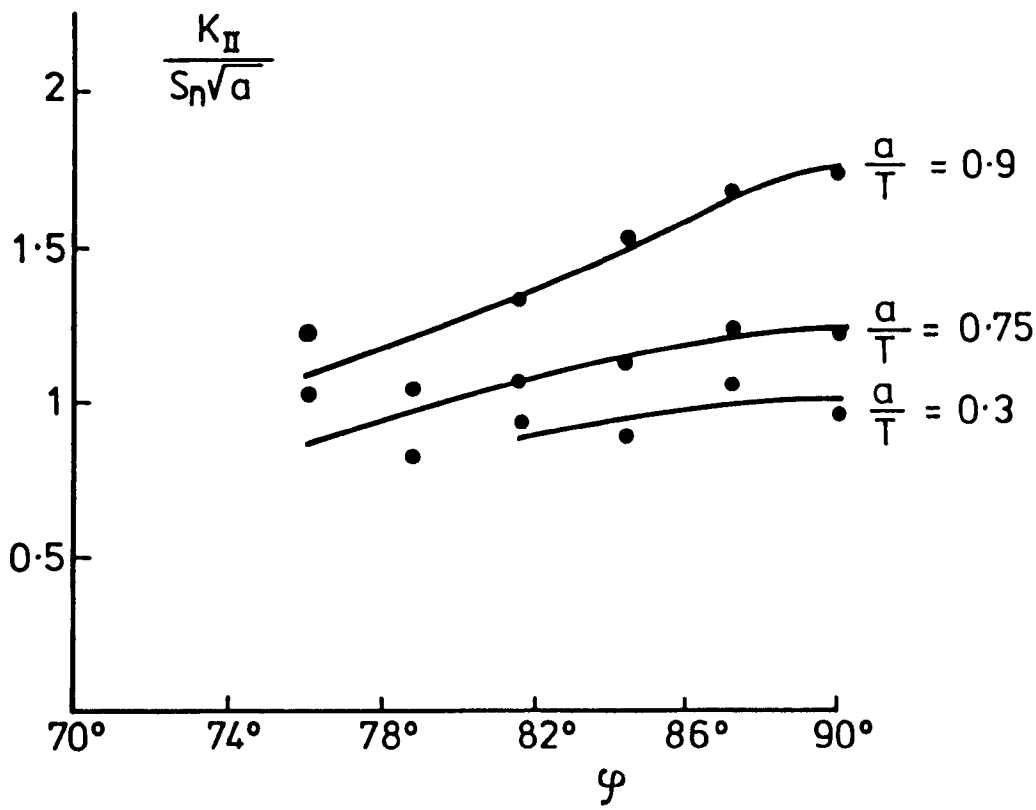
$\frac{K_{II}}{S_n\sqrt{a}}$
2
1·5
1
0·5
70°
74°
78°
82°
86°
90°
φ
$\frac{a}{T}$ = 0·9
$\frac{a}{T}$ = 0·75
$\frac{a}{T}$ = 0·3

Fig 11.24

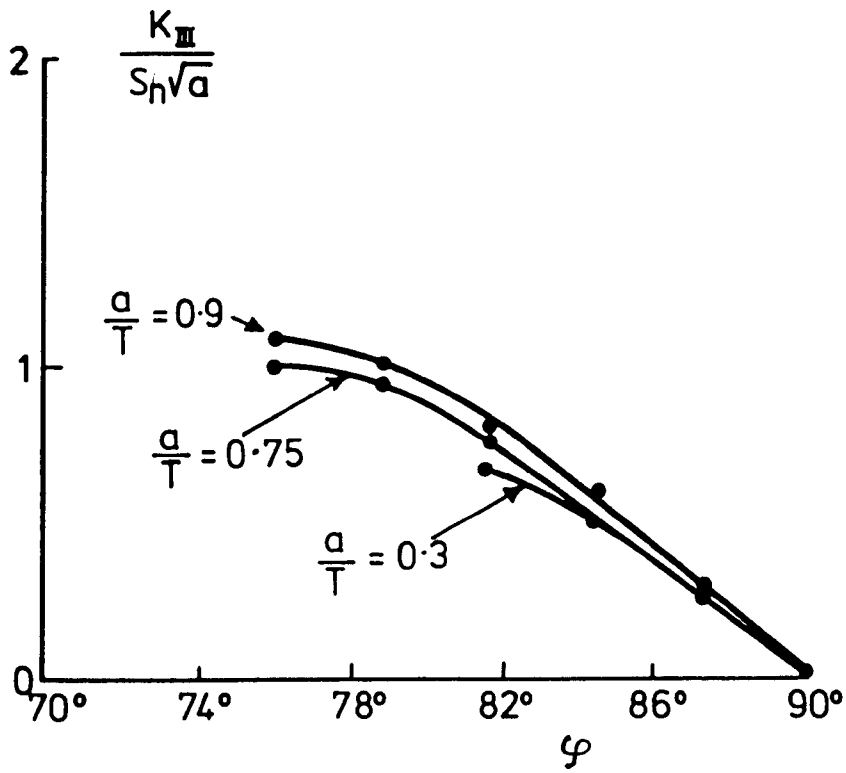
$\frac{K_{III}}{S_n\sqrt{a}}$
2
1
0
$\frac{a}{T} = 0{\cdot}9$
$\frac{a}{T} = 0{\cdot}75$
$\frac{a}{T} = 0{\cdot}3$
70°
74°
78°
82°
86°
90°
φ

Fig 11.25

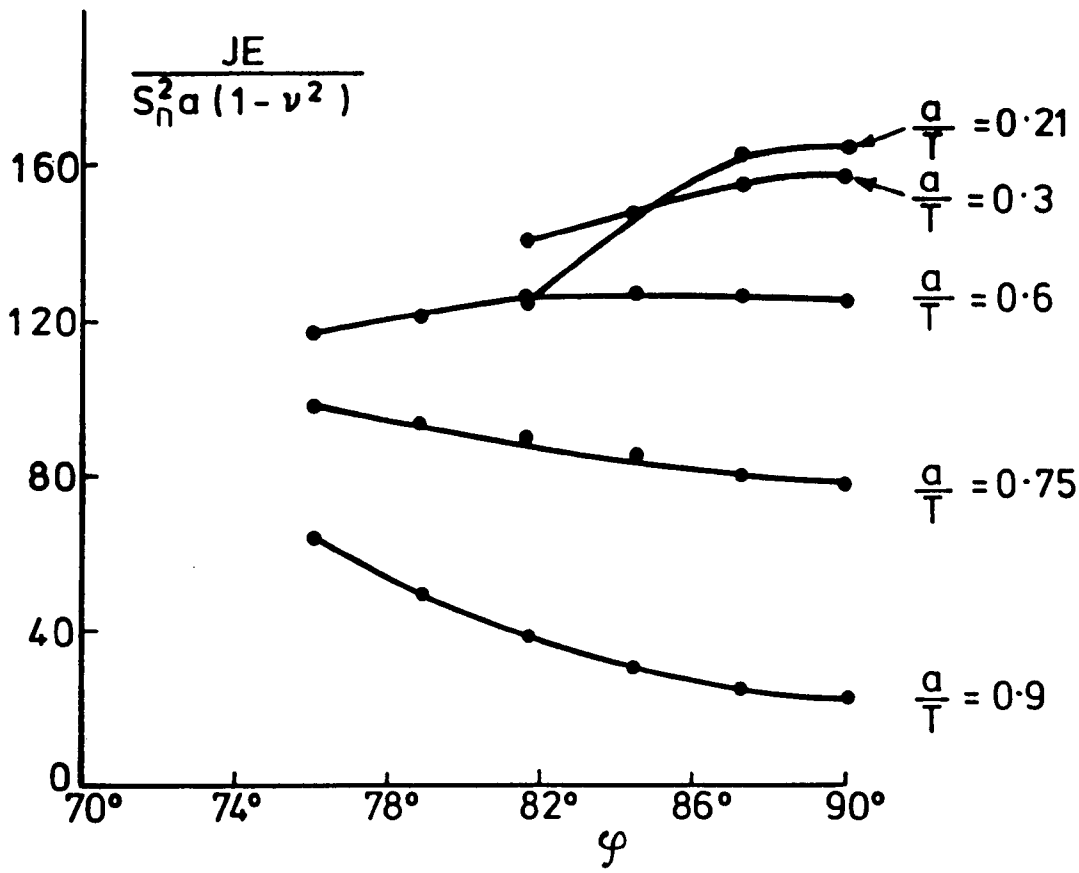
JE / S_n^2 a (1 - ν^2)
160
120
80
40
0
70°
74°
78°
82°
86°
90°
φ
a/T = 0·21
a/T = 0·3
a/T = 0·6
a/T = 0·75
a/T = 0·9

Fig 11.26

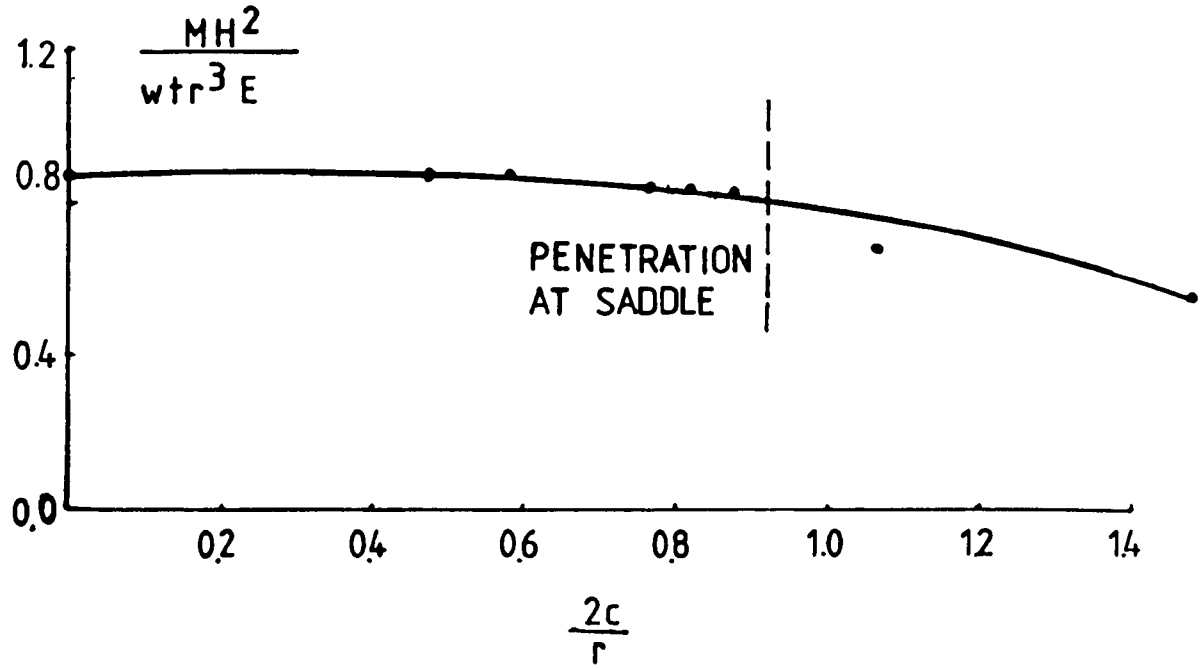
$\frac{MH^2}{wtr^3E}$
1.2
0.8
0.4
0.0
PENETRATION
AT SADDLE
0.2
0.4
0.6
0.8
1.0
1.2
1.4
$\frac{2c}{r}$

Fig 11.27

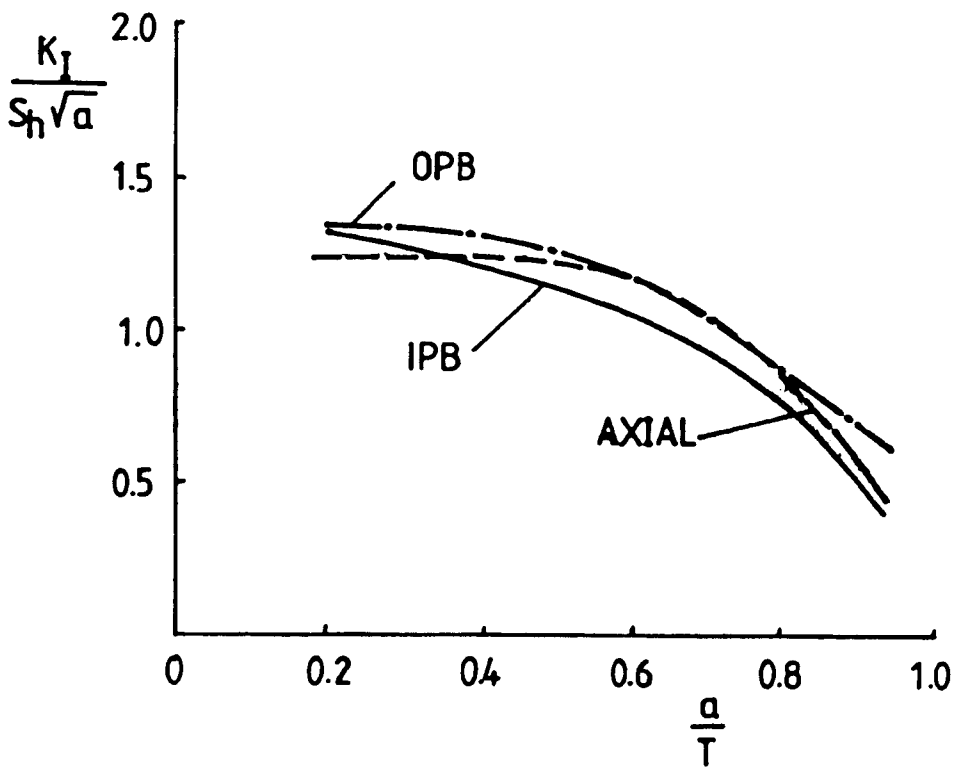

Fig 11.28

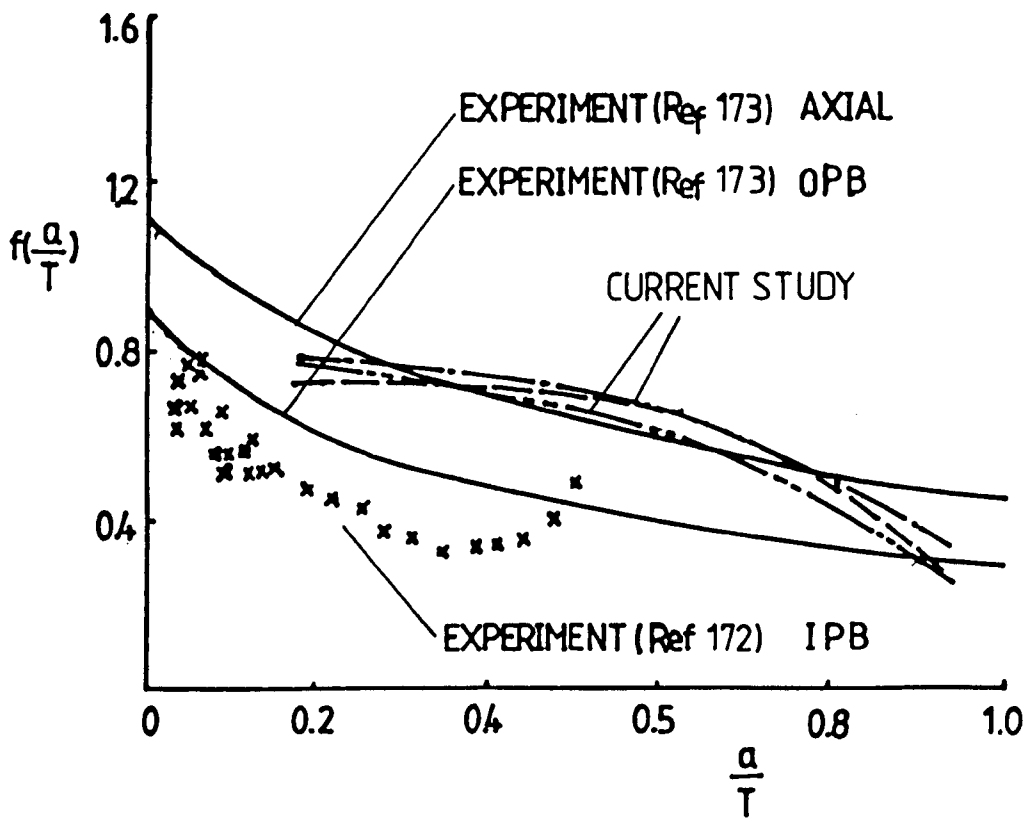
1.6
1.2
0.8
0.4
f(a/T)
EXPERIMENT (Ref 173) AXIAL
EXPERIMENT (Ref 173) OPB
CURRENT STUDY
EXPERIMENT (Ref 172) IPB
0
0.2
0.4
0.5
0.8
1.0
a/T

Fig 11.29

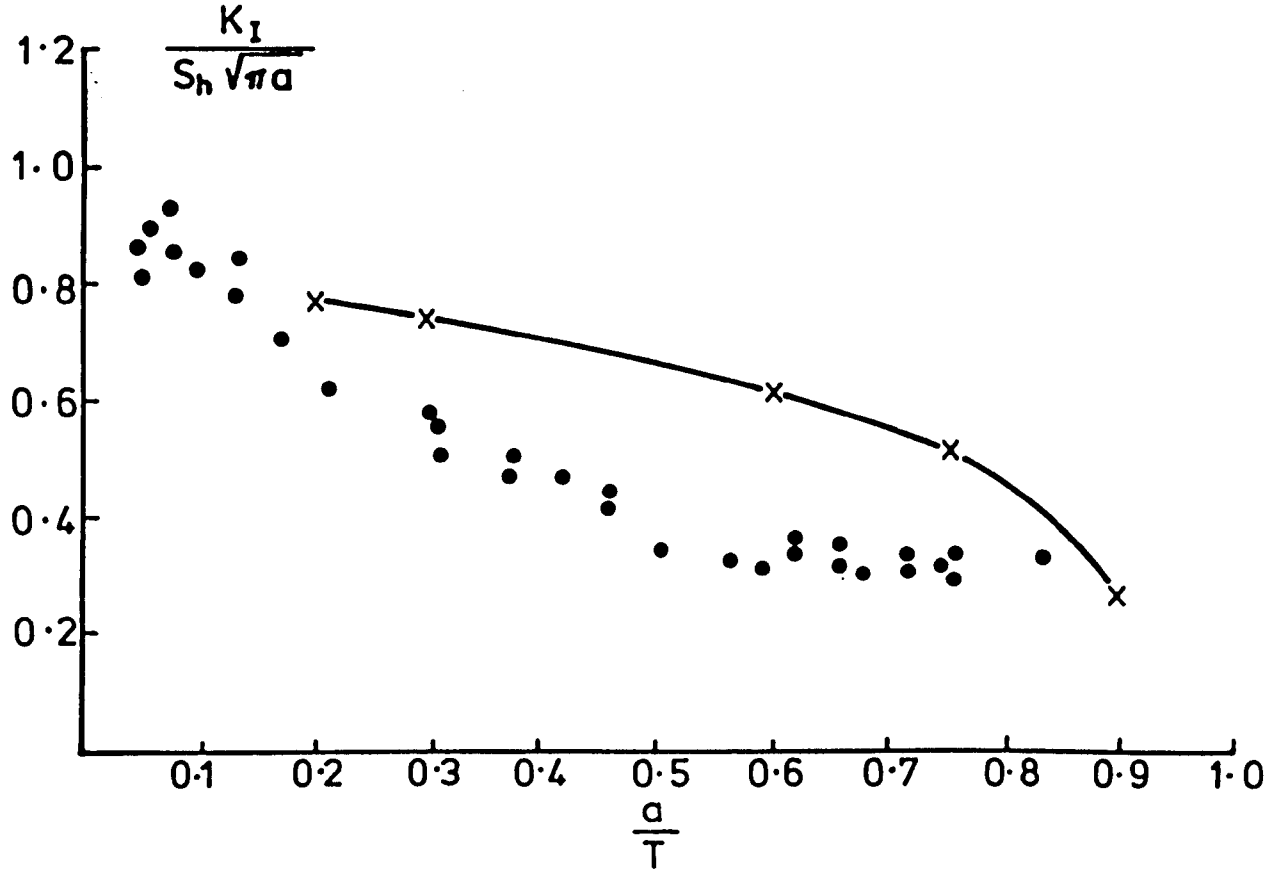
$\frac{K_I}{S_h\sqrt{\pi a}}$
1·2
1·0
0·8
0·6
0·4
0·2
0·1
0·2
0·3
0·4
0·5
0·6
0·7
0·8
0·9
1·0
$\frac{a}{T}$

Fig 11.30

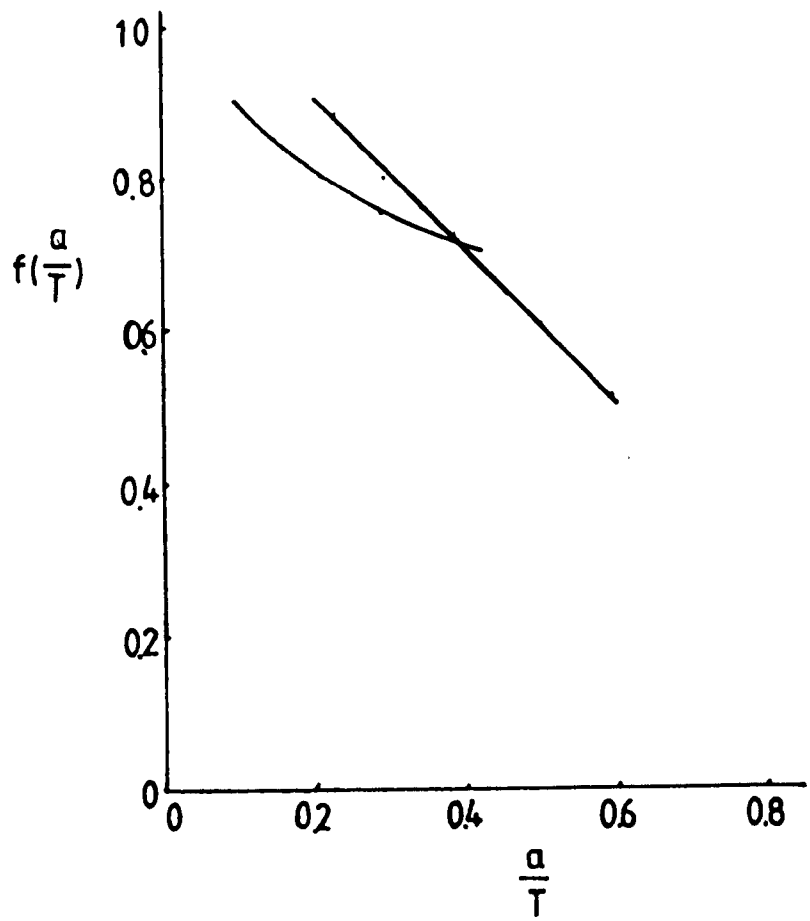

Fig 11.31

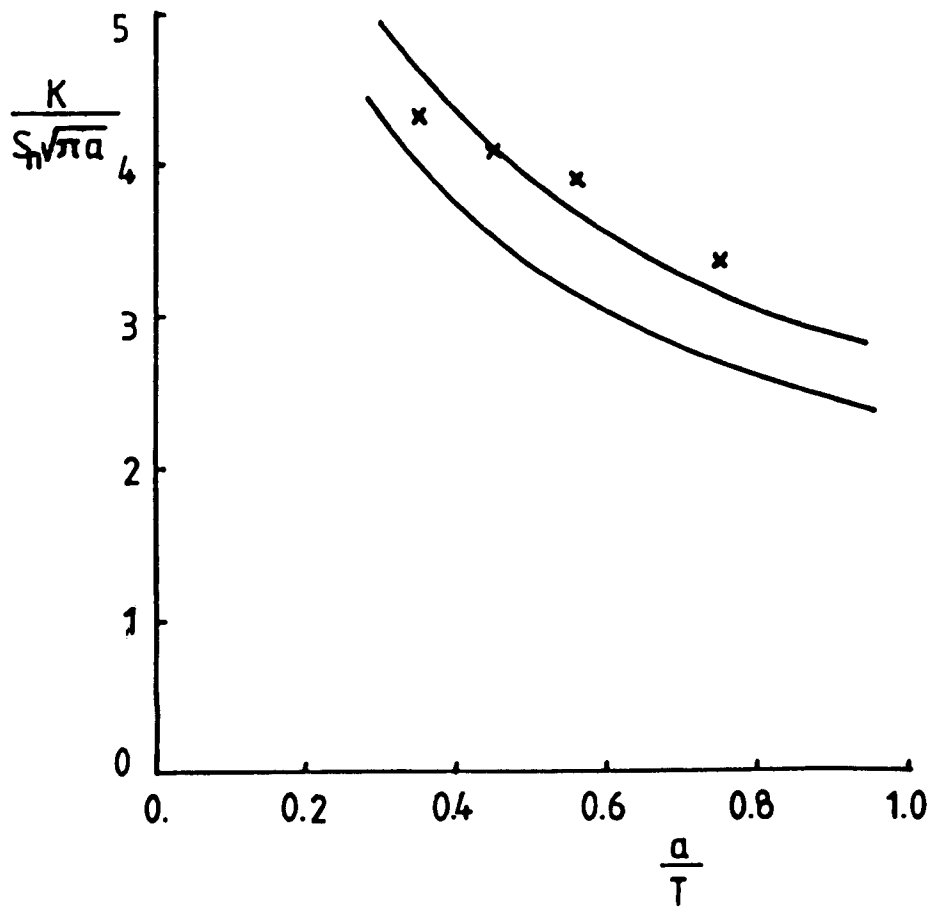

Fig 11.32

CHAPTER 12 PROBABILISTIC ANALYSIS OF THE FATIGUE LIFE OF A TUBULAR JOINT

It is now possible to perform a probabilistic fatigue analysis on the tubular T joint given in Fig 7.1 using fracture mechanics. The randomness of fatigue life was studied using the analytic method presented in Chapter 10. The application of this method requires specific information concerning the fatigue crack propagation in the joint, which is provided by the finite element analysis in Chapter 11.

SECTION 1 Fatigue Life Distribution of a Tubular Joint

In this fracture mechanics assessment of the fatigue life of a tubular joint, the following assumptions have been made:

a. The initial crack depth was arbitrarily assumed to be 10% of the chord wall.

b. The failure criterion was taken as 90% penetration of the chord wall, because beyound this point, plastic tearing may occur which can not be described by the stress intensity factor.

c. The crack shape during propagation is assumed to follow Eq 11.4.

d. There is no interaction between cycles in narrow band random loading. For broad band random loading, it may be possible to account for the interaction effect by introducing a single parameter into the present method. But such an adjustment has not yet been carried out.

Considerations have been given to the tubular welded T joint shown in Fig 7.1 and analysed in Chapter 11. Since the fatigue life was defined by the crack propagation, the deepest point of the crack is of main interest. The opening mode stress intensity factor at the deepest point can be expressed as

$$K_I = f(\frac{a}{T})\ S_n\ C_S\ \sqrt{(\pi a)} \qquad (12.1)$$

where C_S is the hot spot stress consentration factor. f(a/T) can be given as a function of a/T by the polynomial

$$f = C_1 + C_2(\frac{a}{T}) + C_3(\frac{a}{T})^2 + C_4(\frac{a}{T})^3 \qquad (12.2)$$

where C_1, C_2, C_3 and C_4 are constants. For each loading case, four pairs of values of a/T and corresponding opening mode stress intensity factor at the deepest point of the crack are required to input into Eq 12.2, so that a equation set can be produced from which C_1, C_2, C_3 and C_4 can be determined. The values of a/T and the corresponding K_I were obtained from Chapter 11. The stress intensity factor has been extrapolated to a/T<0.2 by Eq 12.2.

The material of the T joint was assumed to be BS 4360 50D steel. Parameters for describing fatigue crack growth rate under constant amplitude loading were given by Gall and Hancock (Ref 125, also see Section 7 in Chapter 10)

$$\mu_\alpha = 8.02 \times 10^{-12} \tag{12.3}$$

and

$$\sigma_\alpha = 1.59 \times 10^{-12} \tag{12.4}$$

The unit for da/dN is m/cycle and for the stress intensity factor is $MN\text{-}m^{-3/2}$. The fatigue loading was assumed to be narrow band random, and the effect of mean load was assumed negligible. In order to make the predictions for different load modes comparable, the fatigue load has been presented in terms of hot spot stresses. In this case, the root mean square of the hot spot stress is a parameter to represent the fatigue loading and was taken as $50MN/m^2$.

These data have been used as input of the computer program PANA (Section 5 in Chapter 10) which predicts the fatigue life distribution and the results are shown in Fig 12.1. The T joint under axial loding, in-plane and out-of-plane bending were considered separately. It can be seen that the life distributions for different modes are similar. For the tubular joint and crack growth route analysed, the present study shows that the hot spot stress can give an approximate indication of the fatigue life.

Perhaps the most important application of the present method is for

assessing the residual life of a cracked joint. A 90% through crack in a tubular joint can be regarded as intolerably dangerous so that for a part through defect, the residual fatigue life can be taken as the period in which the defect propagates to 90% wall penetration. To demonstrate the prediction of residual fatigue life, a half through crack was assumed and other conditions in the prediction of fatigue life were unchanged. The calculated residual life distribution is shown in Fig 12.2

SECTION 2 Corelation with S-N Curve

It is useful to relate the current new method to the traditional methods, therefore the applicability of the present method can be shown immediately. The present method has been used to analyse some experimental S-N data presented by Wylde and McDonald (Ref 167). These data were obtained from constant amplitude fatigue tests on tubular welded T joints. The dimensions of the joints are realistic, for instance the diameter of the chord is 457mm. The fatigue life against loading curve has been presented in terms of hot spot strain range ϵ_h which can be converted into hot spot stress range S_h by

$$S_h = \epsilon_h \times E \qquad (12.5)$$

E is the Young's modulus and has been taken as

$$E = 210 \times 10^9 \ N/m^2 \qquad (12.6)$$

For random fatigue, an equivalent hot spot strain range ϵ_e can be defined as

$$\epsilon_e = \left\{ E\left[\left(\frac{C_s S}{E}\right)^n \right] \right\}^{\frac{1}{2}} \qquad (12.7)$$

which reduces to the hot spot strain range for constant amplitude situations.

Based on this equivalent hot spot strain range and the assumptions made in the last section, the present analysis has been utilized to produce fatigue life predictions which are presented in the form of an ϵ_e against life curve for in plane bending cases. The 95% confidence limits for the ϵ_e vs. N curve have also been compared in Fig 12.3 with the DD55Q curve and experimental data (Ref 167). There is a general agreement between the prediction and the experimental data, although there are a number of differences. One is the difference in the definition of the fatigue life since in the prediction, an initial crack size was assumed, while in experiment, the fatigue life is regarded as the whole experimental period terminated when the limit of the actuating capacity of the machine is reached. The percentage of life to through thickness cracking is about 45% of the total fatigue life in the experiments (Ref 167). Another difference is that the experimental data were collected from experiments using various S_{min}/S_{max} ratios and different loading modes. The third can be identified as differences in the geometry of the tubular joints.

Nevertheless, it can be seen that the theoretical analysis generally describes the relation between hot spot strain range and fatigue life. For longer fatigue life, the analysis is conservative. A

potential use of the analysis is to assist in the production of an S-N curve. In this case, the theoretical prediction can be backed up by a few experimental points. Furthermore, the present analysis can produce S-N curves for different levels of failure probability. Such information is sometimes important as well as enormously costly if experimental methods are used.

In many cases, there are no indications about the scatter of S-N curves and many designs are based on conventional mean S-N curves. Thus the probability of failure of the structures during service can not be eliminated. It can be analysed using the above technique however. This technique can be combined with experiments to produce S-N curves cheaply for different reliability levels which is necessary in full structural analysis.

LIST OF FIGURES FOR CHAPTER 12

Fig 12.1

Probability distribution of fatigue life of the tubular welded T joint.

The solid line represeNts in-plane bending;

The broken line represents axial loading;

The dotted line represents out-of-plane bending.

Fig 12.2

The distribution of residual fatigue life of the tubular welded T joint with a half through crack.

The solid line represents in-plane bending;

The broken line represents axial loading;

The dotted line represents out-of-plane bending.

Fig 12.3

The S-N curve produced by the current analysis for mean life and 95% probability band in comparison with experimental data (Ref 167) and DD55Q curve (Ref 177). One solid line represents the mean life from the current analytic prediction, with two broken lines indicating the 95% confidence

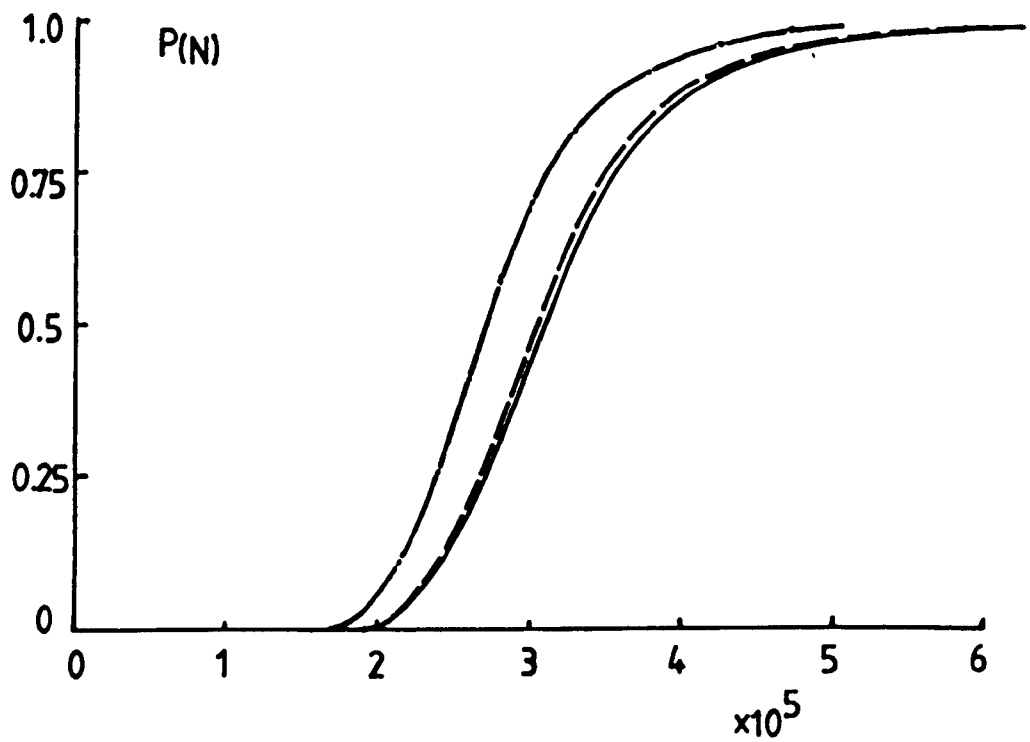

Fig 12.1

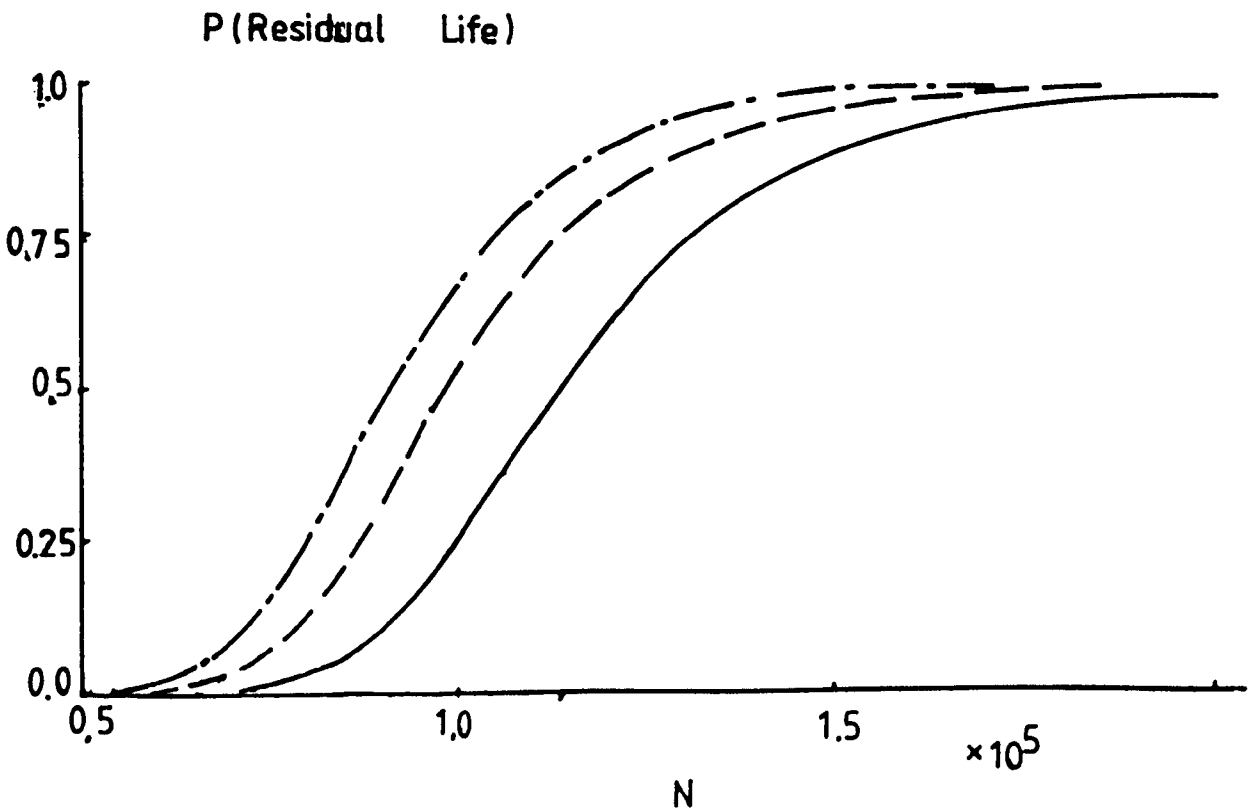

Fig 12.2

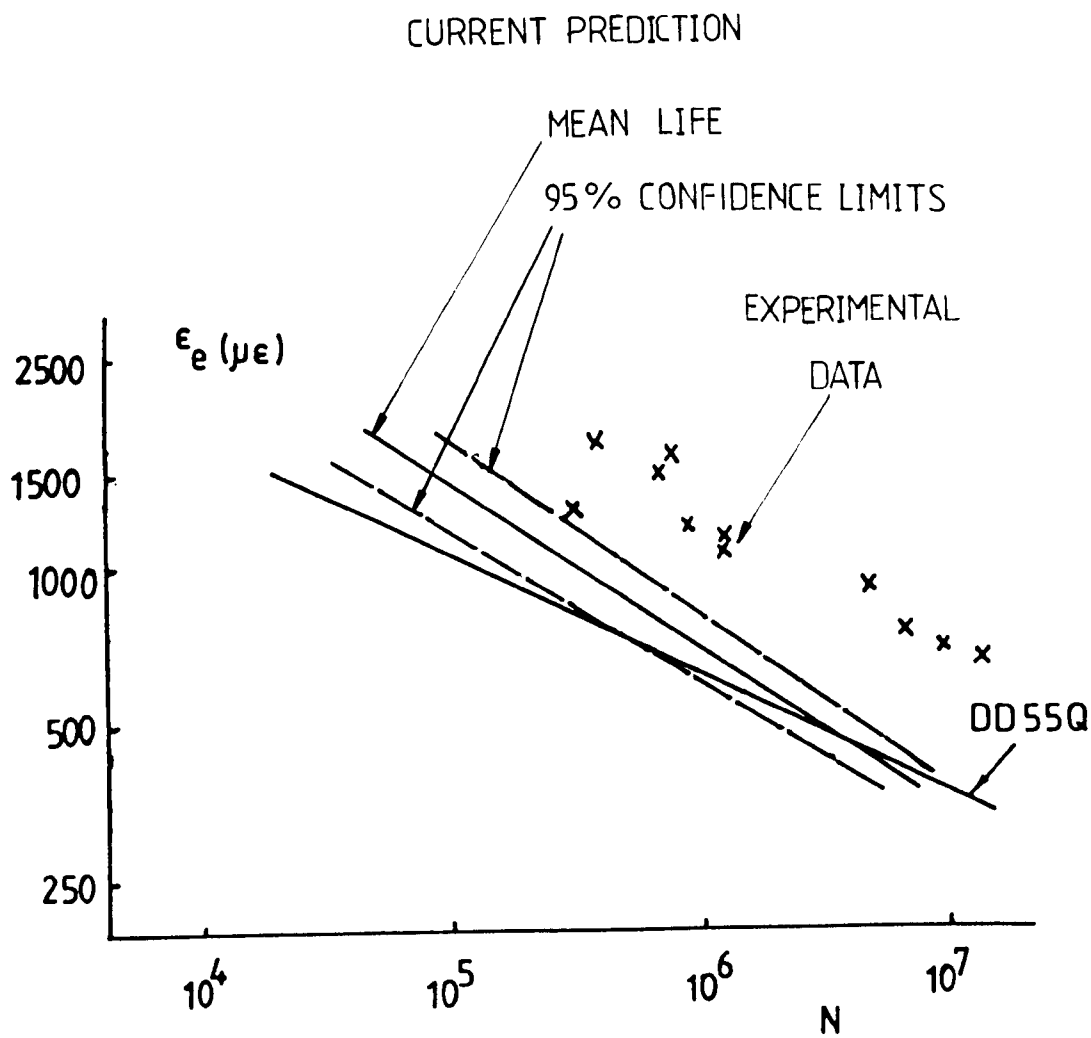
CURRENT PREDICTION
MEAN LIFE
95% CONFIDENCE LIMITS
EXPERIMENTAL
DATA
ϵ_e ($\mu\epsilon$)
2500
1500
1000
500
250
DD55Q
10^4
10^5
10^6
10^7
N

Fig 12.3

ACKNOWLEDGEMENTS

The writer is most grateful to Prof. J.W. Hancock, who supervised this research project and showed patience and encouragement during the last three years. His tremendous help will never be forgotten.

The writer wishes to thank Prof. B.F. Scott, the head of Mechanical Engineering Department of Glasgow University and a supervisor, for allowing the use of facilities. Thanks are also due to Dr. D.K. Brown and Dr. M.J. Cowling in the Department for their advice and enthusiasm.

Appreciation is expressed to Hibbitt, Karlsson and Sorensen, Inc. and Prof. J.W. Hancock for the used of the finite element procedures. A debt is due to the staff of the Computer Service Department of the University and the staff of the University Computer Aided Design Centre for their generous assistance in the calculations.

Acknowledgement is also due to the Chinese Government and the British Council who offered joint financial support of the research work.

Finally, the writer would like to thank his wife Yan Zhou, who carried a heavy burden during this project.

Appendix A

The Monte-Carlo Simulation of Fatigue Crack Propagation

If no interaction effects are considered, the crack length is given by summing the crack increment due to each cycle of the fatigue loading

$$a_f = a_o + \sum_{i=1}^{N} \Delta a_i \qquad \text{(A1)}$$

where the Δa_i indicates the crack growth in the ith cycle. The Paris law can be used to determine the crack growth increment for each cycle

$$\begin{aligned} \Delta a_i &= \alpha \, \Delta K_i^n \\ &= \alpha \left[f S_i \sqrt{(\pi a)} \right]^n \end{aligned} \qquad \text{(A2)}$$

For a simple situation such as a central crack in a infinite plate the geometrical calibration function f is unity. For other cases such as the stress intensity factor for the deepest point of a surface crack in a tubular joint, the geometrical function can be evaluated and represented by a polynomial

$$f\left(\frac{a}{T}\right) = C + C_1\left(\frac{a}{T}\right) + C_2\left(\frac{a}{T}\right)^2 + \ldots \qquad \text{(A3)}$$

The next information needed for the simulation is the stress range in the ith cycle S_i. Random numbers representing S_i can be generated based on the ability of computers to supply random numbers uniformly distributed between 0 and 1. Denoting such a random number as V,

$$p(V) = 1 \qquad (0 < V < 1) \qquad (A4)$$

The required distribution of S in a non-dimensional form is

$$p(\eta) = \frac{\gamma}{(\sqrt{2}\,\gamma)^{\gamma}} \exp\left[- \left(\frac{\eta}{\sqrt{2\gamma}}\right)^{\gamma} \right] \qquad (A5)$$

where

$$\eta = \frac{S}{\sigma} \qquad (A6)$$

The two variables are related by a function which meets the following condition

$$p_{\eta}(\eta) = p_{V}(V) \left| \frac{dV}{dS} \right| \qquad (A7)$$

For the simulations conducted during this research work, a suitable function was found to be

$$S = \gamma\, \sigma\, [- \ln(1-V)]^{1/\gamma} \qquad (A8)$$

Fatigue crack propagation under random loading described by Eq A1 has been used to generated a number of samples, for either a given number of cycles N, or a given crack length. The statistical distribution of the samples are compared with analytical predictions (see Sections 2 and 3 in Chapter 10)

Appendix B

The Romberger Method of Numerical Integration

The Romberg integration method is one of the automatic integration schemes which do not require manual intervention during the excution of the integration. Basically, an estimate from the values of the integrand at a number of points in the interval is compared with the estimate after one more point has been added to the middle of each of the sub-intervals. When the two estimates are within the prescribed tolerance, the number of intervals is not increased further. If the estimates are not close enough, another iteration is conducted in which more evaluation points are added. Since the procedure automatically adds more evaluating points, it is necessary to give a maximum number of iterations if the tolerance condition can not be met.

There are two major advantages of the method. Firstly it avoids defining the divisions of the integration sub-intervals beforehand and secondly, the method uses a particular formula which allows a fast convergence as represented by the decreasing difference between the estimates of the integration in two succesive iterations. For the integrations presented in Eq 10.45, it is very difficult to prescribe a division for the integrations. After the trapezoidal

rule failed to perform the numerical integration, the Romberg method was chosen and the results are satisfactory.

The Romberg method was developed from the trapezoidal rule. Let f(x) be a integrand on [a,b] and the integral be

$$I = \int_a^b f(x)\ dx \tag{B1}$$

If

$$T_o^{(k)} = h\ [\ \frac{1}{2}\ f(a) + f(a+h) + \ldots.$$

$$+ f(a+2^k h - h) + \frac{1}{2}\ f(b)] \tag{B2}$$

where h is the length of subdivisions in the interval and

$$h = \frac{b - a}{2^{-k}} \tag{B3}$$

$T_o^{(k)}$ converges to I as the number k increases. It has been proved (Ref 170) that if f(x) has an infinite degree of differentiation, for a estimate by the trapezoidal rule T(h)

$$T(h) = I + C_1 h + C_2 h^2 + C_3 h^3 \ldots\ldots \tag{B4}$$

where C_1, C_2 .... are independent to h. Therefore

$$T(\frac{h}{2}) = I + \frac{C_1}{4}\ h^2 + \frac{C_2}{16}\ h^4 + \frac{C_3}{64}\ h^6 \ \ldots\ldots \tag{B5}$$

Eq B4 and B5 can be used to speed up the convergence process. By cancelling the term h^2, a new version of the estimate can be

obtained

$$T_1(h) = \frac{4}{3} T(\frac{h}{2}) - \frac{1}{3} T(h) \qquad (B6)$$

The procedure can be then extended into a general form. Let

$$T_m^{(k)} = \frac{4^m}{4^m - 1} T_{m-1}^{(k+1)} - \frac{1}{4^m - 1} T_{m-1}^{(k)} \qquad (B7)$$

a table can be constructed as follows

$$T_o^{(0)}$$

$$T_o^{(1)} \quad T_1^{(1)}$$

$$T_o^{(2)} \quad T_1^{(2)} \quad T_2^{(2)}$$

.....

The $T_i^{(j)}$ which has the highest i in the table is taken as the final Romberg estimate.

For the two dimensional integration in Eq 10.45, two subroutines for the implementing of the Romberg method are needed. In fact, for convenience, they are in the form of functions, one of which is presented here as an example.

```
      REAL FUNCTION ROM(D1,D2,TOLAR)
      DIMENSION T(2,50)
C     THE LIMITS OF THE INTEGRATION INTERVAL IS GIVEN BY D1 AND D2
C     THE INTEGRAND IS FUN( )
```

```
C      THE MAXIMUM NUMBER OF INTERATIONS IS 12
C      THE MINIMUM NUMBER OF INTERATIONS IS 6
       N=2
       M=2
       T(1,1)=(D1-D2)*(FUN(D1)+FUN(D2))/2.
  801  HALF=0.
       DO 810 I=1,N,2
       VAL1=(D2-D1)*FLOAT(I)/FLOAT(N)+D1
  810  HALF=HALF+(D2-D1)/FLOAT(N)*FUN(VAL1)
       T(2,1)=T(1,1)/2.+HALF
       DO 820 J=2,M
  820  T(2,J)=(4.**(FLOAT(J)-1.)*T(2,J-1)-T(1,J-1)
      1/(4.**(FLOAT(J)-1.)-1.)
       IF(M.LT.6) GOTO 833
       IF(ABS(T(2,M)-T(1,M-1)).LT.(TOLAR*T(2,M))) GOTO 850
       IF(M.LT.12) GOTO 833
       WRITE(1,900)
  900  FORMAT(' THE INTEGRATION FAILS TO REACH THE GIVEN
      1 TOLERANCE ONCE)
       GOTO 850
  833  DO 830 J=1,M
  830  T(1,J)=T(2,J)
       M=M+1
       N=N*2
       GOTO 801
  850  ROM=T(2,M)
       RETURN
       END
```

REFERENCES

1. Smith, T.A. and Warwick, R.G.: Int J. of Pressure Vessel and Piping, Vol 2, p 283, 1974.

2. Bush, S. H.: J. of Pressure Vessel Technology, Vol. 97, p 54, 1975.

3. Carlsson, J.: Second Advanced Seminar on Fracture Mechnics, Italy, 1979.

4. DeGroot, M.H., "Probability and statistics", Addison-wesley Publishing Company, Massachusetts, USA, 1975.

5. Weibull, W.: J. of Applied Mechanics, Vol 18, p 293, 1951.

6. Haviland, R.P.: "Engineering probability and long life design", D. Van Nostrand Company, Inc., 1964.

7. Bogdanoff, J. L.: J. Appl. Mech., Vol 45, p 246, 1978.

8. Editors: Korn, G.A. and Korn, T.M., Second edition, "Mathematical handbook for scientists and engineers", McGraw-Hill Book Company,

USA, 1968.

9. Barsom, J.M.: in "Fatigue crack growth under spectrum loads", ASTM STP 595, p 217, 1976.

10. Hudson, C.M.: in "Methods and models for Predicting fatigue crack growth under random loading", ASTM STP 748, p 41, 1981.

11. Rice, S.O.: in "Selected papers on noise and stochastic processes" edited by Nelson Wax, Dover Publications, New York, 1954.

12. Cartwright, D.E. and Longuet-Higgins, M.S.: Proc. Roy. Soc., A237, 1956.

13. Taylor, G.I.: "Diffusion by continuous movements", Proc. Lond. Math. Soc., Ser 2, Vol 22, p 196, 1920.

14. Newland, D.E. "An introduction to random vibrations and spectral analysis", Harlow, 1984.

15. Lighthill, M.J.: "Introduction to Fourier analysis and generalised functions", Cambridge University Press, 1962.

16. Matsuishi, M. and Endo, T., "Fatigue of metals subjected to varying stress", paper presented to Japanese Soc. Mech. Eng., Fukuoka, Japan, 1968.

17. Wirshing, P.H. and Shehata, A.M.: J. of Engng Materials and Technology, Vol. 99, p 205, 1977.

18. Maddox, N.R. and Wildenstein, A.W.: Marine Technology Conference, OTC 2261, p 185, 1975.

19. Dowling, N.E.: J. of Materials, Vol 7, p 71, 1972.

20. Nelson, D.V.: "Cumulative fatigue damage in metals", PhD thesis, University of Stanford, 1978.

21. Hancock, J.W. and Gall, D.S. University of Glasgow Marine Technology Centre Report, 1985.

22. Rice, J.R., Beer, F.P. and Paris, P.C.: in "Acoustical fatigue in aerospace structures", Proceedings of the Second Int. Conf., Dayton, 1964.

23. Palmgren, A.: Ver. deut. Ingr., Vol 68, p 339, 1924 (in Germen).

24. Miner, M.A.: J. of Applied Mechanics, Vol 12, p 159, 1945.

25. American Welding Society Structural Welding Code, American Welding Society, AWS D1.1-72, 1972.

26. Construction and Inspection of Fixed Offshore Structures, Det norske Veritas, Oslo, Norway, 1974.

27. Schijve, J. and Broek, D.: Aircraft Eng., Vol 34, p 314, 1962.

28. Smith, P.W. and Malme, C.I.: J of Acoustical Society of America, Vol. 35, p 43, 1963.

29. Hillberry, B.M.: in "Effect of environment and complex load history on fatigue life, ASTM STP 462, p 167, 1970.

30. Barsom, J.M.: in "Progress in flaw growth and fracture toughness testing", ASTM STP 536, p 55, 1973.

31. Kowalewski, J.: in "Full-scale fatigue testing of air craft structures", p 60, Pergamon, 1961.

32. Swanson, S.R.: Materials Research and Standards, Vol 8, p 10, 1968.

33. Abtahi, A., Albrecht, P. and Irwin, G.R.: J. of the Structural Division, Vol. 102, p 2103, 1976.

34. Wylde, J.G. and McDonald, A.: Second Int. Conf. on Behaviour of Off-shore Structures, London, 1979.

35. Forrest, P.G.: "Fatigue of metals", Pergamon Press, 1962.

36. Corten, H.T. and Dolan, T.J.: Int. Conf. on Fatigue of Metals, London, 1956

37. Wirshing, P.H. and Light, M.C.: J. of the Structural Division, Vol 106, p 1593, 1980.

38. Shin, Y. S. and Lukens, R. W., in "Random fatigue life prediction", ASME PVP Vol 72, p 73, 1983.

39. Shin, Y.S.: J. Pressure Vessel Tech., Vol 102, p 378, 1980.

40. Westergaard, H.M.: J. Appl. Mech., Vol. 61, p A49, 1939.

41. Sih, G.C.: Int. J. on Fracture Mech., Vol 2, p 475, 1966.

42. Pooke, D.P. and Cartwright, D.J.: "Compendium of stress intensity factors", Hillingdon Press, 1976.

43. Tada, H., Paris, P.C. and Irwin, G.R.: "The stress analysis of cracks handbook", Del Research Corporation, Hellertown, Pa., 1973.

44. Srawley, J.E.: Int. J. Fracture, Vol 12, p 475, 1976.

45. Griffith, A.A.: Phil. Trans. Roy. Soc., A221, p 163, 1920.

46. Orowan, E.: Welding Journal, Vol 34, p 1575, 1955.

47. Irwin, G.R.: Appl. Mater. Res., Vol 3, p 65, 1964.

48. Fuchs, H.O. and Stephens, R.I.: "Metal fatigue in engineering", John Wiley and Sons, 1980.

49. Irwin, G.R., Kies, J.A. and Smith, H.L.: Poc. of Am. Soc. Test Material, Vol 58, p 640, 1958.

50. Irwin, G.R.: J. Appl. Mech., Vol 24, p 361, 1957.

51. Pook, L.P.: Eng. Fracture Mech., Vol 3, p 205, 1971.

52. Cartwright, D.J. and Rooke, D.P.: in "A general introduction to fracture mechanics", A Journal of Strain Analysis Monograph, Mechanical Engineering Publications Ltd., 1978.

53. Smith, D.G. and Smith, C.W.: Int. J. Fract. Mech., Vol 6, p 305, 1970.

54. Gallagher, J.P.: Eng. Fract. Mech., Vol 3, p 27, 1971.

55. James, L.A. and Anderson, W.E.: Eng. Fract. Mech., Vol 1, P 565, 1969.

56. Tada, H.: Eng Fract. Mech., Vol 2, p 177, 1970.

57. Irwin, G.R.: in "Structural mechanics", p 557, Pergamon, New York, 1960.

58. Chan S.K., Tuba, I.S. and Wilson, W.K.: Eng. Fract. Mech., Vol 2, p 1, 1970.

59. Rice, J.R. and Levy, N. J. Appl. Mech., Vol 39, p 185, 1972.

60. Brown, W.F. and Strawley, J.E.: in "Plane strain crack toughness testing of high strength metallic meterials", ASTM STP 410, 1967.

61. Parks, D.M.: J. Press. Vessel Tech., Vol 103, p 246, 1981.

62. Raju, J.S. and Newman, J.C.: Eng. Fracture Mech., Vol 11, p 817, 1979.

63. Desvaux, G.J.: "The line spring model for surface flaw, an extension to mode *II* and mode *III*", MSc Thesis of Massachusetts Institute of Technology, 1985.

64. Parks, D.M.: Int. J. of Fracture, Vol 10, p 487, 1974.

65. Parks, D.M.: Comp. Meth. Applied Mech. and Eng. Vol 12, p 353, 1977.

66. Zienkiewicz, O.C.: "Finite element methods in engineering science" McGraw-Hill, 1971.

67. Labbens, R.C., Heliot, J. and Pellissier-Tanon, A.: in "Cracks and fracture", ASTM STP 601, p 448, 1976.

68. Oore, M. and Burns, D. J., J. Pressure Vessel Technology, Vol 102, p 202, 1980.

69. Kassir, M. K. and Sih, G. C. "Three dimensional crack problems", Noordhoff, 1975.

70. Oore, M. and Burns, J.: 4th Int. Conf. on Pressure Vessel Technology, London, 1980.

71. Mowbray, D.F.: Eng. Fract. Mech., Vol 2, p 173, 1970.

72. Tracey, P.M.: Eng. Fract. Mech., Vol 3, p 255, 1971.

73. Walsh, P.F., Int. J. Solids Struct. Vol 7, p 1333, 1971.

74. Vooren, J.V.: J. Basic Eng., Vol 89, p 235, 1967.

75. Isida, M. Eng. Fract. Mech., Vol 2, p 61, 1970.

76. Irwin, G.R.: in "Structural mechanics", p 557, Pergamon, 1960.

77. Irwin, G.R.: J. Basic Eng., Vol 82, p417, 1960.

78. Green, A.E.: and Sneddon, I.N.: Proc. of the Cambridge Philosophical Soc., Vol 46, p 159, 1950.

79. Hartranft, R.T. and Sih, G.C.: in "Methods of analysis of crack", Noordhoft, p 179, 1973.

80. Scott, P.M. and Thorpe, T.W.: "Prediction of semi-elliptic crack shape development during fatigue crack growth", Atomic Energy Research Establishment Report, AERE-R10104, 1981.

81. Newman, J.C.: Eng. Fracture Mech., Vol 4, p 667, 1973.

82. Newman, J.C. and Raju, I.S.: Eng. Fract. Mech., Vol 15, p 185, 1981.

83. Koterazawa, R. and Minamisaka: J. Soc. of Materials Science of Japan, Vol 26, p 1, 1977.

84. Holdbrook, S.J. and Dover, W.D., Eng. Fracture Mech., Vol 12, p 347, 1979.

85. Irwin, G.R.: Trans. ASME, E29, p 651, 1962.

86. Shah, R.C. and Kobayashi, A.S.: Eng Fracture Mech., Vol 3, p71, 1971.

87. Rice, J.R.: J. Appl. Mech., Vol 35, p 379, 1968.

88. Maxey, W.A.: in "Stress corrosion cracking of metals —— A state of the art", ASTM STP 518, p 70, 1972.

89. Hutchinson, J.W.: J. Mech. Phys. Solids. Vol 16, p 13, 1968.

90. Rice, J.R. and Rosengren, G.F.: J. Mech Phys. Solids, Vol 16, p 1, 1968.

91. Hutchinson, J.W. and Paris, P.C.: in "Elastic-plastic fracture", ASTM STP 668, p 37, 1979.

92. Wells, A.A.: In Proc. Crack Propagation Symposium, Cranfield, p 210, 1961.

93. Dugdale, D.S.: J. Mech. Phys. Sol., Vol 8, p 100, 1960.

94. McClintock, F.A. and Irwin, G.R., in "Fracture toughness testing and its applications", ASTM STP 381, p 84, 1965.

95. Parry, G.W. and Mills, R.G.: J. Strain Analysis, Vol 3, p 159, 1968.

96. Veerman, C.C and Muller, T., Eng. Fracture Mech., Vol 4, p 25, 1972.

97. Burdekin, F.M. and Stone, D.E.W.: J. Strain Analysis, Vol 1, p 145, 1966.

98. Dawes, M.G.: Weld Res. Suppl., Sept. 1974.

99. Pook, L.P.: "The role of crack growth in metal fatigue", printed by J.W. Arrowsmith Ltd, Bristol, 1983.

100. Stephens, R.I., Bonner, P.H., Mauritzson, G. and Tindall, G.W.: J. Test. Eval., Vol 7, p 68, 1979.

101. Noordhoek, C. and Verheul, A.: " Comparison of the HCPD method of in depth fetigue crack growth monitoring with the crack front

marking technique", Delft University of Technology Civil Engineering Department Report, 6-86-13, 1984.

102. Forsyth, P.J.E.: "The physical basis of metal fatigue", American Elsevier Publishing Co., New York, 1969.

103. Crooker, T.W., Hasson, D.F. and Yoder, G.R.: in "Fractography-Macroscopic cracking processes", ASTM STP 600, p 205, 1976.

104. Miller, K.J.: in "Fundametals of deformation and fracture", Eshelby Memorial Symposium, Sheffield, 1985.

105. Miller, K.J. and Zachariah, K.P.: J Strain Analysis, Vol 12, p 262, 1977.

106. Pook, L.P. and Greenan, A.F.: in "Fracture mechanics", ASTM STP 677, p 23, 1979.

107. Paris, P.E. and Erdogan, F., J. Basic Eng., Vol 185, p 528, 1963.

108. Liu, H.W.: J. Basic Eng, Vol 85, p 116, 1963.

109. Head, A.K.: J. Appl. Mech., Vol 23, p 497, 1956.

110. Frost, N.E. and Dugdale, D.S.: J of the Mechanics and Physics of Solids. Vol 6, p 93, 1958.

111. Frost, N.E., Pook, L.P. and Denton, K.: Eng. Fract. Mech., Vol 3, p 109, 1971.

112. Davies, K.B. and Fedderson, C.E.: J. Aircraft, Vol 12, p 943, 1975.

113. Forman, R.G., Kearney, V.E. and Engle, R.M.: J. Basic Eng., Vol 89, p 459, 1967.

114. Walker, E. K. in "Effects of environment and complex load history on fatigue life", ASTM STP 462, p 1, 1970.

115. Bowles, C.Q. and Broek, D.: Int. J. Fract. Mech., Vol 8, p 75, 1972.

116. Bates, R.C. and Clark, W.G.: ASME Trans., Vol 62, p 380, 1969.

117. Vosikovsky, O.: Eng. Fract. Mech., Vol 11, p 595, 1979.

118. Cooke, R. J. and Beevers, C.J.: Eng. Fract. Mech., Vol 5, p 1061, 1973.

119. Moutz, J. and Weiss, V.: in "Cracks and fracture", ASTM STP 601, p 154, 1976.

120. Frost, N. E., Marsh, K. J. and Pook, L. P.: "Metal fatigue", Oxford University Press, London, 1974.

121. Crooker, T.W., Bogar, F.D. and Cares, W.R.: in "Corrosion fatigue technology", ASTM STP 642, p 189, 1978.

122. Watson, P., Hoddinott, D.S. and Norman, J.P.: in "Cyclic stress-strain behaviour —— analysis, experimentation, and prediction", ASTM STP 519, p 271, 1973.

123. Manson, S.S., Freche, J.C. and Ensign, C.R.: in "Fatigue crack propagation", ASTM STP 415, p 384, 1967.

124. Priddle, E.K.: Int. J. Pres. Ves. Piping, Vol 4, p 89, 1976.

125. Gall, D.S. and Hancock, J.W.: "Fatigue crack growth under narrow and broad band stationary loading", Part *II*, Glasgow University Marine Technology Report, 1985.

126. Wheeler, O.E.: J. Basic Eng., Vol 94, p 181, 1972.

127. Newman, J.C.(Jr): in "Methods and models for predicting fatigue crack growth under random loading", ASTM STP 748, p 53, 1981.

128. Elber, W.: in "Damage tolerance in aircraft structures", ASTM STP 486, p 230, 1971.

129. Bell, P.D. and Wolfman, A.: in "Mathematical modeling of crack growth interaction effects", ASTM STP 595, p 157, 1976.

130. Newman Jr., J.C.: in "Methods and models for predicting fatigue crack growth under random loading", ASTM STP 748, p 53, 1981.

131. Chang, J.B., Szamossi, M. and Liu, K.W.: in "Methods and models for predicting fatigue crack growth under random loading", ASTM STP 748, p 115, 1981.

132. Dover, W.D., Holdbrook, M.S.J., Hibberd, R.D. and Charlesworth, F.D.W., O.T.C. paper 3252, Houston, 1978.

133. Dover, W.D., Chaudhury, G.K. and Dharmavasan, S., Int. Conf on Steel in Marine Structures, Paris, 1981.

134. Wirshing, P.H. and Wu, Y.-T.; in "Random fatigue life prediction", ASME PVP vol 72, p 107, 1983.

135. Virkler, D.A., Hillberry, B.M. and Goel, P.K.: J. Eng Mater. Tech., vol 101, p 148, 1979.

136. Wei, R.P., Wei, W. and Miller, G.A.: J. Test. Eval., Vol 7, p 90, 1979

137. Clark, W.G. Jr. and Hudak, S.J. Jr.: J. of Test. Eval., Vol 3, p 454, 1975.

138. Sinclair, G.M. and Dolan, T.J., Trans. ASME, Vol 75, p 867, 1953.

139. Salivar, G.C.: Eng Fracture Mech., Vol 12, p 181, 1979.

140. Hunt, R.A., McCartney, L.N.: Int. J. of Fracture, Vol 15, p 365, 1979.

141. Nash, C.D.: in "Random fatigue life prediction", ASME PVP vol 72, p 61, 183.

142. Bogdanoff, J.L.: J. Appl. Mech., Vol 45, p 246, 1978.

143. Lin, Y.K.: "Probabilistic theory of strctural dynamics", McGraw-Hill, 1967.

144. Kozin, F. and Bogdanoff, J.L.: Eng Fract. Mech., Vol 18, p 271, 1983.

145. Lin, Y.K. and Yang, J.N.: Eng Fract. Mech., Vol 18, p 143, 1983.

146. Lin, Y.K. and Yang, J.N.: AIAA J., Vol 23, p 117, 1985.

147. Payne, A.O.: in "Probabilistic aspects of fatigue', ASTM STP 511, p 106, 1972.

148. Payne, A.O. and Graham, A.D.: Eng Fracture Mech., Vol 102, p 329, 1979.

149. Payne, A.O.: Proceedings of the 6th International Congress on Fracture, New Delhi, 1984.

150. Irvine, N.M.: Int. Conf. on Fatigue of Offshore Structural Steels, London, 1981.

151. McDonald, A. and Wylde, J.G.: Int. Conf on Fatigue of Offshore Structural Steels, London, 1981.

152. Kraus, H.: "Thin elastic shells", John Wiley and Sons, 1967.

153. Baker, E.H., Kovalevsky, L. and Rish, F.L.: "Structural analysis of shells", McGraw-Hill, 1972.

154. Scordelis, A.C. and Bouwkamp, J.G.: J. Strut. Division, Vol 96, p 65, 1970.

155. Zienkiewicz, O.C.: "Finite elements and approximation", John Wiley and Sons, 1983.

156. Cheung, Y.K. and Yeo, M.F.: "A practical introduction to finite element analysis", Pitman Publishing Limited, 1979.

157. Wordsworth, A.C. and Smedley, G.P., European Offshore Steels Research Seminar, Welding Institute, 1978.

158. Wordsworth, A.C.: Int. Conf. on Fatigue in Offshore Structural Steels, London, 1981.

159. Elliott, K.S. and Fessler, H.: Int. Conf on Fatigue and Crack Growth in Offshore Structures, London, 1986.

160. Kuang, J.G., Potwin, A.B. and Leick, R.D.: Offshore Technology Conferenece, OTC paper 2205, Houston, 1975.

161. Gibstein, M.B.: European Offshore Research Select Seminar, Cambridge, 1978.

162. Reemsnyder, H.S.: in "Fatigue Testing of Weldments", ASTM STP 648, p 3, 1978.

163. Maddox, S.J.: Int. J. of Fracture, Vol 11, p 221, 1975.

164. Hayes, D.J. and Maddox, S.J.: Weld. Inst. Research Bulletin, Vol 13, p 1, 1972.

165. Albrecht, P. and Yamada, K.: J. of the Struct. Div., Vol 103, p 12742, 1977.

166. Frank, K.H. and Fisher, J.W.: J. of the Struct. Div., Vol 105, p 14823, 1979.

167. Wylde, J.G. and McDonald, A: Int. Conf on Fatigue in Offshore Structural Steel, London, 1981.

168. Dover, W. D. and Holdbrook, S. J.: Proc. 2nd Int. Conf. on the

Behaviour of Offshore Structures, London, 1979.

169. Martin, T.: European Offshore Research Select Seminar, Cambridge, 1978.

170. Clayton, A.M.: "Assessment of U.K.O.S.R.P crack growth data to investigate the remaining life of offshore structures following inspection", U.K.A.E.A Report ND-R-85(R), 1982.

171. Dover, W. D., Hibberd, R. D. and Holdbrook, S. J.: Stress Analysis Conf., University of Sheffield, 1976.

172. Dharmavasan, S. and Dover, W.D.: Second Int. Conf. on Integrity of Offshore Structures, Glasgow, 1981.

173. Dover, W. D. and Dharmavasan, S.: Offshore Technology Conf., OTC paper 4404, Houston, 1982.

174. Dover, W.D. and Connolly, M.: Int. Conf. of Fatigue and Crack Growth in Offshore Structures, London, 1986.

175. Gibstein, M.B.: Int. Conf on Steel in Marine Structures, Paris, 1981.

176. Scott, P.M. and Thorpe, T.W.: Fatigue Eng. Mater. Struct., Vol 4, p 291, 1981.

177. British Standard Institution: "Draft for development: fixed

offshore structures", DD55: 1978.

178. Clayton, A.M.: Int. Conf. on Fatigue in Offshore Structural Steel, London, 1981.

179. Dover, W.D., Holdbrook, M.S.J., Hibberd, R.D. and Charlesworth, F.D.W.: Offshore Tech. Conf., OTC 3252, Houston, 1978.

180. Dharmavasan, S and Dover, W.D.: 6th Int. Conf. on Farcture, New Delhi, 1984.

181. Iida, K., Asano, K., Toyufuku, T. and Ishikawa, K.: 2nd Int. Conf. on Integrity of Offshore Structures, Glasgow, 1981.

182. Davis, P.J. and Pabinowitz, P.: "Methods of numerical integration", Academic Press, 1975.

183. Talreja, R.: Eng. Fract. Mech., Vol 11, p 717, 1979.

184. Gall, D.S.: Private commulication, 1985.

185. Kumar, V., German, M.D., Shih, C.F.: "An engineering approach for elastic-plastic fracture analysis", Electric Power Research Instiute, Inc., 1981.

186. ABAQUS User's Manual, Version 4.5, 1984.

187. Huang, X. and Hancock, J.W.: "Stress intensity factors of

surface cracks in tubular joints" part 2, Glasgow University Marine Technology Centre Report, 1986.

188. Ritchie, D.: private communication, Oct., 1986.